

TECHNISCHE UNIVERSITÄT MÜNCHEN

Anorganisch-Chemisches Institut

**Iridium PNP pincer complexes:
CH activation, oxygenation and oxidation reactions**

Jenni Meiners

Vollständiger Abdruck der von der Fakultät für Chemie der Technischen Universität
München zur Erlangung des akademischen Grades eines

Doktors der Naturwissenschaften (Dr. rer. nat.)

genehmigten Dissertation.

Vorsitzender: Univ.-Prof. Dr. Klaus Köhler

Prüfer der Dissertation:

1. Univ.-Prof. Dr. Sven Schneider
Georg-August Universität Göttingen
2. Univ.-Prof. Dr. Dr. h.c. Bernhard Rieger

Die Dissertation wurde am 20.10.2014 bei der Technischen Universität München eingereicht und durch die Fakultät für Chemie am 03.12.2014 angenommen.

für Lorenz und meine liebe Familie

This thesis originated in the time between March 2008 and October 2014 at the Technical University of Munich, the Friedrich-Alexander-University Erlangen and the Georg-August University Göttingen

I am deeply grateful to my supervisor

Professor Dr. Sven Schneider

Thank you for this fascinating topic, the possibility to work with it, to improve my skills, your interest in my work as well as your great professional knowledge and advice

I also want to express my gratitude to

Professor Dr. Dr. h. c. mult. Wolfgang A. Herrmann

and

Professor Dr. Karsten Meyer

Thank you very much for the possibility to work in your chair, for the excellent infrastructure that I was allowed to use and for the support, which I was granted

This thesis was in part supported by a scholarship of the international doctorate program *NanoCat*

Furthermore, my very special thanks go to:

- My former and actual colleagues in the Schneider group Dr. Alexander Marziale, Dr. Anja Friedrich, Dr. Björn Askevold, Dr. Martina Käß, Dr. Markus Scheibel, Dr. Jorge Nieto, Dr. Giovanni P. Rachiero, Kirsten Heußner, Yanlin Wu, Dr. Markus Finger, Isabel Klopsch, Christian Volkmann, Markus Kinauer and Christian Würtele thank you for ongoing collaboration and support and a wonderful time in the lab and beyond
- Prof. Dr. Dr. h.c. Bernhard Rieger and Prof. Dr. Klaus Köhler (thesis defense)
- Ute Stinzel and Helene Delanoff (examination regulations)
- Arne Glüer, Kirsten Heußner, Andreas Thon, Julian Moegling and my Dad thank you for coming to Munich
- Dr. E. Herdtweck, Dr. B. Bechlars, Dr. F. Heineman, Dr. H. Wolf and Dr. C. Würtele (X-ray diffraction), Dr. M. Khusniyarov and Dr. M. B. Boeddinghaus (SQUID), Prof. Dr. M. v. Holthausen and M. Förster (computations), Prof. Dr. T. Drewello, Prof. Dr. I. Ivanović-Burmazović and Dr. M. v. Gernler (cryo-MS), Dr. M. John (WinDNMR & Nuts assistance)
- U. Ammari, T. Tafelmaier and C. Wronner (elemental analysis)
- The employees of the electronics workshops, mechanical workshops and glassblowing
- Dr. A. Claudia Stückl and Dr. Mathias Moll
- The admins Mrs. I. Grötsch, R. Kaufmann, R. Schuhbauer-Gerl, U. Hansl and D. Griffin
- The workmates of the chairs Prof. W. A. Herrmann and Prof. K. Meyer, all colleagues of the TUM, FAU and GAU and other persons who made it easier to feel at home and settle in
- All my students, especially the trainees/bachelor students Nils Engelbogen, Tobias Berto, Sebastian Grundner, Jürgen Pahl, Alexander Giesa and Arne Glüer
- Dr. Andreas Brück, Dr. Daniel Betz, Dr. Markus Drees, Dr. Bettina Bechlars, Dr. Mirza Coccoja, Dr. Gabi Raudaschl-Sieber, Dr. Evangeline Tosh, Eva Hofmarksrichter, Dr. Sophie Putzien, Sebastian Hensel, Eberhard Bronder, Felix Weiky, Julia Sinn, Diana Beyerlein, Valentin Wessels, Dr. Anna Kluge, Boris Kosog, Dr. Andreas Scheurer, Theresa Mekelburg, Anna Olah, Christopher Hörger, Michael Rosenzweig, Dominik Halter, Sven Herrmann, Robert Fischer, Christian Weidel, Nadine Beyerlein, Julia Dempewolf, Dr. Manfred Küppers, Dr. Benedikte Roberz, Hartmut Drescher, Katharina Feil, Kai Rudolph, Stefan Heyde
- Prof. Hartmut Baumgart for the great chance to be part of the Adam Opel AG
- Dr. Ralf Langendorf for trusting my skills, promoting, growing and supporting me
- Swantje Meiners for understanding all non-chemical PhD-topics and challenges
- My family for their love and support
- Lorenz Siebenbürger for continuous encouragement and the wonderful, incomparably happy and unforgettable time together

Abbreviations

Å	angstrom
BDE	bond dissociation energy
br	broad
calcd.	calculated
CO	carbon monoxide
coa, COA	cyclooctane
coe, COE	cylcooctene
DFT	density functional theory
d	doublet
dd	doublet of doublets
δ	chemical shift(ppm)
dn, d^n	n electrons in valence shell
eq.	equation, equivalent(s)
G	Gibbs energy ($J mol^{-1}$)
H	molar enthalpy($J mol^{-1}$)
Hz	hertz
HMQC	heteronuclear multiple quantum coherence NMR
h	hour(s)
i Pr	isopropyl
is, IS	intermediate spin, Intermediate-Spin
J	coupling constant (Hz)
K	equilibrium constant
k	rate constant
κ	coordinating atom
KIE	kinetic isotope effect
L	ligand
l	liter(s)
ls, LS	low-spin, Low-Spin
M	molar($mol l^{-1}$), transition metal
Me	methyl
MHz	megahertz
MTBE	methyl <i>tert</i> -butyl ether
SBME	methyl <i>sec</i> -butyl ether

NBME	methyl <i>n</i> -butyl ether
m	milli, multiplet (NMR), medium (IR)
min	minute(s)
μ	micro
ML _n	metal center n-fold coordinated
nba, NBA	norbornane
nbe, NBE	norbornene
NMR	nuclear magnetic resonance
ν	wave number (cm ⁻¹)
OTf	trifluoromethanesulfonate
PMe ₃	trimethylphosphine
Ph	phenyl
PPh ₃	triphenylphosphine
ppm	parts per million
q	quartet
R	alkyl, alkenyl, alkynyl or aryl
r.d.s	rate determining step
r.t.	room temperature
S	Entropy (J mol ⁻¹ K ⁻¹)
s	second(s), singlet (NMR), strong (IR)
sept	septet
SP	square planar
tba, TBA	<i>tert</i> -butyl ethane
tbe, TBE	<i>tert</i> -butyl ethylene,
THF	tetrahydrofuran
t	triplet
^t Bu	tertiary butyl
VE	valence electron(s)
vt	virtual triplet

Content

A	Introduction	13
A.1	Late transition metal complexes with aliphatic PNP pincer ligands	14
A.1.1	Abstract	14
A.1.2	Introduction	14
A.1.2.1	Brief overview of metal pincer complexes	14
A.1.2.2	PNP complexes with an aliphatic backbone	18
A.1.3	Electron rich transition metal amides: Bonding, electronic structure, and reactivity	18
A.1.4	16 VE (valence electron) amido, enamido, and dienamido complexes: Probing properties and reactivity	22
A.1.4.1	Synthesis of amine ligands $HL1^R$	22
A.1.4.2	Square-planar 16 VE amine and amido complexes: Synthesis, stability, and N–H acidity	24
A.1.4.3	Functionalization of the pincer backbone: Fine-tuning N→M donation	26
A.1.4.3.1	Amido, enamido, and dienamido pincer ligands: Comparison of the donor properties.	26
A.1.4.3.2	16 VE amido vs. enamido complexes: Consequences for structure and reactivity	29
A.1.5	15 and 14 VE complexes: Control of electronic structure by pincer variation	31
A.1.5.1	Oxidation of 16 VE dialkylamido complexes: Formation of unstable radicals	31
A.1.5.2	Ligand modification: Stabilization of square-planar 15 VE complexes	32
A.1.5.3	Fine-tuning of N→M donation: Low-spin vs. intermediate-spin square-planar 14 VE complexes	33
A.1.5.3.1	$[\text{IrCl}(\text{L}4^{\text{tBu}})]^+$ and $[\text{RuCl}(\text{L}1^{\text{tBu}})]$: Square-planar d^6 low-spin complexes	34
A.1.5.3.2	$[\text{RuCl}\{\text{L}_C^{\text{tBu}}\}]$, $[\text{RuCl}\{\text{L}3^{\text{tBu}}\}]$, and $[\text{RuCl}\{\text{L}4^{\text{tBu}}\}]$: In favour of intermediate-spin	35
A.1.5.4	M(PNP) complexes as platforms for late transition metal nitrides	37
A.1.6	Metal-ligand cooperativity: Hydrogenation and dehydrogenation catalysis	38
A.1.6.1	Cooperative H_2 activation	38
A.1.6.2	Outer-sphere hydrogenation and dehydrocoupling of organic substrates	40
A.1.6.3	De-/Hydrogenation of inorganic substrates: CO_2 , azide and borane-	

	amines	42
A.1.7	Conclusions	44
A.2	Activation of CH bonds	46
A.2.1	CH activation with iridium pincer complexes	60
A.3	Activation of dioxygen and oxygenation reactions	64
A.4	Goal and Motivation	67
B	Results and discussion	69
B.1	Synthesis of a square planar iridium(II) complex and oxydation of the latter to the corresponding square planar iridium(III) complex	70
B.1.1	Introduction	70
B.1.2	Results and discussion	72
B.1.3	Experimental Section	77
B.1.3.1	Materials and synthetic methods	77
B.1.3.2	Analytical methods	77
B.1.3.3	Syntheses	78
B.1.3.3.1	$[\text{IrCl}\{\text{N}(\text{C}_2\text{H}_2\text{P}^t\text{Bu}_2)_2\}]$ (1):	78
B.1.3.3.2	$[\text{IrCl}\{\text{N}(\text{C}_2\text{H}_2\text{P}^t\text{Bu}_2)_2\}]\text{PF}_6$ (2) ^{II} :	78
B.1.3.3.3	Redox equilibrium of 1 with $[\text{FeCp}_2]\text{PF}_6$:	78
B.1.3.3.4	Recovery of 1 from the redox equilibrium with $[\text{FeCp}_2]\text{PF}_6$:	79
B.1.4	Crystallographic details	81
B.1.4.1	X-ray diffraction studies	81
B.1.4.2	Neutron diffraction study of 1	83
B.1.5	Computational examinations	85
B.1.5.1	Methods	85
B.1.5.2	Computational Results	86
B.2	Oxygenation of a dihydrido iridium complex toward a SP-coordinated Ir(III)hydroxo complex	90
B.2.1	Abstract	90
B.2.2	Introduction	91
B.2.3	Results and Discussion	92
B.2.3.1	Synthesis of $[\text{Ir}(\text{H})_2\{\text{HPNP}^t\text{Bu}\}]\text{PF}_6$ (3)	92
B.2.3.2	Reaction of 3 with an excess of dioxygen toward a SP coordinated Ir(III) hydroxo complex 4	93
B.2.3.3	Regeneration of 3 via treatment of 4 with an excess of hydrogen and O ₂ -splitting/hydrogenation cycle	100

B.2.4	Conclusion	101
B.2.5	Experimental Section	102
B.2.5.1	Materials and synthetic methods	102
B.2.5.2	Analytical methods	102
B.2.5.3	Calculation of Eyring plots	102
B.2.5.4	Syntheses:	103
B.2.5.4.1	$[\text{Ir}(\text{H})_2\{\text{HPNP}^{\text{tBu}}\}]\text{PF}_6$ (3):	103
B.2.5.4.2	$[\text{Ir}(\text{H}_2)(\text{H})_2\{\text{HPNP}^{\text{tBu}}\}]\text{PF}_6$ (2):	108
B.2.5.4.3	$[\text{Ir}(\text{OH})\{\text{PNP}^{\text{tBu}}\}]\text{PF}_6$ (4):	111
B.2.5.4.4	Cyclic oxygenation hydrogenation reactions:	121
B.2.5.4.5	Treatment of $[\text{Ir}(\text{H})_2\{\text{HPNP}^{\text{tBu}}\}]\text{PF}_6$ (3) with O_2 at low temperatures and observation of the reaction by NMR spectroscopy:	123
B.2.5.4.6	Treatment of $[\text{Ir}(\text{H})_2\{\text{HPNP}^{\text{tBu}}\}]\text{PF}_6$ (3) with O_2 at low temperatures and observation of the reaction by cryo mass spectroscopy ^{II} :	124
B.3	CH activation of THF by a cationic HPNP iridium(I) complex	125
B.3.1	Introduction	125
B.3.2	Results and Discussion	127
B.3.2.1	Ligand synthesis	127
B.3.2.2	Intramolecular vinylic C-H activation of cyclooctene: Solvent dependent OA/RE	127
B.3.2.3	Intermolecular double C-H activation of THF	131
B.3.2.4	Mechanistic considerations	133
B.3.3	Conclusions	135
B.3.4	Experimental Section	136
B.3.4.1	General Methods	136
B.3.4.2	Analytical Methods	136
B.3.4.3	Syntheses	136
B.3.4.4	Kinetic Experiments	139
B.3.4.5	X-ray Crystal-Structure Determinations	139
B.4	Hydrogen elimination from a PNP Iridium(III) Dihydrido Carbene Complex	142
B.4.1	Abstract	143
B.4.2	Introduction	143
B.4.3	Results and Discussion	146
B.4.3.1	Study of the the subsequent dehydrogenation of a dihydrido iridium	

	carbene complex	146
B.4.3.2	Kinetic investigations of the desymmetrization reaction	148
B.4.3.3	Acceleration of the reaction by the addition of oxygen	149
B.4.3.4	Acceleration of the reaction by addition of [Ir(PNP)OH]PF ₆	152
B.4.4	Mechanistic considerations	153
B.4.5	Conclusion	156
B.4.6	Experimental Section	156
B.4.6.1	Materials and synthetic methods	156
B.4.6.2	Analytical methods	157
B.4.6.3	Syntheses: [IrHPNP ^t Bu=COCH ₂ CH ₂ CH ₂]PF ₆ (2)	157
B.4.6.4	Kinetic experiments: General procedure and air and [Ir] catalyzed, respectively	159
C	Summary and outlook	167
<i>C.1</i>	<i>Overview</i>	168
<i>C.2</i>	<i>Square-planar iridium d⁷ und d⁶ complexes</i>	169
<i>C.3</i>	<i>Oxygen reduction reaction</i>	171
<i>C.4</i>	<i>Intermolecular CH activation</i>	172
<i>C.5</i>	<i>Desymmetrization reaction accelerated by presence of O₂ or an Ir(III) hydroxo complex</i>	173
D	Zusammenfassung und Ausblick	177
<i>D.1</i>	<i>Überblick</i>	178
<i>D.2</i>	<i>Quadratisch-planare Iridium d⁷ und d⁶ Komplexe</i>	178
<i>D.3</i>	<i>Sauerstoff-Reduktions-Reaktion (ORR)</i>	181
<i>D.4</i>	<i>Intermolekulare CH-Aktivierung</i>	182
<i>D.5</i>	<i>Beschleunigte Desymmetrisierung in Anwesenheit von O₂ oder einem Ir(III)-Hydroxokomplex</i>	183
E	List of Publications	187
F	Curriculum Vitae	189

A Introduction

A.1 Late transition metal complexes with aliphatic PNP pincer ligands

The following text is for the most part originated from the paper:

‘Cooperative aliphatic PNP amido pincer ligands: Versatile building blocks for coordination chemistry and catalysis’

S. Schneider, J. Meiners, B. Askevold, *Eur. J. Inorg. Chem.* 2012 (3), 412–429

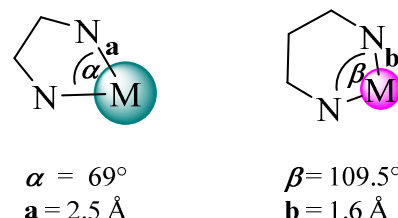
A.1.1 Abstract

In this review, the coordination chemistry of electron rich metal complexes with the simple aliphatic, anionic diphosphinoamido ligand $\{N(CH_2CH_2PR_2)_2\}^-$ is covered and compared with other commonly used, anionic PEP (E = C, N) pincer ligands. The strong π -basicity of this ligand enables both the stabilization of electronically and coordinatively highly unsaturated complexes and their use as cooperating ligands in bifunctional stoichiometric bond activation reactions and catalysis. Versatile ligand backbone dehydrogenation gives access to related enamido and dienamido ligands $\{(R_2PCHCH)N(CH_2CH_2PR_2)\}^-$ and $\{N(CHCHPR_2)_2\}^-$, respectively. This oxidative functionalization enables fine-tuning of the ligand donor properties and thereby of the structural features, electronic structure, and reactivity of the respective complexes, which is discussed for several examples.

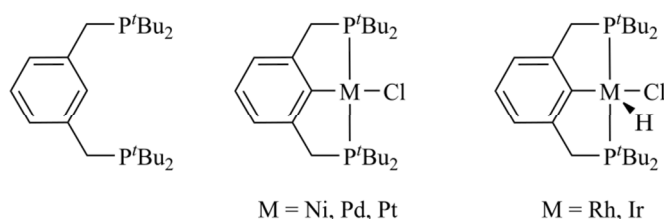
A.1.2 Introduction

A.1.2.1 Brief overview of metal pincer complexes

‘Pincer’ are tridentate chelating ligands, which are bound *meridional* to three adjacent sites of the metal.^[1] (Although it is possible in case of a flexible, aliphatic ‘pincer’ ligand to bind in a facial fashion, the term ‘pincer’ is understood as a binding situation, in which the ligand clips the metal, like a pincette.) If the pincer-metal interaction is inflexible, it provides high thermal stability to the resulting complexes and furthermore, due



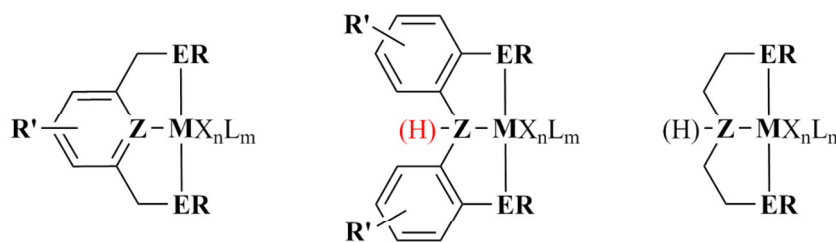
Depiction A.1-1: Ideal geometric values for a five- respective six-membered κ -N,N’ chelating ring.^[3]



Depiction A.1-2: Formula of the precursor (left) of the first PCP ligand 2,6-Bis((di^{tert}butylphosphino)methyl)phenyl and its exemplary complexes (middle and right) with Ni^{II}, Pd^{II}, Pt^{II}, Rh^{III} and Ir^{III}.^[5]

[1] D. Morales-Morales, C. M. Jensen (Eds.), *The Chemistry of Pincer Compounds*, Elsevier, Amsterdam, 2007.

to the constraint, cyclometallation (which can limit the ability to effect CH bond activation of substrates) is hampered.^[2] Due to geometrical conditions (**Depiction A.1-1**) regarding the formation of two chelating, five-membered metallacycles with long metal-heteroatom bonds, high complex building constants, especially toward larger transition metal ions in low oxidation states, can be expected.^[3] The



M = Fe, Co, Ni, Ru, Rh, Pd, Os, Ir, Pt etc.

Z = C, N, etc.

E = P(R)₂, N(R)₂, SR etc.

R = Me, ⁱPr, ^tBu, Ph etc.

R' = Cl, OCH₃, NO₂, OH etc.

L, X⁻ = additional ligands

Depiction A.1-3: Exemplary pincer ligand systems with aromatic backbone (left and center) and saturated backbone (right).^[4]

performed meridional coordination geometry complements excellently with the square planar coordination of d^8 metal centers (e.g. Rh^I, Ir^I, Ni^{II}, Pd^{II}, Pt^{II}) and the square pyramidal or Y-shaped coordination of d^6 metal centers (Ru^{II}, Rh^{III}, Ir^{III}).^[4] Furthermore, the meridional geometry provides the advantage of space for substrates.^[4] The potential dissociation/reductive elimination of one or more *non-pincer* ligand(s) gains the possibility of the formation of reactive, undercoordinated, T-shaped ML₃ d^8 species.

Since their introduction in the late 70s of the last century by *Shaw et al.*^[5] (**Depiction A.1-2**), the ligand class sparked lots of interest in metal organic chemistry due to the defined ligand system, which provides the opportunity to tune the geometrical, sterical and electronically properties of the coordinated metal pointedly. Since then, manifold pincer complexes have been synthesized. For a rough differentiation, the ligand systems are named after their coordinating atoms e.g. PCP, PNP, NCN, SCS, SNS et cetera.

The opportunities for modification of pincer ligands (**Depiction A.1-3**) by rational ligand design are:

(1) The choice of the phosphanyl substituent **R** at the donor group **E**: For many pincer ligand frameworks, bulky substituents are easily introduced, which have large influence on the steric properties of the second coordination sphere of the metal and allow for reactivity control. That includes for example sterical protection of vacant coordination sites or formation of a

[2] C. M. Jensen, *Chem. Commun.* **1999**, 2443–2449.

[3] E. Riedel (Hrsg.), *Moderne Anorganische Chemie (3. Auflage)*, Springer-Verlag, Berlin, **2007**, 476.

[4] M. Albrecht, G. van Koten, *Angew. Chem., Int. Ed. Engl.*, **2001**, *40*, 3750–3781.

[5] C.J. Moulton, B.L. Shaw, *Dalton Trans.*, **1976**, 1020–1024.

hydrophobic, small pocket around the entrance toward the first coordination sphere of the metal.

(2) Electronic effects that arise from pincer modifications, offer further synthetic strategies for catalysis and bond activation reactions. Particularly, at the central ligand framework in *trans*-position to the substrate binding site, electronic modification is fateful. Variation of electron donating/withdrawing substituents **R'** that influences the electronic density at the central donor atom **Z** can affect a differentiation of reactivity. As an example, alteration of **R'** at the aryl backbone of the PCP ligand $\{p\text{-R}'\text{-C}_6\text{H}_4\text{-2,6-(CH}_2\text{PR}_2)_2\}^-$ (R = methyl for computations, R = tert-butyl for experiments) was shown to have a strong influence on the thermodynamics of E'H (E' = H, C) oxidative addition to a d^8 metal center, attributable to M-C_{PCP} π -MO push-pull-interactions.^[6] (Furthermore, **R'** is often a substituent that can be used to immobilize the complex.)

(3) The presence/absence of H ions/atoms in terms of **ZH/Z/Z** and/or in terms of saturated/unsaturated C-C bonds within the ligand backbone provides the opportunity of protonation/deprotonation equilibria, hydrogenation/dehydrogenation equilibria^[7,8] and rearrangement and

tautomerization reactions inside the complex, and thus potential acting of the ligand in bifunctional (cooperative, *Noyori-like*^[9]) processes with a substrate as Brønsted acid/base and/or H₂ donor/acceptor, respectively. For example, rigid, anionic pincer ligands with a central amido unit derived from diarylamines (**Figure 1**, $\{\text{L}_A^R\}^-$) or from pyridine-based chelates upon benzylic deprotonation (**Figure 1**, $\{\text{L}_B^R\}^-$) have recently attracted considerable attention.

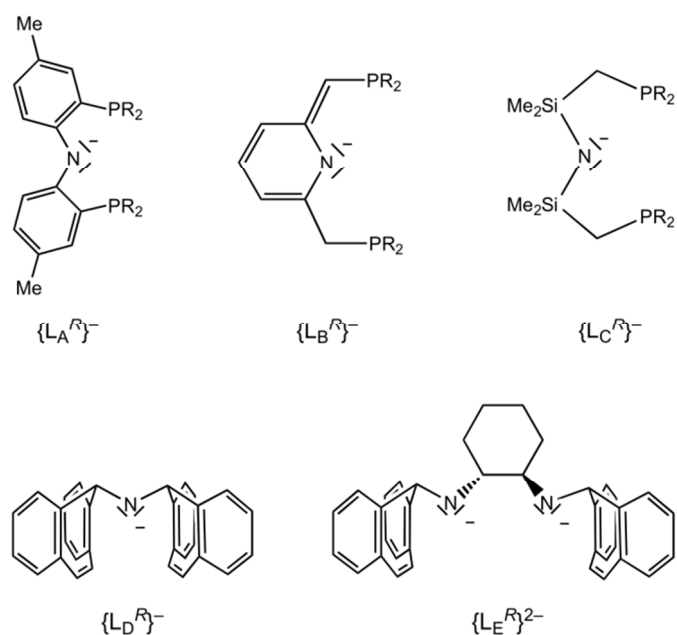


Figure 1: Amido pincer ligands structurally related to the aliphatic PNP ligands discussed here.

[6] K. Krogh-Jespersen, M. Czerw, K. Zhu, B. Singh, M. Kanzelberger, N. Darji, P. D. Achord, K. B. Renkema, A. S. Goldman, *J. Am. Chem. Soc.* 2002, 124, 10797-10809.

[7] *Bifunctional Transition Metal Amido Complexes: Cooperative H₂ Activation and Catalytic Dehydrogenation*, Anja Friedrich PhD Thesis TU München 2010.

[8] a) E. Ben-Ari, G. Leitus, L. J. W. Shimon, D. Milstein, *J. Am. Chem. Soc.* 2006, 128, 15390-15391; b) C. Gunanathan, B. Gnanaprakasam, M. A. Iron, L. J. W. Shimon, D. Milstein, *J. Am. Chem. Soc.* 2010, 132, 14763-14765.

[9] R. Noyori, T. Ohkuma, *Angew. Chem. Int. Ed.*, 2001, 40, 40-73.

The latter were extensively utilized for novel dehydrogenative coupling reactions of polar functional groups as metal-ligand cooperative catalysts based on reversible amide/pyridine de-/aromatization.^[1,10,11,12]

A *redox-non-innocence* contribution of the ligand to the reactivity of the complex is in principal achievable by lifting or lowering of the MOs with significant ligand character due to

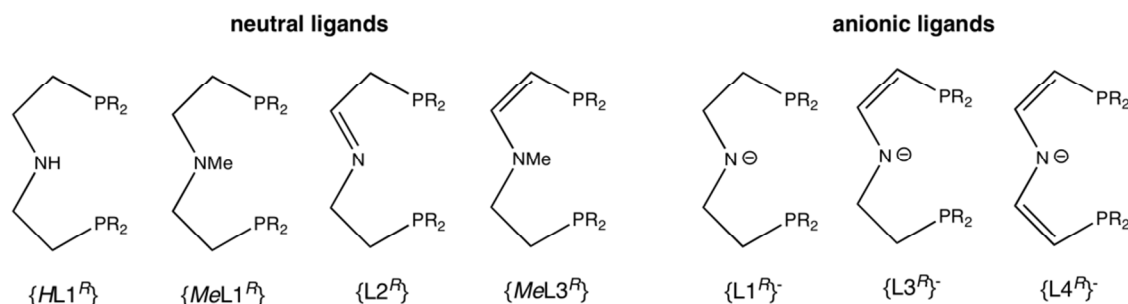


Figure 2: Neutral and anionic ligands derived from parent $\text{HN}(\text{CH}_2\text{CH}_2\text{PR}_2)_2$.

electron withdrawal or supply by the substituents, similarly as redox-non-innocent behavior was previously shown for a few instances of pincer complexes.^[13]

Consequently, pincer complexes are able to perform within a wide variety of stoichiometric and catalytic applications,^[14] such as molecular sensing,^[4,15] switching,^[16] activation of small molecules (e.g. CO_2 ^[17], N_2 ^[18]), carbon-halogen bond formation^[19], oxidative addition of CO and CF bonds^[20], polymerization of alkenes^[21,22] and alkynes^[23], alkane dehydrogenation^[2,24,25], alkane metathesis^[26], transfer hydrogenation^[2,27] and metal centered bond activation.^[25,28]

[10] L.-C. Liang, *Coord. Chem. Rev.* **2006**, *250*, 1152-1177.

[11] a) O. V. Ozerov, C. Guo, V. A. Papkov, B. M. Foxman, *J. Am. Chem. Soc.* **2004**, *126*, 4792-4793; b) L. Fan, L. Yang, C. Guo, B. M. Foxman, O. V. Ozerov, *Organometallics* **2004**, *23*, 4778-4787; c) W. Weng, C. Guo, C. Muora, L. Yang, B. M. Foxman, O. V. Ozerov, *Organometallics* **2005**, *24*, 3487-3499; d) L. Fan, O. V. Ozerov, *Chem. Commun.* **2005**, 4450-4452; e) L. Fan, S. Parkin, O. V. Ozerov, *J. Am. Chem. Soc.* **2005**, *127*, 16772-16773.

[12] a) J. I. van der Vlugt, J. N. H. Reek, *Angew. Chem.* **2009**, *121*, 8990-9004; *Angew. Chem. Int. Ed.* **2009**, *48*, 8832-8846; b) D. Milstein, *Top. Catal.* **2010**, *53*, 915-923; c) C. Gunanathan, D. Milstein, *Acc. Chem. Res.* **2011**, *44*, 588-602.

[13] a) S. C. Bart, K. Chlopek, E. Bill, M. W. Bouwkamp, E. Lobkovsky, F. Neese, K. Wieghardt, P. J. Chirik, *J. Am. Chem. Soc.* **2006**, *128*, 13901-13912.; b) A. T. Radosevich, J. G. Melnick, S. A. Stoian, D. Bacciu, C.-H. Chen, B. M. Foxman, O. V. Ozerov, D. G. Nocera, *Inorg. Chem.* **2009**, *48*, 9214-9221; c) D. Adhikari, S. Mossin, F. Basuli, J. C. Huffman, R. K. Szilagyi, K. Meyer, D. J. Mendiola, *J. Am. Chem. Soc.* **2008**, *130*, 3676-3682; d) M. G. Scheibel, B. Askevold, F. W. Heinemann, E. J. Reijerse, B. B. de, S. Schneider, *Nat. Chem.* **2012**, *4*, 552-558; e) M. G. Scheibel, Y. Wu, A. C. Stückl, L. Krause, E. Carl, D. Stalke, B. de Bruin, S. Schneider, *J. Am. Chem. Soc.* **2013**, *135*, 17719-17722; f) C. C. Hojilla Atienza, C. Milsman, S. P. Semproni, Z. R. Turner, P. J. Chirik, *Inorg. Chem.* **2013**, *52*, 5403-5417; g) A. K. Hui, R. L. Lord, K. G. Caulton, *Dalton Trans.* **2014**, *43*, 7958; h) S. Musa, S. Fronton, L. Vaccaro, D. Gelman, *Organometallics* **2013**, *32*, 3069-3073.

[14] M. E. van der Boom, D. Milstein, *Chem. Rev.* **2003**, *103*, 1759-1792.

[15] Albrecht, M./; Gossage, R.A.; Lutz, M.; Spek, A. L.; van Koten, G. *Chem.-Eur. J.* **2000**, *6*, 1431-1445.

[16] Steenwinkel, P.; Grove, D. M.; Veldman, M.; Spek, A. L.; van Koten, G. *Organometallics* **1998**, *17*, 5647-5655.

[17] Lee, D. W.; Jensen, C. M.; Morales-Morales, D. *Organometallics* **2003**, *22*, 4744-4749.

[18] Vigalok, A.; Ben-David, Y.; Milstein, D. *Organometallics* **1996**, *15*, 1839-1844.

[19] Beletskaya, I. P.; Cheprakov, A. V. *Chem. Rev.* **2000**, *100*, 3009-3066.

[20] Choi, J.; Wang, D. Y.; Kundu, S.; Choliy, Y.; Emge, T. J.; Krogh-Jespersen, K.; Goldman, A. S. *Science* **2011**, *332*, 1545-1548.

[21] McGuinness, D. S.; Gibson, V. C.; Steed, J. W. *Organometallics* **2004**, *23*, 6288-6292.

[22] McGuinness, D. S.; Gibson, V. C.; Wass, D. F.; Steed, J. W. *J. Am. Chem. Soc.* **2003**, *125*, 12716-12717.

[23] Yao, J.; Wong, W.T.; Jia, G. *J. Organomet. Chem.* **2000**, *598*, 228-234.

[24] Liu, F.; Pak, E.B.; Singh, B.; Jensen, C. M.; Goldman, A. S. *J. Am. Chem. Soc.* **1999**, *121*, 4086-4087.

[25] J. Choi, A. H. R. McArthur, M. Brookhart, A. S. Goldman, *Chem. Rev.* **2011**, *111*, 1761-1779.

[26] Goldman, A. S.; Roy, A. H.; Huang, Z.; Ahuja, R.; Schinski, W.; Brookhart, M. *Science* **2006**, *312*, 257-261.

[27] a) D. Morales-Morales, *Rev. Soc. Quím. Méx.* **2004**, *48*, 338-346; b) Dani, P.; Karlen, T.; Gossage, R. A.; Gladiali, S.; van Koten, G. *Angew. Chem., Int. Ed.* **2000**, *39*, 743-745; c) ACS Symposium Series 885, *Activation and Functionalization of C-H Bonds*, **2004** Chapter 12, 198-215: "Alkane Transfer-Dehydrogenation Catalyzed by a Pincer-Ligated Iridium Complex" A. S. Goldman, K. B. Renkema, M. Czerw, K. Krogh-Jespersen.

[28] a) M. Albrecht, G. van Koten, *Angew. Chem.* **2001**, *113*, 3866-3898; *Angew. Chem. Int. Ed.* **2001**, *40*, 3750-3781; b) W. Leis, H. A. Mayer, W. C. Kaska, *Coord. Chem. Rev.* **2008**, *252*, 1787-1797.

A.1.2.2 PNP complexes with an aliphatic backbone

In comparison, despite seminal work from Fryzuk's group using a disilylamido PNP ligand (**Figure 1**, $\{L_C^R\}^-$) in combination with d^6 and d^8 metal ions, aliphatic amido pincer ligands were neglected for some time.^[29] Amido ligands with C–H bonds in α -position are generally prone to β -hydride elimination giving rise to imine formation.^[30] Hence, the expected lower thermal stabilities and more complex reactivity patterns from ligand chemical non-innocence might have impeded the use of alkylamido ligands to some extent.

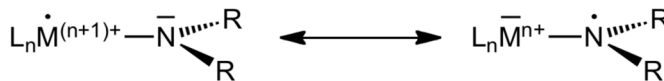


Figure 3: Canonic Lewis-structures for open shell amido complexes.

However, chelating amido ligands exhibit higher barriers for imine extrusion compared to terminal amides. Particularly the great success of 'bifunctional catalysis' for the hydrogenation of polar multiple bonds sparked great interest in flexible, chelating ligands which can facilitate H_2 heterolysis by the stabilization of both amido and amino intermediates which occur during ionic hydrogenation.^[31]

This review covers the recent work with aliphatic, anionic PNP ligands, particularly ethylene bridged ligand $N(CH_2CH_2PR_2)_2^-$ ($\{L1^R\}^-$), and related ligands derived by simple ligand backbone functionalization (**Figure 2**). These oxidative ligand modifications are discussed in combination with their impact on donor properties and electronic structure and reactivity of the respective complexes. After a concise introduction into bonding and reactivity of amido ligands coordinated to electron rich transition metal centers (**section A.1.3**), the properties of PNP amido, enamido, and dienamido ligands are compared with other common pincer ligands (**section A.1.4**). Finally, their use for the stabilization of unusual, electronically unsaturated complexes (**section A.1.5**) and for metal-ligand cooperative bond activation and catalysis (**section A.1.6**) are discussed.

A.1.3 Electron rich transition metal amides: Bonding, electronic structure, and reactivity

Covalently bound π -donating ligands, such as amido ligand (NR_2^-), are frequently used to stabilize complexes of electron poor (early) transition metals in high oxidation states.^[32] In contrast, until more recently electron rich (late) transition metal complexes in low oxidation

[29] a) M. D. Fryzuk, P. A. McNeil, *J. Am. Chem. Soc.* **1981**, *103*, 3592-3593; b) M. D. Fryzuk, P. A. McNeil, *Organometallics* **1983**, *2*, 355-356; c) M. D. Fryzuk, P. A. McNeil, S. J. Rettig, *Organometallics* **1986**, *5*, 2469-2476.

[30] Representative examples: a) S. E. Diamond, F. Mares, *J. Organomet. Chem.* **1977**, *142*, C55-C57; b) J. M. Mayer, C. J. Curtis, J. E. Bercaw, *J. Am. Chem. Soc.* **1983**, *105*, 2651-2660; c) J. F. Hartwig, S. Richards, D. Barañano, F. Paul, *J. Am. Chem. Soc.* **1996**, *118*, 3626-3633; d) J. F. Hartwig, *J. Am. Chem. Soc.* **1996**, *118*, 7010-7011; e) S. Wagaw, R. A. Rennels, S. L. Buchwald, *J. Am. Chem. Soc.* **1997**, *119*, 8451-8458; f) J. Zhao, H. Hesslink, J. F. Hartwig, *J. Am. Chem. Soc.* **2001**, *123*, 7220-7227; g) P. Zhao, J. F. Hartwig, *J. Am. Chem. Soc.* **2005**, *127*, 12066-12073; h) I. Matas, J. Campora, P. Palma, E. Alvarez, *Organometallics* **2009**, *28*, 6515-6523.

[31] a) R. Noyori, T. Okhuma, *Angew. Chem.* **2001**, *113*, 40-75; *Angew. Chem. Int. Ed.* **2001**, *40*, 40-73; b) S. E. Clapham, A. Hadzovic, R. H. Morris, *Coord. Chem. Rev.* **2004**, *248*, 2201-2237; c) K. Muñoz, *Angew. Chem.* **2005**, *117*, 6780-6785; *Angew. Chem. Int. Ed.* **2005**, *44*, 6622-6627; d) H. Grützmacher, *Angew. Chem.* **2008**, *120*, 1838-1842; *Angew. Chem. Int. Ed.* **2008**, *47*, 1814-1818. e) J. S. M. Samec, J.-E. Bäckvall, P. G. Andersson, P. Brandt, *Chem. Soc. Rev.* **2006**, *35*, 237-248; f) T. Ikariya, A. J. Blacker, *Acc. Chem. Res.* **2007**, *40*, 1300-1308; e) M. Ito, T. Ikariya, *Chem. Commun.* **2007**, 5134-5142.

[32] a) R. Kempe, *Angew. Chem.* **2000**, *112*, 478-504; *Angew. Chem. Int. Ed.* **2000**, *39*, 468-493; b) M. Lappert, P. Power, A. Protchenko, A. Seeber in *Metal Amide Chemistry*, Wiley, Chichester, **2009**.

states ($d^6 - d^{10}$) with these ligands were comparatively rare.^[33] However, the participation of late transition metal amido complexes in catalytic transformations, such as C–N cross coupling reactions,^[34] has stimulated several studies about M–NR₂ bonding. Pearson’s hard and soft acid and base (HSAB) theory predicts weak bonding of hard, π -donating amido ligands with electron rich metal centers.^[35] However, Bercaw and co-workers demonstrated a linear relationship of M–R (M = Ru^{II}, Pt^{II}; R = alkyl, aryl, acetylide, hydride, alkoxide and amide) bond dissociation energies (BDE) with the respective H–R BDE’s.^[36] On the other hand, comparison of metal amido hydrogenolysis along the transition series ($L_nM-NR_2 + H_2 \rightleftharpoons L_nM-H + HNR_2$) provides some qualitative information with respect to relative M–N_{amido} bond energetics:^[37] While d^6 and d^8 anilido complexes

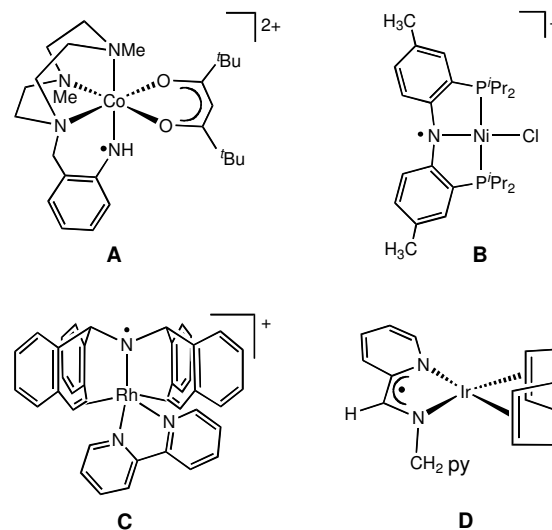


Figure 4: Representative examples for radical complexes with predominant aminyl character (py = 2-pyridyl).

[Cp*₂Ru(NHPh)(PMe₃)₂] or [PtH(NHPh)(PEt₃)₂] readily react with H₂ to give the corresponding hydride complex and free amine, [Cp*₂Zr(H)₂] exhibits reverse reactivity and releases H₂ with NH₂Ph.^[36,38] This reactivity is in line with calculated relative BDE’s (BDE_{M–H} - BDE_{M–N}: 151 kJ/mol (Cp*₂Ru(PMe₃)₂); 121 kJ/mol (PtH(PEt₃)₂); 4 kJ/mol (Cp*₂ZrH)). These results can be rationalized on the basis of M–N bonding: High anionic charge density on the nitrogen atom is expected as a result of polar metal-amido σ -bonding.^[39] If vacant metal orbitals for N→M π -donation are available, the charge will be effectively delocalized, strengthening the M–N bond as in the case of d^0 complex [Cp*₂Zr(NHPh)(H)].^[40] For metal centers without empty d -orbitals of suitable symmetry and energy, e.g. octahedral d^6 or square-planar d^8 complexes, no net M–N π -bond results from the M–N π -interaction.^[41]

[33] a) H. E. Bryndza, W. Tam, *Chem. Rev.* **1988**, *88*, 1163-1188; b) M. D. Fryzuk, C. D. Montgomery, *Coord. Chem. Rev.* **1989**, *95*, 1-40; c) D. M. Roundhill, *Chem. Rev.* **1992**, *92*, 1-27; d) R. G. Bergman, *Polyhedron* **1995**, *14*, 3227-3237; e) J. R. Fulton, A. W. Holland, D. J. Fox, R. G. Bergman, *Acc. Chem. Res.* **2002**, *35*, 44-56; f) T. B. Gunnoe, *Eur. J. Inorg. Chem.* **2007**, 1185-1203.

[34] (a) J. F. Hartwig, *Acc. Chem. Res.* **1998**, *31*, 852-860; (b) J. F. Hartwig, *Synlett* **2006**, 1283-1294; (d) J. F. Hartwig, *Nature* **2008**, *455*, 314-322.

[35] R. G. Pearson, *J. Am. Chem. Soc.* **1963**, *85*, 3533-3539.

[36] H. E. Bryndza, L. K. Fong, R. A. Paciello, W. Tam, J. E. Bercaw, *J. Am. Chem. Soc.* **1987**, *109*, 1444-1456.

[37] For an excellent discussion, *c. f.* ref 33e.

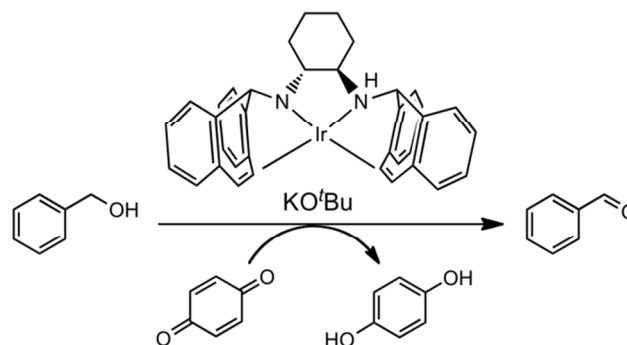
[38] a) G. L. Hillhouse, J. E. Bercaw, *J. Am. Chem. Soc.* **1984**, *106*, 5472-5478; (b) R. L. Cowan, W. C. Troglor, *J. Am. Chem. Soc.* **1989**, *111*, 4750-4761.

[39] P. L. Holland, R. A. Andersen, R. G. Bergman, *Comm. Inorg. Chem.* **1999**, *21*, 115-129.

[40] L. A. Goj, E. D. Blue, S. A. Delp, T. B. Gunnoe, T. R. Cundari, A. W. Pierpont, J. L. Petersen, P. D. Boyle, *Inorg. Chem.* **2006**, *45*, 9032-9045.

[41] K. G. Caulton, *New J. Chem.* **1994**, *18*, 25-41.

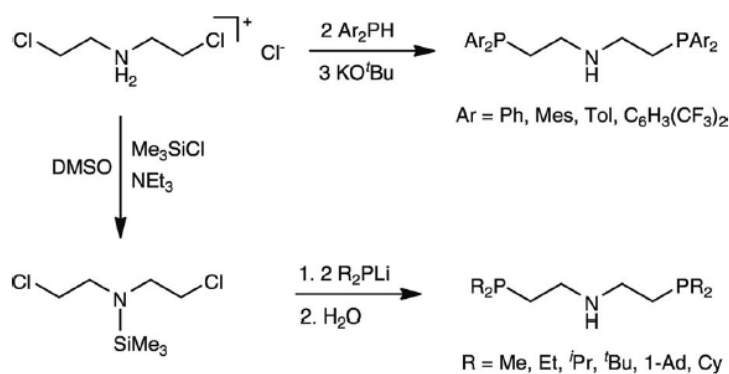
This lack of charge delocalization results in high basicity and nucleophilicity of the amido ligand, exemplified by C–N coupling with C-electrophiles.^[42,43] Proton transfer to the amido ligand upon H₂ heterolysis was first demonstrated by Fryzuk and co-workers for *d*⁶ and *d*⁸ complexes with disilylamido pincer ligand {Lc^R}⁻.^[44] This reaction was later recognized as key step for



Scheme 1: Oxidative dehydrogenation of alcohols catalyzed by an iridium amido complex.

‘bifunctional’ (also denoted ‘metal-ligand cooperative’ or ‘Noyori-Morris-type’ catalysis or initially as ‘N-H effect’) hydrogenation catalysis and was therefore extensively studied.^[31] Other than H₂, weakly acidic sp, sp², and sp³ C–H bonds were also shown to add across M–N_{amido} bonds.^[43a,45]

However, cooperativity of amido ligands is not restricted to acid-base chemistry. A mainly N-centered HOMO suggests potential ligand redox non-innocence for amido radical complexes, or in terms of a simple Lewis-formalism a description as aminyl (N-radical) rather than amido (metalloradical)



Scheme 2: Synthesis of PNP amine ligands HL1^R (1-Ad = 1-adamantyl, Cy = cyclohexyl, Mes = mesityl, Tol = *p*-tolyl).

complex (**Figure 3**).^[46] The electronic structure of amido radical complexes is of relevance for catalysis, e.g., oxidative dehydrogenation of amines, which is particularly well promoted by metals of the iron-triad.^[47] The oxidation of alcohols to aldehydes catalyzed by the

[42] S. Park, A. L. Rheingold, D. M. Roundhill, *Organometallics* **1991**, *10*, 615-623.

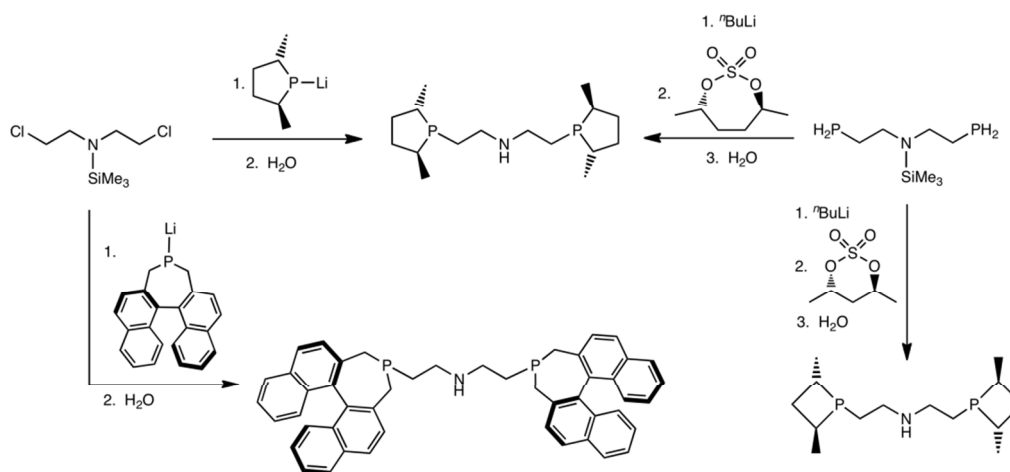
[43] a) J. R. Fulton, M. W. Bouwkamp, R. G. Bergman, *J. Am. Chem. Soc.* **2000**, *122*, 8799-8800; b) T. Büttner, F. Breher, H. Grützmacher, *Chem. Commun.* **2004**, 2820-2821; c) P. Maire, F. Breher, H. Schönberg, H. Grützmacher, *Organometallics* **2005**, *24*, 3207-3218; d) T. Büttner, J. Geier, G. Frison, J. Harmer, C. Calle, A. Schweiger, H. Schönberg, H. Grützmacher, *Science* **2005**, *307*, 235-238.

[44] a) M. D. Fryzuk, P. A. McNeil, *Organometallics* **1983**, *2*, 682-684; b) M. D. Fryzuk, P. A. McNeil, S. J. Rettig, *Organometallics* **1985**, *4*, 1145-1147; c) M. D. Fryzuk, P. A. McNeil, S. J. Rettig, *J. Am. Chem. Soc.* **1987**, *109*, 2803-2812.

[45] a) D. Rais, R. G. Bergman, *Chem. Eur. J.* **2004**, *10*, 3970-3978; b) D. Conner, K. N. Jayaprakash, T. R. Cundari, T. B. Gunnoe, *Organometallics* **2004**, *23*, 2724-2733; c) A. N. Walstrom, L. A. Watson, M. Pink, K. G. Caulton, *Organometallics* **2004**, *23*, 4814-4816; d) Y. Feng, M. Lail, N. A. Foley, T. B. Gunnoe, K. A. Barakat, T. R. Cundari, J. L. Petersen, *J. Am. Chem. Soc.* **2006**, *128*, 7982-7994.

[46] Selected reviews and comments on non-innocent ligands: a) K. Ray, T. Petrenko, K. Wieghardt, F. Neese, *Dalton Trans.* **2007**, 1552-1566; b) R. G. Hicks, *Angew. Chem.* **2008**, *120*, 7503-7505; *Angew. Chem. Int. Ed.* **2008**, *47*, 7393-7395; W. Kaim, *Science* **2005**, *307*, 216-217; c) W. Kaim, *Inorg. Chem.*, DOI: 10.1021/ic2003832.

[47] F. R. Keene, *Coord. Chem. Rev.* **1999**, *187*, 121-149.



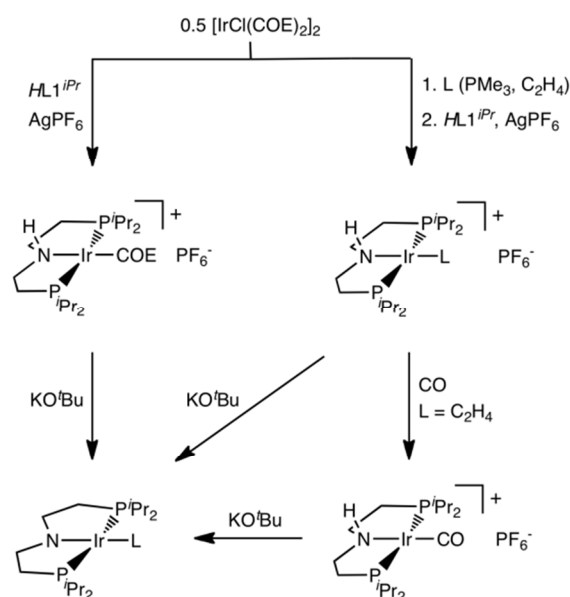
Scheme 3: Synthesis of chiral PNP ligands $HL1^R$.

oxidoreductase enzyme galactose oxidase provides a related example in nature.^[48] In the active site, the copper phenoxide moiety undergoes both metal and ligand centered one electron redox steps to accomplish the overall 2-electron redox reaction.

para-Aryl C–C-coupling was reported in early studies as a consequence of platinum(II) anilide oxidation, pointing towards ligand-centered radical reactivity.^[49] EPR spectroscopic characterization revealed some metal-to-ligand spin transfer for radical complex $[Cp^*Mn(CO)_2(N(H)C_6H_4-4-NMe_2)]$ ($Cp^* = \eta^5-C_5Me_5$).^[50]

Wieghardt and co-workers isolated the first examples that could be unequivocally assigned to persistent anilino radical complexes (**Figure 2A**).^[51] In recent years,

several other aminyl complexes were spectroscopically characterized or isolated (**Figure 2**).^[43d,52,53,54,55,56] For example, spectroscopic and quantumchemical examination of the radical



Scheme 4: Synthesis of iridium(I) PNP amine and amido complexes.

[48] L. Que Jr., W. B. Tolman, *Nature* **2008**, 455, 333-340.

[49] a) N. W. Alcock, R. D. O'Sullivan, A. W. Parkins, *J. Chem. Soc., Chem. Commun.* **1980**, 1216-1218; b) R. D. O'Sullivan, A. W. Parkins, N. W. Alcock, *J. Chem. Soc., Dalton Trans.* **1986**, 571-575.

[50] R. Gross, W. Kaim, *Inorg. Chem.* **1987**, 26, 3596-3600.

[51] F. N. Penkert, T. Weyhermüller, E. Bill, P. Hildebrandt, S. Lecomte, K. Wieghardt, *J. Am. Chem. Soc.* **2000**, 122, 9663-9673.

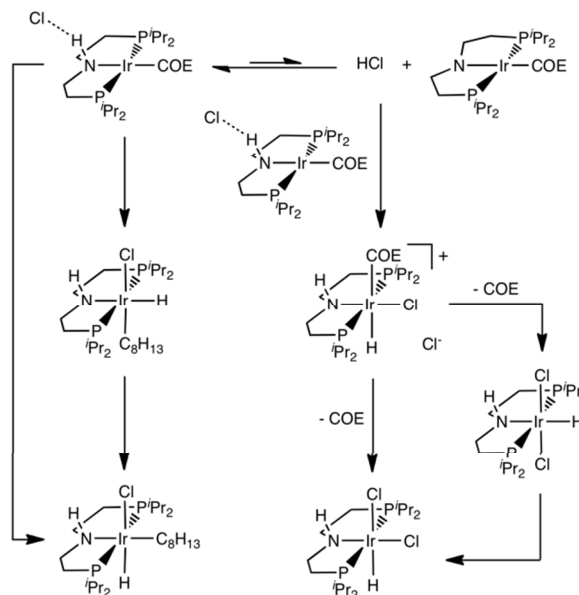
[52] a) P. Maire, M. Königsmann, A. Sreekanth, J. Harmer, A. Schweiger, H. Grützmacher, *J. Am. Chem. Soc.* **2006**, 128, 6578-6580; b) N. Donati, D. Stein, T. Büttner, H. Schönberg, J. Harmer, S. Anadaram, H. Grützmacher, *Eur. J. Inorg. Chem.* **2008**, 4691-4703.

complex $[\text{NiCl}\{\text{L}_A^{iPr}\}]^+$ (**Figure 2 B**) indicates considerable spin-density delocalization into the diarylamido PNP pincer ligand and, in turn, nickel(II) as the most appropriate assignment for the metal oxidation state.^[53] Besides the relevance of transient aminyl complexes as possible intermediates in oxidation catalysis, more persistent aminyl complexes might allow for the utilization of amido non-innocence in metal–ligand cooperative catalysis.^[57] As a rare example, Grützmacher and co-workers presented the use of an iridium amido complex as catalyst for the oxidation of alcohols with benzoquinone (**Scheme 1**). The authors proposed a mechanism with an intermediate aminyl radical complex as the crucial intermediate, undergoing C–H hydrogen abstraction from the substrate ligand.^[58]

A.1.4 16 VE (valence electron) amido, enamido, and dienamido complexes: Probing properties and reactivity

A.1.4.1 Synthesis of amine ligands $HL1^R$

Nucleophilic substitution of *N,N*-bis-(2-chloroethyl)amine^[59] provides versatile access to amine ligands $\text{HN}(\text{CH}_2\text{CH}_2\text{PR}_2)_2$ ($HL1^R$, **Figure 2**) with a wide variety of aromatic and aliphatic substituents at the phosphine moiety. The synthesis of diphenylphosphino derivative $HL1^{Ph}$ was reported via reaction of $\text{HN}(\text{CH}_2\text{CH}_2\text{X})_2$ ($\text{X} = \text{Cl}, \text{Br}$) with KPh_2 , or more conveniently from hydrochloride $[\text{H}_2\text{N}(\text{CH}_2\text{CH}_2\text{Cl})_2]\text{Cl}$ with diphenylphosphine and excess KO^tBu (**Scheme 2**).^[60,61] This route also affords the aryl phosphines $HL1^R$ ($\text{R} = \text{mesityl}, p\text{-tolyl}, \text{C}_6\text{H}_3\text{-3,5-}$



Scheme 5: $[\text{Ir}(\text{COE})\{\text{HL1}^{iPr}\}]\text{Cl}$, which decomposes in non-protic solvents.

[53] Y. Miyazato, T. Wada, J. T. Muckerman, E. Fujita, K. Tanaka, *Angew. Chem.* **2007**, *119*, 5830-5832; *Angew. Chem. Int. Ed.* **2007**, *46*, 5728-5730.

[54] D. Adhikari, S. Mossin, F. Basuli, J. C. Huffmann, R. K. Szilagy, K. Meyer, D. J. Mindiola, *J. Am. Chem. Soc.* **2008**, *130*, 3676-3682.

[55] (a) C. Tejel, M. A. Ciriano, M. Pilar del Rio, D. G. H. Hetterscheid, N. Tschlis i Spithas, J. M. N. Smits, B. de Bruin, *Chem. Eur. J.* **2008**, *14*, 10932-10936.

(b) C. Tejel, M. P. del Rio, M. A. Ciriano, E. J. Reijerse, F. Hartl, S. Zalis, D. G. H. Hetterscheid, N. Tschlis i Spithas, B. de Bruin, *Chem. Eur. J.* **2009**, *15*, 11878-11889.

[56] N. P. Mankad, W. E. Antholine, R. K. Szilagy, J. C. Peters, *J. Am. Chem. Soc.* **2009**, *131*, 3878-3880.

[57] a) P. J. Chirik, K. Wieghardt, *Science* **2010**, *327*, 794-795; b) W. I. Dzik, J. I. van der Vlugt, J. N. H. Reek, B. de Bruin, *Angew. Chem.* **2011**, *123*, 3416-3418; *Angew. Chem. Int. Ed.* **2011**, *50*, 3356-3358.

[58] M. Königsmann, N. Donati, D. Stein, H. Schönberg, J. Harmer, A. Sreekanth, H. Grützmacher *Angew. Chem.* **2007**, *119*, 3637-3640; *Angew. Chem. Int. Ed.* **2007**, *46*, 3567-3570.

[59] Free amine $\text{HN}(\text{CH}_2\text{CH}_2\text{Cl})_2$ and its hydrochloride salt are carcinogenic and should be handled with care. The related compounds $\text{RN}(\text{CH}_2\text{CH}_2\text{Cl})_2$ ($\text{R} = \text{Me}, \text{Et}, \text{CH}_2\text{CH}_2\text{Cl}$) were produced as chemical warfare agents ('nitrogen mustards') and used as antitumor drugs. Their cytotoxicity relies on the formation of aziridinium salts upon intramolecular electrophilic substitution. Ring opening by nucleobases results in irreversible DNA damage by interstrand cross-linking: S. M. Rink, M. J. Solomon, M. J. Taylor, S. B. Rajur, L. W. McLaughlin, P. B. Hopkins, *J. Am. Chem. Soc.* **1993**, *115*, 2551-2557.

[60] a) L. Sacconi and R. Morassi, *J. Chem. Soc. A* **1968**, 2997-3002; b) M. M. T. Khan, E. R. Rao, *Polyhedron* **1987**, *6*, 1727-1735.

[61] a) M. E. Wilson, R. G. Nuzzo, G. E. Whitesides, *J. Am. Chem. Soc.* **1978**, *100*, 2269-2270; b) R. G. Nuzzo, S. L. Haynie, M. E. Wilson, G. M. Whitesides, *J. Org. Chem.* **1981**, *46*, 2861-2867.

(CF₃)₂).^[62] The primary phosphine ligand *HL1^H* is similarly obtained in high yield from [H₂N(CH₂CH₂Cl)₂]₂Cl and PH₃ in basic conditions (KOH/DMSO).^[63] Initial attempts to synthesize dialkylphosphino ligands *HL1^{Me}* and *HL1^{Et}* from HN(CH₂CH₂Cl)₂ and NaPMe₂ in liquid ammonia or from [H₂N(CH₂CH₂Cl)₂]₂Cl and LiPEt₂ in THF, respectively, suffered from moderate to poor yields.^[64] Synthesis of ligands with bulkier dialkylphosphino substituents failed on this route. The low yield is attributed to the formation of aziridines (CH₂CH₂N)CH₂CH₂PR₂ as side products.^[65] This base-promoted nucleophilic cyclization can be avoided by silyl-protection of the amine. Deprotection of the product is easily achieved by

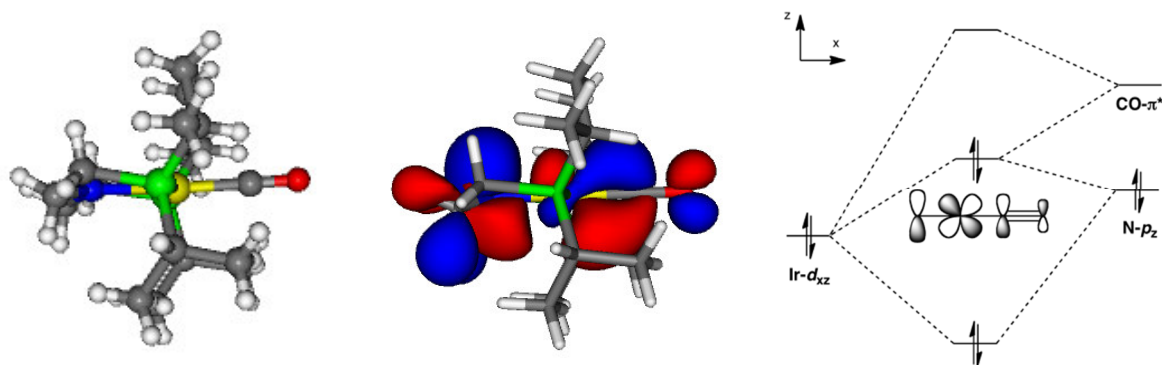


Figure 5: Molecular structure of [Ir(CO){L1^{iPr}}] from X-ray diffraction (left), DFT computed HOMO (center), and qualitative representation of the N–Ir–CO orbital π -interaction (right).

refluxing in H₂O or treatment with KF or [ⁿBu₄N]F in MeOH.^[65,66,67] This pathway affords a wide range of dialkylphosphino ligands *HL1^R* (R = Me, Et, ⁱPr, ^tBu, 1-adamantyl, cyclohexyl) with good yields (**Scheme 2**).^[65,68,69] Particular mention should be made of the possibility to introduce very bulky groups, such as P^tBu₂ or PAd₂, which was not reported for the popular diarylamido pincer ligands (**Figure 1**, {*HL_A*}).

Chiral, non-racemic derivatives were also reported. Bis(2-((2*S*,5*S*)-2,5-dimethylphospholanoethyl))amine (*HL1^{S,S-Me₂Phospholane}*) can be synthesized by reaction of (2*S*,5*S*)-2,5-dimethyl-1-phenylphospholyllithium with Me₃SiN(CH₂CH₂Cl)₂ (**Scheme 3**).^[67] Alternatively, another pathway towards chiral phospholane ligands is provided by deprotonation of the *N*-protected primary phosphine Me₃SiN(CH₂CH₂PH₂)₂ with ⁿBuLi and subsequent reaction with chiral, cyclic 2*S*,4*S*-2,4-pentandiol sulfate or 2*S*,5*S*-2,5-hexandiol sulfate, respectively

[62] W. Kuriyama, T. Matsumoto, Y. Ino, O. Ogata (Takasago Int.), WO 2011048727, 2011.

[63] A. Heßler, S. Kücken, O. Stelzer, W. S. Sheldrick *J. Organomet. Chem.* **1998**, 553, 39-52.

[64] A. A. Danopoulos, P. G. Edwards, *Polyhedron* **1989**, 8, 1339-1344.

[65] A. A. Danopoulos, A. R. Wills, P. G. Edwards, *Polyhedron* **1990**, 9, 2413-2418.

[66] B. Askevold, S. Schneider, *unpublished results*

[67] a) M. J. Burk, J. E. Feaster, R. L. Harlow, *Tetrahedron Asymmetry* **1991**, 2, 569-592; b) M. J. Burk (Du Pont), WO 92/19630, **1992**.

[68] a) K. Abdur-Rashid, US 20050107638, **2005**; b) Z. E. Clarke, P. T. Maragh, T. P. Dasgupta, D. G. Gusev, A. J. Lough, K. Abdur-Rashid, *Organometallics* **2006**, 25, 4113-4117; c) K. Abdur-Rashid, T. Graham, C.-W. Tsang, X. Chen, R. Guo, W. Jia, D. Amoroso, C. Sui-Seng (Kanata Chem. Tech.), WO 2008/141439, **2008**.

[69] J. Meiners, A. Friedrich, E. Herdtweck, S. Schneider, *Organometallics* **2009**, 28, 6331-6338.

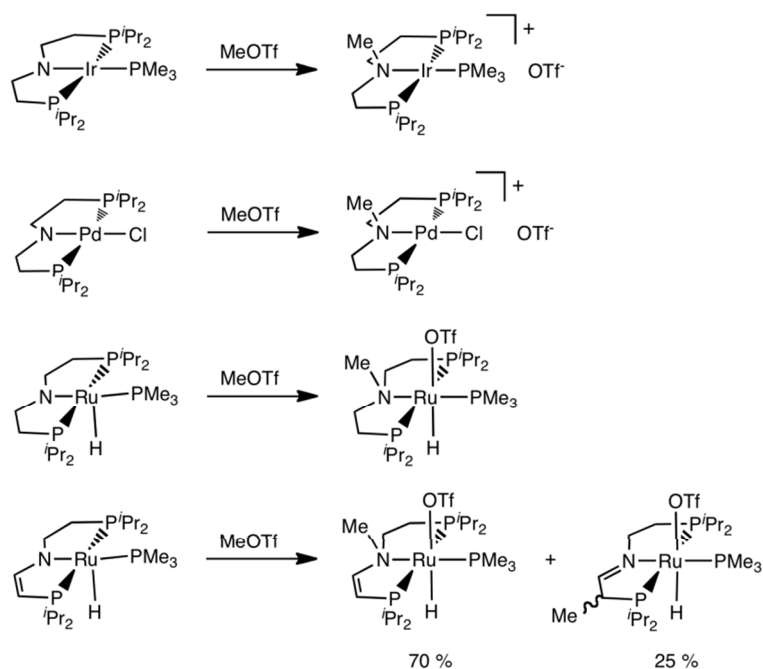
(Scheme 3).^[68a] Axially chiral binaphthyl ligand ($HL1^{Binaph}$) is obtained by *P*-lithiation of enantiomerically pure 4-chloro-4,5-dihydro-3*H*-4-phosphacyclohepta[2,1-*c*;1',2'-*e*]phosphepine,^[70] subsequent reaction with $Me_3SiN(CH_2CH_2Cl)_2$, and *N*-deprotection (Scheme 3).^[68a]

A.1.4.2 Square-planar 16 VE amine and amido complexes: Synthesis, stability, and N–H acidity

Reaction of $[IrCl(COE)_2]_2$ (COE = cyclooctene) with $HL1^{iPr}$ in 2-propanol affords iridium(III) complex $[Ir(H)_2Cl\{HL1^{iPr}\}]$.^[68a]

Using THF as solvent provides access to a wide range of stable, square-planar d^8 amine complexes, $[IrL\{HL1^{iPr}\}]^+$ (L = CO, COE, C_2H_4 , C_3H_6 , PMe_3)

(Scheme 4).^[71] However, exchange of chloride *vs.*



Scheme 6: Reactions of amido and enamido complexes with MeOTf.

a weakly coordinating counter anion is crucial. In non-protic solvents the chloride anion of $[Ir(COE)\{HL1^{iPr}\}]Cl$ is hydrogen bonded to the N–H proton, evidenced by a strong downfield shift in the 1H NMR spectrum, accompanied by decomposition towards an equimolar mixture of amide $[Ir(COE)\{L1^{iPr}\}]$ and iridium(III) complex $[Ir(Cl)_2H\{HL1^{iPr}\}]$, and minor amounts of cyclooctenyl complex $[IrCl(C_8H_{13})H\{HL1^{iPr}\}]$ (Scheme 5). Kinetic examinations indicate that the amido complex results from HCl elimination, which oxidatively adds to the initial cyclooctene complex. Intramolecular, vinylic C–H activation and subsequent trapping by chloride is kinetically competitive with this reaction.^[72] In comparison, $[Ir(COE)\{HL1^{tBu}\}]Cl$ and $[IrCl(C_8H_{13})H\{HL1^{tBu}\}]$ form a strongly solvent dependent equilibrium.^[69] The increased steric bulk favours the vinyl hydride over olefin

[70] a) Y. Chi, X. Zhang, *Tetrahedron Letters*, **2002**, 43, 4849-4852; c) H. Klein, R. Jackstell, K.-D. Wiese, C. Borgmann M. Beller, *Angew. Chem.* **2001**, *113*, 3505-3508; *Angew. Chem. Int. Ed.*, **2001**, *40*, 3408-3411.

[71] A. Friedrich, R. Ghosh, R. Kolb, E. Herdtweck, S. Schneider, *Organometallics* **2009**, *28*, 708-718.

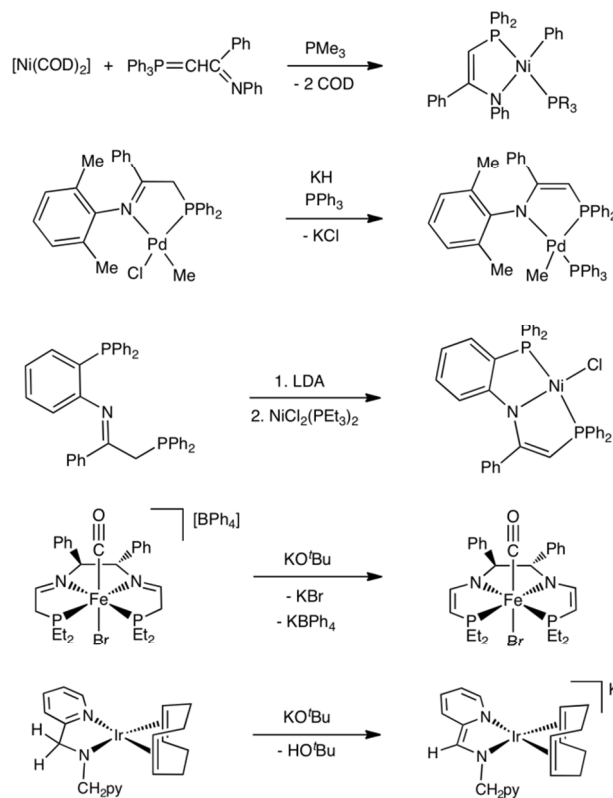
[72] Selected examples for vinylic COE C–H oxidative addition: (a) M. J. Fernandez, M. J. Rodriguez, L. A. Oro, F. J. Lahoz, *J. Chem. Soc., Dalton Trans.* **1989**, 2073-2076; (b) D. Hermann, M. Gandelman, H. Rozenberg, L. J. W. Shimon, D. Milstein, *Organometallics* **2002**, *21*, 812-818; (c) M. Iimura, D. R. Evans, T. C. Flood, *Organometallics* **2003**, *22*, 5370-5373.

isomer, slows down C–H oxidative addition/reductive elimination, and renders chloride trapping of iridium(III) reversible.

Deprotonation of $[\text{IrL}\{\text{HL}^{\text{iPr}}\}]$ provides access to iridium(I) amido complexes $[\text{IrL}\{\text{L}^{\text{iPr}}\}]$ ($\text{L} = \text{CO}, \text{COE}, \text{C}_2\text{H}_4, \text{PMe}_3$), which are thermally relatively robust towards β -H elimination (**Scheme 4**).^[71,73]

Likewise, palladium(II) PNP amido complexes $[\text{PdX}\{\text{L}^{\text{iPr}}\}]$ ($\text{X} = \text{Cl}, \text{Me}, \text{Ph}$) and $[\text{PdL}\{\text{L}^{\text{iPr}}\}]\text{PF}_6$ ($\text{L} = \text{PMe}_3, \text{CN}^t\text{Bu}$) were synthesized.^[74] The large hypsochromic shift ($\Delta\nu = 68 \text{ cm}^{-1}$, Table 1) of the $[\text{Ir}(\text{CO})\{\text{L}^{\text{iPr}}\}]$ C–O stretching vibration and the large $[\text{Ir}(\text{olefin})\{\text{L}^{\text{iPr}}\}]$ olefinic ^{13}C NMR highfield shifts ($\Delta\delta^{\text{C}_2\text{H}_4} = 22.1 \text{ ppm}$; $\Delta\delta^{\text{COE}} = 20.8 \text{ ppm}$) upon deprotonation of the respective amine complexes indicate a very electron rich $\text{Ir}\{\text{L}^{\text{R}}\}$ -

fragment. In turn, the ligand *trans* to the nitrogen atom has a profound effect on the amine $\text{p}K_{\text{a}}$ value which varies over more than 7 orders of magnitude (in dmsO) within the series $\text{L} = \text{CO}$ (14.9(3)), COE (16.0(4)), PMe_3 (22.0(1)).^[73] In comparison, the value for the olefin complex is close to square-planar *cis*-diamine-diolefin Rh^{I} complex $[\text{Rh}\{\text{H}_2\text{L}_E\}]^+$ ($\text{p}K_{\text{a}}^{\text{dmsO}} = 15.7$) but considerably less acidic than the corresponding Ir^{I} complex $[\text{Ir}\{\text{H}_2\text{L}_E\}]^+$ ($\text{p}K_{\text{a}}^{\text{dmsO}} = 10.5$).^[58,75] However, the $\text{p}K_{\text{a}}$ -trend within the $[\text{IrL}\{\text{HL}^{\text{iPr}}\}]^+$ -series can be rationalized with a $\text{N} \rightarrow \text{Ir} \rightarrow \text{L}$ *push-pull*-interaction which stabilizes the $\text{N}-\text{Ir} \pi^*$ orbital (HOMO) if *trans*-ligand L is a π -acceptor ligand, such as CO or olefins (**Figure 5**). The same bonding situation was found for iridium(I) olefin amido complex $[\text{Ir}(\text{COD})\{\kappa^2\text{-bpa}\}]$ ($\text{COD} = \text{cyclooctadiene}$; $\text{bpa} = \text{N}(\text{CH}_2\text{C}_5\text{H}_4\text{N})_2$).^[55b] High nucleophilicity of the amido group towards C -nucleophiles is also observed. $[\text{Ir}(\text{PMe}_3)\{\text{L}^{\text{iPr}}\}]$ and $[\text{PdCl}\{\text{L}^{\text{iPr}}\}]$ are selectively attacked by MeOTf at the nitrogen atom (**Scheme 6**) and an iridium(III) methyl complex was not observed.^[73,74]



Scheme 7: Syntheses of chelating enamido complexes.

[73] B. Askevold, A. Friedrich, M. R. Buchner, B. Lewall, A. C. Filippou, E. Herdtweck, S. Schneider, *J. Org. Chem.* 2013, 744, 35–40.

[74] A. N. Marziale, E. Herdtweck, J. Eppinger, S. Schneider *Inorg. Chem.* 2009, 48, 3699–3709.

[75] P. Maire, F. Breher, H. Grützmacher, *Angew. Chem.* 2005, 117, 6483–6487; *Angew. Chem. Int. Ed.* 2005, 44, 6325–6329.

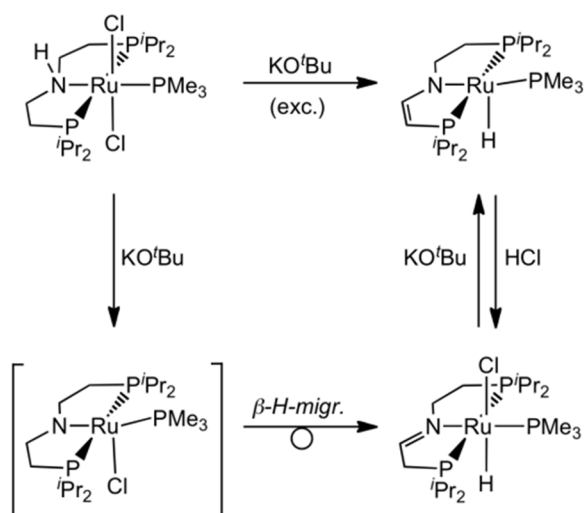
A.1.4.3 Functionalization of the pincer backbone: Fine-tuning N→M donation

A.1.4.3.1 Amido, enamido, and dienamido pincer ligands: Comparison of the donor properties.

Dehydrogenation of the chelate backbone bridges towards enamido and dienamido ligands $\{L3^R\}^-$ and $\{L4^R\}^-$ (**Figure 2**) provides another approach to fine-tune electronic properties and reactivity. These enamido ligands are related to chelating (2-phosphino)vinylalcoholates, which are used in the Shell Higher Olefin Process (SHOP).^[76] In analogy, Braunstein and co-workers prepared the enamido nickel(II) complexes $[\text{Ni}(\text{Ph})\text{L}\{\text{N}(\text{Ph})\text{CPhCHPPH}_2\}]$ ($\text{L} = \text{PMe}_3, \text{PMe}_2\text{Ph}, \text{PMePh}_2$) by P–Ph

oxidative addition of an α -iminophosphorous ylide to $[\text{Ni}(\text{COD})_2]$ (**Scheme 7**).^[77] However, deprotonation of coordinated or free imine ligands at the C–H-acidic α -position represents a more general approach to phosphinoenamido ligands.^[78,79] For example, Morris recently reported the synthesis of dienamido PNNP iron(II) complexes by deprotonation of the corresponding imines (**Scheme 7**).^[80] Both catalyse the transfer hydrogenation of ketones

with comparable rates, suggesting that ligand backbone proton transfer reactions might be involved in a metal-ligand cooperating hydrogenation mechanism. Deprotonation of bis(2-picoly)amido ligands coordinated to rhodium(I) and iridium(I) affords ‘dearomatized’ vinylenediamido complexes $[\text{M}(\text{COD})\{\text{RNC}(\text{H})\text{C}_5\text{H}_4\text{N}\}]^-$ ($\text{M} = \text{Rh}, \text{Ir}; \text{COD} = \text{cyclooctadiene}; \text{R} = \text{CH}_2\text{C}_5\text{H}_4\text{N}$) (**Scheme 7**).^[55b,81] Synthetic access to the free ligands $\{L3^R\}^-$ and $\{L4^R\}^-$ has not been reported, yet. Their metal complexes are obtained starting from coordinated amine, imine, or amido precursors on several routes which are discussed in the subsequent sections. However, comparison of parent amido complexes carrying $\{L1^R\}^-$



Scheme 8: Synthesis and proposed mechanism of enamido complex $[\text{Ru}(\text{H})\text{PMe}_3\{\text{L}3^{iPr}\}]$.

[76] W. Keim, *Angew. Chem.* **1990**, *102*, 251-260; *Angew. Chem. Int. Ed. Engl.* **1990**, *29*, 235-244.

[77] P. Braunstein, J. Pietsch, Y. Chauvin, S. Mercer, L. Saussine, A. DeCian, J. J. Fischer, *J. Chem. Soc., Dalton Trans.* **1996**, 3571-3574.

[78] a) K. S. Coleman, M. L. H. Green, S. I. Pascu, N. H. Rees, A. R. Cowley, L. H. Rees, *J. Chem. Soc., Dalton Trans.* **2001**, 3384-3395; b) S. Pascu, G. D. W. Anderson, M. L. H. Green, J. C. Green, N. H. Rees, A. R. Cowley, *Inorg. Chim. Acta* **2006**, *359*, 3677-3692.

[79] Z.-X. Wang, L. Wang, *Chem. Commun.* **2007**, 2423-2425.

[80] a) P. O. Lagaditis, A. J. Lough, R. H. Morris, *Inorg. Chem.* **2010**, *49*, 10057-10066; b) P. O. Lagaditis, A. J. Lough, R. H. Morris, *J. Am. Chem. Soc.* **2011**, *133*, 9662-9665.

[81] C. Tejel, M. Pilar del Río, L. Asensio, F. J. van den Bruele, M. A. Ciriano, N. Tschilch i Spithas, D. G. H. Hetterscheid, B. de Bruin, *Inorg. Chem.* **2011**, *50*, 7524-7534.

with related enamido and dienamido complexes formally derived from it ($\{L3^R\}^-$ and $\{L4^R\}^-$) and with complexes of other popular PEP (E = N, C) pincer ligands is informative at this point to understand reactivity trends. CO stretching vibrations (ν_{CO}) can serve as a probe in trying to scale the electronic effects of backbone dehydrogenation.

complex	ν_{CO} [cm^{-1}]	ref.
<i>[Ir(CO){HLL^{iPr}}]PF₆</i>	1976 ^[a]	71
[Ir(CO){C ₅ H ₃ N(CH ₂ P ^t Bu ₂) ₂]PF ₆	1962 ^[e]	82
[Ir(CO){C ₆ H ₃ (OP ^t Bu ₂) ₂ }]	1949 ^[d]	83
[Ir(CO)Cl(P ⁱ Pr ₃) ₂]	1939 ^[a]	84
<i>[Ir(CO)(L^A^{Bu})]</i>	1937 ^[a]	85
[Ir(CO){NC ₅ H ₃ (CHP ^t Bu ₂)(CH ₂ P ^t Bu ₂)}]	1932 ^[e]	86
[Ir(CO){L _C ^{iPr} }]	1930 ^[c]	29c
[Ir(CO){L _A ^{iPr} }]	1930 ^[c]	87
[Ir(CO){C ₆ H ₃ (CH ₂ P ⁱ Pr ₂) ₂ }]	1928 ^[b]	6
[Ir(CO){CpFeC ₅ H ₂ (CH ₂ P ⁱ Pr ₂) ₂ }]	1926 ^[f]	88
[Ir(CO){C ₇ H ₄ (CHP ^t Bu ₂)(CH ₂ P ^t Bu ₂)}]	1919 ^[h]	89a
<i>[Ir(CO)(L^I^{iPr})]</i>	1908 ^[a]	71
[Ir(CO){C ₇ H ₅ (CH ₂ P ^t Bu ₂) ₂ }]	1905 ^[h]	89b
<i>[RuCl(CO)(L^A^{Bu})]</i>	1916 ^[a]	85
[RuCl(CO){CpFeC ₅ H ₂ (CH ₂ P ^t Bu ₂) ₂ }]	1914 ^[g]	90
[RuCl(CO){C ₆ H ₃ (CH ₂ P ^t Bu ₂) ₂ }]	1909 ^[a]	91
<i>[RuCl(CO)(L³^{Bu})]</i>	1896 ^[a]	85
<i>[RuCl(CO)(L¹^{Bu})]</i>	1888 ^[a]	85
[RuCl(CO){CH(CH ₂ CH ₂ P ^t Bu ₂) ₂ }]	1887 ^[a]	92
Sample preparation: ^[a] Nujol mull; ^[b] cyclooctane solution; ^[c] THF solution; ^[d] pentane solution; ^[e] neat film; ^[f] hexane solution; ^[g] CH ₂ Cl ₂ solution; ^[h] KBr pellet		

Table A.1-1: Comparison of M(CO){PEP} (E = N, C) CO stretching vibrations. Complexes with ligands derived from HLL^R in italics.

[82] S. M. Kloeck, M. Heinekey, K. I. Goldberg, *Organometallics* **2006**, *25*, 3007–3011.

[83] I. Göttker-Schnetmann, P. S. White, M. Brookhart, *Organometallics* **2004**, *23*, 1766–1776.

[84] R. Meij, D. J. Stufkens, K. Vrieze, W. van Gerresheim, C. H. Stam, *J. Organomet. Chem.* **1979**, *164*, 353–370.

[85] *Late Transition Metal Amido Complexes: Electronic Structure and Reactivity*, Bjoern B. Askevold PhD Thesis TU München 2012.

[86] L. Schwartsburd, M. A. Iron, L. Konstantinovskii, Y. Diskin-Posner, G. Leitun, L. J. W. Shimon, D. Milstein, *Organometallics* **2010**, *29*, 3817–3827.

[87] M. T. Whithead, R. H. Grubbs, *J. Am. Chem. Soc.* **2008**, *130*, 5874–5875.

[88] S. A. Kulkin, A. M. Sheloumov, F. M. Dolgushin, M. G. Ezernitskaya, A. S. Peregudov, P. V. Petrovskii, A. A. Koridze, *Organometallics* **2006**, *25*, 5466–476.

[89] a) A. M. Winter, K. Eichele, H.-G. Mack, W. C. Kaska, H. A. Mayer, *Organometallics* **2005**, *24*, 1837–1844; b) *Dalton Trans.* **2008**, 527–532.

[90] A. M. Sheloumov, F. M. Dolgushin, M. V. Kondrashov, P. V. Petrovskii, K. A. Barbakadze, O. I. Lekashvili, A. A. Koridze, *Russ. Chem. Bull. Int. Ed.* **2007**, *6*, 1757–1764.

[91] D. G. Gusev, M. Madott, F. M. Dolgushin, K. A. Lyssenko, M. Y. Antipin, *Organometallics* **2000**, *19*, 1734–1739.

[92] D. G. Gusev, A. J. Lough, *Organometallics* **2002**, *21*, 5091–5099.

Table A.1-1 shows representative examples of square-planar $[\text{Ir}^{\text{I}}(\text{CO})\{\text{PEP}\}]$ and five-coordinate $[\text{Ru}^{\text{II}}\text{Cl}(\text{CO})\{\text{PEP}\}]$ complexes ($\text{E} = \text{N}, \text{C}$), all carrying bulky dialkylphosphine (P^iPr_2 or P^tBu_2) substituents but different pincer backbones.^[93] Amine and amido complexes

$[\text{Ir}(\text{CO})\{\text{HL}1^{iPr}\}]^+$
($\nu_{\text{CO}} = 1976 \text{ cm}^{-1}$)
and $[\text{Ir}(\text{CO})\{\text{L}1^{iPr}\}]$
($\nu_{\text{CO}} = 1908 \text{ cm}^{-1}$)

represent the upper and lower ends of a wide range of CO stretching vibrations found for cationic and neutral

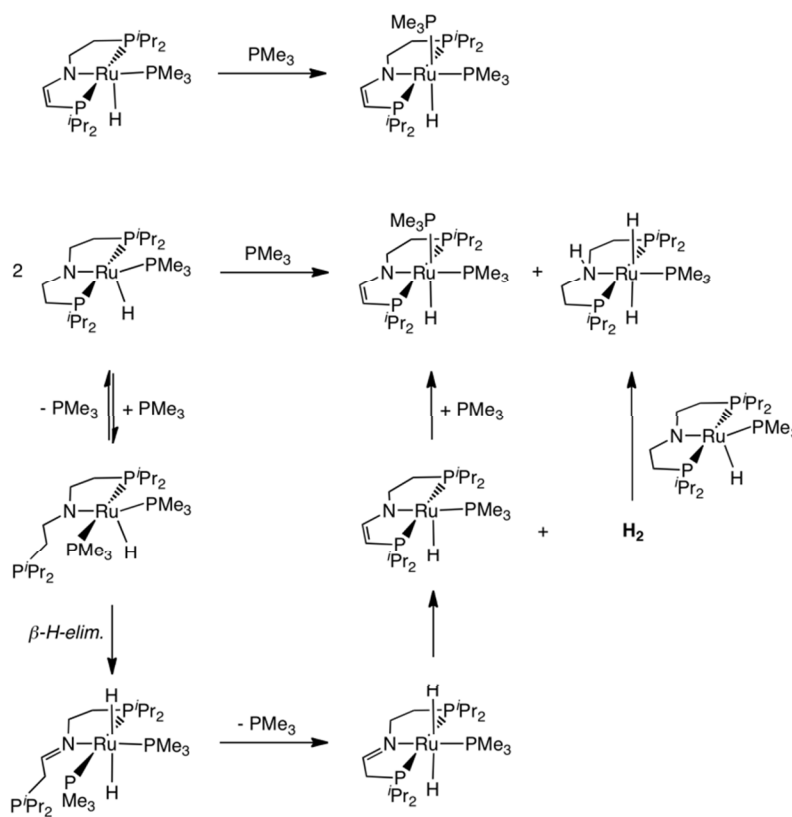
$[\text{Ir}^{\text{I}}(\text{CO})\{\text{PEP}\}]^{+0}$ pincer complexes.

On the other hand, fully dehydrogenated

pincer complex $[\text{Ir}(\text{CO})\{\text{L}4^{tBu}\}]$

(**Scheme 11**) exhibits an

intermediate ν_{CO} (1937 cm^{-1}).^[85] This observation suggests reduced $\text{N} \rightarrow \text{Ir}$ electron donation upon oxidative ligand backbone functionalization, owing to stabilization of the N -lone-pair by $\text{C}(\text{p})-\text{N}(\text{p})$ overlap, i.e. the vinyl substituents acting as π -acceptors. These qualitative considerations are further reflected within the series $[\text{RuCl}(\text{CO})\{\text{L}1^{tBu}\}]$ ($\nu_{\text{CO}} = 1888 \text{ cm}^{-1}$), $[\text{RuCl}(\text{CO})\{\text{L}3^{tBu}\}]$ ($\nu_{\text{CO}} = 1896 \text{ cm}^{-1}$), and $[\text{RuCl}(\text{CO})\{\text{L}4^{tBu}\}]$ ($\nu_{\text{CO}} = 1916 \text{ cm}^{-1}$), which can be prepared by reaction of CO with the respective 4-coordinate complexes.^[85] As for the square-planar Ir^{I} platform, the 5-coordinate Ru^{II} complexes span a range of about 30 cm^{-1} , indicating comparable electronic effects for the different metals and coordination geometries upon backbone dehydrogenation. $[\text{RuCl}(\text{CO})\{\text{L}1^{tBu}\}]$ and $[\text{RuCl}(\text{CO})\{\text{CH}(\text{CH}_2\text{CH}_2\text{P}^t\text{Bu}_2)_2\}]$ exhibit almost identical ν_{CO} . Hence, weaker $\text{E} \rightarrow \text{Ru}$ ($\text{E} = \text{N}, \text{C}$) σ -donation of the amido vs. alkyl ligand is offset by $\text{N} \rightarrow \text{Ru}$ π -donation. Other frequently used anionic pincer ligands, such as the aryl pincer $\{\text{C}_6\text{H}_3(\text{CH}_2\text{P}^i\text{Pr}_2)_2\}^-$, diarylamido pincer $\{\text{L}_A\}^-$, disilylamido pincer



Scheme 9: Reactions of enamide $[\text{RuH}(\text{PMe}_3)\{\text{L}3^{iPr}\}]$ (top) and amide $[\text{RuH}(\text{PMe}_3)\{\text{L}1^{iPr}\}]$ (bottom) with PMe_3 and proposed mechanism for the latter.

[93] All ruthenium complexes in **Table A.1-1** exhibit square-pyramidal molecular structures with CO in the apical position.

$\{L_C\}^-$, or pyridine based ‘dearomatized’ pincer $\{L_B\}^-$, fall within a relatively narrow range between $\{L3\}^-$ and $\{L4\}^-$ with respect to their donor properties, as judged by their CO stretching vibrations.

A.1.4.3.2 16 VE amido vs. enamido complexes: Consequences for structure and reactivity

The molecular structure and reactivity of $[\text{RuH}(\text{PMe}_3)\{\text{L1}^{iPr}\}]$, as compared with $[\text{RuH}(\text{PMe}_3)\{\text{L3}^{iPr}\}]$, provides further information. The enamido complex is quantitatively obtained from $[\text{RuCl}_2(\text{PMe}_3)\{\text{HL1}^{iPr}\}]$ with excess KO^tBu (Scheme 8).^[94] Decomposition of the tentative amido intermediate $[\text{RuCl}(\text{PMe}_3)\{\text{L1}^{iPr}\}]$ by β -hydride migration and backbone deprotonation of the resulting imine provides a reasonable mechanism.^[95] $[\text{RuH}(\text{PMe}_3)\{\text{L3}^{iPr}\}]$ adds two equiv. H_2 to give amine complex $[\text{Ru}(\text{H})_2(\text{PMe}_3)\{\text{HL1}^{iPr}\}]$

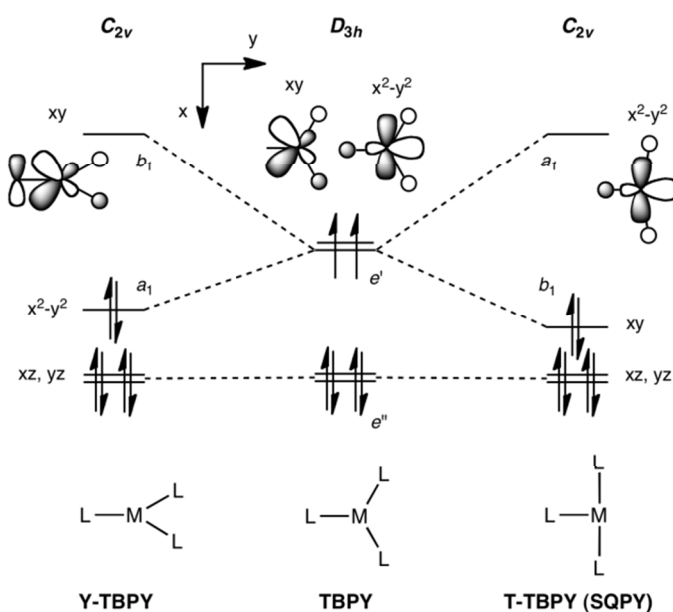


Figure 6: Qualitative valence d -orbital splitting in a TBPY (D_{3h}) ligand field (center) with d^6 occupation (d_{22} LUMO omitted) and lifted degeneracy of the e' -orbitals upon Y-shaped (left) and T-shaped (right) distortion, respectively. The respective LUMO's indicate the suitability in the Y-TBPY case for π -bonding with a π -donor ligand.

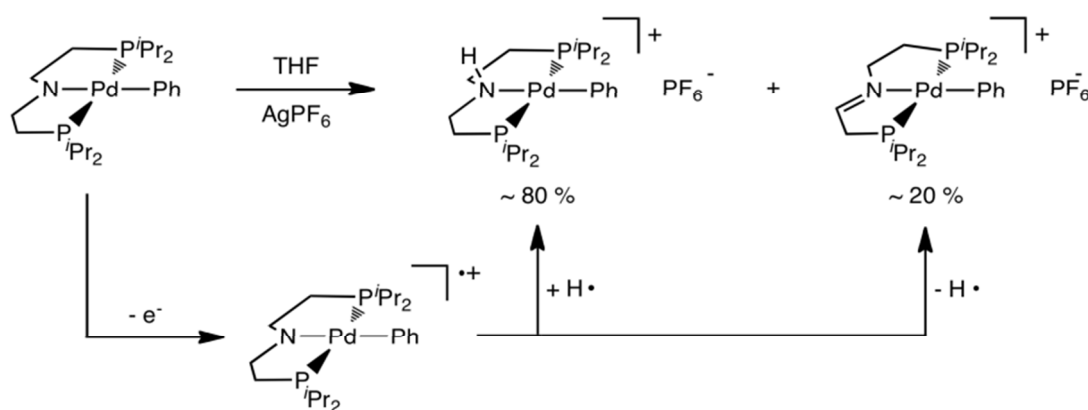
(Scheme 9). This reaction is fully reversible but elimination of the first equivalent is considerably faster (see below) rendering amido complex $[\text{RuH}(\text{PMe}_3)\{\text{L1}^{iPr}\}]$ easily isolable.

The molecular structures of both $[\text{RuH}(\text{PMe}_3)\{\text{L1}^{iPr}\}]$ (X-ray) and $[\text{RuH}(\text{PMe}_3)\{\text{L3}^{iPr}\}]$ (DFT) can be described starting from trigonal-bipyramidal (TBPY) geometry, with N, H, and PMe_3 in equatorial positions, but with different modes of distortion from ideal TBPY.^[94] For

[94] M. Käß, A. Friedrich, M. Drees, S. Schneider, *Angew. Chem.* **2009**, *121*, 922-924; *Angew. Chem. Int. Ed.* **2009**, *48*, 905-907.

[95] A. Friedrich, M. Drees, M. Käß, E. Herdtweck, S. Schneider, *Inorg. Chem.* **2010**, *49*, 5482-5494.

[RuH(PMe₃){L1^{iPr}}], the strongly compressed H–Ru–PMe₃ angle (76.0(7) °) and widened H–Ru–N (124.8(7) °) and N–Ru–PMe₃ (159.12(3) °) angles indicate a ‘Y-shaped’ distortion from TBPY coordination. This geometry is typically found for five-coordinate *d*⁶ complexes with a strong π-donor ligand to avoid repulsive filled-filled N(*p*)-M(*d*) π–interactions and instead maintain stabilizing N→M π–bonding with the coordinatively unsaturated metal center (**Figure 6**).^[96,97] In contrast, [RuH(PMe₃){L3^{iPr}}] (H–Ru–PMe₃: 84.6°; H–Ru–N: 102.5°; N–Ru–PMe₃: 172.6°) exhibits stronger resemblance of ‘T-shaped’ distortion from TBPY (i.e. square-pyramidal (SQPY) geometry) suggesting again attenuated π–donation by the enamido nitrogen atom. This interpretation is further backed by comparison of the Ru–N Wiberg Bond Indices for [RuH(PMe₃){L1^{iPr}}] (0.50) and [RuH(PMe₃){L3^{iPr}}] (0.37), indicating a lower degree of covalent bonding for the latter.



Scheme 10: Chemical oxidation of amido complex [PdPh{L1^{iPr}}] and proposed mechanism via aminyl radical complex [PdPh{L1^{iPr}}]^{*+}.

Hence, the ruthenium centre in the enamido complex exhibits a higher degree of electronic unsaturation, which is reflected in the reactivity with nucleophiles. [RuH(PMe₃){L3^{iPr}}] shows Lewis-acidic reactivity, typical for SPQY Ru^{II} complexes, exemplified by the formation of octahedral [RuH(PMe₃)₂{L3^{iPr}}] with PMe₃ (**Scheme 9**).^[95] In contrary, [RuH(PMe₃){L1^{iPr}}] does not form an isolable six-coordinate amido complex. Upon addition of PMe₃, broadening of all signals in the ³¹P NMR spectrum indicates rapid ligand exchange. Furthermore, slow ligand disproportionation towards amine [Ru(H)₂(PMe₃){HL1^{iPr}}] and enamide [RuH(PMe₃)₂{L3^{iPr}}] is observed, attributed to the mechanism in **Scheme 9**. The instability of proposed imine intermediate [Ru(H)₂(PMe₃){L2^{iPr}}] towards H₂ elimination was confirmed by DFT computations (**Scheme 15**). The reactivity towards electrophiles was also examined. With MeOTf, [Ru(H)(PMe₃){L1^{iPr}}] forms the expected tertiary amine complex

[96] a) D. L. Thorn, R. Hoffmann, *New J. Chem.* **1979**, 3, 39-45; b) J. F. Riehl, Y. Jean, O. Eisenstein, M. Pélessier, *Organometallics* **1992**, 11, 729-737.

[97] a) H. Werner, A. Höhn, M. Dziallas, *Angew. Chem.* **1986**, 98, 1112-1112; *Angew. Chem. Int. Ed. Engl.* **1986**, 25, 1090-1092; b) M. D. Fryzuk, P. A. McNeil, R. G. Ball, *J. Am. Chem. Soc.* **1986**, 108, 6414-6416.

[Ru(H)OTf(PMe₃){MeL1^{iPr}}] selectively. [Ru(H)(PMe₃){L3^{iPr}}] exhibits reactivity with both nucleophilic positions on the ligand backbone, resulting in a mixture of enamine [Ru(H)OTf(PMe₃){MeL3^{iPr}}] and the products from backbone C-methylation to a minor extent (**Scheme 6**).

A.1.5 15 and 14 VE complexes: Control of electronic structure by pincer variation

A.1.5.1 Oxidation of 16 VE dialkylamido complexes: Formation of unstable radicals

The *d*⁸ amido complexes [IrL{L1^{iPr}}] (L = CO, COE, PMe₃) and [PdCl{L1^{iPr}}] in THF exhibit irreversible oxidation waves in the cyclic voltammograms (THF) at scan speeds up to 1 Vs⁻¹), suggesting rapid chemical degradation of initially formed radical cations on the experimental timescale.^[73] As for the p*K*_a values of the conjugate acids (see above), the

oxidation potentials of the

series [IrL{L1^{iPr}}] are

highly dependent on the

ligand in *trans*-position to

the nitrogen atom (L = CO:

-0.39 V, COE: -0.49 V,

PMe₃: -1.09V vs. Fc/Fc⁺).

Chemical oxidation of

[IrPMe₃{L1^{iPr}}] and

[PdPh{L1^{iPr}}] with AgPF₆

gives the amine complexes

[IrPMe₃{HL1^{iPr}}]⁺ or [PdPh{HL1^{iPr}}]⁺ in around 90% and 80% yield, respectively, and a

minor amount of the corresponding imines [IrPMe₃{L2^{iPr}}]PF₆ and [PdPh{L2^{iPr}}]PF₆.^[73,74]

Deuterium labelling in case of Pd supports initial formation of radical cation [PdPh{L1^{iPr}}]⁺

which undergoes competitive hydrogen abstraction from the solvent (THF) and ligand

backbone disproportionation (**Scheme 10**). Hence, the reactivity indicates ‘redox non-

innocent’ behaviour of the dialkylamido ligand. Accordingly, DFT computations (B3LYP/6-

311+G***) for [IrCO{L1^{iPr}}]⁺ indicate about 63 % of the Mulliken spin-density to be located

on the nitrogen atom, and the SOMO of [IrCO{L1^{iPr}}]⁺ (**Figure 7**) represents the N(*p*)–Ir(*d*_{xz})

π*-orbital resulting from removal of an electron from the HOMO of parent [IrCO{L1^{iPr}}]

(**Figure 5**).

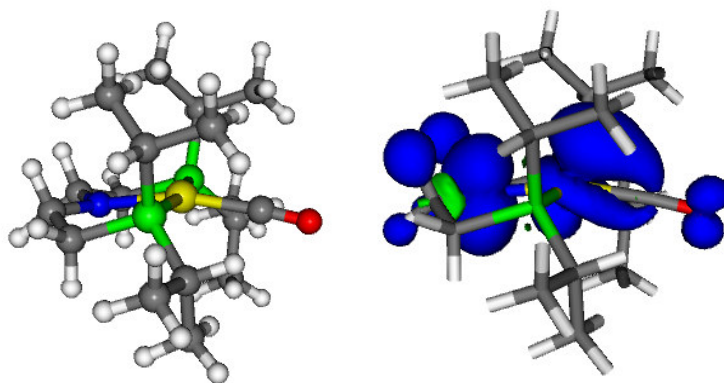
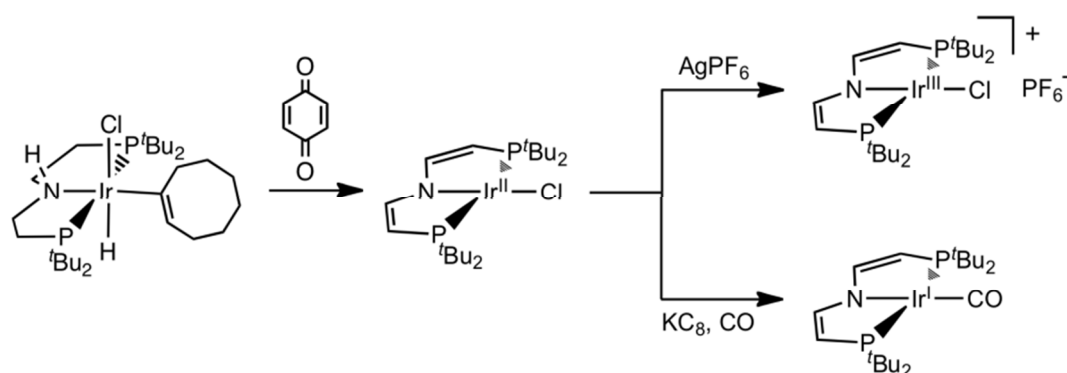


Figure 7: DFT computed molecular structure of [Ir(CO)(L1^{iPr})]⁺* (left) and spin density (right).

A.1.5.2 Ligand modification: Stabilization of square-planar 15 VE complexes

The decomposition mechanism of PNP dialkylamido iridium and palladium radical complexes suggests a simple synthetic strategy for the isolation of persistent open-shell complexes.^[98] Replacement of the backbone ethylene with vinylene bridges (**Figure 2**), prevents putative aminoyl ligand disproportionation towards amine and imine complexes. In fact, in contrast to transient $[\text{IrPMe}_3\{\text{L}1^{iPr}\}]^{+\bullet}$ (see above), disilylamido complex $[\text{IrCl}\{\text{L}_C^{tBu}\}]$ was isolated and characterized by EPR spectroscopy.^[99] Furthermore, this modification should also stabilize a 15 VE radical complex electronically by delocalization of the *N*-lone-pair. Hence, the SOMO of enamido and dienamido radical complexes should



Scheme 11: Synthesis of iridium(I), iridium(II), and iridium(III) dienamido complexes.

exhibit less *N*(p) character as compared with an analogous dialkylamido radical complex, providing further stabilization with respect to possible ligand centered radical decomposition reactions.^[100] Oxidation of amine $[\text{IrH}(\text{C}_8\text{H}_{13})\text{Cl}\{\text{HL}1^{tBu}\}]$ with benzoquinone gives dienamido complex $[\text{IrCl}\{\text{L}4^{tBu}\}]$ in good yield (**Scheme 11**).^[101] As for $[\text{IrCl}\{\text{L}_C^{tBu}\}]$, the large anisotropy of the *g*-values is in agreement with predominant d^7 metalloradical character. DFT computations confirmed 67 % spin density to be located at the Ir metal. Unlike for the 3*d* homologue cobalt (and to some extent for rhodium) isolable, monomeric d^7 complexes of iridium still remain relatively rare.^[99,102]

[98] Selected reviews on open-shell platinum metal complexes: a) K. K. Pandey, *Coord. Chem. Rev.* **1992**, *121*, 1-42; b) D. G. DeWit, *Coord. Chem. Rev.* **1996**, *147*, 209-246; c) B. de Bruin, D. G. Hetterscheid, A. J. J. Koekoek, H. Grützmacher, *Progr. Inorg. Chem.* **2007**, *55*, 247-354.

[99] N. P. Tsvetkov, M. F. Laird, H. Fan, M. Pink, K. G. Caulton, *Chem Commun.* **2009**, 4578-4580.

[100] B. de Bruin, D. G. H. Hetterscheid, *Eur. J. Inorg. Chem.* **2007**, 211-230.

[101] J. Meiners, M. G. Scheibel, M.-H. Lemée-Cailleau, S. A. Mason, M. B. Boeddinghaus, T. F. Fässler, E. Herdtweck, M. M. Khusniyarov, S. Schneider, *Angew. Chem.* **2011**, *123*, 8334-8337; *Angew. Chem. Int. Ed.* **2011**, *50*, 8184-8187.

[102] a) M. P. García, M. V. Jimenez, L. A. Oro, F. J. Lahoz, P. J. Alonso, *Angew. Chem.* **1992**, *104*, 1512-1514; *Angew. Chem. Int. Ed. Engl.* **1992**, *31*, 1527-1529; b) A. B. Danopoulos, G. Wilkinson, B. Hussain-Bates, M. B. Hursthouse, *J. Chem. Soc. Dalton Trans.* **1992**, 3165-3170; c) H. Zhai, A. Bunn, B. Wayland, *Chem. Commun.* **2001**, 1294-1295; d) B. de Bruin, T. P. J. Peters, S. Thewissen, A. N. J. Blok, J. B. M. Wilting, R. de Gelder, J. M. M. Smits, A. W. Gal, *Angew. Chem.* **2002**, *114*, 2239-2242; *Angew. Chem. Int. Ed.* **2002**, *41*, 2135-2138; e) A. S. Ionkin, W. J. Marshall, *Organometallics* **2004**, *23*, 6031-6041; f) D. G. H. Hetterscheid, J. Kaiser, E. Reijerse, T. P. J. Peters, S. Thewissen, A. N. J. Blok, J. M. M. Smits, R. de Gelder, B. de Bruin, *J. Am. Chem. Soc.* **2005**, *127*, 1895-1905; g) W. I. Dzik, L. F. Arruga, M. A. Siegler, A. L. Spek, J. N. H. Reek, B. de Bruin, *Organometallics* **2011**, *30*, 1902-1913.

A.1.5.3 Fine-tuning of N→M donation: Low-spin vs. intermediate-spin square-planar 14 VE complexes

Ligand field considerations for square-planar complexes (D_{4h}) with strong-field ligands predict splitting of the d -orbital manifold into three nonbonding orbitals with b_{2g} (d_{xy}) and e_g (d_{xz} , d_{yz}) symmetry, weakly antibonding d_{z^2} (a_{1g}) orbital (stabilized by valence s -orbital mixing), and the high lying $d_{x^2-y^2}$ (b_{1g}) orbital, respectively. Hence, for d^6 ions an intermediate-spin ($S = 1$) electronic configuration is expected (**Figure 8A**).^[103] Iron(II) porphyrinato and bisdithiolato complexes provide well examined examples.^[104,105] In contrast, four-coordinate 14 VE complexes of the platinum metals are usually found in a sawhorse (*cis*-divacant octahedral) conformation with electronic low-spin ($S = 0$) configuration and stabilizing C–H agostic interactions at the vacant coordination sites.^[106] DFT computations also suggested an intermediate-spin electronic ground state for square-planar alkyl PCP pincer complex $[\text{RuCl}\{\text{HC}(\text{CH}_2\text{NHP}^t\text{Bu}_2)_2\}]$.^[107] This species was postulated as a transient intermediate in the equilibrium formed by the closed-shell α - and β -hydrogen elimination

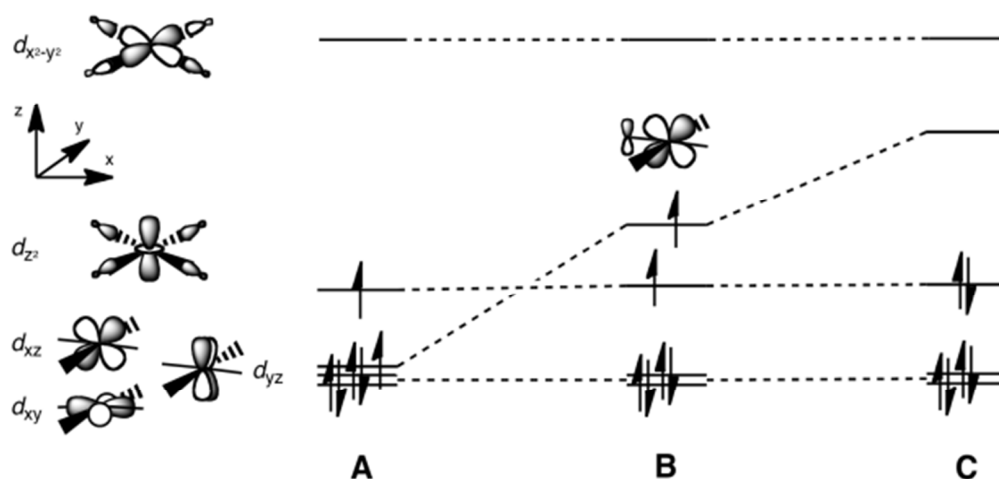


Figure 8: Valence d -orbital splitting in square-planar coordination for a d^6 ion with pure σ -donor ligands (A) and one weak (B) or strong (C) single faced, perpendicular π -donor, respectively.

products (**Scheme 12**). The high reaction rate of hydrido alkylidene and olefin isomer interconversion was attributed to two-state reactivity^[108] via triplet intermediate $[\text{RuCl}\{\text{HC}(\text{CH}_2\text{NHP}^t\text{Bu}_2)_2\}]$. The introduction of one perpendicular single-faced π -donor, such as an amido ligand, further perturbs the valence orbital splitting by lifting the d_{xz}/d_{yz}

[103] S. Alvarez, J. Cirera, *Angew. Chem.* **2006**, *118*, 3078-3087; *Angew. Chem. Int. Ed.* **2006**, *45*, 3012-3020.

[104] a) B. W. Dale, R. J. P. Williams, C. E. Johnson, T. L. Thorp, *J. Chem. Phys.* **1968**, *49*, 3441-3444; b) H. Goff, G. N. La Mar, C. A. Reed, *J. Am. Chem. Soc.* **1977**, *99*, 3641-3646.

[105] K. Ray, A. Begum, T. Weyhermüller, S. Piligkos, J. van Slageren, F. Neese, K. Wieghardt, *J. Am. Chem. Soc.* **2005**, *127*, 4403-4415.

[106] a) G. Ujaque, A. C. Cooper, F. Maseras, O. Eisenstein, K. G. Caulton, *J. Am. Chem. Soc.* **1998**, *120*, 361-365; b) W. Baratta, E. Herdtweck, P. Rigo, *Angew. Chem.* **1999**, *111*, 1733-1735; *Angew. Chem. Int. Ed.* **1999**, *38*, 1629-1631; c) J. P. Lee, Z. Ke, M. A. Ramirez, T. B. Gunnoe, T. R. Cundari, P. D. Boyle, J. L. Petersen, *Organometallics* **2009**, *28*, 1758.

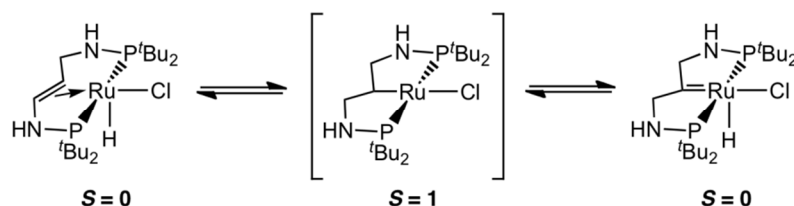
[107] V. F. Kuznetsov, K. Abdur-Rashid, A. J. Lough, D. G. Gusev, *J. Am. Chem. Soc.* **2006**, *128*, 14388-14396.

[108] a) D. Schröder, S. Shaik, H. Schwarz, *Acc. Chem. Res.* **2000**, *33*, 139-145; b) R. Poli, J. N. Harvey, *Chem. Soc. Rev.* **2003**, *32*, 1-8.

degeneracy. If the π -donor is located along the x-axis, the d_{xz} -orbital will be considerably destabilized, subject to the extent of N→Ir π -donation (**Figure 8B/C**). For iridium(II) complex $[\text{IrCl}\{\text{L4}^{t\text{Bu}}\}]$, the expected $(xy,yz,z^2)^6(xz)^1(x^2-y^2)^0$ occupation was obtained from calculations. However, two electronic configurations can arise from the removal of one further electron: An intermediate-spin ($S = 1$) electronic ground state with the N–M π^* -orbital being singly occupied ($(xy,yz,z^2)^5(xz)^1(x^2-y^2)^0$; **Figure 8B**) or a low-spin configuration ($S = 0$) where this orbital is vacant ($(xy,yz,z^2)^6(xz)^0(x^2-y^2)^0$, **Figure 8C**). Therefore, N→M π -bonding should directly influence the singlet-triplet gap, eventually favouring a low-spin over intermediate-spin ground state if the spin pairing energy is overcompensated.

A.1.5.3.1 $[\text{IrCl}(\text{L4}^{t\text{Bu}})]^+$ and $[\text{RuCl}(\text{L1}^{t\text{Bu}})]$: Square-planar d^6 low-spin complexes

Electrochemical characterization of $[\text{IrCl}\{\text{L4}^{t\text{Bu}}\}]$ indicates reversible oxidation at $E_{1/2} = +0.02$ V (vs. $\text{FeCp}_2/\text{FeCp}_2^+$).^[101] Accordingly, diamagnetic d^6 -complex $[\text{IrCl}\{\text{L4}^{t\text{Bu}}\}]\text{PF}_6$ can be synthesized upon chemical oxidation with AgPF_6 , as a unique example for a square-planar Ir^{III} complex (**Scheme 11**). DFT calculations confirm for the singlet state to be more stable by >4 kcal/mol (ZORA-B3LYP/TZVP), attributable to strong N→Ir π -donation. This complex is isoelectronic with Shaw's 'classic' carbene complex $[\text{IrCl}\{=\text{C}(\text{CH}_2\text{CH}_2\text{P}^t\text{Bu})_2\}]$.^[109] Square-



Scheme 12: Equilibrium of $[\text{Ru}(\text{H})\text{Cl}\{\text{P}^t\text{Bu}_2\text{PNHCH}=\text{CHCH}_2\text{NHP}^t\text{Bu}_2\}]$ and $[\text{Ru}(\text{H})\text{Cl}\{\text{C}(\text{CH}_2\text{NHP}^t\text{Bu}_2)_2\}]$ attributed to two-state reactivity via triplet intermediate $[\text{RuCl}\{\text{CH}(\text{CH}_2\text{NHP}^t\text{Bu}_2)_2\}]$.

planar Ru^{II} complex $[\text{RuCl}\{\text{L1}^{t\text{Bu}}\}]$ is obtained by HCl elimination from $[\text{RuCl}_2\{\text{HL1}^{t\text{Bu}}\}]$ (**Scheme 13**).^[110] Like $[\text{IrCl}\{\text{L4}^{t\text{Bu}}\}]^+$, $[\text{RuCl}\{\text{L1}^{t\text{Bu}}\}]$ is diamagnetic, as evidenced by sharp NMR signals. DFT computations suggested a small singlet-triplet gap. The short Ru–N bond derived by single-crystal X-ray diffraction (1.890(2) Å) is in agreement with the DFT optimized structure for the singlet state (1.90 Å) and considerably shorter than the one computed for the triplet state (1.99 Å). This structural feature is particularly indicative for the spin state since the N–M π^* -orbital is vacant in the singlet state (**Figure 8C**) but singly occupied in the triplet state (**B**). Furthermore, the NMR spectra (^1H and ^{31}P) exhibit some unusual chemical shifts with strong temperature dependence. Population of an energetically

[109] D. Empsall, E. M. Hyde, R. Markham, W. S. McDonald, M. C. Norton, B. L. Shaw, W. Weeks, *J. Chem. Soc. Chem. Comm.* **1977**, 589-590.

[110] B. Askevold, M. M. Khusniyarov, E. Herdtweck, K. Meyer, S. Schneider, *Angew. Chem.* **2010**, *122*, 7728-7731; *Angew. Chem. Int. Ed.* **2010**, *49*, 7566-7569.

low lying triplet state was proposed as explanation and the thermodynamic parameters were estimated by fitting of the NMR data ($\Delta H = 10.6 \pm 0.3 \text{ kJmol}^{-1}$; $\Delta S = 4.2 \pm 0.8 \text{ Jmol}^{-1}\text{K}^{-1}$).^[110]

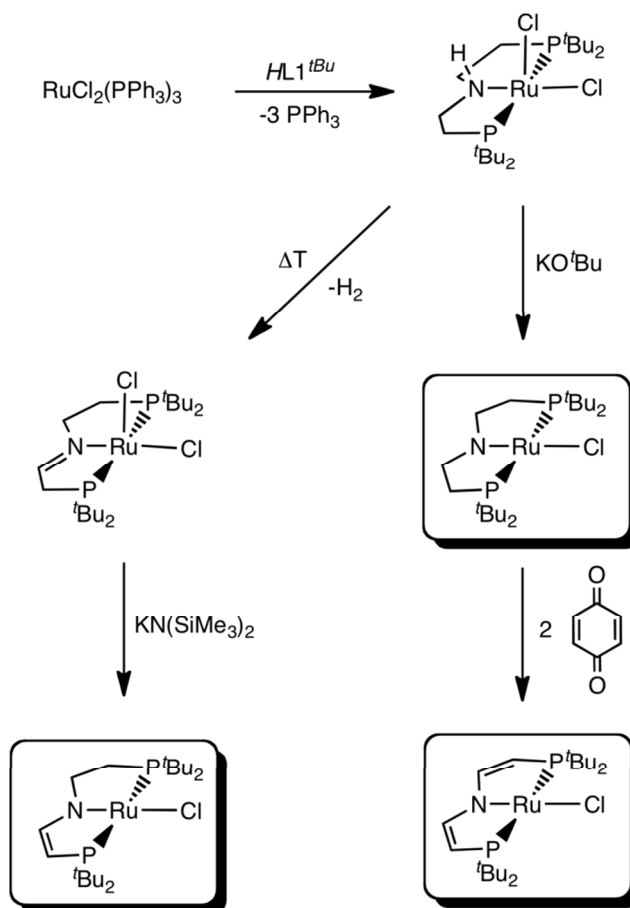
A.1.5.3.2 $[\text{RuCl}\{\text{L}_C^{t\text{Bu}}\}]$, $[\text{RuCl}\{\text{L}3^{t\text{Bu}}\}]$, and $[\text{RuCl}\{\text{L}4^{t\text{Bu}}\}]$: In favour of intermediate-spin

In contrast, Caulton's disilylamido complex $[\text{RuCl}\{\text{L}_C^{t\text{Bu}}\}]$ exhibits strongly paramagnetically shifted signals in the ^1H NMR spectrum and no ^{31}P NMR signal was detected.^[111] At

298 K, the magnetic susceptibility is in agreement with two unpaired electrons ($\chi_{\text{M}}T = 1.03$), and the triplet state was calculated to be favoured by 10 kcal/mol.^[112]

However, at low temperatures $\chi_{\text{M}}T$ drops to near zero indicating a non-magnetic ground state.^[111] These results were rationalized with a spin triplet ground state which is further split into the nonmagnetic $|S = 1, M_S = 0\rangle$ microstate placed below $|S = 1, M_S = \pm 1\rangle$ owing to zero-field-splitting (ZFS).^[113]

Fitting of the magnetic data gave a large axial ZFS parameter ($D = +273 \text{ cm}^{-1}$). The intermediate-spin ground state, also observed for $[\text{RuX}\{\text{L}_C^{t\text{Bu}}\}]$ ($X = \text{F}, \text{OTf}$), $[\text{OsI}\{\text{L}_C^{t\text{Bu}}\}]$, and hydrolysis product $[\text{Ru}(\text{OSiMe}_2\text{CH}_2\text{P}^t\text{Bu}_2)_2]$, is highly unusual for second and third row transition metal complexes.^[112,114] The magnetic properties are reminiscent of the $\text{Ru}^{\text{II}}/\text{Ru}^{\text{II}}$ paddlewheel complexes $[\text{Ru}_2(\text{O}_2\text{CR})_4]$ ($R = \text{CH}_3, \text{Ph}$) which exhibit two unpaired electrons



Scheme 13: Synthesis of square-planar Ru^{II} amido, enamido, and dienamido complexes.

[111] L. A. Watson, O. V. Ozerov, M. Pink, K. G. Caulton, *J. Am. Chem. Soc.* **2003**, *125*, 8426-8427.

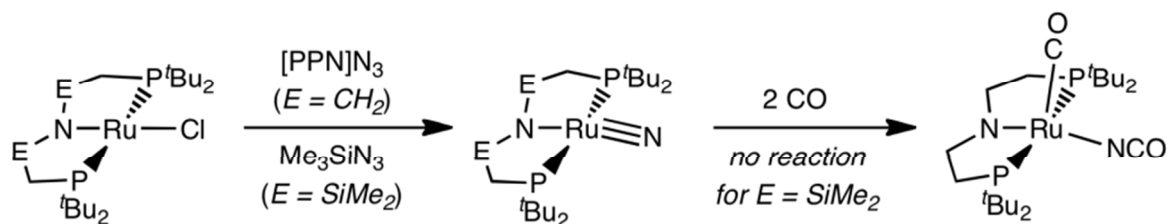
[112] X. Yang, A. Walstrom, N. Tsvetkov, M. Pink, K. G. Caulton, *Inorg. Chem.* **2007**, *46*, 4612-4616.

[113] R. Boca, *Coord. Chem. Rev.* **2004**, *248*, 757-815.

[114] a) A. Walstrom, M. Pink, N. P. Tsvetkov, H. Fan, M. Ingleson, K. G. Caulton, *J. Am. Chem. Soc.* **2005**, *127*, 16780-16781; b) A. Walstrom, M. Pink, K. G. Caulton, *Inorg. Chem.* **2006**, *45*, 5617-5620; c) N. Tsvetkov, M. Pink, H. Fan, J.-H. Lee, K. G. Caulton, *Eur. J. Inorg. Chem.* **2010**, 4790-4800.

but are essentially non-magnetic at low temperatures due to a $\sigma^2\pi^4\delta^2\delta^{*2}\pi^{*2}$ electronic triplet configuration of the Ru^{4+} core and large ZFS.^[115]

Direct comparison of $[\text{RuCl}\{\text{L}1^{t\text{Bu}}\}]$ and $[\text{RuCl}\{\text{L}_C^{t\text{Bu}}\}]$ suggests that the different electronic structure might be attributed to stronger N→M π -donation by the dialkyl- vs. disilylamido ligand. In terms of donor properties, enamido and dienamido ligands scale closer to disilylamides (see above). Therefore, the respective square-planar Ru^{II} complexes $[\text{RuCl}\{\text{L}3^{t\text{Bu}}\}]$ and $[\text{RuCl}\{\text{L}4^{t\text{Bu}}\}]$ were prepared to probe this qualitative picture (Scheme 13).^[85] Both complexes exhibit two unpaired electrons at room temperature, as



Scheme 14: Synthesis of square-planar ruthenium(IV) nitrido complexes and reactivity with CO.

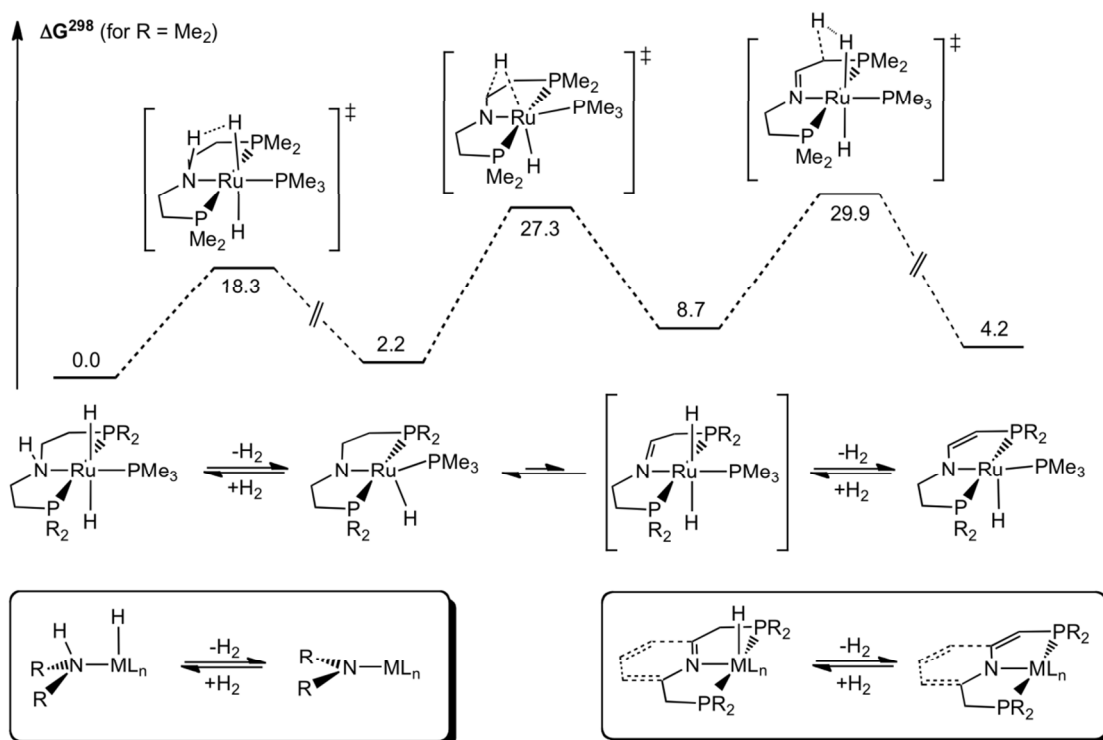
judged by SQUID magnetometry and NMR data. In analogy to $[\text{RuCl}\{\text{L}_C^{t\text{Bu}}\}]$, χ_{MT} drops to near zero at low temperatures. Fitting of the magnetic data to a model with $S = 1$ gave large axial ZFS parameters at around $+380 \text{ cm}^{-1}$ ($[\text{RuCl}\{\text{L}3^{t\text{Bu}}\}]$) and $+230 \text{ cm}^{-1}$ ($[\text{RuCl}\{\text{L}4^{t\text{Bu}}\}]$), respectively, as found for $[\text{RuCl}\{\text{L}_C^{t\text{Bu}}\}]$ ($D = +273 \text{ cm}^{-1}$). To exclude a gradual spin-transition as an alternative explanation for the magnetic data, the molecular structure of $[\text{RuCl}\{\text{L}4^{t\text{Bu}}\}]$ was derived by single crystal X-ray diffraction over a wide temperature range (30 - 200 K). Both the Ru–N distance ($1.994(2) \text{ \AA}$) and the N–Ru–Cl angle (180.0°) are invariant. DFT computations confirmed that both structural parameters should be sensitive indicators for the spin multiplicity ($\Delta_{\text{Ru-N}} = 0.07 \text{ \AA}$; $\Delta_{\text{N-Ru-Cl}} = 15.2^\circ$).

Hence, the bulky ligands $\{\text{L}1^{t\text{Bu}}\}^-$, $\{\text{L}3^{t\text{Bu}}\}^-$, and $\{\text{L}4^{t\text{Bu}}\}^-$ enable the isolation of square-planar 15 and 14 VE Ir^{II} , Ir^{III} , and Ru^{II} complexes. In case of Ru^{II} , the ligand variation allows for control of the electronic structure, attributed to modified N→M π -donation. As pointed out by Caulton and co-workers, other factors such as pincer ligand conformational variations, certainly affect M–N π -bonding, as well, and therefore the generally small singlet-triplet gap for this class of compounds.^[112] As for $[\text{IrCl}\{\text{L}4^{t\text{Bu}}\}]^+$, the supposedly weakest π -donor within the series $\{\text{L}1^R\}^- / \{\text{L}3^R\}^- / \{\text{L}4^R\}^-$ is sufficient to effect spin pairing which is probably an effect of the charge and generally stronger d -orbital splitting compared with Ru^{II} .

[115] F. A. Cotton, V. M. Miskowski, B. Zhong, *J. Am. Chem. Soc.* **1989**, *111*, 6177-6182.

A.1.5.4 M(PNP) complexes as platforms for late transition metal nitrides

The coordinatively and electronically highly unsaturated 14 VE complexes should be suitable platforms for the stabilization of multiply bonded ligands. Accordingly, diamagnetic Ru^{IV} nitrides [RuN{L^{*t*Bu}}] and [RuN{L1^{*t*Bu}}] are isolated in high yield from the corresponding chloro complexes by salt metathesis with azides and N₂ elimination (**Scheme 14**).^[116,117] Terminal nitrido complexes with *dⁿ*-electron counts *n* > 2 are exceedingly rare.^[118] At variance with more common Ru^{VI} nitrides,^[119] [RuN{L^{*t*Bu}}] exhibits a nucleophilic nitrido



Scheme 15: Center: H₂ addition/elimination equilibrium of [Ru(H)₂PMe₃{HL1^{*i*Pr}}], [Ru(H)PMe₃{L1^{*i*Pr}}], and [Ru(H)PMe₃{L3^{*i*Pr}}] and proposed intermediate [Ru(H)₂PMe₃{L2^{*i*Pr}}] (H₂-complex intermediates omitted). Top: Computed energies for the PME₂ truncated model (kcal/mol). Bottom: Analogies with Noyori-type (left) and Milstein-type (right) catalysts.

ligand, exemplified by methylation with MeOTf and lack of reactivity with phosphines.^[120] However, while [RuN{L^{*t*Bu}}] does not react with CO, selective nitride-CO coupling was observed for [RuN{L1^{*t*Bu}}] (**Scheme 14**).^[117] Nitride hydrogenolysis with H₂ was also

[116] A. Walstrom, M. Pink, X. Yang, J. Tomaszewski, M.-H. Baik, K. G. Caulton, *J. Am. Chem. Soc.* **2005**, *127*, 5330-5331.

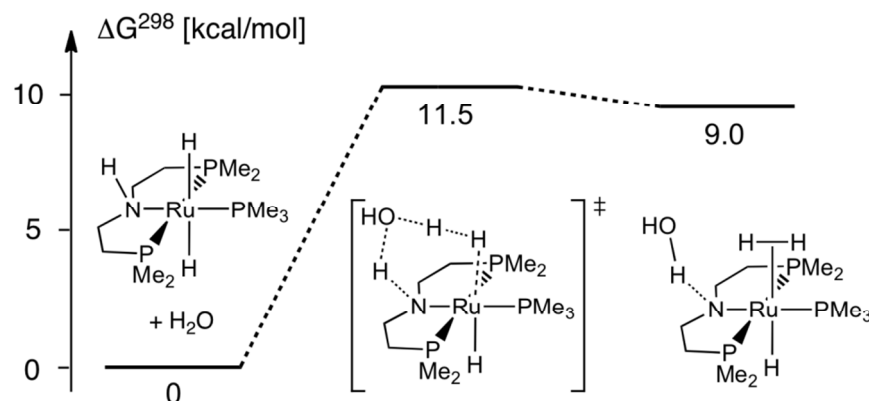
[117] B. Askevold, J. T. Nieto, S. Tussupbayev, M. Diefenbach, E. Herdtweck, M. C. Holthausen, S. Schneider, *Nature Chem.* **2011**, *3*, 532-537.

[118] a) T. A. Betley, J. C. Peters, *J. Am. Chem. Soc.* **2004**, *126*, 6252-6254; b) C. Vogel, F. W. Heinemann, J. Sutter, C. Anthon, K. Meyer, *Angew. Chem.* **2008**, *120*, 2721-2724; *Angew. Chem. Int. Ed.* **2008**, *47*, 2681-2684; c) J. J. Scepaniak, M. D. Fulton, R. P. Bontchev, E. N. Duesler, M. L. Kirk, J. M. Smith, *J. Am. Chem. Soc.* **2008**, *130*, 10515-10517; d) J. J. Scepaniak, J. A. Young, R. P. Bontchev, J. M. Smith, *Angew. Chem.* **2009**, *121*, 3204-3206; *Angew. Chem. Int. Ed.* **2009**, *48*, 3158-3160; e) J. Schöffel, A. Y. Rogachev, S. DeBeer George, P. Burger, *Angew. Chem.* **2009**, *121*, 4828-4832; *Angew. Chem. Int. Ed.* **2009**, *48*, 4734-4738; f) C. C. H. Atienza, A. C. Bowman, E. Lobkovsky, P. J. Chirik, *J. Am. Chem. Soc.* **2010**, *132*, 16343-16345; g) J. J. Scepaniak, C. S. Vogel, M. M. Khusniyarov, F. W. Heinemann, K. Meyer, J. M. Smith, *Science* **2011**, *331*, 1049-1052.

[119] R. A. Eikey, M. M. Abu-Omar, *Coord. Chem. Rev.* **2003**, *243*, 83-124.

[120] A. Walstrom, H. Fan, M. Pink, K. G. Caulton, *Inorg. Chim. Acta* **2010**, *363*, 633-636.

examined and will be discussed in section 4.3. The mechanism of N–CO coupling was not reported, but the lack of reactivity towards the π -acid CO^[121] for [RuN{L^{*t*Bu}}] possibly indicates weaker nucleophilicity of its nitride ligand. As a consequence of the mutual *trans*-



Scheme 16: DFT computed water catalyzed H₂ heterolysis.

configuration of two strong π -donors (nitride and amide), both nitrido complexes exhibit molecular structures with considerable deviation from planarity by N–Ru–N angle bending. Weaker Ru≡N bonding in case of [RuN{L1^{*t*Bu}}] is indicated by the comparatively low stretching vibration ($\nu_{\text{Ru}=\text{N}} = 976 \text{ cm}^{-1}$; [RuN{L_C^{*t*Bu}}]: 1030 cm^{-1}).^[122]

A.1.6 Metal-ligand cooperativity: Hydrogenation and dehydrogenation catalysis

A.1.6.1 Cooperative H₂ activation

The twofold H₂ elimination/addition equilibrium of amine, amido, and enamido complexes [Ru(H)₂PMe₃{HL1^{*i*Pr}}], [Ru(H)PMe₃{L1^{*i*Pr}}], and [Ru(H)PMe₃{L3^{*i*Pr}}] was investigated by kinetic examinations and DFT computations for the PMe₂-truncated model (**Scheme 15**).^[95] H₂ elimination from amine complex [Ru(H)₂PMe₃{HL1^{*i*Pr}}] (**Scheme 15** left branch) proceeds via proton transfer from the amine group to the *syn*-coplanar hydride ligand giving a dihydrogen complex (omitted in **Scheme 15**) with a moderate barrier ($\Delta G^\ddagger = 18.3 \text{ kcal/mol}$ for PMe₂-model), which loses H₂ almost barrierless. The reverse, H₂ heterolysis by amido complexes, was well examined experimentally and computationally for several related systems in the context of hydrogenase model reactivity and metal-ligand cooperative hydrogenation of ketones.^[31,123]

[121] C. Lee, W. Yang, R. G. Parr, *J. Mol. Struct. (Theochem)* **1988**, *163*, 305-313.

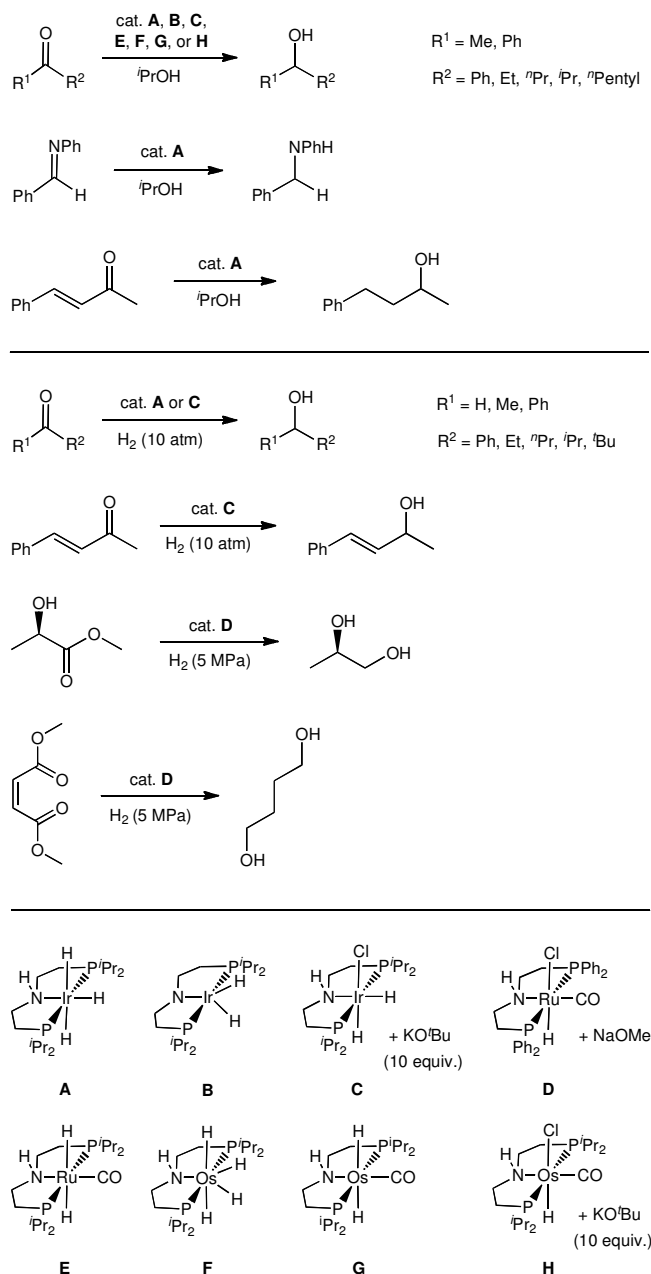
[122] J. F. Berry, *Comments Inorg. Chem.* **2009**, *30*, 28-66.

[123] G. J. Kubas, *Chem. Rev.* **2007**, *107*, 4152-4205; b) J. C. Gordon, G. J. Kubas, *Organometallics* **2010**, *29*, 4682-4701.

On the right branch of the equilibrium reaction, i.e. elimination of H₂ from the ligand backbone, considerably higher barriers were obtained from computations and H/D exchange kinetics (**Figure 15**).^[95] The putative imine intermediate

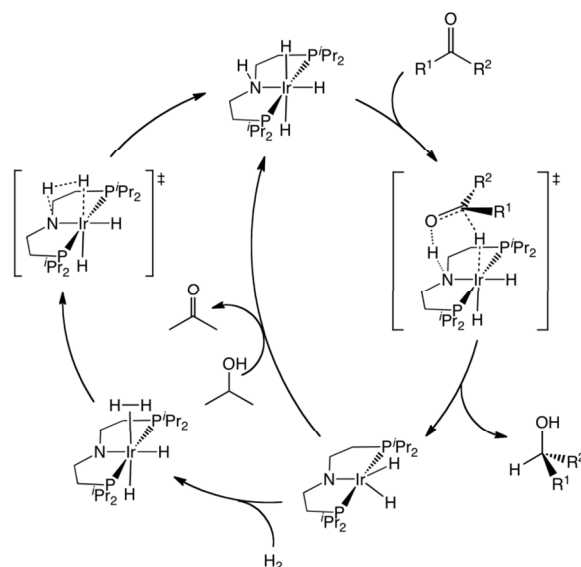
[Ru(H)₂PMe₃{L2^{iPr}}] was not detected spectroscopically. Accordingly, the calculations predict that it is unstable towards both H₂ elimination and migrative imine insertion. Dihydrogen complex [Ru(H)₂(H)PMe₃{L3^{iPr}}]

(omitted in **Scheme 15**) was located as an intermediate on the H₂-elimination path, losing H₂ almost barrierless. The computations indicate that C–H proton transfer from the ligand backbone to the hydride ligand is kinetically feasible without dissociation of one of the pincer ‘arms’. However, predissociation might considerably lower the barrier for amide β-H elimination which could account for the more rapid disproportionation of [Ru(H)PMe₃{L1^{iPr}}] in the presence of PMe₃ (see above). The equilibrium L_nM(H){L2^R} ⇌ L_nM{L3^R} + H₂ provides an aliphatic analogue of Milstein’s pyridine and acridine based PNP pincer catalysts, which operate upon reversible ligand backbone aromatization/dearomatization (**Scheme 15**).^[12]



Scheme 17: Transfer-hydrogenation and direct hydrogenation of carbonyl and carboxyl groups catalyzed by HL1^R-complexes.

Several studies for related ‘Noyori-Morris-type’ metal-ligand cooperative catalysts suggest that Brønsted acids catalyze the H₂ heterolysis step.^[124] For [Ru(H)₂PMe₃{HL1^{iPr}}], proton exchange rates with H₂O were studied by ¹H-EXSY NMR spectroscopy.^[125] The examinations indicate stereoselective H⁺/H⁻ exchange of water with the hydride ligand that is *syn*-coplanar with the N–H proton. This observation is in line with a water catalyzed proton shuttle mechanism for H₂



Scheme 18: Proposed catalytic cycles for transfer-hydrogenation (inner cycle) and direct hydrogenation (outer cycle) of ketones with [Ir(H)₃{HL1^{iPr}}].

heterolysis upon hydrogen bonding with the secondary amine (**Scheme 16**). Accordingly, tertiary amine complex [Ru(H)₂PMe₃{MeL1^{iPr}}] shows considerably slower and unselective H⁺/H⁻ exchange of both hydride ligands with H₂O. DFT computations confirm the proposed mechanism indicating that water catalysis reduces the kinetic barrier for H₂ heterolysis by around 8 kcal/mol for the PMe₂-truncated model (**Scheme 16**). Similarly, computations for proton transfer (‘dearomatization’) from the ligand backbone to a hydride ligand in [Ir(H)₂Ph{NC₅H₃(CH₂PMe₂)₂}] indicate water catalysis, as well.^[126]

A.1.6.2 Outer-sphere hydrogenation and dehydrocoupling of organic substrates

Early studies reported about olefin hydrogenation with [RhCl{HL1^{Ph}}] and [IrCl{HL1^{Ph}}] as pre-catalysts.^[127,128] However, the observation of the ‘N-H-effect’ by Noyori and co-workers sparked interest in these ligands for metal-ligand cooperative (‘bifunctional’) catalysis.^[31] As a rare example, iridium(III) complex [Ir(H)₂Cl{HL1^{iPr}}] catalyzes both the hydrogenation of a wide range of aldehydes and ketones and the transfer hydrogenation of ketones and imines at

[124] a) R. Hartmann, P. Chen, *Angew. Chem.* **2001**, *113*, 3693-3697; *Angew. Chem. Int. Ed.* **2001**, *40*, 3581-3585; b) M. Ito, M. Hirakawa, K. Murata, T. Ikariya, *Organometallics* **2001**, *20*, 379-381; c) V. Rautenstrauch, X. Hoang-Cong, R. Churland, K. Abdur-Rashid, R. H. Morris, *Chem. Eur. J.* **2003**, *9*, 4954-4967; d) C. Hedberg, K. Källström, P. I. Arvidsson, P. Brandt, P. G. Andersson, *J. Am. Chem. Soc.* **2005**, *127*, 15083-15090; e) W. Baratta, K. Siega, P. Rigo, *Chem. Eur. J.* **2007**, *13*, 7479-7486; f) A. Hadzovic, D. Song, C. M. MacLaughlin, R. H. Morris, *Organometallics* **2007**, *26*, 5987-5999.

[125] A. Friedrich, M. Drees, J. Schmedt auf der Günne, S. Schneider, *J. Am. Chem. Soc.* **2009**, *131*, 17552-17553.

[126] M. A. Iron, E. Ben-Ari, R. Cohen, D. Milstein, *Dalton Trans.* **2009**, 9433-9439.

[127] a) M. M. T. Khan, B. T. Khan, S. Nazeeruddin, K. Nazeeruddin, *J. Mol. Catal.* **1984**, *26*, 207-217; b) M. M. T. Khan, B. T. Khan, S. Begum, *J. Mol. Catal.* **1986**, *34*, 9-18; c) M. M. T. Khan, B. T. Khan, S. Begum, S. M. Ali, *J. Mol. Catal.* **1986**, *34*, 283-291; d) M. M. T. Khan, E. R. Rao, M. R. H. Siddiqui, B. T. Khan, S. Begum, S. M. Ali, J. Reddy, *J. Mol. Catal.* **1988**, *45*, 35-50.

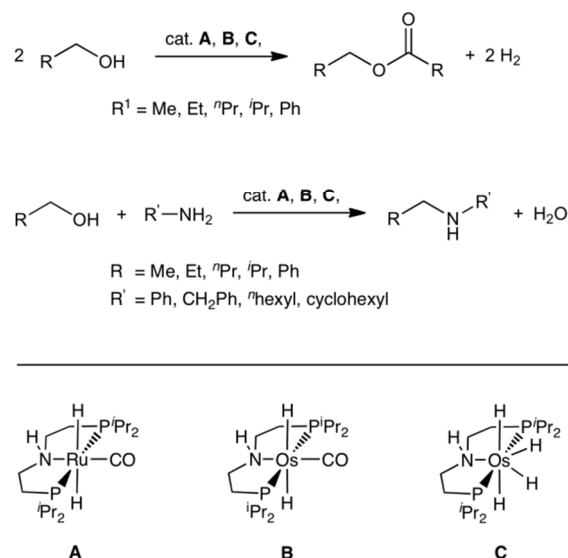
[128] Tertiary amine ligands RL1Ph (R ≠ H) were also used, e.g. in chemoselective hydrogenation of α,β -unsaturated ketones, asymmetric hydrogenation, and transfer hydrogenation, but are not subject of this review: a) C. Bianchini, E. Farnetti, M. Graziani, G. Nardin, A. Vacca, F. Zanobini, *J. Am. Chem. Soc.* **1990**, *112*, 9190-9197; b) C. Bianchini, E. Farnetti, L. Glendenning, M. Graziani, G. Nardin, M. Peruzzini, E. Rocchini, F. Zanobini, *Organometallics* **1995**, *14*, 1489-1502; c) C. Bianchini, L. Glendenning, F. Zanobini, E. Farnetti, M. Graziani, E. Nagy, *J. Mol. Catal. A* **1998**, *132*, 13-19; d) M. S. Rahman, P. D. Prince, J. W. Steed, K. K. M. Hii, *Organometallics* **2002**, *21*, 4927-4933.

mild reaction conditions upon activation with base (**Scheme 17**).^[68b,129] Chemoselective direct hydrogenation of the carbonyl group is observed for benzylideneacetone, while transfer hydrogenation results in the saturated alcohol.

Amine and amido complexes $[\text{Ir}(\text{H})_3\{\text{HL1}^{iPr}\}]$ and $[\text{Ir}(\text{H})_2\{\text{L1}^{iPr}\}]$ catalyze the reaction with comparable rates without base activation. Therefore, a metal-ligand cooperating, ‘Noyori-Morris-type’ mechanism, with concerted H^+/H^- -transfer to the substrate was proposed for hydrogenation and transfer-

hydrogenation (**Scheme 18**) and DFT computations confirmed this suggestion.^[130] Ruthenium and Osmium catalysts with ligand HL1^R ($R = iPr, \text{Ph}$) were also reported as excellent bifunctional catalysts for transfer hydrogenation of ketones,^[131] and for direct hydrogenation of esters to alcohols (**Scheme 17**).^[62] α -Hydroxy esters and β -boc-amino esters are hydrogenated with retention of the configuration. Despite the availability of chiral PNP ligands, asymmetric hydrogenation was not reported, yet.

Microscopic reversibility suggests that these catalysts could be suitable for acceptorless dehydrocoupling and reactions using the ‘borrowing hydrogen’ methodology, as well.^[132] Beller and co-workers reported the highly efficient ($\text{TON} > 40000$; $\text{TOF}_{\text{max}} > 14000 \text{ h}^{-1}$) release of H_2 and acetone from neat 2-propanol at very mild conditions ($90 \text{ }^\circ\text{C}$) with $[\text{RuH}_2(\text{CO})(\text{PPh}_3)_3] / \text{HL1}^{iPr}$ (4.0 ppm loading) in the absence of base. Interestingly, the addition of base (e.g. NaOiPr) results in considerably smaller TOF and the dehydrogenation of the PNP-ligand backbone in the presence of base (see above) provides a possible explanation.^[133] Ruthenium and osmium complexes with ligand HL1^{iPr} were also used for dehydrocoupling of primary alcohols to symmetric esters and for amine alkylation with



Scheme 19: Dehydrogenative coupling reactions with ruthenium and osmium PNP complexes.

[129] X. Chen, W. Jia, R. Guo, T. W. Graham, M. A. Gullons, K. Abdur-Rashid, *Dalton Trans.*, **2009**, 1407-1410.

[130] S. Bi, Q. Xie, X. Zhao, Y. Zhao, X. Kong, *J. Organomet. Chem.* **2008**, 693, 633-638.

[131] a) M. Bertoli, A. Choualeb, A. J. Lough, B. Moore, D. Spasyuk, D. G. Gusev, *Organometallics* **2011**, 30, 3479-3482; b) M. Bertoli, A. Choualeb, D. G. Gusev, A. J. Lough, Q. Major, B. Moore, *Dalton Trans.*, DOI: 10.1039/c1dt10342c.

[132] a) M. H. S. A. Hamid, P. A. Slatford, J. M. J. Williams, *Adv. Synth. Catal.* **2007**, 349, 1555-1575; b) A. Friedrich, S. Schneider, *ChemCatChem* **2009**, 1, 72-73; c) T. D. Nixon, M. K. Whittlesey, J. M. J. Williams, *Dalton Trans.* **2009**, 753-762; d) A. J. A. Watson, J. M. J. Williams, *Science* **2010**, 329, 635-636; e) G. E. Dobreiner, R. H. Crabtree, *Chem. Rev.* **2010**, 110, 681-703; f) G. Guillena, D. J. Ramón, M. Yus, *Chem. Rev.* **2010**, 110, 1611-1641; g) J. Choi, A. H. R. McArthur, M. Brookhart, A. S. Goldman, *Chem. Rev.* **2011**, 111, 1761-1779.

[133] M. Nielsen, A. Kammer, D. Cozzula, H. Junge, S. Gladiali, M. Beller, *Angew. Chem.* **2011**, 123, 9767-9771; *Angew. Chem. Int. Ed.* **2011**, 50, 9593-9597.

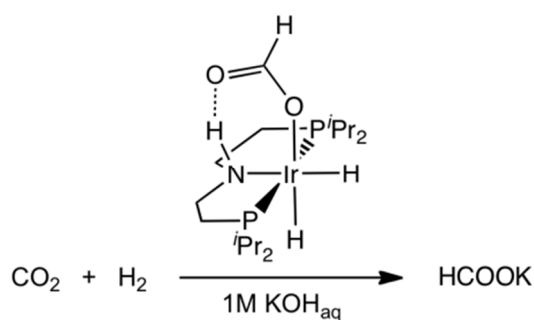
alcohols exhibiting high turn-over numbers (**Scheme 19**).^[131] The latter reaction was reported for $[\text{Ir}(\text{H})_2\text{Cl}\{\text{HL1}^{iPr}\}]$ / base as pre-catalyst, as well.^[134]

A.1.6.3 De-/Hydrogenation of inorganic substrates: CO₂, azide and borane-amines

The d^6 -complexes $[\text{Re}(\text{H})_2\text{NO}\{\text{HL1}^{iPr}\}]$ and $[\text{Ir}(\text{H})_3\{\text{HL1}^{iPr}\}]$ rapidly insert CO₂ into a metal-hydride bond to form the formiato complexes $[\text{Re}(\text{O}_2\text{CH})\text{NO}(\text{H})\{\text{HL1}^{iPr}\}]$ and $[\text{Ir}(\text{O}_2\text{CH})(\text{H})_2\{\text{HL1}^{iPr}\}]$, respectively.^[135,136] The latter catalyzes the hydrogenation of CO₂ to formiate in basic, aqueous solution with high activity (**Scheme 20**). In analogy to ‘Noyori-Morris-type’ ketone hydrogenation, an outer-sphere hydrogen transfer mechanism to the substrate was proposed, supported by DFT computations.

Nitrido complexes could serve as model compounds to examine ammonia formation *en route* to a highly desirable homogeneous catalyst for N₂ hydrogenation at ambient conditions. However, only a few examples were reported that show reactivity towards H₂.^[137] Otherwise, terminal nitrides are surprisingly inert towards H₂,^[138] including $[\text{RuN}\{\text{Lc}^{tBu}\}]$.^[120] In contrast, nitrido complex $[\text{RuN}\{\text{L1}^{tBu}\}]$ reacts with H₂ at relatively mild conditions (1 bar, 50 °C).^[117] Unprecedented formation of ammonia and polyhydride $[\text{RuH}_4\{\text{HL1}^{tBu}\}]$ is observed in high yield (**Scheme 21**). Preliminary mechanistic examination are in agreement with initial, rate determining heterolytic hydrogen splitting across the Ru-amido bond followed by stepwise proton transfer reactions to the nitride via, imido, amido, and ammine intermediates.

Hence, the role of the PNP pincer ligand is two-fold: Weakening Ru–N bonding to the *trans*-nitrido ligand (see above) and acceleration of the reaction by metal-ligand cooperative H₂ activation. Recycling of the ruthenium product by protonolysis followed by reaction with azide and base with high yields was also demonstrated, giving an overall synthetic cycle for catalytic hydrogenation of azide to NH₃ (**Scheme 21**).



Scheme 20: Hydrogenation of CO₂ in aqueous solution catalyzed by $[\text{Ir}(\text{O}_2\text{CH})(\text{H})_2\{\text{HL1}^{iPr}\}]$.

[134] N. Andrushko, V. Andrusjko, P. Roose, K. Moonen, A. Börner, *ChemCatChem* **2010**, 2, 640-643.

[135] T. J. Schmeier, G. E. Dobreiner, R. H. Crabtree, N. Hazari, *J. Am. Chem. Soc.* **2011**, 133, 9274-9277.

[136] A. Choualeb, A. J. Lough, D. G. Gusev, *Organometallics* **2007**, 26, 3509-3515.

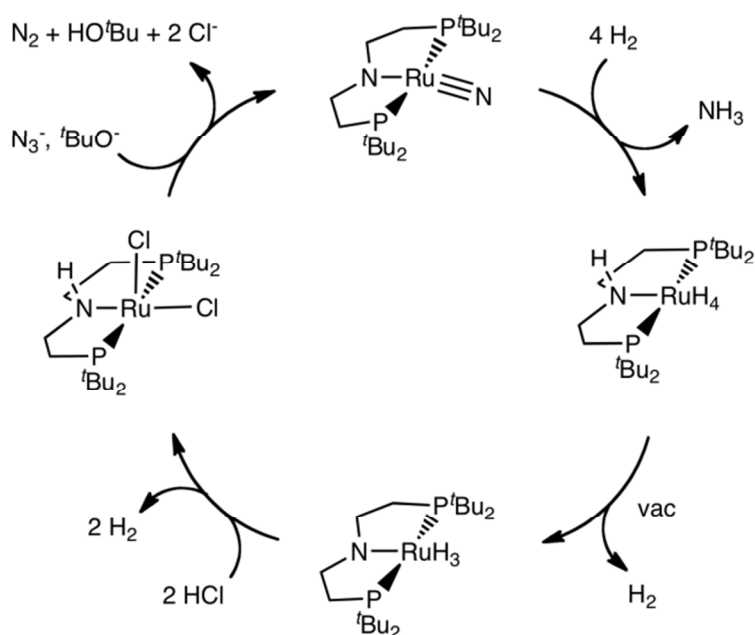
[137] a) S. D. Brown, M. P. Mehn, J. C. Peters, *J. Am. Chem. Soc.* **2005**, 127, 13146-13147; b) J. Schöffel, A. Y. Rogachev, S. DeBeer George, P. Burger, *Angew. Chem.* **2009**, 121, 4828-4832; *Angew. Chem. Int. Ed.* **2009**, 48, 4734-4738.

[138] M. P. Shaver, M. D. Fryzuk, *Adv. Synth. Catal.* **2003**, 345, 1061-1076.

In recent years, the dehydrogenation of borane-amine adducts has attracted considerable interest for chemical hydrogen storage and the synthesis of novel inorganic polymers and B-N-ceramics.^[139,140]

Both $[\text{Ru}(\text{H})\text{PMe}_3\{\text{L1}^{iPr}\}]$ and $[\text{Ru}(\text{H})_2\text{PMe}_3\{\text{HL1}^{iPr}\}]$ catalyse the release of H_2 (1 equiv.) from $\text{H}_3\text{N}-\text{BH}_3$ (AB) solutions with high activities ($\text{TOF} = \sim 20 \text{ s}^{-1}$) and turn over numbers ($\text{TON} > 3000$)

without base at room temperature (Scheme 22).^[94] According to ^{11}B -MQ-MAS spectra of the AB dehydrocoupling product, linear polyaminoboranes $\text{H}_3\text{N}-[\text{H}_2\text{B}-\text{H}_2\text{N}]_n-\text{BH}_3$ are formed.^[7] Dehydrocoupling of $\text{MeH}_2\text{N}-\text{BH}_3$ towards linear, high molecular-mass poly-*N*-methylaminoborane $\text{MeH}_2\text{N}-[\text{H}_2\text{B}-\text{MeHN}]_n-\text{BH}_3$ and of $\text{Me}_2\text{HN}-\text{BH}_3$ towards aminoborane dimer $[\text{Me}_2\text{N}-\text{BH}_2]_2$ were reported, as well.^[141,142] The related catalyst $[\text{RuCl}_2(\text{H}_2\text{NCH}_2\text{CH}_2\text{P}^t\text{Bu}_2)_2]$ (with 10 equiv. KO^tBu) was used for dehydrogenation of borane amine adducts, as well.^[143,144] Based on DFT computations, Fagnou proposed for this catalyst a metal-ligand cooperative ('Noyori-Morris-type') mechanism with concerted H^+/H^- transfer from the substrate to a catalyst amido species and subsequent, turn-over limiting H_2 elimination from the amine complex. In fact, for $\text{H}_3\text{N}-\text{BH}_3$ dehydrocoupling catalyzed by $[\text{Ru}(\text{H})\text{PMe}_3\{\text{L1}^{iPr}\}]$ high kinetic isotope effects upon deuteration of the substrate both at the *N*- and at the *B*-termini were reported, as expected for such a mechanism.^[94] However, the experimental rate law is first order in substrate, indicating a different rate-determining step for this catalyst. Iridium(III) complexes $[\text{Ir}(\text{Cl})_2\text{H}\{\text{HL1}^{tBu}\}]$ and $[\text{Ir}(\text{C}_8\text{H}_{13})\text{HCl}\{\text{HL1}^{tBu}\}]$ were



Scheme 21: Synthetic cycle for the hydrogenation of azide to ammonia.

[139] a) F. H. Stephens, V. Pons, R. T. Baker, *Dalton Trans.* **2007**, 2613-2626; b) C. W. Hamilton, R. T. Baker, A. Staubitz, I. Manners, *Chem. Soc. Rev.* **2009**, 38, 279-293; c) N. C. Smythe, J. C. Gordon, *Eur. J. Inorg. Chem.* **2010**, 509-521; d) A. Staubitz, A. P. M. Robertson, I. Manners, *Chem. Rev.* **2010**, 110, 4079-4124.

[140] a) T. J. Clark, K. Lee, I. Manners, *Chem. Eur. J.* **2006**, 12, 8634-8648; b) A. Staubitz, A. P. M. Robertson, M. E. Sloan, I. Manners, *Chem. Rev.* **2010**, 110, 4023-4078.

[141] A. Staubitz, M. E. Sloan, A. Robertson, A. Friedrich, S. Schneider, P. J. Gates, J. Schmedt, a. d. Günne, I. Manners, *J. Am. Chem. Soc.* **2010**, 132, 13332-13345.

[142] A. Friedrich, M. Drees, S. Schneider, *Chem. Eur. J.* **2009**, 15, 10339-10342.

[143] N. Blaquiere, S. Diallo-Garcia, S. I. Gorelsky, D. A. Black, K. Fagnou, *J. Am. Chem. Soc.* **2008**, 130, 14034-14035.

[144] S. S. Mal, F. H. Stephens, R. T. Baker, *Chem. Commun.* **2011**, 47, 2922-2924.

also reported to be efficient catalysts for the hydrolysis of ammonia borane in *i*PrOH/H₂O solution, mediating the rapid release of almost 3 equiv. H₂ (approx. 9 wt.-%).^[145]

A.1.7 Conclusions

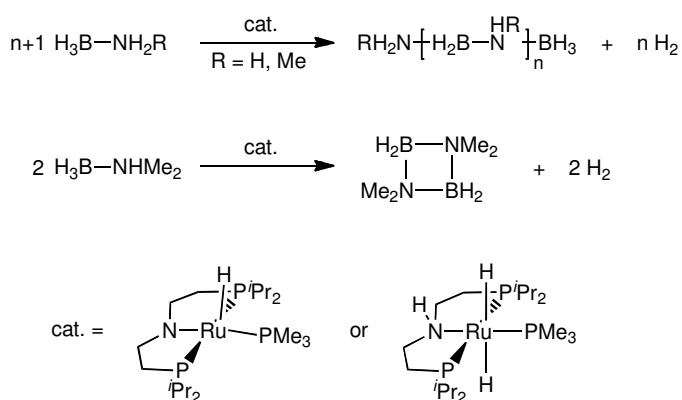
The present review emphasizes the remarkable versatility of the chelating amido, imine, enamido, and dienamido ligands derived from ethylene bridged amine HN(CH₂CH₂PR₃)₂ by deprotonation or oxidative backbone functionalization, respectively. The parent amine, arguably one of the simplest PEP (E = C, N) pincer ligand platforms, is synthetically easily accessible with a wide range of available substituents including very bulky and some chiral examples. Most importantly, backbone dehydrogenation allows for electronic fine-tuning of the ligand donor properties, giving rise to a relatively wide range as compared with many other popular pincer ligand platforms.

The strong π -basicity of the dialkylamide {L1^R}⁻ accounts for the main properties, such as ligand centered nucleophilicity.

Hence, these ligands are ideal building blocks for metal-ligand cooperative (,Noyori-Morris-type') stoichiometric bond activation reactions and catalysis, exemplified by several efficient hydrogenation and dehydrocoupling reactions of organic and inorganic substrates.

Besides the bifunctional reactivity of the amido moiety, the easily obtained enamido ligand {L3^R}⁻ represents an aliphatic analogue of

another ligand class, which is successfully applied in hydrogenation and dehydrocoupling catalysis, i.e. Milstein's ,dearomatized' PNP ligands. In addition to nitrogen centered basic reactivity, the π -basicity also affects the electronic structure of coordinatively and electronically unsaturated complexes. Strong N(*p*)→M(*d*) π -donation by the dialkylamido ligand results in considerable nitrogen contribution to the HOMO of square-planar 16 VE complexes. Consequently, 1-electron oxidation of such iridium(I) and palladium(II) amides gives unstable radical complexes with predominant aminyl character. In turn, *d*⁶ dialkylamides in this geometry are strongly stabilized by the N→M π -donation. The d-orbital



Scheme 22: Dehydrocoupling of borane-amine adducts catalyzed by [Ru(H)PMe₃{HL1^{*i*Pr}}} and [Ru(H)₂PMe₃{HL1^{*i*Pr}}}.

[145] T. W. Graham, C.-W. Tsang, X. Chen, R. Guo, W. Jia, S.-M. Lu, C. Sui-Seng, C. B. Ewart, A. Lough, D. Amoroso, K. Abdur-Rashid, *Angew. Chem.* **2010**, *122*, 8890-8893; *Angew. Chem. Int. Ed.* **2010**, *49*, 8708-8711.

needed for π -bonding is vacant in the electronic low-spin configuration found for $[\text{RuCl}\{\text{L1}^{1B_u}\}]$ and $[\text{IrCl}\{\text{L4}^{1B_u}\}]^+$, which can therefore be described as 16 VE complexes. In case of ruthenium(II), the use of weaker π -donating ligands, $\{\text{L}_C\}^-$, $\{\text{L3}\}^-$, or $\{\text{L4}\}^-$, enables the control of the ground state spin multiplicity. Hence, it will be an interesting goal for future developments to assess if the relatively unusual and to some extent adjustable electronic structure of these compounds will translate into unusual reactivity and reactivity.

A.2 Activation of CH bonds

Functionalization of CH bonds^[146] denotes the conversion of at least one C_{sp3}-H, C_{sp2}-H or C_{sp}-H bond into a C_{sp3}-X, C_{sp2}-X or C_{sp}-X (X = any functional group) bond or into the half of an additional C-C bond (in case of a dehydrogenation reaction). The *activation* of CH bonds is widely understood as the breaking of a CH bond and can be the first step and a prerequisite for an overall functionalization process. The term ‘CH activation’ is often linked to those reactions in which a metal center is *significantly* involved in the CH bond breaking step and therefore is reserved for certain specific metal organic reactions by many authors.^[147] Different CH activation mechanisms are established (**Scheme A.2-1**, **Scheme A.2-2**, **Scheme A.2-3** and **Scheme A.2-4**):^[148] Electrophilic activation,^[149] oxidative addition,^[26,150] σ -bond metathesis,^[151] σ -complex-assisted metathesis (σ -CAM),^[152] metallo radical reaction,^[153] 1,2 CH addition,^[154] ligand based H atom abstraction,^[155] and carbene^[156] and nitrene^[156e,157] insertion, whereby the four latter ones are not in the above-mentioned, strict sense CH activations but bifunctional and ligand centered mechanisms, respectively.^[158,159,160] Some

[146] a) P. M. Doyle, K. I. Goldberg, *Acc. Chem. Res.* **2012**, *45* (6), 777; b) foreword to a special issue by R. H. Crabtree, *Chem. Rev.* **2010**, *110*, 575.

[147] a) B. A. Arndtsen, R. G. Bergman, T. A. Mobley, T. H. Peterson, *Acc. Chem. Res.* **1995**, *28*, 154-162; b) R. A. Periana, G. Bhalla, W. J. Tenn III, K. J. H. Young, X. Y. Liu, O. Mironov, C. J. Jones, V. R. Ziatdinov, *J. Mol. Catal. A: Chem.* **2004**, *220*, 7-25; c) W. B. Tolman, “Activation of small molecules. Organometallic and bioinorganic perspectives”, Wiley-VCH, Weinheim, **2006** s 246; d) A. E. Shilov, G. B. Shul’pin, *Chem. Rev.* **1997**, *97*, 2879-2932; e) Robert H. Crabtree, *J. Organomet. Chem.* **2004**, *689*, 4083-4091.

[148] J. A. Labinger, J. E. Bercaw, *Nature* **2002**, *417*, 507-514.

[149] a) A. E. Shilov, A. A. Shteinman, *Coord. Chem. Rev.* **1977**, *24*, 97-143 (the first time the reaction was presented, though russian-speaking, was here: *Zh. Fiz. Khim.* **1969**, *43*, 2174); b) S. S. Stahl, J. A. Labinger, J. E. Bercaw, *Angew. Chem. Int. Ed.* **1998**, *37*, 2180-2192; c) H. A. Zhong, J. A. Labinger, J. E. Bercaw, *J. Am. Chem. Soc.* **2002**, *124*, 1378-1399; d) R. A. Periana, *Science* **1998**, *280*, 560-564.

[150] a) A. H. Janowicz, R. G. Bergman, *J. Am. Chem. Soc.* **1983**, *105*, 3929-3939; b) A. H. Janowicz, R. G. Bergman, *J. Am. Chem. Soc.* **1982**, *104*, 352-4; c) J. S. Yeston, B. K. McNamara, R. G. Bergman, *Chem. Commun.* **2000**, 19, 3442-3446; d) J. S. Yeston, B. K. McNamara, R. G. Bergman, *Organometallics* **2000**, *19*, 3442-3446.

[151] a) P. L. Watson, *J. Am. Chem. Soc.* **1983**, *105*, 6491-6493; b) C. M. Fendrick, T. J. Marks, *J. Am. Chem. Soc.* **1984**, *106*, 2214-2216; c) A. D. Sadow, T. D. Tilley, *J. Am. Chem. Soc.* **2003**, *125*, 7971-7977.

[152] a) R. N. Perutz, S. Sabo-Etienne, *Angew. Chem. Int. Ed.* **2007**, *46*, 2578-2592; b) S. M. Ng, W. H. Lam, C. C. Mak, C. W. Tsang, G. Jia, Z. Lin, C. P. Lau, *Organometallics* **2003**, *22*, 641-651; c) J. F. Hartwig, K. S. Cook, M. Hapke, C. D. Incarvito, Y. Fan, C. E. Webster, M. B. Hall, *J. Am. Chem. Soc.* **2005**, *127*, 2538-2552; d) K. M. Waltz, J. F. Hartwig, *J. Am. Chem. Soc.* **2000**, *122*, 11358-11369; e) C. E. Webster, Y. Fan, M. B. Hall, D. Kunz, J. F. Hartwig, *J. Am. Chem. Soc.* **2003**, *125*, 858-859; f) W. H. Lam, G. Jia, Z. Lin, C. P. Lau, O. Eisenstein, *Chem. Eur. J.* **2003**, *9*, 2775-2782; g) K. M. Waltz, J. F. Hartwig, *Science* **1997**, *277*, 211-213; h) B. A. Vastine, M. B. Hall, *Coordination Chemistry Reviews* **2009**, *253*, 1202-1218; i) J. F. Hartwig, *Acc. Chem. Res.* **2012**, *45*, 864-873; j) G. Choi, H. Tsurugi, K. Mashima, *J. Am. Chem. Soc.* **2013**, *135*, 13149-13161; k) C. S. Wei, C. A. Jiménez-Hoyos, M. F. Videa, J. F. Hartwig, M. B. Hall, *J. Am. Chem. Soc.* **2010**, *132*, 3078-3091; l) C. Cheng, B. G. Kim, D. Guironnet, M. Brookhart, C. Guan, D. Y. Wang, K. Krogh-Jespersen, A. S. Goldman, *J. Am. Chem. Soc.* **2014**, *136*, 6672-6683.

[153] a) F. F. Puschmann, H. Grützmacher, B. de Bruin, *J. Am. Chem. Soc.* **2010**, *132*, 73-75; b) A. E. Sherry, B. B. Wayland, *J. Am. Chem. Soc.* **1990**, *112*, 1259-1261; c) B. B. Wayland, S. Ba, A. E. Sherry, *J. Am. Chem. Soc.* **1991**, *113*, 5305-5311; d) H. Lu, H. Jiang, L. Wojtas, X. P. Zhang, *Angew. Chem. Int. Ed.* **2010**, *49*, 10192-10196; e) Y. W. Chan, K. S. Chan, *J. Am. Chem. Soc.* **2010**, *132*, 6920-6922; f) C. Qin, H. M. L. Davies, *J. Am. Chem. Soc.* **2014**, *136*, 140616162229006.

[154] a) P. J. Walsh, F. J. Hollander, R. G. Bergman, *J. Am. Chem. Soc.* **1988**, *110*, 8729-8731; b) C. C. Cummins, S. M. Baxter, P. T. Wolczanski, *J. Am. Chem. Soc.* **1988**, *110*, 8731-8733; c) C. C. Cummins, C. P. Schaller, G. D. van Duyne, P. T. Wolczanski, A. W. E. Chan, R. Hoffmann, *J. Am. Chem. Soc.* **1991**, *113*, 2985-2994; d) J. L. Bennett, P. T. Wolczanski, *J. Am. Chem. Soc.* **1994**, *116*, 2179-2180; e) C. P. Schaller, J. B. Bonanno, P. T. Wolczanski, *J. Am. Chem. Soc.* **1994**, *116*, 4133-4134; f) J. B. Bonanno, T. P. Henry, D. R. Neithamer, P. T. Wolczanski, E. B. Lobkovsky, *J. Am. Chem. Soc.* **1996**, *118*, 5132-5133; g) C. P. Schaller, C. C. Cummins, P. T. Wolczanski, *J. Am. Chem. Soc.* **1996**, *118*, 591-611; h) J. de With, A. D. Horton, *Angew. Chem. Int. Ed. Engl.* **1993**, *32*, 903-905; i) T. R. Cundari, N. Matsunaga, E. W. Moody, *J. Phys. Chem.* **1996**, *100*, 6475-6483; j) J. L. Bennett, P. T. Wolczanski, *J. Am. Chem. Soc.* **1997**, *119*, 10696-10719; k) D. F. Schafer, P. T. Wolczanski, *J. Am. Chem. Soc.* **1998**, *120*, 4881-4882; l) L. M. Slaughter, P. T. Wolczanski, T. R. Klinckman, T. R. Cundari, *J. Am. Chem. Soc.* **2000**, *122*, 7953-7975; m) T. R. Cundari, T. R. Klinckman, P. T. Wolczanski, *J. Am. Chem. Soc.* **2002**, *124*, 1481-1487; n) J. R. Webb, S. A. Burgess, T. R. Cundari, T. B. Gunnoe, *Dalton Trans* **2013**, *42*, 16646-16665.

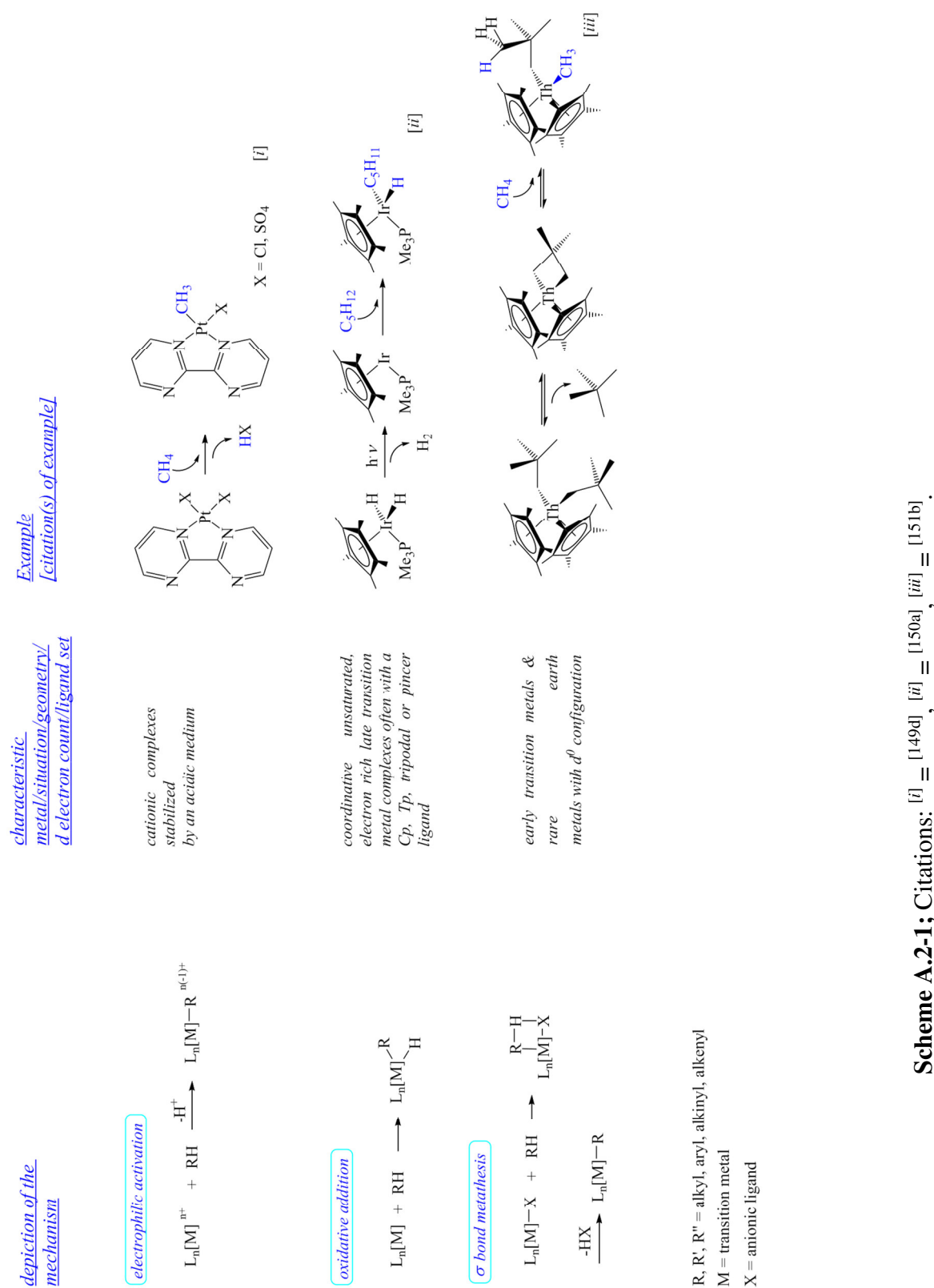
[155] a) O. A. Olatunji-Ojo, T. R. Cundari, *Inorg. Chem.* **2013**, *52*, 8106-8113; b) Sazama, G. Thomas, PhD Thesis **2013**, “Late First-Row Transition Metals in Weak Ligand Fields - Correlating High-Spin Electronic Structure and Reactivity”; c) J. T. Groves, G. A. McClusky, *J. Am. Chem. Soc.* **1976**, *98*, 859-861; recent articles about cytochromes P450: d) T. D. H. Bugg, *Tetrahedron* **2003**, *59*, 7075-7101; e) D. Hamdane, H. Zhang, P. Hollenberg, *Photosynth Res* **2008**, *98*, 657-666; f) B. Meunier, S. P. de Visser, S. Shaik, *Chem. Rev.* **2004**, *104*, 3947-3980; g) S. Shaik, S. Cohen, S. P. de Visser, P. K. Sharma, D. Kumar, S. Kozuch, F. Ogliaro, D. Danovich, *Eur. J. Inorg. Chem.* **2004**, *2004*, 207-226; h) S. G. Sligar, T. M. Makris, I. G. Denisov, *Biochem. Biophys. Res. Comm.* **2005**, *338*, 346-354; i) C. R. Nishida, P. R. Ortiz de Montellano, *ibid.* **2005**, *338*, 437-445; more recent studies: j) I. F. Sevrioukova, T. L. Poulos, *Dalton Trans.* **2013**, *42*, 3116; k) J. Rittle, M. T. Green, *Science* **2010**, *330*, 933-937.

[156] a) A. Demonceau, A. F. Noels, A. J. Hubert, P. Teyssie, *J. Chem. Soc., Chem. Commun.* **1981**, 688; b) M. P. Doyle, L. J. Westrum, W. N. E. Wolthuis, M. M. See, W. P. Boone, V. Bagheri, M. M. Pearson, *J. Am. Chem. Soc.* **1993**, *115*, 958-964; c) H. M. L. Davies, S. A. Panaro, *Tetrahedron Lett.* **1999**, *40*, 5287-5290; d) H. M. L. Davies, T. Hansen, D. W. Hopper, S. A. Panaro, *J. Am. Chem. Soc.* **1999**, *121*, 6509-6510; e) E. Nakamura, N. Yoshikai, M. Yamanaka, *J. Am. Chem. Soc.* **2002**, *124*, 7181-7192; f) H. M. L. Davies, R. E. J. Beckwith, *Chem. Rev.* **2003**, *103*, 2861-2904; g) H. M. L. Davies, *Angew. Chem. Int. Ed.* **2006**, *45*, 6422-6425; h) H. M. L. Davies, J. R. Manning, *Nature* **2008**, *451*, 417-424; i) M. M. Diaz-Requejo, P. J. Pérez, *Chem. Rev.* **2008**, *108*, 3379-3394; j) M. P. Doyle, R. Duffy, M. Ratnikov, L. Zhou, *Chem. Rev.* **2010**, *110*, 704-724; k) A. Caballero, E. Despagne-Ayoub, M. Mar Diaz-Requejo, A. Diaz-Rodriguez, M. E. Gonzalez-Nunez, R. Mello, B. K. Munoz, W.-S. Ojo, G. Asensio, M. Etienne et al., *Science* **2011**, *332*, 835-838; l) M. A. Fuentes, A. Olmos, B. K. Muñoz, K. Jacob, M. E. González-Núñez, R. Mello, G. Asensio, A. Caballero, M. Etienne, P. J. Pérez, *Chemistry - A European Journal* **2014**, n/a-n/a.

[157] a) C. Liang, F. Robert-Peillard, C. Fruit, P. Müller, R. H. Dodd, P. Dauban, *Angew. Chem. Int. Ed.* **2006**, *45*, 4641-4644; b) X. Lin, C. Zhao, C.-M. Che, Z. Ke, D. L. Phillips, *Chem. Asian J.* **2007**, *2*, 1101-1108; c) X.-Q. Yu, J.-S. Huang, X.-G. Zhou, C.-M. Che, *Org. Lett.* **2008**, *2*, 2233-2236; d) C. Liang, F. Collet, F. Robert-Peillard, P. Müller, R. H. Dodd, P. Dauban, *J. Am. Chem. Soc.* **2008**, *130*, 343-350.

[158] P. J. Perez, Editor., “Alkane C-H Activation by Single-Site Metal Catalysis”, *Catal. Met. Complexes*, **38**, Springer, **2012**.

bifunctional heterolytical activation reactions e.g. across covalent late metal amido bonds of *alkenyl* and *alkynyl* CH bonds have been observed as well (e.g. **Scheme A.2-5**).^[161]



Scheme A.2-1; Citations: [i] = [149d], [ii] = [150a], [iii] = [151b].

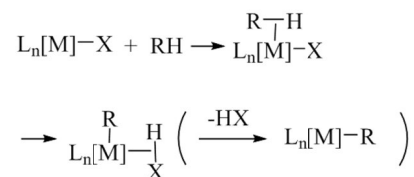
[159] *Organometallic C–H Bond Activation: An Introduction* Alan S. Goldman and Karen I. Goldberg ACS Symposium Series 885, **2004**, 1–43.

[160] a) D. Balcells, E. Clot, O. Eisenstein, *Chem. Rev.* **2010**, *110*, 749–823; b) R. A. Periana, G. Bhalla, W. J. Tenn III, K. J. H. Young, X. Y. Liu, O. Mironov, C. J. Jones, V. R. Ziatdinov, *J. Mol. Catal. A: Chem.* **2004**, *220*, 7–25.

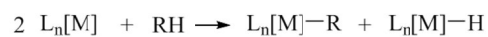
[161] e.g. J. R. Fulton, M. W. Bouwkamp, R. G. Bergman, *J. Am. Chem. Soc.* **2000**, *122*, 8799.

depiction of the mechanism

σ - complex-assisted metathesis (σ -CAM)



metallo radical reaction



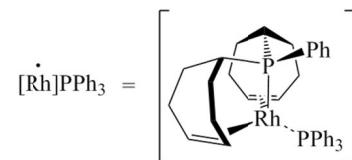
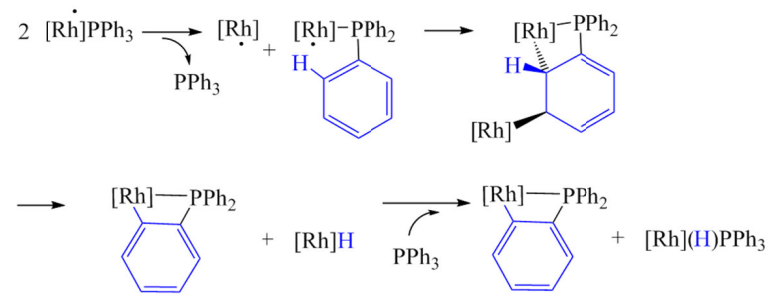
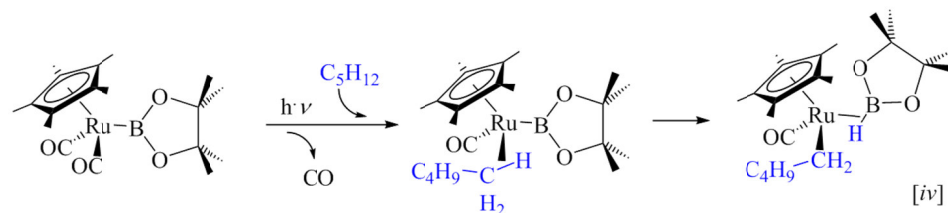
R, R', R'' = alkyl, aryl, alkynyl, alkenyl
M = transition metal
X = anionic ligand

characteristic metal/situation/geometry/d electron count/ligand set

possibility to interconvert σ ligands (H-H, H-BR₂, H-CR₃, H-SiR₃) without change of oxidation state of the metal

heavy transition metals, often binuclear porphyrinorhodium(II) complexes

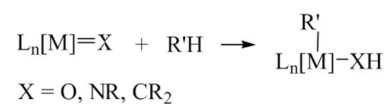
Example [citation(s) of example]



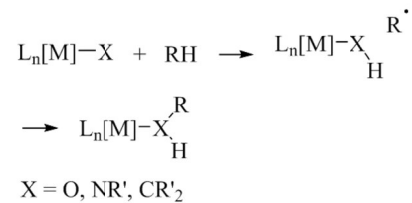
Scheme A.2-2; Citations: ^[iv] = [152d], ^[v] = [153a].

depiction of the mechanism

1,2 CH addition



ligand based H atom abstraction



R, R', R'' = alkyl, aryl, alkynyl, alkenyl

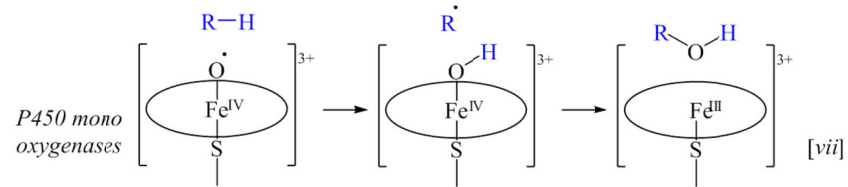
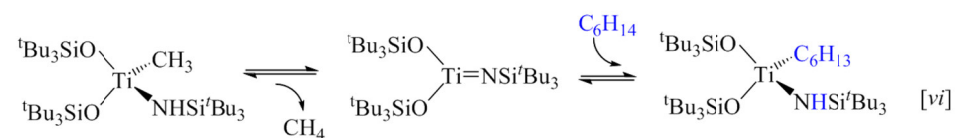
M = transition metal

X = anionic ligand

characteristic metal/situation/geometry/d electron count/ligand set

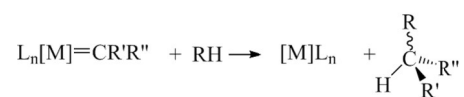
cooperative ligand set,
d⁰ Ti, Zr or Ta, via oxo,
imido or carbene complex

Example [citation(s) of example]



depiction of the mechanism

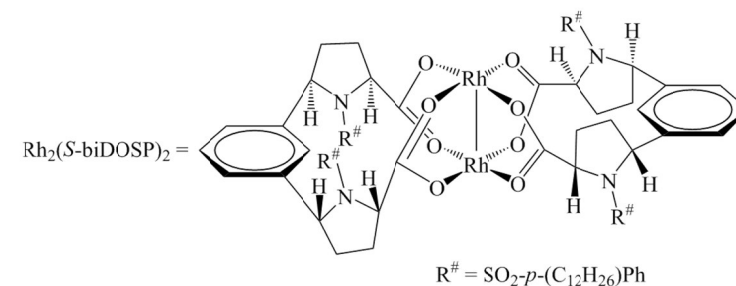
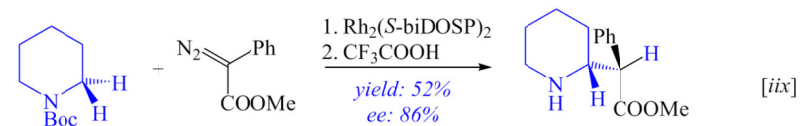
carbene insertion



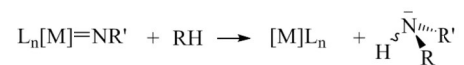
characteristic metal/situation/geometry/d electron count/ligand set

Cu, Ru or Di-Rh complexes with highly electrophilic carbene ligands generated from Diazo-compounds

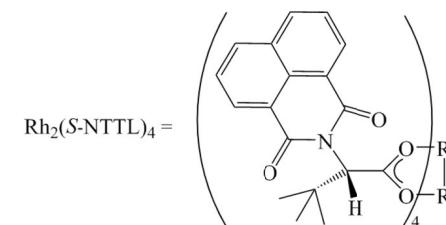
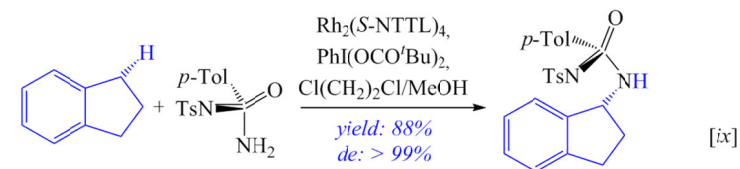
Example [citation(s) of example]



nitrene insertion



highly electrophilic nitrene ligands generated from transient Iminoiodane



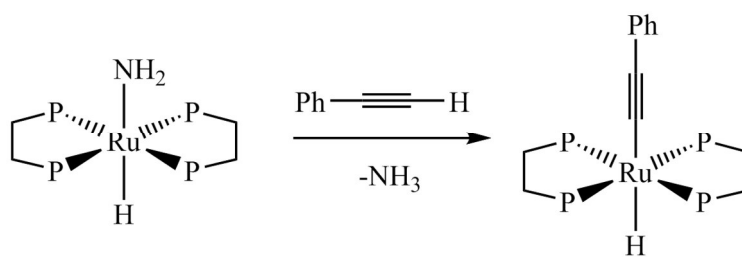
R, R', R'' = alkyl, aryl, alkynyl, alkenyl

M = transition metal

X = anionic ligand

Scheme A.2-4; Citations: [ix] = [156c-d,h], [ix] = [157a].

The chemistry of hydrocarbons depends on fossil resources in terms of natural gas, oil and coal. This dependency, which is difficult due to the limitation of these resources, leads to extensive efforts in the research area of



Scheme A.2-5: Nucleophilic splitting of a CH bond in phenylacetylene at a bifunctional Ru-N-bond.

the activation and functionalization of CH bonds, particularly in small hydrocarbons, to use the natural gas methane resources, which are estimated to be in store in a higher quantity than that of oil^[162] (furthermore, methane can be produced from renewable biogas^[163]), for the construction of larger hydrocarbons. Beyond that, industrial *cracking*^[164] of fossil resources, which involves high energy consumption, mainly leads to the branched and unsaturated hydrocarbons (with exception of *hydrocracking*^[165]). The latter will be functionalized mainly by addition to the double bond afterwards, instead of directly functionalizing the saturated hydrocarbons.^[158] Methane is transformed by *steam reforming* to *syngas* H₂ + CO, which then is converted to methanol by *ICI process* or built up to longer chained hydrocarbons by the *Fischer Tropsch process*.

Thus, economically more suitable process steps for an effective usage of resources would e.g. be the directly oxidative coupling reaction of methane (OCM), the direct oxy-functionalization of methane to methanol and the direct oxidative functionalization of CH bonds from oil.

Unfortunately, methane is a difficult substrate for selective activation, because of the poor reactivity of the H₃C-H bond (BDE_{CH} = 439 kJ/mol^[166,147c167]). Hence, if high energy processes are used for the activation of methane, radical or carbocation reactions are facilitated, which is not (yet) combinable with selective oxidative coupling or oxidation steps, but with increase of side reactions. Furthermore, due to the higher reactivity of the H₂(OH)C-H bond of methanol (BDE_{CH} = 402 kJ/mol)^[166] toward oxidation as compared with

[162] Global resources [EJ] of natural gas are currently estimated to be approx. equivalent to 1.8 times of the resources of oil according to e.g. "Energy Study. Reserves, Resources and Availability of Energy Resources 2013" *Federal Institute for Geosciences and Natural Resources Germany*, Hannover 2013

[163] a) A. D. Cuéllar, M. E. Webber, *Environ. Res. Lett.* 2008, 3, 34002; b) Brian K. Richards, Robert J. Cummings, Thomas E. White, William J. Jewell, *Biomass and Bioenergy* 1991, 1, 65–73 ; c) Brian K. Richards, Frederick G. Herndon, William J. Jewell, Robert J. Cummings, Thomas E. White, *Biomass and Bioenergy* 1994, 6, 275–282.

[164] a) P. M. Zimmerman, D. C. Tranca, J. Gomes, D. S. Lambrecht, M. Head-Gordon, A. T. Bell, *Journal of the American Chemical Society* 2012, 134, 19468–19476; b) R. Gounder, E. Iglesia, *Journal of the American Chemical Society* 2009, 131, 1958–1971; c) C. Sievers, A. Onda, A. Guzman, K. S. Otillinger, R. Olindo, J. A. Lercher, *The Journal of Physical Chemistry C* 2007, 111, 210–218; d) B. S. Greensfelder, H. H. Voge, G. M. Good, *Industrial & Engineering Chemistry* 1949, 41, 2573–2584; e) H. H. Voge, G. M. Good, *Journal of the American Chemical Society* 1949, 71, 593–597.

[165] a) H. González, O. S. Castillo, J. L. Rico, A. Gutiérrez-Alejandre, J. Ramírez, *Industrial & Engineering Chemistry Research* 2013, 52, 2510–2519; b) S. Gamba, L. A. Pellegrini, V. Calemma, C. Gambaro, *Industrial & Engineering Chemistry Research* 2009, 48, 5656–5665.

[166] S. J. Blanksby, G. B. Ellison, *Acc. Chem. Res.* 2003, 36, 255–263; Ref [147]c: BDE_{(CH)HCOH} = 389 kJ/mol.

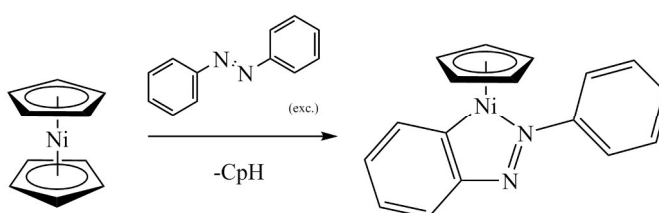
[167] V. N. Cavaliere, D. J. Mendiola, *Chem. Sci.* 2012, 3, 3356.

the substrate methane, oxygenation resulting in CO/CO₂ and water is favored over selective oxygenation toward H₃COH or formaldehyde H₂CO.^[168]

Optimized, indirect, high-temperature conversion of CH₄ to CH₃OH (>800 °C) leads to expensive, high energy consumption.^[169] A published low temperature process due to Cu doped Zeolites is selective but proceeds only with low yields.^[170]

However, *Shilov et al.* showed as early as in 1969^[149a], the possibility to first selectively activate RH₂C-H with Pt(II) salts in an electrophilic step, followed by oxidation of the [Pt^{II}]CH₂R species, attack of a nucleophile X⁻ and finally liberation of RH₂CX. Unfortunately, only expensive H₂Pt^{IV}Cl₆ in stoichiometric amounts was found to selectively oxidize the [Pt^{II}]CH₂R species.

Furthermore, it is possible to trap the MeOH after the first activation step in an *esterification* as *Periana et al.* realized with Au and Pt (Scheme A.2-1) complexes in oleum as oxidizing agent with >90% selectivity for MeOH formation and >40% yield.^[149d,171]



Scheme A.2-6: First known example of homogenous CH activation at a metal center.

These processes appeared to be hampered by difficult separation and recycling of the molecular catalyst, but efforts are made to immobilize the catalysts to overcome this disadvantage.^[171d] Recently, *Periana et al.* even showed stoichiometric oxidation of i.a. methane toward methyltrifluoroacidester with Pb^{IV} and Tl^{III} salts via electrophilic CH activation in 100% selectivity and >70% yield. If the reoxidation of the generated Pb^{II} and Tl^I salts is possible, a catalytic scenario should be available.^[172]

Research toward satisfying, reasonably priced OCM and partial oxidation of methane to methanol processes via metal complexes that are e.g. strongly acidic electrophiles, strongly basic and electron rich or ambiphilic is a lively area of current research.^[169] Singular, prominent examples for the feasible selective oxygenation of CH₄ are the enzymes methane mono oxygenase (MMO), which are able to produce methanol from natural gas. The reaction- and chemo-selectivity of MMO is mainly caused by a constricted, hydrophobic binding

[168] see e.g. Q. Zhang, D. He, Q. Zhu, *J. Nat. Gas Chem.* 2008, 17, 24–28.

[169] B. G. Hashiguchi, S. M. Bischof, M. M. Konnick, R. A. Periana, *Acc. Chem. Res.* 2012, 45, 885–898.

[170] E. M. C. Alayon, M. Nachtegaal, M. Ranocchiari, J. A. van Bokhoven, *CHIMIA* 2012, 66, 668–674.

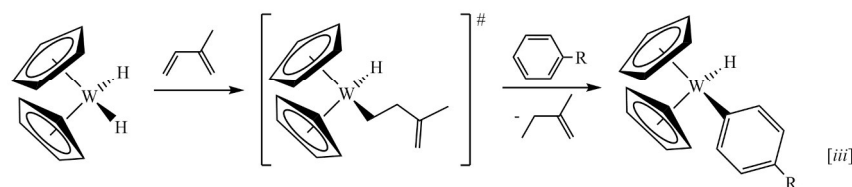
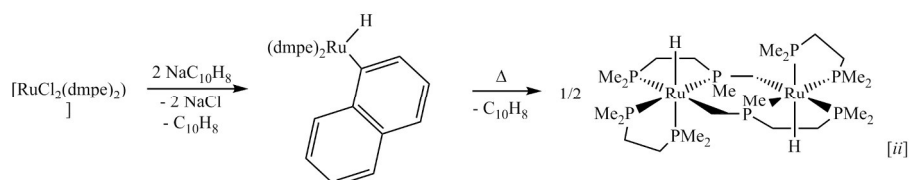
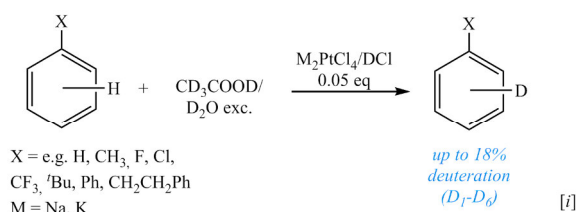
[171] a) C. J. Jones, D. Taube, V. R. Ziatdinov, R. A. Periana, R. J. Nielsen, J. Oxgaard, W. A. Goddard, *Angew. Chem. Int. Ed.* 2004, 43, 4626–4629; b) R. A. Periana, G. Bhalla, W. J. Tenn III, K. J. H. Young, X. Y. Liu, O. Mironov, C. J. Jones, V. R. Ziatdinov, *J. Mol. Catal. A: Chem.* 2004, 220, 7–25; c) B. L. Conley, W. J. Tenn, K. J. H. Young, S. K. Ganesh, S. K. Meier, V. R. Ziatdinov, O. Mironov, J. Oxgaard, J. Gonzales, W. A. Goddard et al., *J. Mol. Catal. A: Chem.* 2006, 251, 8–23; d) R. Palkovits, M. Antonietti, P. Kuhn, A. Thomas, F. Schüth, *Angew. Chem. Int. Ed.* 2009, 48, 6909–6912.

[172] B. G. Hashiguchi, M. M. Konnick, S. M. Bischof, S. J. Gustafson, D. Devarajan, N. Gunsalus, D. H. Ess, R. A. Periana, *Science* 2014, 343, 1232–1237.

pocket: Presumably the small, unpolar substrate methane is associated by van der Waals bonds and the polar product methanol is in return extruded quickly.^[173,147c]

Historically, the first example of homogeneous *aryl* CH activation (electrophilic *ortho* CH activation of azobenzene) was found in the early 1960s (Scheme A.2-6).^[174]

Afterwards numerous examples of *aryl*, *alkenyl*, *alkinyl* and even *alkyl* CH activation reactions were presented (e.g. Scheme A.2-7).^[175]



Scheme A.2-7: Pioneering examples of *aryl* and *alkyl* CH bond activation (Citations: [i] = [175a], [ii] = [175b], [iii] = [175c]); *i* scrambling of aromatic CH bonds by electrophilic Pt salts, *ii* aromatic CH activation of naphthalene and alkyl activation of dmpe by Ru⁰, *iii* aromatic CH activation by proposed transient Cp₂W.

Mechanistically, CH activation resembles many aspects of H₂ activation,^[176] which was investigated earlier in detail^[177] and can be related to HB and HSi activation reactions as well.^[178] In every CH activation process, no matter which reaction mechanism, coordination of the substrate via a hydrocarbon σ -complex preceding the actual reaction, is widely accepted as a crucial step that can even be rate-determining.^[179] The σ -CH bond has a relatively low lying HOMO and a relatively high lying LUMO, accordingly both the σ CH $\sigma \rightarrow d$ donation and $\pi d \rightarrow$ CH σ^* back donation are very weak. In case of σ -BH

[173] a) R. L. Lieberman, A. C. Rosenzweig, *Nature* **2005**, *434*, 177–182; b) A. C. Rosenzweig, C. A. Frederick, S. J. Lippard, P. Nordlund, *Nature* **1993**, *366*, 537–543.

[174] J. P. Kleiman, M. Dubeck, *J. Am. Chem. Soc.* **1963**, *85*, 1544–1545.

[175] e.g. a) J. L. Garnett, R. J. Hodges, *J. Am. Chem. Soc.* **1967**, *89*, 4546–4547; b) J. Chatt, J. M. Davidson, *J. Chem. Soc.* **1965**, 843; c) M. L. Green, P. J. Knowles, *J. Chem. Soc. D* **1970**, 1677.

[176] a) A. S. Goldman, K. I. Goldberg, *Organometallic C–H Bond Activation: An Introduction*, ACS Symposium series 885, S. 1–43; b) R. H. Crabtree, *Chem. Rev.* **1985**, *85*, 245–269.

[177] a) L. Vaska, M. F. Werneke, *Ann NY Acad Sci* **1971**, *172*, 546–562; b) J. Y. Saillard, R. Hoffmann, *J. Am. Chem. Soc.* **1984**, *106*, 2006–26; c) R. H. Crabtree, M. Lavin, *J. Chem. Soc., Chem. Commun.* **1985**, 794–5; d) R. H. Crabtree, M. Lavin, L. Bonneviot, *J. Am. Chem. Soc.* **1986**, *108*, 4032–4037; e) Robert H. Crabtree, Douglas G. Hamilton in *Adv. Organomet. Chem.* (Eds.: F.G.A. Stone, Robert West), Academic Press, **1988**; f) R. H. Crabtree, *Acc. Chem. Res.* **1990**, *23*, 95–101; g) D.-H. Lee, B. P. Patel, R. H. Crabtree, E. Clot, O. Eisenstein, *Chem. Commun.* **1999**, 297–298.

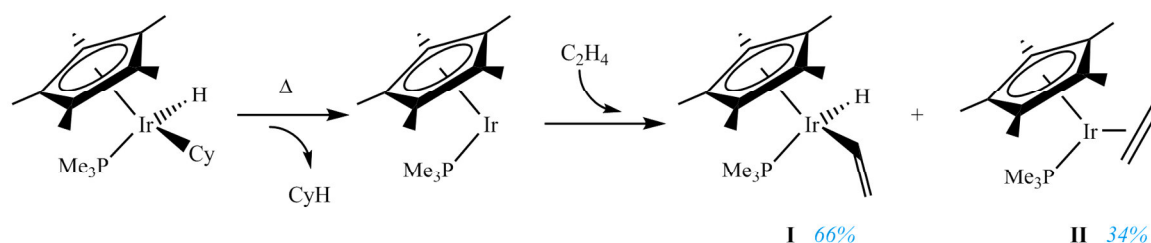
[178] a) J. F. Hartwig, *Organotransition metal chemistry. From bonding to catalysis*, University Science Books, Sausalito, Calif., ©**2010**; b) J. J. Schneider, *Angew. Chem.* **1996**, *108*, 1132–1139.

[179] G. S. Chen, J. A. Labinger, J. E. Bercaw, *Proc. Nat. Acad. Sci.* **2007**, *104*, 6915–6920.

complexes, the LUMO is represented by a comparatively low lying, empty p_z orbital of the B atom that is located perpendicular to the H-BRR' plane which opens the possibility for effective back donation.^[177] The bond strengths in HH σ -complexes are higher than in CH σ -complexes as well, which is presumably due to steric factors. The discovery of *intramolecular*, chelating C–H units (C–H agostic bonds), is due to entropic effects repeatedly found^[180], but the isolation or at least spectroscopic characterization of *intermolecular* CH σ -complexes is a substantial challenge and until now, there are only few examples known.^[181]

The coordination of the σ -complex is more facile in case of aromatic and olefinic substrates than in case of alkanes, owing to higher nucleophilicity originating from the presence of π -electrons. Additionally, the presence of relatively low lying, vacant π^* -molecular orbitals (compared to σ^*) promotes the metal-to-ligand $d\pi$ -backbonding, which enhances substrate coordination.^[158]

Starting from a σ -complex, several different pathways are possible, which can be evaluated for an according substrate / metal complex pair, whereby differentiated energy reaction-coordinate diagrams can be calculated. If the difference between the energies and the geometrical structures of several spin states is very small in a so called *minimum energy crossing point* (MECP) on the hypersurface, a conversion between these spin states is possible. This opens up additional reaction pathways for compounds which are capable of



Scheme A.2-8: Thermolysis of $[\text{Cp}^*(\text{PMe}_3)\text{Ir}(\text{H})\text{Cy}]$ in the presence of ethylene.

two-state-reactivity (TSR).^[108a,182] *Bergman et al.*^[183] and *Poli et al.*^[184] e.g. investigated the reaction of transient CpIrPR_3 with $\text{H}_2\text{C}=\text{CH}_2$ in which the distribution of the products and the

[180] a) M. Brookhart, M. L. H. Green, L.-L. Wong, *Prog. Inorg. Chem.* **1988**, *36*, 1–124; b) M. Brookhart, M. L. H. Green, G. Parkin, *Proc. Nat. Acad. Sci.* **2007**, *104*, 6908–6914.

[181] a) E. P. Wassermann, C. B. Moore, R. G. Bergman, *Science* **1992**, *255*, 315–318; b) A. A. Bengali, R. H. Schultz, C. B. Moore, R. G. Bergman, *J. Am. Chem. Soc.* **1994**, *116*, 9585–9589; c) S. E. Bromberg, *Science* **1997**, *278*, 260–263; d) S. Geftakis, G. E. Ball, *J. Am. Chem. Soc.* **1998**, *120*, 9953–9954; e) B. K. McNamara, J. S. Yeston, R. G. Bergman, C. B. Moore, *J. Am. Chem. Soc.* **1999**, *121*, 6437–6443; f) I. Castro-Rodriguez, H. Nakai, P. Gantzel, L. N. Zakharov, A. L. Rheingold, K. Meyer, *J. Am. Chem. Soc.* **2003**, *125*, 15734–15735; g) D. J. Lawes, S. Geftakis, G. E. Ball, *J. Am. Chem. Soc.* **2005**, *127*, 4134–4135; h) D. J. Lawes, T. A. Darwish, T. Clark, J. B. Harper, G. E. Ball, *Angew. Chem. Int. Ed.* **2006**, *45*, 4486–4490; i) G. E. Ball, C. M. Brookes, A. J. Cowan, T. A. Darwish, M. W. George, H. K. Kawanami, P. Portius, J. P. Rourke, *Proc. Nat. Acad. Sci.* **2007**, *104*, 6927–6932; j) W. H. Bernskoetter, C. K. Schauer, K. I. Goldberg, M. Brookhart, *Science* **2009**, *326*, 553–556.

[182] H. Schwarz, *Angew. Chem.* **2011**, *123*, 10276–10297.

[183] a) J. Silvestre, M. J. Calhorda, R. Hoffmann, P. O. Stoutland, R. G. Bergman, *Organometallics* **1986**, *5*, 1841–1851; b) P. O. Stoutland, R. G. Bergman, *J. Am. Chem. Soc.* **1985**, *107*, 4581–4582; c) *ibid.* **1988**, *110*, 5732–5744; d) B. A. Arndtsen, R. G. Bergman, T. A. Mobley, T. H. Peterson, *Acc. Chem. Res.* **1995**, *28*, 154–162.

[184] K. M. Smith, R. Poli, J. N. Harvey, *Chem. Eur. J.* **2001**, *7*, 1679–1690.

evaluated rate constants were not *prima facie* explainable, at least not on the basis of a supposed singlet single-state-reactivity pathway. The two different reaction products, the vinylhydride CpIr(H)-CH=CH_2 (**I**) and the olefin complex $\text{CpIrPR}_3(\text{H}_2\text{C=CH}_2)$ (**II**), were

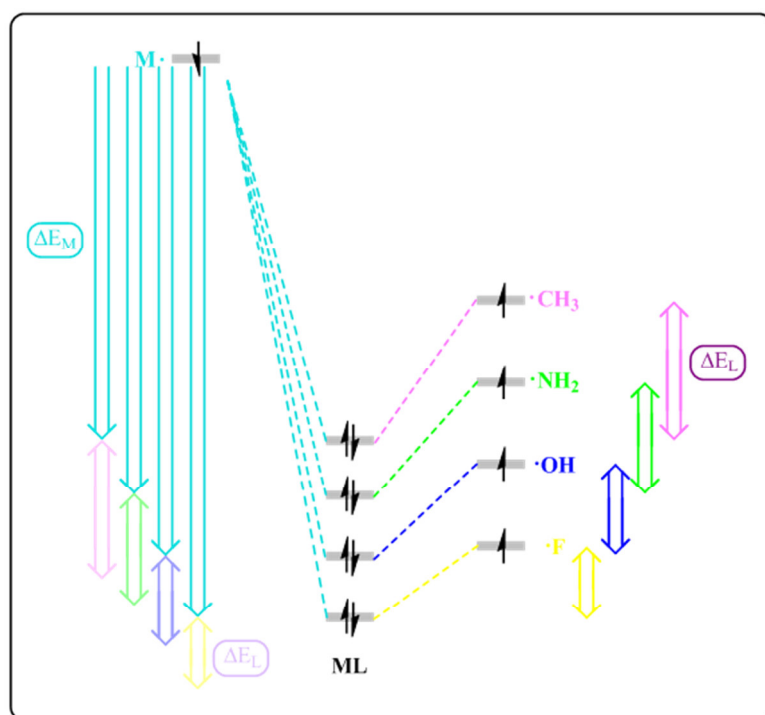


Figure A.2-1: Qualitative contributions of orbital stabilization energies of late metal complexes^[187]

obtained in a 2:1 mixture (**Scheme A.2-8**). Leading the reaction under thermal conditions revealed that **II** was not an intermediate on the way to **I** but the thermodynamic product. DFT calculations disclosed that the complex CpIrPR_3 , which is formed by thermolysis of the precursor $\text{CpIrPR}_3(\text{H})\text{Cy}$, is represented by a triplet ground state ($S = 1$) that possesses several MECPs with the singlet surface. It turned out that crossing the states on an early MECP leads to a pathway via a singlet transition state ($S = 0$) that enables a reaction pathway predominantly toward the product **I**, whereas reaction via a triplet transition state results mainly in formation of **II**.

Regarding thermodynamic factors, metal organyl bonds are normally very weak, relative to other metal ligand bonds, to the metal hydride bond and to the preceding hydrocarbon CH bond. Previously, *Landis et al.*^[185] had disclosed a relationship between increasing calculated $\text{H}_n\text{M-R}$ bond dissociation energies (BDEs) of early and late metals M and the ascending electronegativity of the ligand R ($R = \text{CH}_3, \text{CH}_2\text{Me}, \text{CHMe}_2, \text{CMe}_3, \text{CH=CH}_2, \text{CH}_2\text{Ph}, \text{Ph}, \text{NH}_2, \text{NHMe}, \text{NMe}_2, \text{OH}, \text{OMe}, \text{OPh}$ and F). Calculations of bond energies (BE) of late transition metal bonds $[\text{M}]-\text{X}$ for $\text{X} = \text{CH}_3, \text{NH}_2, \text{OH}$ and F ($M = \text{Pt}, \text{Ru}, \text{Rh}, \text{Ir}$) by energy decomposition analysis (EDA)^[186] by *Ess et al.*^[187] reveal, that the destabilization by *Pauli repulsion* which includes closed-shell $d\pi-p\pi$ repulsion generally decreases (with some fluctuation in some examples) along the ligand series and therefore does not generally control

[185] J. Uddin, C. M. Morales, J. H. Maynard, C. R. Landis, *Organometallics* 2006, 25, 5566–5581.

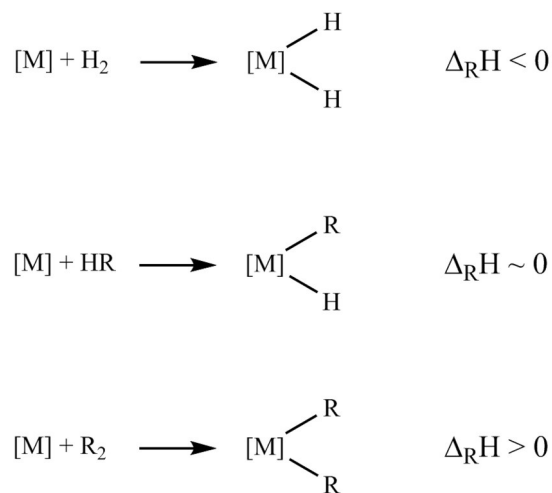
[186] M. v. Hopffgarten, G. Frenking, *WIREs Comput Mol Sci* 2012, 2, 43–62.

[187] D. Devarajan, T. B. Gunnoe, D. H. Ess, *Inorg. Chem.* 2012, 51, 6710–6718.

late metal M–X bond strengths. Stabilizing *electrostatic interactions* generally decrease along the investigated row as well.^[187] However, offsetting the latter effects, the orbital charge transfer stabilization energy ϵ_{orb} increases significantly along the alkyl to heteroatom ligand row. This can be rationalized by the impact of electronegativity on the X ligand fragment which results in increasing orbital stabilization for the neutral metal radical fragment that represents the majority of the overall orbital stabilization energy (**Figure A.2-1**).

Consequently, the equation $[M] + XY \rightarrow [M]XY$ of the CH-activation step alone, without combination with other reactions, tends to be a) exergonic, b) ergoneutral and c) endergonic for a) X,Y = H, b) X = H, Y = organyl and c) X,Y = organyl (**Scheme A.2-9**).^[188] Regarding the differences in bond energies, a hydrogenation reaction, starting from a d^8 square planar ML_4 compound and H_2 results in exergonic addition of H_2 toward $L_4M(H)_2$, due to the sufficient M-H BDE, whereas the similar reaction with a hydrocarbon as the substrate is approximately ergoneutral. By utilizing reactive compounds such as bent CpML or T-shaped ML_3 complexes, generated e.g. by heating of a corresponding precursor ($ML_3L' \rightarrow ML_3 + L'$ or $CpMLXY \rightarrow CpML$), this thermodynamical disadvantage can be compensated. Therefore those reactive metalorganic complexes are paralleling strained (entatic^[189]) states in metalloenzymes.

The M-C bond strength of the CH addition product is the higher, the stronger the preceding H-C bond in the substrate was, by the relationship: $BDE_{([M]R)} = a \cdot BDE_{(HR)} + b$. The slope a is usually found between 0.5 till 2.0 and the intercept b between -50 till -180 kcal, whereby both a and b depend on the metal center and the ligand environment.^[188,190] CH_3 often represents an exception due to its weaker bonding than estimated by the correlation. The steady growth of $BDE_{([M]R)}$ with increasing $BDE_{(HR)}$ is mainly influenced by more s-hybridization character in $H-C_{sp^2}$ or $H-C_{sp}$ substrates, which react toward $[M]-C_{sp^2}$



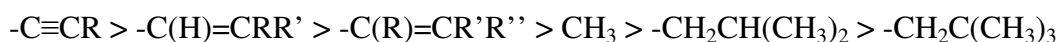
Scheme A.2-9: Thermodynamic trends for the addition of H-H, H-C and C-C bonds to a metal center.

[188] J. Halpern, *Inorg. Chim. Acta* 1985, 100, 41–48.

[189] a) B. L. Vallee, R. J. P. Williams, *Proc. Nat. Acad. Sci.* 1968, 59, 498–505; b) M. W. G. de Bolster, *Pure Appl. Chem.* 1997, 69, 1251–1304; c) M. Nič, J. Jiráč, B. Košata, A. Jenkins, A. McNaught, *IUPAC Compendium of Chemical Terminology*, IUPAC, Research Triangle Park, NC, 2009.

[190] H. E. Bryndza, P. J. Domaille, W. Tam, L. K. Fong, R. A. Paciello, J. E. Bercaw, *Polyhedron* 1988, 7, 1441–1452.

or [M]-C_{sp} products and therefore, is again a function of the orbital electronegativity of the R group.^[187] However, the main impact on the slope *a*, which is frequently > 1,^[191] is supposed to be based on sterical effects.^[147e,188,192,185] Therefore, the bond strengths of metal-organyl bonds decrease in the following order:^[185,193]



Regarding the regioselectivity of an *aliphatic* CH functionalization, in case of a *radical route* (e.g. free radical substitution reactions), radicals abstract an H atom from alkanes, leading to preferred formation of the most stable radical, which is in this case the most substituted one.^[194] An *acidic pathway*, in which superacids abstract H⁺ from RH or protonates RH, leads predominantly to the most substituted carbocation as well.^[194a,195] The subsequent formation of the final product therefore results mainly in the highest substituted or branched, products by non-metal-catalyzed radical or acidic routes.^[196]

The *activation* of *aliphatic* CH bonds RH by low valent transition metal complexes [M] results selectively in the formation of the most stable metal alkyl bond [M]-R, which is the metal bond toward the least substituted carbon atom.^[197] Hence, in contrast to radical or acid pathways, *aliphatic CH functionalization* by metal complexes leads to the formation of the corresponding *n*-alkyl products.^[196,198]

A combination of the CH-activation step with a continuative functionalization is practicable if the allover sum of Gibbs energies of the connected processes is < 0. E.g. insertion of additional substrates with multiple bonds like olefins, alkynes or CO, which is favored into the [M]-C bond over insertion into the [M]-H bond due to [M]-C bond weakness, is an opportunity to provide an exergonic substep.^[192]

Until today, there are only a few direct CH functionalization processes which have been brought to technical use. Particularly, there exists unfortunately not any commercial functionalization of C_{sp3}-H bonds as yet, due to the challenges that were discussed above. However, some exemplary processes involving C_{sp2}-H and C_{sp}-H bond activation and some

[191] *Calculated *R*_{MC/HC} ratios are largest among the group 3 metals, decreasing across the early metals. For late metals, *R*_{MC/HC} ratios generally fall between 1.2 and 1.5.* see ref [185]

[192] P. O. Stoutland, R. G. Bergman, S. P. Nolan, C. D. Hoff, *Polyhedron* 1988, 7, 1429–1440.

[193] a) J. M. Buchanan, J. M. Stryker, R. G. Bergman, *J. Am. Chem. Soc.* **1986**, 108, 1537–50; b) D. D. Wick, W. D. Jones, *Organometallics* 1999, 18, 495–505.

[194] a) M. Smith, J. March, *March's advanced organic chemistry. Reactions, mechanisms, and structure*, Wiley-Interscience, Hoboken, N.J, **2007**; b) R. Bruckner, *Advanced organic chemistry. Reaction mechanisms*, Harcourt/Academic Press, San Diego, 2002.

[195] a) Abstraction of hydrides from alkanes: G. A. Olah, J. Lukas, *J. Am. Chem. Soc.* 1967, 89, 4739–4744; b) Multiple Protonation of CH₄ toward CH₇³⁺: G. A. Olah, G. Rasul, *Acc. Chem. Res.* **1997**, 30, 245; c) H. Wittcoff, B. G. Reuben, J. S. Plotkin, *Industrial organic chemicals*, Wiley-Interscience, Hoboken, N.J, 2004; d) G. A. Olah, D. A. Klumpp, *Superelectrophiles and their chemistry*, Wiley-Interscience, Hoboken, N.J, **2008**; e) G. A. Olah, *Superacid chemistry*, Wiley, Hoboken, N.J, **2009**

[196] *The Organometallic Chemistry of the Transition Metals* 4th ed., R. Crabtree (Wiley, **2005**).

[197] a) T. C. Flood, K. E. Janak, M. Imura, H. Zhen, *J. Am. Chem. Soc.* **2000**, 122, 6783–6784; b) T. O. Northcutt, D. D. Wick, A. J. Vetter, W. D. Jones, *J. Am. Chem. Soc.* **2001**, 123, 7257–7270; c) W. D. Jones, *Acc. Chem. Res.* **2003**, 36, 140–146.

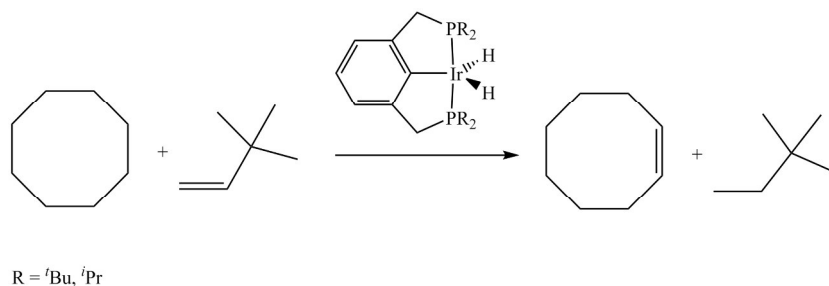
[198] this circumstance has, strictly speaking, only for ch activation reactions with the participation of low-coordinated metal centers absolute validity. According to reference[204a] e.g., in case of oxidation reactions of alkyls in sulfuric acid the selectivity for the rupture of the C-H bond decreases according to the sequence: 3° > 2° > 1° (if russian-speaking see here: Rudakov, E. S.; Lutsyk, A. I. *Neftekhimiya* 1980, 20(2), 163-79).

feasible reactions and models, which point toward a prospective use, will be outlined in the following.^[158]

Functionalization of sp^3 hybridised CH bonds in compounds, which possess heteroatoms: In these compounds, during the CH bond activation step, the heteroatom can coordinate and direct the metal center, activate the CH bond and stabilize the product. Some examples of catalytic methods that are developed: Heteroatom directed Rh catalyzed CC bond formation^[199], Pd catalyzed arylation^[200], α -arylation of carbonyl and carboxyl compounds and their synthetic equivalents^[201] and the *Murai reaction*^[202]: Ru catalyzed addition of aromatic and olefinic CH bonds to olefins.

Oxidative functionalization of Alkyl ethers through reaction of hetero cumulenes with an iridium PNP pincer carbene complex: This reaction which was found by *Grubbs et al.*^[203] is described in detail within the section **B.3 CH activation of THF by a cationic HPNP iridium(I) complex.**

Functionalization of alkanes via electrophilic CH activation: The single most famous example, which is very early as well, as mentioned before (vide infra), is the reaction by *Shilov et al.*^[149a,204], who used aqueous solutions of Pt(II) salts as catalysts and one equivalent of Pt(IV) to functionalize methane. The latter and related systems, based on Rh, Ir, Pd, Pt, Cu, Au, Hg and Tl, which are in parts very active, selective and long living, could unfortunately not yet be incorporated into larger processes.^[205,206] The mechanism^[207] of the CH activation step of these reactions, which are frequently performed in acid solutions, is assumed



Scheme A.2-10: Transferhydrogenation by the example of the reaction $\text{coa} + \text{tbe} \rightarrow \text{coe} + \text{tba}$.

[199] D. A. Colby, R. G. Bergman, J. A. Ellman, *Chem. Rev.* 2010, 110, 624–655.

[200] O. Daugulis, H.-Q. Do, D. Shabashov, *Acc. Chem. Res.* 2009, 42, 1074–1086.

[201] F. Bellina, R. Rossi, *Chem. Rev.* 2010, 110, 1082–1146.

[202] a) S. Murai, F. Kakiuchi, S. Sekine, Y. Tanaka, A. Kamatani, M. Sonoda, N. Chatani, *Nature* 1993, 366, 529–531; b) F. Kakiuchi, S. Murai, *Acc. Chem. Res.* 2002, 35, 826–834.

[203] M. T. Whited, R. H. Grubbs, *J. Am. Chem. Soc.* 2008, 130, 16476–16477.

[204] a) A. E. Shilov, G. B. Shul'pin, *Chem. Rev.* 1997, 97, 2879–2932; b) C. L. Hill, *Activation and functionalization of alkanes*, Wiley, New York, 1989.

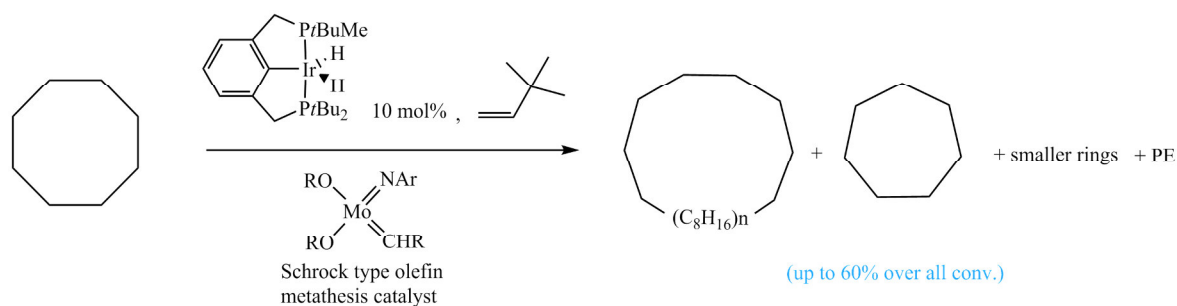
[205] S. S. Stahl, J. A. Labinger, J. E. Bercaw, *Angewandte Chem. Int. Ed.* 1998, 37, 2180–2192.

[206] M. Lersch, M. Tilset, *Chem. Rev.* 2005, 105, 2471–2526.

[207] a) R. A. Periana, D. J. Taube, E. R. Evitt, D. G. Löffler, P. R. Wentrcsek, G. Voss, T. Masuda, *Science* 1993, 259, 340–343; b) U. Fekl, K. I. Goldberg, *Adv. Inorg. Chem.* 2003, 54, 259–319; c) R. A. Periana, D. J. Taube, S. Gamble, H. Taube, T. Satoh, H. Fujii, *Science* 1998, 280, 560–564; d) B. L. Conley, W. J. Tenn, K. J. H. Young, S. K. Ganesh, S. K. Meier, V. R. Ziatdinov, O. Mironov, J. Oxgaard, J. Gonzales, W. A. Goddard et al., *J. Mol. Catal. A: Chem.* 2006, 251, 8–23; e) J. A. Labinger, *J. Mol. Catal. A: Chem.* 2004, 220, 27–35.

to take place via electrophilic coordination of an alkyl or aryl ligand and liberation of a proton H^+ . Afterwards, an inter- or intramolecular nucleophilic attack by e.g. halides, H_2O or HSO_3^- to the activated hydrocarbyl ligand is proposed.

Borylation of alkyl CH bonds: An effective protocol to derive boranes from metal boryls and hydrocarbons by photo induction was found by *Hartwig et al.*^[208] in the 1990ies and was successively extended to a wide scope of metal (W, Re, Fe, Ru, Rh, Ir) catalysts and substrates.



Scheme A.2-11: Alkan metathesis by the example of a ring expansion, contraction, and metathesis-polymerization of coa.^[213a]

Dehydrogenation of alkanes: This endothermic process can be realized in high temperature processes and/or by usage of a sacrificial olefin (which makes the reaction on the whole exothermic, e.g. NBE, TBE)^[209] with Rh^I or Ir^I complexes or Rh^{III} , Ir^{III} or Re^{VII} hydrides as the precursor.^[210] When *Tanaka et al.* found that alkanes were dehydrogenated by photolysis of $RhCO(PR_3)_2Cl$ ^[211], the implementation of monoanionic PCP pincer ligands to Ir^{VIII} and Rh^{VIII} centers by *Kaska et Jensen et al*^[212] (**Scheme A.2-10**) and later highly effective POCOP ligands to Ir^{VIII} by *Goldman et al.*^[26,213] were the next steps towards highly active transferhydrogenation and acceptorless dehydrogenation catalysts.

Alkane metathesis: *n*-Alkanes are selectively transformed into their lower and higher homologues at moderate temperatures. This process can be realized by a dual catalyzed

[208] a) K. M. Waltz, X. He, C. Muhoro, J. F. Hartwig, *J. Am. Chem. Soc.* **1995**, *117*, 11357–11358; b) K. M. Waltz, J. F. Hartwig, *Science* **1997**, *277*, 211–21; c) K. M. Waltz, J. F. Hartwig, *J. Am. Chem. Soc.* **2000**, *122*, 11358–11369; d) H. Chen, S. Schlecht, T. C. Semple, J. F. Hartwig, *Science* **2000**, *287*, 1995–1997.
 [209] G. A. Olah, Á. Molnár, *Hydrocarbon chemistry*, Wiley-Interscience, Hoboken, N.J., **2003**.
 [210] a) R. H. Crabtree, J. M. Mihelcic, J. M. Quirk, *J. Am. Chem. Soc.* 1979, *101*, 7738–7740; b) D. Baudry, M. Ephritikhine, H. Felkin, *J. Chem. Soc., Chem. Commun.* 1980, 1243–1244; c) D. Baudry, M. Ephritikhine, H. Felkin, R. Holmes-Smith, *J. Chem. Soc., Chem. Commun.* 1983, 788–789; d) M. J. Burk, R. H. Crabtree, C. P. Parnell, R. J. Uriarte, *Organometallics* 1984, *3*, 816–817.
 [211] a) Toshiyasu Sakakura, Touru Sodeyama, Yuko Tokunaga, Masato Tanaka, *Chem. Lett.* 1988, *17*, 263–264; b) J. A. Maguire, W. T. Boese, A. S. Goldman, *J. Am. Chem. Soc.* 1989, *111*, 7088–7093; c) J. A. Maguire, W. T. Boese, M. E. Goldman, A. S. Goldman, *Coord. Chem. Rev.* 1990, *97*, 179–192; d) J. A. Maguire, A. S. Goldman, *J. Am. Chem. Soc.* 1991, *113*, 6706–6708; e) Kun Wang, Martin E. Goldman, Thomas J. Emge, Alan S. Goldman, *J. Organomet. Chem.* 1996, *518*, 55–68.
 [212] a) J. K. Perry, G. Ohanessian, W. A. Goddard, *Organometallics* 1994, *13*, 1870–1877; b) M. Gupta, C. Hagen, R. J. Flesher, W. C. Kaska, C. M. Jensen, *Chem. Commun.* 1996, 2083; c) M. Gupta, C. Hagen, W. C. Kaska, R. E. Cramer, C. M. Jensen, *J. Am. Chem. Soc.* 1997, *119*, 840–841; d) W.-w. Xu, G. P. Rosini, K. Krogh-Jespersen, A. S. Goldman, M. Gupta, C. M. Jensen, W. C. Kaska, *Chem. Commun.* 1997, 2273–2274; e) F. Liu, E. B. Pak, B. Singh, C. M. Jensen, A. S. Goldman, *J. Am. Chem. Soc.* 1999, *121*, 4086–4087; f) F. Liu, A. S. Goldman, *Chem. Commun.* 1999, 655–656; g) K. B. Renkema, Y. V. Kissin, A. S. Goldman, *J. Am. Chem. Soc.* 2003, *125*, 7770–7771; h) I. Göttker-Schnetmann, P. White, M. Brookhart, *J. Am. Chem. Soc.* 2004, *126*, 1804–1811.
 [213] a) R. Ahuja, S. Kundu, A. S. Goldman, M. Brookhart, B. C. Vicente, S. L. Scott, *Chem. Commun.* 2008, 253; b) Z. Huang, E. Rolfé, E. C. Carson, M. Brookhart, A. S. Goldman, S. H. El-Khalafy, A. H. R. MacArthur, *Adv. Synth. Catal.* 2010, *352*, 125–135; c) M. C. Haibach, S. Kundu, M. Brookhart, A. S. Goldman, *Acc. Chem. Res.* 2012, *45*, 947–958; d) C. Gunanathan, D. Milstein, *Science* 2013, *341*, 1229712; e) A. J. Nawara-Hultsch, J. D. Hackenberg, B. Punji, C. Supplee, T. J. Emge, B. C. Bailey, R. R. Schrock, M. Brookhart, A. S. Goldman, *ACS Catal.* 2013, *3*, 2505–2514; f) K. B. Renkema, Y. V. Kissin, A. S. Goldman, *J. Am. Chem. Soc.* **2003**, *125*, 7770–7771; g) I. Göttker-Schnetmann, M. Brookhart, *J. Am. Chem. Soc.* **2004**, *126*, 9330–9338.

tandem reaction of dehydrogenation / olefin metathesis / hydrogenation of alkanes. Whether heterogenous^[214], homogenous or with immobilized metalorganic catalysts, respectively^[2,25,26,213] (**Scheme A.2-11**).

Oxygenation of CH bonds: see A.3 Activation of dioxygen and oxygenation reactions

Carbene and nitrene

insertion into C–H

Bonds: The principal

insertion of organic

carbenes CR₂ into

alkyl CH bonds^[215]

is well known.

Intramolecular

insertion of highly

electrophilic metal

organic carbenes,

generated from

diazoalkanes, was

enabled with Cu^[156j] or more often with dirhodium compounds^[156f-h,j].

Intermolecular insertion could be realized by dirhodium^[156a-e] or Cu, Ag and Au^[156i] systems. Even

functionalization of methane was recently shown with Ag complexes^[156k-l].

Intermolecular nitrene insertions via transient nitren complexes are possible with dirhodium systems or Mn or Ru porphyrinato complexes as well.^[156g-h,j,157]

A.2.1 CH activation with iridium pincer complexes

Nucleophilic and electrophilic, organic singlet carbenes CR₂ react i.a. in CH insertion

reactions (though with selectivity for 3° > 2° > 1° CH bonds^[216]).

CH activation via oxidative addition is consistently facilitated by metalorganic complexes which are isolobal^[217] to

carbene CH₂ (**Figure A.2-2**, **Figure A.2-4**), i. e. the following species^[159,217,218]: 16 VE

butterfly *d*⁸ ML₄, 16 VE bent *d*⁸ CpML^[219] and TpML (M = Rh, Ir) and 14 VE bent *d*¹⁰ ML₂

(M = Pt).

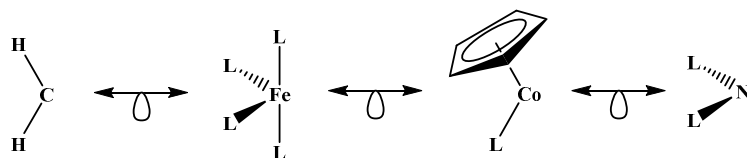


Figure A.2-2: Examples of complexes which are isolobal to CH₂.^[218]

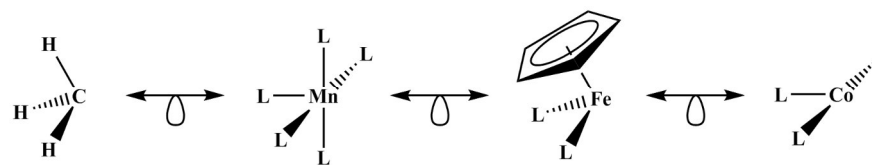


Figure A.2-3: Examples of complexes which are isolobal to CH₃.^[218]

[214] a) R. Burnett, *J. Catal.* 1973, 31, 55–64; V. Vidal, A. Théolier, J. Thivolle-Cazat, J.-M. Basset, *Science* 1997, 276, 99–102; b) J. M. Basset, C. Copéret, L. Lefort, B. M. Maunders, O. Maury, E. Le Roux, G. Saggio, S. Soignier, D. Soulivong, G. J. Sunley et al., *J. Am. Chem. Soc.* 2005, 127, 8604–8605; c) E. Le Roux, M. Taoufik, A. Baudouin, C. Copéret, J. Thivolle-Cazat, J.-M. Basset, B. M. Maunders, G. J. Sunley, *Adv. Synth. Catal.* 2007, 349, 231–237; d) J.-M. Basset, C. Copéret, D. Soulivong, M. Taoufik, J. T. Cazat, *Acc. Chem. Res.* 2010, 43, 323–334.

[215] W. von E. Doering, R. G. Buttery, R. G. Laughlin, N. Chaudhuri, *J. Am. Chem. Soc.* 1956, 78, 3224.

[216] I. Fleming, *Molecular orbitals and organic chemical reactions*, Wiley, Chichester, 2011.

[217] a) R. Hoffmann, *Angew. Chem. Int. Ed. Engl.* 1982, 21, 711–724; b) J. Y. Saillard, R. Hoffmann, *J. Am. Chem. Soc.* 1984, 106, 2006–26.

[218] Y. Jean, *Molecular orbitals of transition metal complexes*, Oxford University Press, Oxford, 2005.

[219] a) J. K. Hoyano, W. A. G. Graham, *J. Am. Chem. Soc.* 1982, 104, 3723–3725; b) A. H. Janowicz, R. G. Bergman, *J. Am. Chem. Soc.* 1982, 104, 352–4; c) W. D. Jones, F. J. Feher, *J. Am. Chem. Soc.* 1982, 104, 4240–4242; d) A. H. Janowicz, R. G. Bergman, *J. Am. Chem. Soc.* 1983, 105, 3929–3939; e) J. K. Hoyano, A. D. McMaster, W. A. G. Graham, *J. Am. Chem. Soc.* 1983, 105, 7190–7191; f) W. D. Jones, F. J. Feher, *J. Am. Chem. Soc.* 1984, 106, 1650–1663; g)

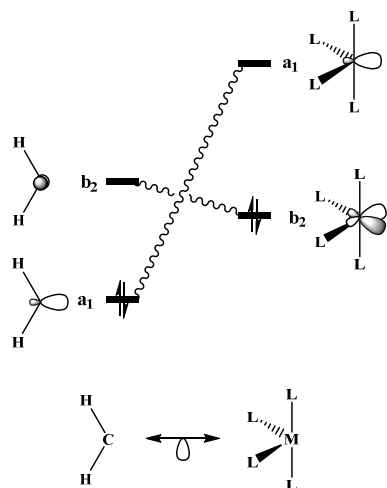


Figure A.2-4: Qualitative representation of the sp^2 and p_y orbitals of CH_2 and the isolobal $d_{x^2-y^2}/p_x$ and sp orbitals of a c_{2v} -symmetric $d^8 ML_4$ complex.^[218]



Figure A.2-5: Qualitative representation of the frontier orbitals of a T-symmetric 14(15) VE $d^{8(9)} ML_3$ complex.^[218]

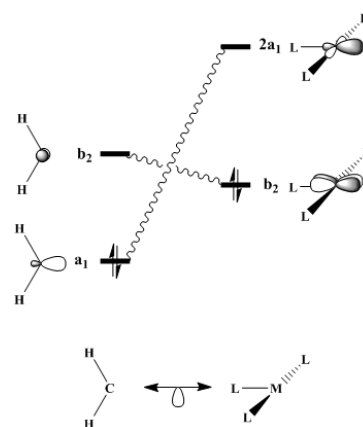
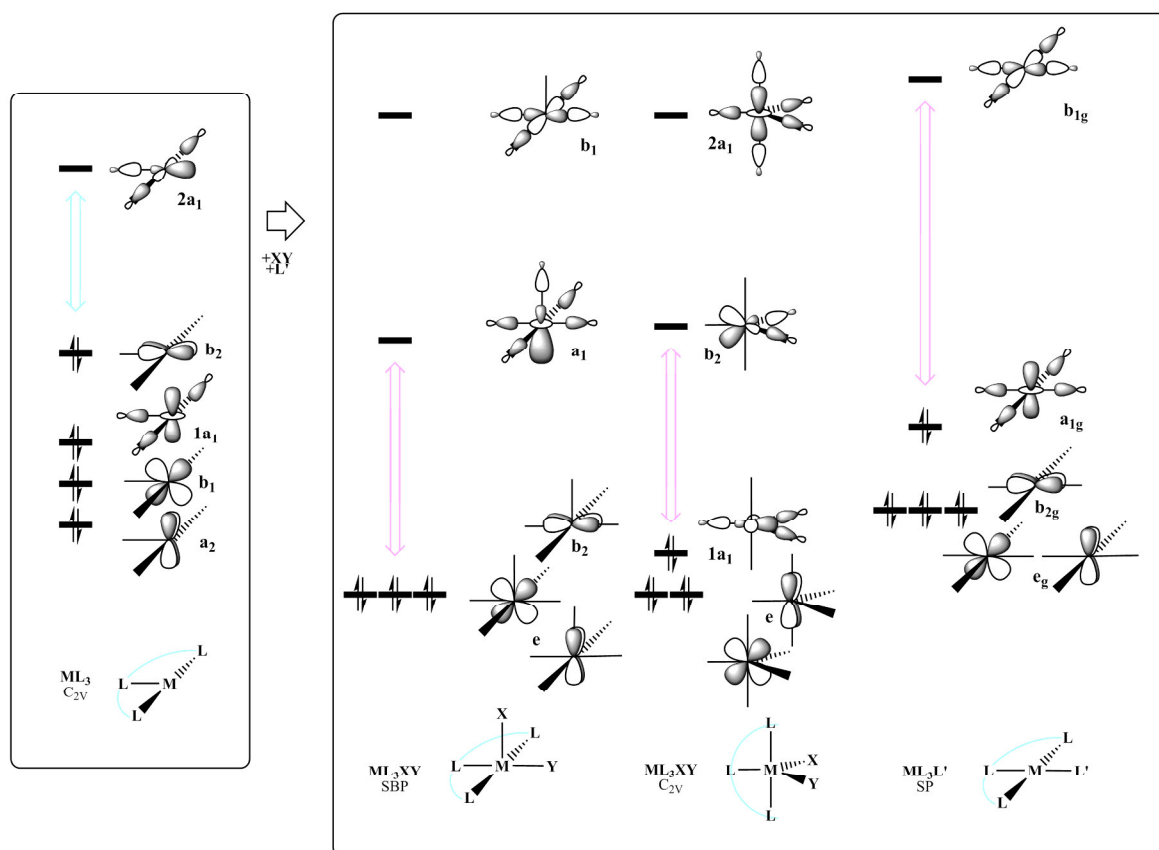


Figure A.2-6: Qualitative representation of the sp^2 and p_y orbitals of CH_2 and the isolobal $d_{x^2-y^2}/p_x$ and d_{xy} orbitals of a c_{2v} -symmetric $d^8 ML_3$ complex in case of order changing HOMO/HOMO-1 due to influences of the ligand setting.

15 VE T-symmetric $d^9 ML_3$ (**Figure A.2-5**) complexes are basically described as isolobal to CH_3 (**Figure A.2-3**) by Hoffmann^[217a] and Jean^[218]. 14 VE T-symmetric $d^8 ML_3$ complexes should therefore be isolobal to CH_3^+ with $2a_1$ as LUMO, $1a_1$ as HOMO and b_2 as HOMO-1 (**Figure A.2-5**). However, depending on the ligand environment $MLL'L'$ π -effects can influence first the ordering of the levels insofar, that $1a_1$ and b_2 exchanges the order and ML_3 becomes isolobal to CH_2 ^[220f] (**Figure A.2-6**). Second, the magnitude of the HOMO-LUMO gap can be affected and thereby the one of the singlet triplet gap^[220e-g] as well.^[220]

Energetically, a relatively low lying LUMO and a relatively high lying HOMO, resulting in a relatively small HOMO-LUMO gap is favorable for coordination of the σ -CH complex due to both effective $\sigma CH_\sigma \rightarrow d$ donation and $\pi d \rightarrow CH_\sigma$ back donation. Starting from higher coordinated precursor compounds, the resulting d^8 T-symmetric ML_3 complex contains such a small gap (**Scheme A.2-12**).

J. M. Buchanan, J. M. Stryker, R. G. Bergman, *J. Am. Chem. Soc.* **1986**, *108*, 1537–1550; h) R. A. Periana, R. G. Bergman, *J. Am. Chem. Soc.* **1986**, *108*, 7332–7346.
 [220] a) R. H. Crabtree, E. M. Holt, M. Lavin, S. M. Morehouse, *Inorg. Chem.* **1985**, *24*, 1986–1992; b) N. Koga, K. Morokuma, *J. Phys. Chem.* **1990**, *94*, 5454–5462; c) T. R. Cundari, *J. Am. Chem. Soc.* **1994**, *116*, 340–347; d) C. Hall, R. N. Perutz, *Chem. Rev.* **1996**, *96*, 3125–3146; e) M.-D. Su, S.-Y. Chu, *J. Am. Chem. Soc.* **1997**, *119*, 10178–10185; f) M.-D. Su, S.-Y. Chu, *J. Phys. Chem. A* **1998**, *102*, 10159–10166; g) M.-D. Su, S.-Y. Chu, *Int. J. Quant. Chem.* **1998**, *70*, 961–971.



Scheme A.2-12: Qualitative representation of the d -orbitals of a T-symmetric d^8 ML_3 complex (left) obtained from square based pyramidal (middle-left) or Y-shaped d^6 ML_3XY (middle-right) complex or from square planar d^8 ML_3L' (right) complex by reductive elimination of XY or respective dissociation of L' . Notice the different sizes of the HOMO-LUMO gaps for the ML_3 compound (petrol) compared to the precursor complexes (pink).

Regarding the formation of the preceding σ hydrocarbon complex as well as the effective CH-bond breaking step, a *relatively* small HOMO-LUMO gap but with large energy difference in total, yields a high LFSE and therefore increases the bond strength. Experimentally and theoretically, the metal hydrocarbyl bond strength is higher in case of heavier ($5d > 4d > 3d$) transition metals in contrast to lighter transition metals, due to a better overlap of the ligand orbitals with the dp hybrids of the metal, especially for the 3rd row, in which additionally relativistic effects take place, leading to an overall less endothermic CH activation process in the former case.^[185,192,221] Regarding trends in computed BDEs in H_nM-CH_3 along the rows, within the 1st row the bond strengths altogether decrease from left to right (with some fluctuation) to reach a minimum at Co and then increase again. The bond strengths within the 2nd row just decrease from left to right (again with fluctuations) and within the 3rd row show no trend but just fluctuate.^[185]

[221] T. Ziegler, V. Tschinke, A. Becke, *J. Am. Chem. Soc.* 1987, 109, 1351–1358.

For the activation of hydrocarbons, which are singlet substrates, reaction in a concerted, singlet oxidative-addition-pathway is desirable, instead of a free-radical-pathway. Since reaction with a triplet compound would be spin forbidden, the metal organic species should be either a singlet compound as well or be capable of TSR to follow a nonadiabatic^[222] pathway, which, again, is easier in case of late, heavy transition metals due to increased spin-orbit coupling.

In favor to preorganize a T-shaped, 3rd row d^8 ML_3 species, the PNP Ir^{I/III} fragment plus one neutral or respective two monoanionic ligand(s), which can dissociate/eliminate during the reaction, is an ideal precursor for CH activation reactions.

Most of the success in CH activation processes due to Ir-pincer complexes so far was achieved by several transfer hydrogenation reactions (see above).

[222] K. J. Laidler, *Pure Appl. Chem.* 1996, 68.

A.3 Activation of dioxygen and oxygenation reactions

The activation of O₂ is an elongation or a partial or full cleavage of the O=O bond and is exemplified in nature by the respiration in the mitochondria. The reduction of O₂ with 4 electrons e⁻ toward 2 H₂O under binding of 4 protons H⁺ inside the cell and translocation of 4 additional H⁺ to fuel the ATP synthase is catalyzed by *complex IV*. The metal centers Fe⁺² and Cu⁺¹ within the previously reduced binuclear cytochrome a₃-Cu_B center are bridged by a hydroxo ligand. This ligand is protonated under loss of H₂O, resulting in a void which can be filled by O₂. The currently accepted mechanism involves immediate oxygen-oxygen bond cleavage by a rapid four electron reduction, which likely avoids any intermediate to form superoxide.^[223]

O₂ activation is of technical interest in fuel cells in terms of the oxygen reduction reaction (ORR) and as the microscopical reversible reaction of water cleavage.

An oxygenation includes, as well as an O₂ activation reaction, an incorporation of molecular oxygen into a substrate which is in nature realized by oxygenase enzymes as e.g. cytochromes P450 (**Scheme A.2-3**), *non-heme-oxygenases* (e.g. methane mono oxygenase MMO) or multicopper oxidases.

The mechanistical picture of the oxygenation of unactivated hydrocarbon bonds for the metabolism of aliphatic acids, degradation of drugs or detoxification reactions catalyzed by cytochromes P450 and especially the identity of the competent O-transfer complex, called *P450 compound I*, was discussed for many years^[155d-j] but finally uncovered in 2010 by *Green et al.*^[155k]. The catalytic cycle involves reduction of a ferric Fe(III) enzyme toward a ferrous Fe(II) enzyme by acceptance of one electron e⁻, binding of oxygen, forming an oxy-heme complex, which under acceptance of two protons H⁺ and one additional e⁻ heterolytically cleaves the O-O bond to form H₂O and *P450 compound I*. The latter is proved to be a ferryl S = 1 Fe(IV)oxo species exchange coupled with an S = 1/2 ligand-based radical delocalized over the non-innocent porphyrin and thiolate ligands. The actual oxygenation step takes place via an abstraction of hydrogen from substrate by *compound I*, leading to an Fe(IV)hydroxide that rapidly recombines with the substrate radical to yield the hydroxylated product, which exactly represents the *oxygen rebound mechanism* that was suggested by *Groves et al.* as early as in 1976.^[155c]

Although the characterization or moreover the quantitative synthesis of the Fe(IV)oxo species *P450 compound I* was not accessible for many years, a shortcut to oxygenate substrates without dioxygen starting from the ferric Fe(III) heme species and reduced single-oxygen

[223] a) M. J. Baldwin, E. C. Long, *Bioinorganic chemistry. Cellular systems and synthetic models*; ACS symposium series, Washington, DC, **2009**; b) M. Fabian, W. W. Wong, R. B. Gennis, G. Palmer, *Proc. Nat. Acad. Sci.* **1999**, 96, 13114–13117; c) O. Hammerich, J. Ulstrup, *Bioinorganic electrochemistry*, Springer, Dordrecht, London, **2008**; d) D. A. Proshlyakov, M. Pressler, C. DeMaso, J. Leykam, D. DeWitt, G. Babcock, *Science* **2000**, 290, 1588–1591; e) T. Tsukihara, H. Aoyama, E. Yamashita, T. Tomizaki, H. Yamaguchi, K. Shinzawa-Itoh, R. Nakashima, R. Yaono, S. Yoshikawa, *Science* **1995**, 269, 1069–1074; f) G. T. Babcock, *Proc. Nat. Acad. Sci.* **1999**, 96, 12971–12973.

donors such as organic hydroperoxides was found for the first time in 1973^[224]. Shortly thereafter, similar reactions could be performed with e.g. H₂O₂, hypochlorites, NaClO₂, PhIO and KHSO₅ as O-atom-donors via this pathway as well, which was retrospectively called the *peroxide-shunt*.^[225]

The mechanism^[226] of oxygenation reactions in non-heme Fe oxygenases is in principle close to that of P450 enzymes and in particular high-valent iron-oxo, Fe(IV)=O or oxygen bridged, binuclear Fe(IV)(O)₂Fe(IV) species are postulated as the competent oxidant, albeit the metal-ligand-framework is in some reaction steps overall less oxidized in the non-heme case, probably because of the stronger non-innocence character of the porphyrinato/thiolato environment in case of the cytochrome containing enzymes.

A model, which likely copies the *function* of oxygenases, is the very early found *Fenton system*^[227], the oxygenation of methylene groups with H₂O₂ in the presence of FeSO₄, presumably radically. The mimicry of non heme oxygenases, starting at tripodal or otherwise tetradentate coordinated Fe(II) or Fe(III) complexes^[228] in the presence of H₂O₂, results in remarkable success e.g. in terms of stereospecific alkane hydroxylation.^[228b] Further effort to copy the function of oxygenases is in progress, e.g. in terms of syntheses of high reactive metal oxo compounds.^[229] The oxygenation reactions of methylene groups with systems of Fe(II) ligated by bulky, tetradentate 2-((S)-2-[(S)-1-(pyridin-2-ylmethyl)pyrrolidin-2-yl]pyrrolidin-1-yl)methylpyridine (PDP) in the presence of H₂O₂, which can be performed with striking, predictable site-selectivities, aroused great interest.^[230]

Reactions which involve a combination of CH bond activation and oxidation via O₂ or O-nucleophiles are e.g. the *functionalization of olefins via nucleopalladation*^[231]:

The well-known *Wacker process*, which contains a hydroxypalladation step of ethylene and reoxidation of the Pd catalyst via cocatalytic Cu/O₂, is the most prominent example of this

[224] F. F. Kadlubar, K. C. Morton, D. M. Ziegler, *Biochem. Biophys. Res. Comm.* **1973**, *54*, 1255–1261.

[225] P. R. Ortiz de Montellano, *Cytochrome P450*, Springer US, Boston, MA, **2005**.

[226] a) H. Basch, K. Mogi, D. G. Musaev, K. Morokuma, *J. Am. Chem. Soc.* **1999**, *121*, 7249–7256; b) K. E. Liu, A. M. Valentine, D. Qiu, D. E. Edmondson, E. H. Appelman, T. G. Spiro, S. J. Lippard, *J. Am. Chem. Soc.* **1995**, *117*, 4997–4998; c) M. Merckx, D. A. Kopp, M. H. Sazinsky, J. L. Blazyk, J. Müller, S. J. Lippard, *Angew. Chem. Int. Ed.* **2001**, *40*, 2782–2807.

[227] H. J. H. Fenton, *J. Chem. Soc., Trans.* **1894**, *65*, 899.

[228] a) T. Okuno, S. Ito, S. Ohba, Y. Nishida, *J. Chem. Soc., Dalton Trans.* **1997**, 3547–3551; b) C. Kim, K. Chen, J. Kim, L. Que, *J. Am. Chem. Soc.* **1997**, *119*, 5964–5965; c) K. Chen, L. Q. Jr., *Chem. Commun.* **1999**, 1375–1376.

[229] a) A. Gunay, K. H. Theopold, *Chem. Rev.* **2010**, *110*, 1060–1081; b) A. Paul, J. F. Hull, M. R. Norris, Z. Chen, D. H. Ess, J. J. Concepcion, T. J. Meyer, *Inorg. Chem.* **2011**, *50*, 1167–1169.

[230] a) M. S. Chen, M. C. White, *Science* **2007**, *318*, 783–787; b) N. A. Vermeulen, M. S. Chen, M. Christina White, *Tetrahedron* **2009**, *65*, 3078–3084; c) M. S. Chen, M. C. White, *Science* **2010**, *327*, 566–571.

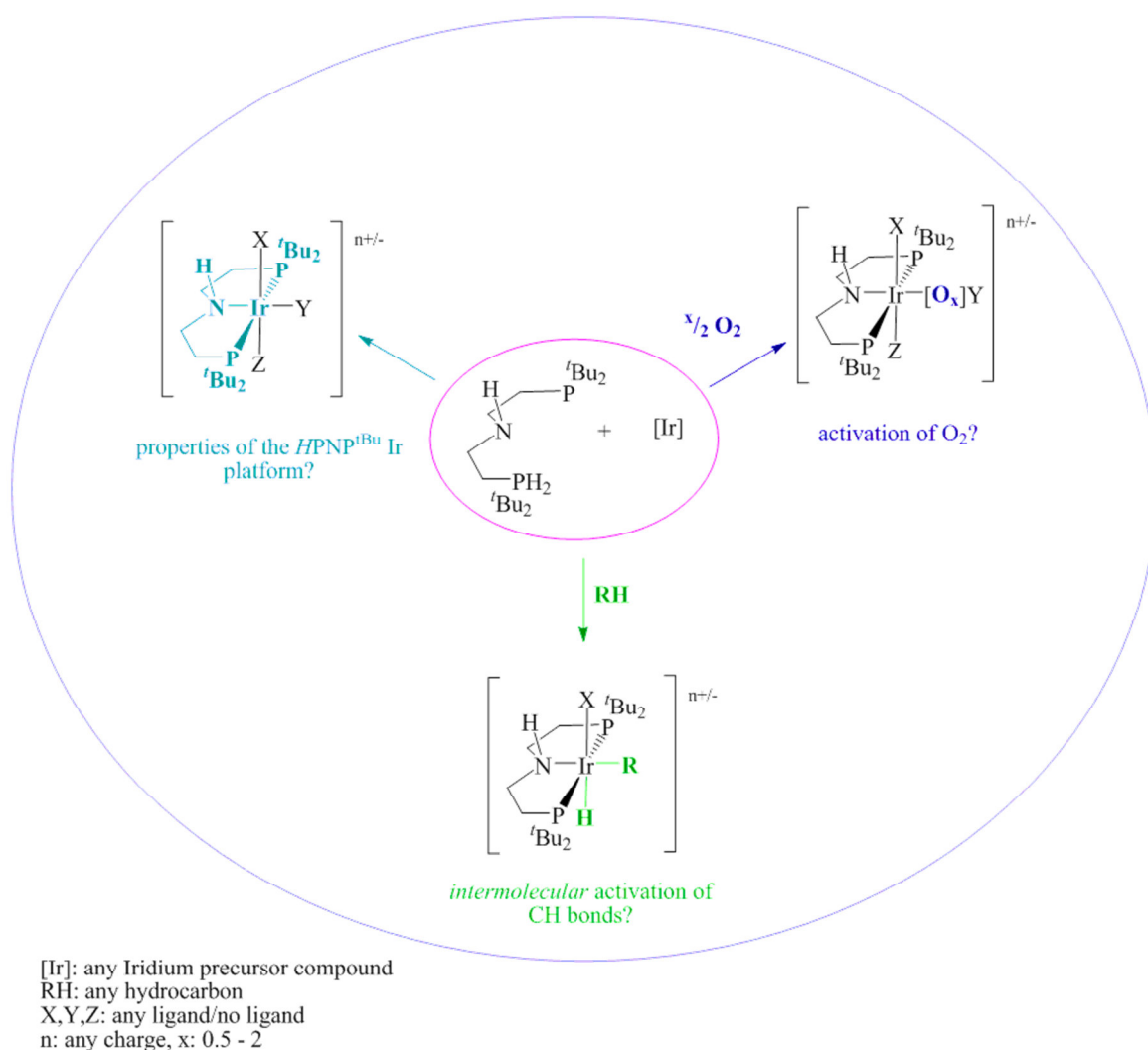
[231] a) S. S. Stahl, J. A. Labinger, J. E. Bercaw, *Angew. Chem. Int. Ed.* **1998**, *37*, 2180–2192; b) B. V. Popp, S. S. Stahl, *J. Am. Chem. Soc.* **2007**, *129*, 4410–4422; c) B. V. Popp, S. S. Stahl, *Chem. Eur. J.* **2009**, *15*, 2915–2922; d) C. C. Scarborough, A. Bergant, G. T. Sazama, I. A. Guzei, L. C. Spencer, S. S. Stahl, *Tetrahedron* **2009**, *65*, 5084–5092; e) A. N. Campbell, P. B. White, I. A. Guzei, S. S. Stahl, *J. Am. Chem. Soc.* **2010**, *132*, 15116–15119; f) M. M. Konnick, N. Decharin, B. V. Popp, S. S. Stahl, *Chem. Sci.* **2011**, *2*, 326; g) N. Decharin, S. S. Stahl, *J. Am. Chem. Soc.* **2011**, *133*, 5732–5735; h) A. N. Campbell, E. B. Meyer, S. S. Stahl, *Chem. Commun.* **2011**, 47, 10257; i) N. Decharin, S. S. Stahl, *J. Am. Chem. Soc.* **2011**, *133*, 5732–5735; j) A. E. Wendlandt, A. M. Suess, S. S. Stahl, *Angew. Chem. Int. Ed.* **2011**, *50*, 11062–11087; k) P. B. White, S. S. Stahl, *J. Am. Chem. Soc.* **2011**, *133*, 18594–18597; l) N. Decharin, B. V. Popp, S. S. Stahl, *J. Am. Chem. Soc.* **2011**, *133*, 13268–13271; m) R. I. McDonald, G. Liu, S. S. Stahl, *Chem. Rev.* **2011**, *111*, 2981–3019; n) P. Teo, Z. K. Wickens, G. Dong, R. H. Grubbs, *Org. Lett.* **2012**, *14*, 3237–3239; o) A. B. Weinstein, S. S. Stahl, *Angew. Chem. Int. Ed.* **2012**, *51*, 11505–11509; p) J. E. Redford, R. I. McDonald, M. L. Rigsby, J. D. Wiensch, S. S. Stahl, *Org. Lett.* **2012**, *14*, 1242–1245; q) Z. Lu, S. S. Stahl, *Org. Lett.* **2012**, *14*, 1234–1237; r) A. N. Campbell, S. S. Stahl, *Acc. Chem. Res.* **2012**, *45*, 851–863; s) C. Martínez, Y. Wu, A. B. Weinstein, S. S. Stahl, G. Liu, K. Muñiz, *J. Org. Chem.* **2013**, *78*, 6309–6315; t) X. Ye, P. B. White, S. S. Stahl, *J. Org. Chem.* **2013**, *78*, 2083–2090; u) D. Wang, Y. Izawa, S. S. Stahl, *J. Am. Chem. Soc.* **2014**, *136*, 9914–9917; v) T. Diao, S. S. Stahl, *Polyhedron* **2014**, na, na.

reaction type. It can be carried out via inter- or intramolecular attack of the oxy-, amino- or carbo-nucleophile in larger olefins or aryl-substituted olefins as well. The reoxidation of the Pd catalyst is executed by various stoichiometric oxidants e.g. Benzoquinone (BQ), hypervalent iodine or the substrate itself. In case of BQ it is discovered that the oxidant promotes the C-O reductive elimination of the product as well, presumably by a ‘*push*’ mechanism, involving oxidatively induced C–O bond formation.^[231v] Using 4,5-diazafluorenone as a ligand, which probably enhances back-bonding from the Pd^{II} center and thereby facilitates reductive elimination, aerobic allylic acetoxylation of several terminal olefins without other oxidants was demonstrated by *Stahl et al.*^[231e]. Mechanistic studies for this reaction are mostly consistent with a ‘*pull*’ mechanism which contains reversible C–O bond formation from an allyl-palladium(II) species and trapping of the Pd⁰ intermediate by O₂.^[231v]

A.4 Goal and Motivation

At first the aliphatic PNP platform should be investigated regarding the electronic donor properties, geometries, oxidation and spin states, potential non-innocent and cooperative behavior and the impact of these features on the reactivity.

Also of great interest in this context is to evaluate the potential activation of dioxygen and the formation of selective oxidation and oxygenation products with O₂ to gain information about potential selective reactions of the iridium pincer complexes with dioxygen and the possibility of selective oxygenation of previously activated substrates with well-priced and “green” dioxygen.



Scheme A.4-1: Fields of interest within this thesis.

Furthermore, the coordination chemistry of iridium with the ethylene-bridged, bulky PNP pincer ligand $\text{HN}(\text{CH}_2\text{CH}_2\text{P}^t\text{Bu}_2)_2$ ($\text{HPNP}^{t\text{Bu}}$) regarding CH activation should be examined. Preliminary results in case of the similarly ^iPr substituted $\text{HPNP}^{i\text{Pr}}$ ligand revealed i.a. the

formation of the vinyl complex $[\text{IrHCl}(\text{C}_8\text{H}_{13})(\text{HPNP}^{iPr})]^{[232]}$ by *intramolecular* CH activation of cyclooctene (coe). However, in favor of a potential functionalization, an *intermolecular* CH activation step is desired. The influence of the sterically more demanding (relatively to *i*Pr), neutral (\rightarrow leading to a cationic complex), Brønsted acidic (\rightarrow potentially capable of bifunctional reactivity) HPNP^{tBu} ligand toward chemoselectivity of the CH activation step should be evaluated.

Even if this is a preview it should be noted that: As the results that are presented here were discovered, *Grubbs et al.* ^[203] were publishing similar CH activation results with a related pincer system. This system was very effective, so that a catalytic functionalization could be implemented. Therefore the focus was on the illumination of parts of the reaction mechanism in more detail in case of the $\text{HN}(\text{CH}_2\text{CH}_2\text{P}^t\text{Bu}_2)_2$ platform.

Accordingly, important sections concerning the mentioned iridium PNP system, which will be discussed in the following, are (**Scheme A.4-1**): The *investigation of the iridium PNP platform, its reactivity towards oxygen and the reactivity towards CH bonds.*

[232] A. Friedrich, R. Ghosh, R. Kolb, E. Herdtweck, S. Schneider, *Organometallics* **2009**, 28, 708–718.

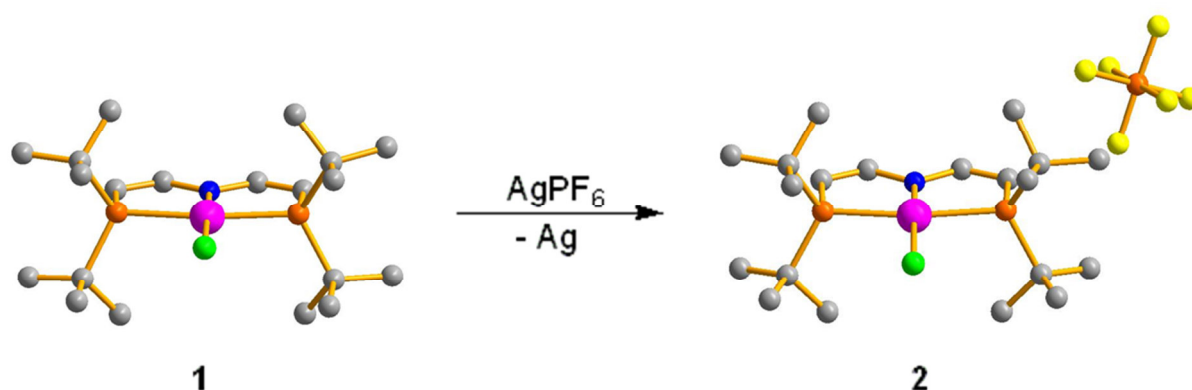
B Results and discussion

B.1 Synthesis of a square planar iridium(II) complex and oxydation of the latter to the corresponding square planar iridium(III) complex

This chapter is originated from the paper:

*Square-Planar Iridium(II) and Iridium(III) Amido Complexes
Stabilized by a PNP Pincer Ligand*

J. Meiners, M. G. Scheibel, M.-H. Lemée-Cailleau, S. A. Mason, M. B. Boeddinghaus, T. F. Fässler, E. Herdtweck, M. M. Khusniyarov, S. Schneider, *Angew. Chem.* **2011**, *123*, 8334-8337; *Angew. Chem. Int. Ed.* **2011**, *50*, 8184-8187.



B.1.1 Introduction

Coordination compounds of the precious metals are of enormous importance in homogeneous catalysis. Generally, their electronic structures favor closed-shell states, thus explaining the typical preference of two-electron (oxidative addition/reductive elimination) over one-electron redox reactions.^[233] However, the importance of the latter was more recently emphasized for platinum metal complexes, for example in radical H₂, C-H, and C-C activation reactions or catalytic oxidations.^[234,235,236,237] Nevertheless, fully characterized metalloradical complexes of these metals remain scarce.^[238] Alternatively, radical complexes with the spin density mainly located on redox non-innocent ligands have been described, such as strongly N-centered radical complexes resulting from oxidation of Rh^I and Ir^I

[233] P. J. Chirik, K. Wieghardt, *Science* **2010**, *327*, 794.

[234] a) K. J. Del Rossi, B. B. Wayland, *J. Chem. Soc., Chem. Commun.* **1986**, 1653; b) M. R. Ringenberg, S. L. Kokatam, Z. M. Heiden, T. B. Rauchfuss, *J. Am. Chem. Soc.* **2008**, *130*, 788; c) J. Wassenaar, B. de Bruin, M. A. Siegler, A. L. Spek, J. N. H. Reek, J. I. van der Vlugt, *Chem Commun.* **2010**, *46*, 1232.

[235] a) R. S. Paonessa, N. C. Thomas, J. Halpern, *J. Am. Chem. Soc.* **1985**, *107*, 4333; b) K. J. del Rossi, B. B. Wayland, *J. Am. Chem. Soc.* **1985**, *107*, 7941; c) B. B. Wayland, S. Ba, A. E. Sherry, *J. Am. Chem. Soc.* **1991**, *113*, 5305; d) K. M. Smith, R. Poli, J. N. Harvey, *Chem. Eur. J.* **2001**, *7*, 1679; e) F. F. Puschmann, H. Grützmacher, B. de Bruin, *J. Am. Chem. Soc.* **2010**, *132*, 73.

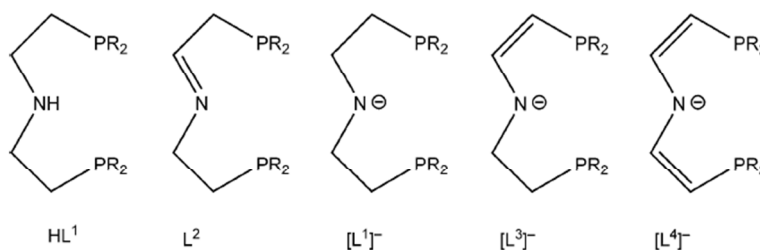
[236] K. S. Chan, X. Z. Li, W. I. Dzik, B. de Bruin, *J. Am. Chem. Soc.* **2008**, *130*, 2051.

[237] a) B. de Bruin, P. H. M. Budzelaar, A. W. Gal, *Angew. Chem. Int. Ed.* **2004**, *43*, 4142; b) M. Königsmann, N. Donati, D. Stein, H. Schönberg, J. Harmer, A. Sreekanth, H. Grützmacher, *Angew. Chem.* **2007**, *119*, 3637; *Angew. Chem. Int. Ed.* **2007**, *46*, 3567.

[238] a) K. K. Pandey, *Coord. Chem. Rev.* **1992**, *121*, 1. b) D. G. DeWitt, *Coord. Chem. Rev.* **1996**, *147*, 209; c) R. Poli, *Chem. Rev.* **1996**, *96*, 2135; d) B. de Bruin, D. G. H. Hetterscheid, A. J. J. Koekoek, H. Grützmacher, *Progr. Inorg. Chem.* **2007**, *55*, 247.

dialkylamides.^[237b,239] However, in contrast to rhodium, these iridium aminyl radicals were described as being transient intermediates. In analogy, upon oxidation of the Pd^{II} amide [PdPh(L¹)] (with R = *i*Pr), only the follow-up products [PdPh(HL¹)]⁺ and [PdPh(L²)]⁺ (R = *i*Pr) were obtained (Scheme 1).^[240]

Similarly, complexes of the platinum metals with an even number of valence electrons in high-spin configuration are extremely rare owing to the generally larger ligand field splitting of the 4d/5d metal ions compared to their 3d homologues. An exception is provided by the square-planar d⁶ disilylamido complexes [MX(L⁵)] (M = Ru, Os; X = F, Cl, I, trifluoromethanesulfonate (OTf); L⁵ = N(SiMe₂-CH₂PtBu₂)₂), which exhibit an electronic intermediate-spin configuration, in analogy to iron(II).^[241,242] However, the stronger N→M π-donation in the related dialkylamido complex [RuCl(L¹)] (R = *t*Bu) results in a low-spin ground state.^[243]



Scheme 1. PNP chelating ligands derived from HN(CH₂CH₂PR₂)₂.

These examples demonstrate the importance to rationalize the parameters that control the electronic structure and therefore the reactivity of such radical complexes and coordinatively strongly unsaturated complexes of the platinum metals. Regarding the PNP pincer ligands used in our group (Scheme 1), the dehydrogenation of one of the chelate backbone ethylene bridges to ligand L³ allows the donor properties to be fine-tuned.^[244]

Herein, we present the versatile ligand functionalization towards the novel dieneamido ligand (L⁴)₋ (R = *t*Bu; Scheme 1), which afforded the isolation of iridium(II) amido complex [IrCl(L⁴)] (**1**; R = *t*Bu). Oxidation of **1** gives diamagnetic [IrCl(L⁴)]PF₆ (**2**; R = *t*Bu)^[245], the first example of a square-planar iridium(III) complex.

[239]a) T. Büttner, J. Geier, G. Frison, J. Harmer, C. Calle, A. Schweiger, H. Schönberg, H. Grützmacher, *Science* **2005**, *307*, 235; b) P. Maire, M. Königsmann, A. Sreekanth, J. Harmer, A. Schweiger, H. Grützmacher, *J. Am. Chem. Soc.* **2006**, *128*, 6578; c) N. Donati, D. Stein, T. Büttner, H. Schönberg, J. Harmer, S. Anadaram, H. Grützmacher, *Eur. J. Inorg. Chem.* **2008**, 4691.

[240] A. Marziale, E. Herdtweck, J. Eppinger, S. Schneider, *Inorg. Chem.* **2009**, *48*, 3699.

[241]a) L. A. Watson, O. V. Ozerov, M. Pink, K. G. Caulton, *J. Am. Chem. Soc.* **2003**, *125*, 8246; b) A. Walstrom, M. Pink, N. P. Tsvetkov, H. Fan, M. Ingleson, K. G. Caulton, *J. Am. Chem. Soc.* **2005**, *127*, 16780; c) X. Yang, A. Walstrom, N. Tsvetkov, M. Pink, K. G. Caulton, *Inorg. Chem.* **2007**, *46*, 4612; c) N. P. Tsvetkov, M. Pink, J.-H. Lee, K. G. Caulton, *Eur. J. Inorg. Chem.* **2010**, 4790.

[242]a) B. W. Dale, R. J. P. Williams, C. E. Johnson, T. L. Thorp, *J. Chem. Phys.* **1968**, *49*, 3441; b) H. Geoff, G. N. La Mar, C. A. Reed, *J. Am. Chem. Soc.* **1977**, *99*, 3641; c) K. Ray, A. Begum, T. Weyhermüller, S. Piligkos, J. van Slageren, F. Neese, K. Wieghardt, *J. Am. Chem. Soc.* **2005**, *127*, 4403; d) E. J. Hawrelak, W. H. Bernskoetter, E. Lobkovsky, G. T. Yee, E. Bill, P. J. Chirik, *Inorg. Chem.* **2005**, *44*, 3103.

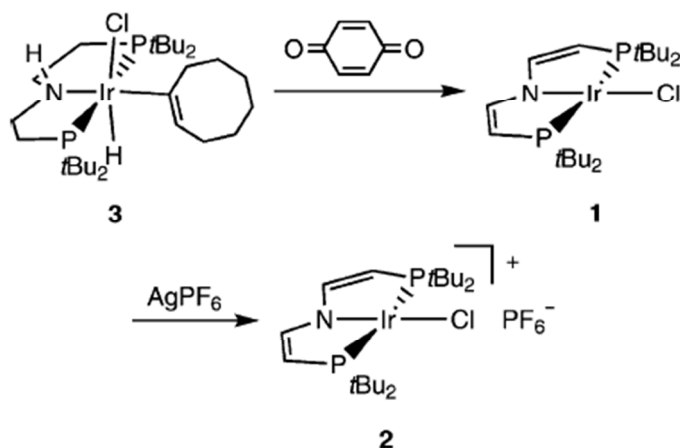
[243]a) B. Askevold, M. M. Khusniyarov, E. Herdtweck, K. Meyer, S. Schneider, *Angew. Chem.* **2010**, *122*, 7728; *Angew. Chem. Int. Ed.* **2010**, *49*, 7566; b) B. Askevold, J. T. Nieto, S. Tussupbayev, M. Diefenbach, E. Herdtweck, M. C. Holthausen, S. Schneider, *Nature Chem.*, in press (DOI:10.1038/nchem.1051).

[244] a) M. Käb, A. Friedrich, M. Drees, S. Schneider, *Angew. Chem.* **2009**, *121*, 922; *Angew. Chem. Int. Ed.* **2009**, *48*, 905; b) A. Friedrich, M. Drees, M. Käb, E. Herdtweck, S. Schneider, *Inorg. Chem.* **2010**, *49*, 5482.

[245] Complex **2** was synthesized by Markus Scheibel.

B.1.2 Results and discussion

$[\text{Ir}(\text{H})\text{Cl}(\text{C}_8\text{H}_{13})(\text{HL}^1)]$ (**3**; $\text{R} = t\text{Bu}$)^[246] can be oxidized *in situ* with benzoquinone (2.5 equiv) to give turquoise complex **1** in yields of isolated product of up to 60% (Scheme 2).^[247] A ³¹P NMR spectrum of **1** exhibits no signals. The three broad signals in the ¹H NMR spectrum are strongly paramagnetically shifted and can be assigned to the *t*Bu substituents ($\delta = 10.5$ ppm) and two sets of ligand backbone C-H protons ($\delta = -6.8, -138.2$ ppm), respectively, indicating C_{2v} symmetry on the NMR spectroscopy timescale.



Scheme 2. Synthesis of iridium complexes **1** and **2**.

The potential redox non-innocence of amido ligands has attracted considerable interest in recent years.^[237b,239,248,249] For example, radical complexes with related, chelating amido ligands, such as $[(\text{cod})\text{Ir}\{\text{N}(\text{CHC}_5\text{H}_5\text{N})(\text{CH}_2\text{C}_5\text{H}_5\text{N})\}]$ (cod = 1,5-cyclooctadiene) or $[\text{NiCl}\{\text{N}(\text{C}_6\text{MeH}_3\text{P}i\text{Pr}_2)_2\}]^+$, were reported to exhibit strongly ligand-centered spin densities.^[249c,d] Thus, resonance structures which describe **1** in terms of an iridium(II) amido or iridium(I) aminyl complex provide conceivable alternatives. Mononuclear iridium(II) complexes were frequently postulated as transient reaction intermediates. However, fully characterized examples are considerably more rare than those of rhodium(II).^[238,250] The rhombic EPR spectrum of **1** indicates a large anisotropy of the *g* tensor, suggesting a metal-centered radical (Figure 1). Hyperfine coupling with iridium is not resolved (86 K). Similar EPR parameters were reported for other iridium(II) complexes.^[250e,g] The spectroscopic results

[246] J. Meiners, A. Friedrich, E. Herdtweck, S. Schneider, *Organometallics* **2009**, *28*, 6331.

[247] For experimental, crystallographic and quantum chemical details see Supporting Information.

[248] R. G. Hicks, *Angew. Chem.* **2008**, *120*, 7503; *Angew. Chem.* **2008**, *47*, 7393.

[249] a) F. N. Penkert, T. Weyhermüller, E. Bill, P. Hildebrandt, S. Lecomte, K. Wieghardt, *J. Am. Chem. Soc.* **2000**, *122*, 9663; b) Y. Miyazato, T. Wada, J. T. Muckerman, E. Fujita, K. Tanaka, *Angew. Chem.* **2007**, *119*, 5830; *Angew. Chem. Int. Ed.* **2007**, *46*, 5728. c) D. Adhikari, S. Mossin, F. Basuli, J. C. Huffman, R. K. Szilagyí, K. Meyer, D. J. Mindiola, *J. Am. Chem. Soc.* **2008**, *130*, 3676; d) C. Tejel, M. A. Ciriano, M. P. del Rio, D. G. H. Hetterscheid, N. Tschlis i Spithas, J. M. M. Smits, B. de Bruin, *Chem. Eur. J.* **2008**, *14*, 10932.

[250] a) M. P. Garcia, M. V. Jimenez, L. A. Oro, F. J. Lahoz, P. J. Alonso, *Angew. Chem.* **1992**, *104*, 1512; *Angew. Chem. Int. Ed. Engl.* **1992**, *31*, 1527; b) A. B. Danaopoulos, G. Wilkinson, B. Hussain-Bates, M. B. Hursthouse, *J. Chem. Soc. Dalton Trans.* **1992**, 3165; c) H. Zhai, A. Bunn, B. Wayland, *Chem. Commun.* **2001**, 1294; d) B. de Bruin, T. P. J. Peters, S. Thewissen, A. N. J. Blok, J. B. M. Wilting, R. de Gelder, J. M. M. Smits, A. W. Gal, *Angew. Chem.* **2002**, *114*, 2239; *Angew. Chem. Int. Ed.* **2002**, *41*, 2135; e) A. S. Ionkin, W. J. Marshall, *Organometallics* **2004**, *23*, 6031; f) D. G. H. Hetterscheid, J. Kaiser, E. Reijerse, T. P. J. Peters, S. Thewissen, A. N. J. Blok, J. M. M. Smits, R. de Gelder, B. de Bruin, *J. Am. Chem. Soc.* **2005**, *127*, 1895; g) N. P. Tsvetkov, M. F. Laird, H. Fan, M. Pink, K. G. Caulton, *Chem. Commun.* **2009**, 4578.

are supported by DFT calculations, suggesting 67% of the spin density to be located at the metal center. The magnetic moment in the solid state (Supporting Information, Figure S1) confirms the doublet ground state of **1** ($\mu_{\text{eff}} = 2.2 \mu_{\text{B}}$; $g = 2.5$) and is in agreement with the EPR spectrum ($g_{\text{av}} = ((g_1^2 + g_2^2 + g_3^2)/3)^{1/2} = 2.41$).

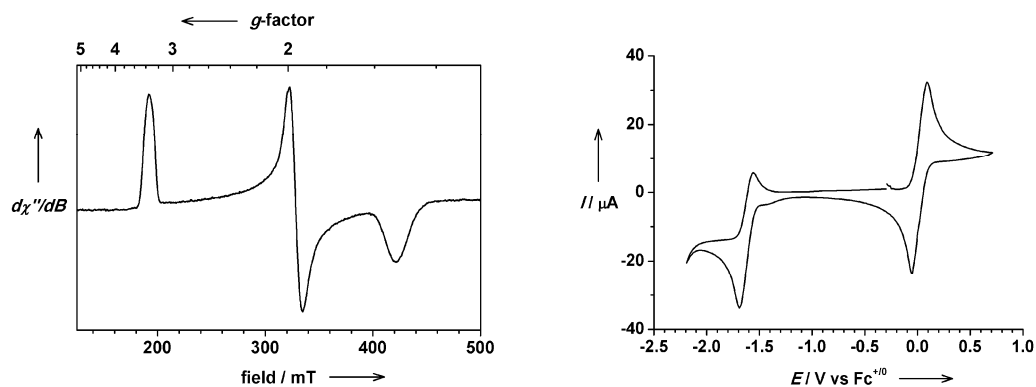
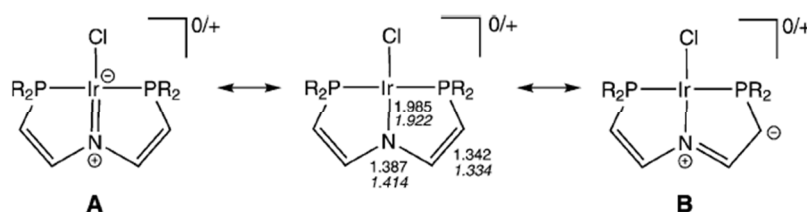


Figure 1. Left: X-Band EPR spectrum of **1** (Et₂O/Toluol glass, 86 K, freq. 8.9931 GHz, power 0.5 mW, modulation 1 mT/100 kHz). right: Cyclic voltammogram of **1** in CH₂Cl₂ at room temperature (glassy carbon electrode, 0.15 M [N*n*Bu₄]PF₆, scan rate 100 mV s⁻¹). Fc = ferrocene.

Single-crystal X-ray diffraction of **1** confirms a C_{2v}-symmetric molecular structure (Figure 2a). The metal center has a square-planar coordination geometry with an ideally linear N1-Ir-Cl1 axis. The Ir1-N1 distance (1.985(2) Å) of **1** compares well with the iridium(I)amido complex [Ir(C₂H₄)(L¹)] (R = *i*Pr; **4**; 1.99(2) Å) and is slightly shorter than in [Ir(CO)(L¹)] (R = *i*Pr; **5**; 2.035(4) Å).^[251] The planar nitrogen atom (sum of angles 360.08°) and the short C2-C3 (1.342(3) Å; **4** 1.50(3)/1.56(3) Å; **5** 1.521(9)/1.528(9) Å) and N1-C2 distances (1.387(2) Å; **4** 1.43(3)/1.48(3) Å; **5** 1.438(7)/1.464(8) Å) are in agreement with the dehydrogenation of both pincer backbone ethylene bridges and formation of the novel (L⁴)⁻ dieneamido ligand with considerable C=C and C=N double bonding contributions.



Scheme 3. Selected resonance structures and bond lengths (center) for **1** and **2**^[245] (italics).

The mass spectrum of **1** provides no indication for further hydrido ligands at the vacant coordination sites. The IR spectrum of **1** shows three very weak absorptions between 1870

[251]A. Friedrich, R. Ghosh, R. Kolb, E. Herdtweck, S. Schneider, *Organometallics* **2009**, *28*, 708.

und 1960 cm^{-1} . However, although open-shell hydrido complexes are very rare,^[252] the presence of a hypothetical iridium(IV) complex $[\text{Ir}(\text{H})_2\text{Cl}(\text{L}^4)]$ ($\text{R} = t\text{Bu}$) could not be fully excluded on the basis of these results. Interestingly, the synthesis of iridium(IV)dihydrido complexes $[\text{Ir}(\text{H})_2(\text{Cl})_2(\text{PR}_3)_2]$ ($\text{R} = i\text{Pr}$, cyclohexyl) had been reported earlier, but reevaluation of these results could not confirm their existence.^[253,254] Therefore, single crystals of **1** were also characterized by neutron diffraction (Supporting Information, Figure S4).^[247,255] The neutron-diffraction results confirm the square-planar geometry around the metal center and the absence of further hydride ligands. Furthermore, the localization of the hydrogen atoms indicates the absence of significant $\text{Ir}\cdots\text{H}_\text{C}$ interactions at the vacant coordination sites.

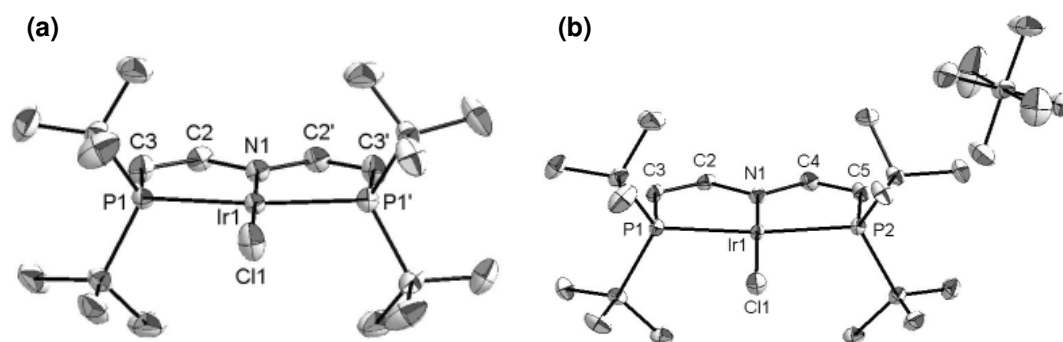


Figure 4. DIAMOND plots of the molecular structures of a) **1** and b) **2**^[245] from single crystal X-ray diffraction (ellipsoids set at 50% probability, hydrogen atoms and one THF solvent molecule in of **2** are omitted for clarity). Selected bond lengths [\AA] and angles [$^\circ$]: **1**: Ir1–Cl1 2.3390(7), Ir1–N1 1.985(2), Ir1–P1 2.3190(6), N1–C2 1.387(2), C2–C3 1.342(3); N1–Ir1–Cl1 180.0, P1–Ir1–P1' 166.22(2). **2**: Ir1–Cl1 2.2966(6), Ir1–N1 1.922(2), Ir1–P1 2.3416(6), Ir1–P2 2.3443(6), N1–C2 1.414(3), N1–C4 1.415(3), C2–C3 1.335(3), C4–C5 1.334(3); N1–Ir1–Cl1 174.93(6), P1–Ir1–P2 167.56(2).

Oxidative addition of H_2 is a typical reaction of square-planar iridium(I) complexes, but was not observed for iridium(II) compound **1** over a prolonged period of time. The cyclic voltamogram of **1** (Figure 1; Supporting Information, Figure S2) exhibits a reduction wave at $E_{1/2} = -1.61\text{ V}$ (vs. $\text{Fe}(\text{C}_5\text{H}_5)_2/\text{Fe}(\text{C}_5\text{H}_5)_2^+$) that is quasireversible only at high scan rates ($>800\text{ mVs}^{-1}$). Accordingly, all efforts to isolate the corresponding iridium(I) complex $[\text{IrCl}(\text{L}^4)]^-$ ($\text{R} = t\text{Bu}$) were unsuccessful to date. However, reversible oxidation at $E_{1/2} = +0.02\text{ V}$ (100 mVs^{-1}) is observed, even at low scan rates. This result is particularly surprising, as the chemical

[252] R. Poli in *Recent Advances in Hydride Chemistry* (Hrsg.: M. Peruzzini, R. Poli), Elsevier, Amsterdam, **2001**, S. 139.

[253] a) P. Mura, *J. Am. Chem. Soc.* **1986**, *108*, 351; b) P. Mura, A. Segre, *Angew. Chem.* **1986**, *98*, 453; *Angew. Chem. Int. Ed. Engl.* **1986**, *25*, 460.

[254] a) A. Albinati, V. I. Bakmutov, K. G. Caulton, E. Clot, J. Eckert, O. Eisenstein, D. G. Gusev, V. V. Grushin, B. E. Hauger, W. T. Klooster, T. F. Koetzle, R. K. McMullan, T. J. O'Loughlin, M. Pelissier, J. S. Ricci, M. P. Sigalas, A. B. Vymenits, *J. Am. Chem. Soc.* **1993**, *115*, 7300; b) D. Capitani, P. Mura, *Inorg. Chim. Acta* **1997**, *258*, 169.

[255] Owing to the small crystal size ($1 \times 1 \times 0.5\text{ mm}^3$), the neutron diffraction investigation was carried out on VIVALDI, the thermal neutron Laue diffractometer at the ILL: a) C. Wilkinson, J.A. Cowan, D. A. A. Myles, F. Cipriani, G. J. McIntyre, *Neutron News* **2002**, *13*, 37; b) G. J. McIntyre, M.-H. Lemée-Cailleau, C. Wilkinson, *Phys. B* **2006**, *385-386*, 1055-

oxidation of the related complex $[\text{Ir}^{\text{II}}\text{Cl}\{\text{N}(\text{SiMe}_2\text{CH}_2\text{PtBu}_2)_2\}]$ resulted in the isolation of subsequent products after *PtBu* cyclometalation.^[250g]

In contrast, the reversible electrochemical oxidation of **1** is also observed by chemical redox titration, which can be monitored by ¹H NMR spectroscopy: An equimolar mixture of **1** and $[\text{Fe}(\text{C}_5\text{H}_5)_2]\text{PF}_6$ in CD_2Cl_2 exhibits a broad signal at $\delta=7.4$ ppm, which is assignable to one averaged signal for the *tBu* substituents of $[\text{IrCl}(\text{L}^4)]$ ($\text{R}=\textit{tBu}$; $\delta_{\text{Bu}}=10.7$ ppm) and $[\text{IrCl}(\text{L}^4)]^+$ ($\delta_{\text{Bu}}=2.3$ ppm; see below), which form a fast redox equilibrium on the NMR timescale (Supporting Information, Figure S3). From this solution, **1** can be recovered without decomposition almost quantitatively. Reaction of **1** with AgPF_6 enables the isolation of the primary oxidation product, $[\text{IrCl}(\text{L}^4)]\text{PF}_6$ (**2**)^[245] in yields of about 40% (Scheme 2). Compound **2** is thermally labile, and complete decomposition to several products is observed after about 4 h in solution at room temperature. The sharp NMR signals for **2** point towards a diamagnetic, C_{2v} -symmetric cation. The diamagnetism of **2** is unexpected, as square-planar d^6 complexes with a formal 14-valence-electron count typically exhibit an electronic intermediate-spin ($S=1$) configuration.^[243a]

The molecular structure of **2**^[245] in the crystalline state confirms the square-planar geometry (Figure 2b). The steric bulk of the *tBu* substituents or the planarization of the ligand backbone possibly contribute to the stabilization of squareplanar instead of saw-horse coordination, which is generally observed for four-coordinate iridium(III).^[256] However, DFT calculations predict a square-planar structure for the less sterically encumbered model complex $[\text{IrCl}(\text{L}^4)]^+$ ($\text{R}=\text{Me}$; **2**^{Me}), as well (see below). The structural parameters of **2** and **1** in the crystalline state are very similar. As the most striking difference, the Ir1-N1 bond shortens considerably upon oxidation (**2** 1.922(2), **1** 1.985(2)). The comparison with the Ir1-C11 bond lengths (**2** 2.2966(6), **1** 2.3390(7)) suggests that the Ir-N bond contraction cannot only be attributed to the smaller ionic radius of iridium(III). Furthermore, significant elongation of the pincer backbone N-C bonds and slight contraction of the C-C bonds are also observed (Scheme 3). These structural features indicate stronger weighting of mesomeric structure **A** for **2** compared with structure **B**, which is tantamount to enhanced $\text{N}\rightarrow\text{Ir}$ π donation. This qualitative bonding picture was further substantiated by electronic structure calculations using DFT methods for the model complexes $[\text{IrCl}(\text{L}^4)]$ ($\text{R}=\text{Me}$; **1**^{Me}) and $[\text{IrCl}(\text{L}_4)]^+$ ($\text{R}=\text{Me}$; **2**^{Me}). The optimized geometries of **1**^{Me} (doublet state) and **2**^{Me} (singlet state) are in good agreement with the crystallographic results for the respective $\{\text{Ir}(\text{L}^4)\}^{0/+}$ fragments.^[247] **2**^{Me} (triplet state) is found at higher energies with respect to the singlet state by around 4.1 kcal mol⁻¹ (B3LYP) or 9.3 kcal mol⁻¹ (BP). Furthermore, the Ir-N bond length is considerably

[256] G. Ujaque, A. C. Cooper, F. Maseras, O. Eisenstein, K. G. Caulton, *J. Am. Chem. Soc.* **1998**, *120*, 361.

overestimated in the triplet state ($\Delta d_{\text{Ir-N}} = 0.08 \text{ \AA}$). The structural trends are easily explained by consideration of the frontier orbitals. The SOMO of **1** exhibits considerable N-Ir π^* character. Therefore, removal of this electron by oxidation towards **2** in the singlet state effects reinforcement of the N-Ir π bond (Figure 3). Therefore, the unusual electronic low-spin configuration of **2** is attributed to strong N \rightarrow Ir π donation as in the case of $[\text{RuCl}(\text{L}^1)]$ (R =

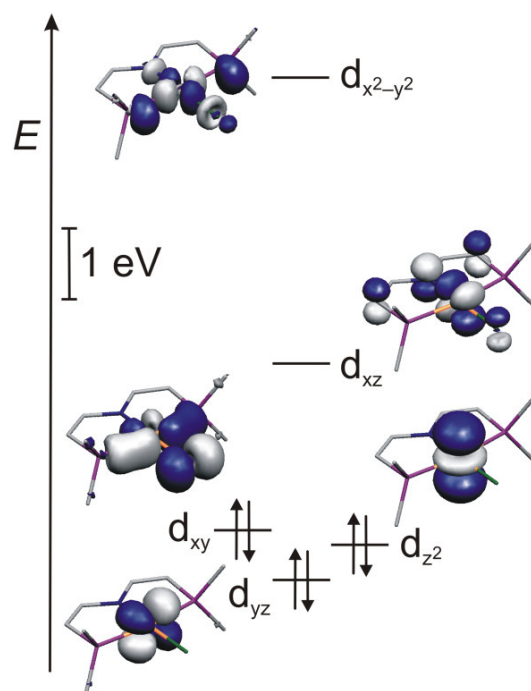


Figure 3. Metal centred Kohn-Sham frontier orbitals of 2^{Me} in the singlet state from spin-unrestricted ZORA-B3LYP-DFT calculations (the z-axis is perpendicular to the $\{\text{Ir}(\text{L}4)\}$ plane).

$t\text{Bu}$).^[243] While the π -donor properties of the L^1 ligand should be weakened by dehydrogenation to L^4 , this effect is counterbalanced by the cationic charge and the change from a 4d to a 5d metal, which should strengthen M-N bonding.^[257]

In conclusion, simple oxidative ligand functionalization of the PNP chelate ligand framework allows for the versatile isolation of unusual square-planar d^7 and d^6 iridium complexes. Surprisingly, the square-planar d^8 complex of the redox series, $[\text{IrCl}(\text{L}^4)]^-$ (R = $t\text{Bu}$), was not stable under the experimental electrochemical and synthetic conditions. Compared to the ethylene-bridged PNP amido ligand, the $(\text{L}^4)^-$ pincer is characterized by higher conformational rigidity but electronic flexibility: While the radical complexes from the oxidation of iridium(I) dialkylamides are generally transient species, the metalloradical **1** and

[257] The valence tautomeric description of diamagnetic **2** resulting from ligand centered oxidation of **1** and antiferromagnetic coupling of the ligand with the metal centre ($(\text{L}^4)^{\cdot-}/\text{Ir}^{\text{II}}$) cannot be fully excluded. However, a broken-symmetry solution was not found by DFT and the present experimental results (for example, the Ir-N bond lengths) do not point towards such an electronic structure. Thus, we prefer the more simple description as $(\text{L}^4)^{\cdot-}/\text{Ir}^{\text{III}}$ (see also: M. Gallagher, N. L. Wieder, V. K. Dioumaev, P. J. Carroll, D. H. Berry, *Organometallics* **2010**, *29*, 591).

the oxidation product **2** are sufficiently stable to be easily isolated.^[239,245,73] Thus the new dieneamido ligand opens up the opportunity to examine an unusual one-electron reactivity of iridium.

B.1.3 Experimental Section

B.1.3.1 Materials and synthetic methods

All experiments were carried out under an atmosphere of argon using Schlenk and glove-box techniques. Solvents were dried over Na/benzophenone/tetraglyme (benzene) and Na/benzophenone (THF, toluene), distilled under argon and deoxygenated prior to use. Pentanes and CH₂Cl₂ were dried by passing through columns packed with activated alumina. Deuterated solvents were obtained from Euriso-Top GmbH, dried over Na/K (C₆D₆) or CaH₂ (CD₂Cl₂), distilled by trap-to-trap transfer *in vacuo*, and degassed by three freeze-pump-thaw cycles. AgPF₆ (ABCR) and [FeCp₂]PF₆ (Acros) were used as purchased. 1,4-Benzoquinone (Merck) was sublimed in prior to use. [IrCl(COE)₂]₂ and (HPNP)^{tBu} were prepared according to published procedures.^[258,246]

B.1.3.2 Analytical methods

Elemental analyses were obtained from the Microanalytical Laboratory of Technische Universität München. NMR spectra were recorded on a Bruker Avance III 400 spectrometer and were calibrated to the residual proton resonance of the solvent (CHDCl₂: δH = 5.32; C₆HD₅: δH = 7.16 ppm). ³¹P NMR chemical shifts are reported relative to external phosphoric acid (δP = 0.0 ppm). Signal multiplicities are abbreviated as: s (singlet), d (doublet), t (triplet), q (quartet), m (multiplet), br (broad). The mass spectrometry was performed with a Finnigan-MAT 90 mass spectrometer. EPR spectra were recorded on a JEOL CW spectrometer JESFA200 equipped with an X-band Gunn diode oscillator bridge, a cylindrical mode cavity, and a helium cryostat. Cyclic voltammograms were recorded with CompactStat instrument from Ivium Technologies, a platinum wire counter electrode, a platinum wire pseudo-reference electrode, and a glassy carbon working electrode. Ferrocene/ferrocenium couple was used as an internal standard. Temperature-dependent magnetic susceptibility data were recorded on an MPMS XL Quantum Design SQUID magnetometer in the temperature range of 5 – 300 K. The experimental magnetic susceptibility data were corrected for underlying diamagnetism and temperature-independent paramagnetism (TIP). The program JulX v.1.5 was used to fit experimental data.^[259]

[258] A. L. Onderlinden, A. van der Ent, *Inorg. Chim. Acta* **1972**, 6, 420.

[259] E. Bill, *JulX version 1.5*, MPI for Bioinorganic Chemistry, Mülheim an der Ruhr, Germany, **2008**.

B.1.3.3 Syntheses

B.1.3.3.1 [IrCl{N(C₂H₂P^tBu₂)₂}] (1):

An orange solution of (HPNP)^{tBu} (489 mg; 1.36 mmol) and [Ir(COE)₂Cl]₂ (596 mg; 665 μmol) in THF (25 mL) is stirred for 5 minutes at r.t. A solution of 1,4-benzoquinone (376 mg; 3.48 mmol) in THF (5 ml) is added and the resulting dark green reaction mixture is stirred for 16 hrs at r.t. The solvent is removed *in vacuo* and the residue is extracted with toluene/pentanes 1:1 (3 x 10 mL). The solvent is concentrated *in vacuo*. Crystallization from the saturated solution at -40 °C gives moderately air-sensitive **1** as blue-green crystals (Yield: 318 mg; 544 μmol; 41 %). Anal. calcd. for C₂₀H₄₀ClIrNP₂ (584.16): C, 41.12; H, 6.90; N, 2.40. Found: C, 41.09; H, 7.11; N, 2.44. NMR (C₆D₆, [ppm]) ¹H NMR (400.13 MHz, 20°C): δ = -138.17 (br, 2 H, 2 CH), -6.77 (br, 2 H, 2 CH), 10.45 (br, 36H, 4 × C(CH₃)₃). No signal was found by ³¹P NMR spectroscopy. FAB-MS: m/z = 584.1 ([M]⁺, 100 %), 528.1 ([M - CH₂CMe₂]⁺, 39 %), 472.0 ([M - 2 CH₂CMe₂]⁺, 43 %).

B.1.3.3.2 [IrCl{N(C₂H₂P^tBu₂)₂}]PF₆ (2)^[245]:

A mixture of **1** (11.3 mg; 19.3 μmol) and AgPF₆ (4.9 mg; 19.3 μmol) was dissolved in cold THF (0.5 mL) and stirred for 5 minutes at -60 °C. The solvent is removed *in vacuo*, the residue is washed with pentanes (3 x 0.5 mL), rapidly extracted with THF (3 x 1 mL) at r.t. and filtered into a cooled flask at -60 °C. After removal of the solvent, the residue is washed with toluene (3 x 0.5 mL) and dried *in vacuo*. The product is isolated as a temperature sensitive black powder (Yield: 5.5 mg; 7.5 μmol; 39%). NMR (CD₂Cl₂, [ppm]) ¹H NMR (400.13 MHz, 20°C): δ = 1.8 (t, ³J_{HP} = 7 Hz, 2H, NCHCHP), 2.34 (A₁₈XX'A'₁₈, N | ³J(H,P) + ⁵J(H,P) | = 7.8 Hz, 36H, CH₃), 4.70 (AMXX', N = | ²J(H,P) + ⁴J(H,P) | = 16.3 Hz, ³J(H,H) = 5.7 Hz, 2H, NCHCHP). ³¹P NMR (101.25 MHz, 20°C): δ = 7.8 (s, 2P), -145.0 (q, ¹J_{PF} = 711 Hz, 1P, PF₆). Anal. calcd. for C₂₀H₄₀ClF₆IrNP₃ × 0.2 THF (729.12): C, 33.60; H, 5.64; N, 1.88. Found: C, 34.08; H, 5.88; N, 1.78. THF could not be fully removed by drying over long time without partial decomposition of the sample. However, the amount of THF correlates with the ¹H NMR spectrum.

B.1.3.3.3 Redox equilibrium of **1** with [FeCp₂]PF₆:

A mixture of 4.0 mg (6.8 μmol) [IrCl{N(C₂H₂P^tBu₂)₂}] (**1**) and 2.3 mg (6.9 μmol) [FeCp₂]PF₆ is dissolved in 0.5 ml of CD₂Cl₂ in a J-Young NMR tube. The solution turns from violet-blue to green. ¹H-NMR (Figure S3): δ = 7.36 (br, PCCH₃), 18.62 (br, Fe(C₅H₅)). No signal was observed by ³¹P NMR spectroscopy. The molar ratios of **1** (x_{Ir(II)} = [Ir^{II}]/([Ir^{II}] + [Ir^{III}]) = 0.60)

and **2** ($x_{\text{Ir(III)}} = [\text{Ir}^{\text{III}}]/([\text{Ir}^{\text{II}}]+[\text{Ir}^{\text{III}}]) = 0.40$) can be calculated from the averaged *t*Bu chemical shift ($\delta_{\text{ave}} = 7.36$ ppm) and the chemical shifts of pure **1** ($\delta_{\text{Ir(II)}} = 10.74$ ppm) and **2** ($\delta_{\text{Ir(III)}} = 2.34$ ppm) applying:

$$\delta_{\text{ave}} = \delta_{\text{Ir(II)}}x_{\text{Ir(II)}} + \delta_{\text{Ir(III)}}x_{\text{Ir(III)}} \quad (\text{eq. 1})$$

$$x_{\text{Ir(II)}} + x_{\text{Ir(III)}} = 1 \quad (\text{eq. 2})$$

Molar ratios of $x_{\text{Ir(II)}} = 0.60$ and $x_{\text{Ir(III)}} = 0.40$ are also predicted for this experiment from the Nernst equation using the limiting potential at small scan rates ($E_{\text{Ir(II)/Ir(III)}}^0 = +0.02$ V vs. $\text{FeCp}_2/\text{FeCp}_2^+$) with $[\text{Fe}^{\text{III}}] = [\text{Ir}^{\text{II}}]$ and $[\text{Ir}^{\text{III}}] = [\text{Fe}^{\text{II}}]$:

$$0.059 \cdot \log([\text{Fe}^{\text{III}}]/[\text{Fe}^{\text{II}}]) = +0.02\text{V} + 0.059 \cdot \log([\text{Ir}^{\text{III}}]/[\text{Ir}^{\text{II}}]) \quad (\text{eq. 3})$$

B.1.3.3.4 Recovery of **1** from the redox equilibrium with $[\text{FeCp}_2]\text{PF}_6$:

1 (46.9 mg; 80.3 μmol) and $[\text{FeCp}_2]\text{PF}_6$ (25.5 mg; 77.0 μmol) are dissolved in CH_2Cl_2 (10 mL) and stirred for 30 min at r.t. The green solution is evaporated until the onset of $[\text{FeCp}_2]\text{PF}_6$ precipitation which is completed by addition of pentanes. The dark solid is washed (3 x 3 ml) with pentanes and dried *in vacuo* and identified as $[\text{FeCp}_2]\text{PF}_6$ by ^1H NMR spectroscopy (CD_2Cl_2 , 400.13 MHz: $\delta[\text{ppm}] = 33.24$ (br)). The combined green filtrates are reduced to dryness and the remaining dark solid is dried *in vacuo* (Yield: 43.6 mg; 74.6 μmol ; 93 %). The product was identified as **1** by ^1H NMR spectroscopy.

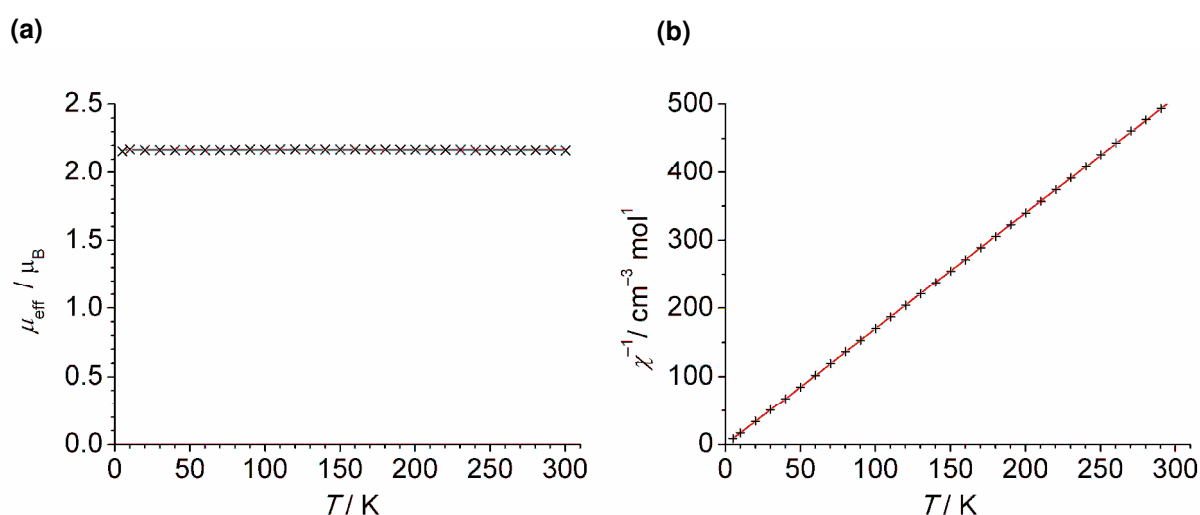


Figure S1. Temperature dependence of the effective magnetic moment μ_{eff} (a) and the reciprocal molar magnetic susceptibility χ^{-1} (b) of a microcrystalline sample of **1** recorded at 0.1 T. The solid lines in red represent the best fit obtained with $S = 1/2$, $g = 2.50$, $\text{TIP} = 2.74 \times 10^{-4} \text{ cm}^3 \text{mol}^{-1}$.

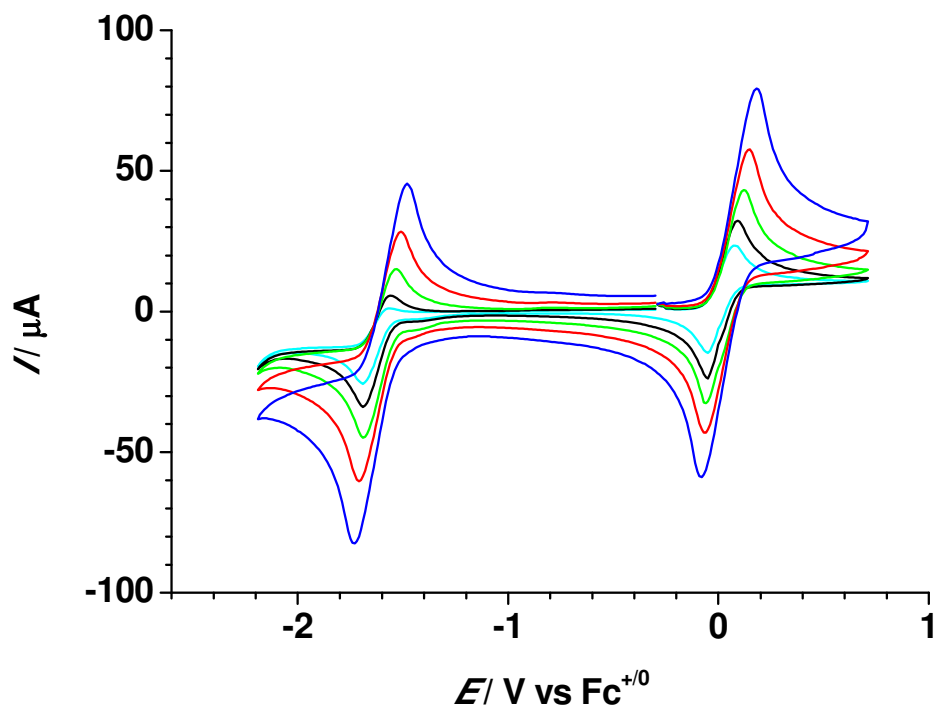


Figure S2. Cyclic voltammograms (room temperature, CH_2Cl_2 , glassy carbon working electrode, 0.15 M $[\text{NnBu}_4]\text{PF}_6$) of **1** at different scan rates: 800 (blue), 400 (red), 200 (green), 100 (black), and 50 (turquoise) mV s^{-1} .

scan rate [mV s^{-1}]	$E_{1/2}^1$ [V]	$ I_a^1 / I_c^1 $	$E_{1/2}^2$ [V]	$ I_a^2 / I_c^2 $
800	-1.61	1.0	0.05	0.9
400	-1.61	1.2	0.05	1.0
200	-1.61	1.3	0.03	1.0
100	-1.63	1.5	0.02	1.0
50	-1.63	1.7	0.02	1.0

Table S1. Electrochemical data for **1** from cyclic voltammetry (vs. $\text{FeCp}_2/\text{FeCp}_2^+$) at room temperature (conditions c.f. Figure S1, $E_{1/2}$: half wave potential; I_a / I_c : anodic/cathodic peak currents)

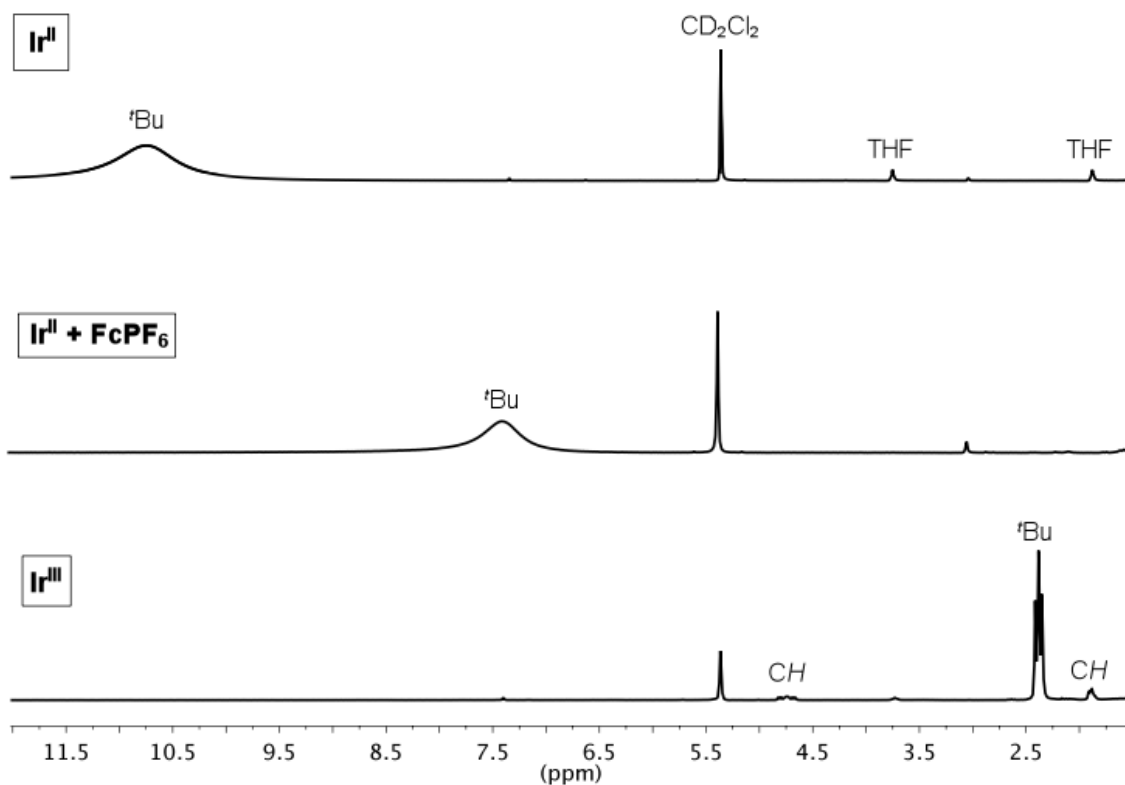


Figure S3. Comparison of the ^1H NMR spectra (CD_2Cl_2) of **1** (top) and **2** (bottom) with an equimolar mixture of **1** and $[\text{Fe}(\text{Cp})_2]\text{PF}_6$ (middle) as described above.

B.1.4 Crystallographic details

B.1.4.1 X-ray diffraction studies

Preliminary examination and data collection were carried out on an area detecting system (APEX II, κ -CCD) at the window of a rotating anode (Bruker AXS, FR591) and graphite monochromated MoK_α radiation ($\lambda = 0.71073 \text{ \AA}$). Raw data were corrected for Lorentz, polarization, and, arising from the scaling procedure, for latent decay and absorption effects. The structures were solved by a combination of direct methods and difference Fourier syntheses. All non-hydrogen atoms were refined with anisotropic displacement parameters. Methyl hydrogen atoms were refined as part of rigid rotating groups. All other hydrogen atoms were placed in calculated positions and refined using a riding model. Full-matrix least-squares refinements were carried out by minimizing $\sum w(F_o^2 - F_c^2)^2$ with SHELXL-97 weighting scheme. The final residual electron density maps showed no remarkable features. Neutral atom scattering factors for all atoms and anomalous dispersion corrections for the non-hydrogen atoms were taken from *International Tables for Crystallography*.^[260]

[260] a) APEX suite of crystallographic software. APEX2 Version 2008.4. Bruker AXS Inc., Madison, Wisconsin, USA, 2008; b) SAINT, Version 7.56a and SADABS Version 2008/1. Bruker AXS Inc., Madison, Wisconsin, USA, 2008; c) A. Altomare, G. Cascarano, C. Giacovazzo, A. Guagliardi, M. C. Burla, G. Polidori, M. Camalli, *SIR92*, *J. Appl. Crystallogr.* **1994**, *27*, 435; d) International Tables for Crystallography, vol. C, Tables 6.1.1.4 (pp. 500), 4.2.6.8 (pp. 219), and 4.2.4.2 (pp. 193), (Ed.: A. J. C. Wilson), Kluwer Academic Publishers, Dordrecht, The Netherlands, 1992; e) G. M. Sheldrick, *SHELXL-97*, University of Göttingen, Göttingen, Germany, 1998; f) A. L. Spek, *PLATON*, A Multipurpose Crystallographic Tool, Utrecht University, Utrecht, The Netherlands, 2008; g) L. J. Farrugia, *WinGX* (Version 1.70.01 January 2005), *J. Appl. Crystallogr.* **1999**, *32*, 837.

Crystallographic data (excluding structure factors) for the structures obtained by X-ray diffraction reported in this paper have been deposited with the Cambridge Crystallographic Data Centre as supplementary publication no. CCDC-822068 (**1**) and CCDC-822070 (**2**). Copies of the data can be obtained free of charge on application to CCDC, 12 Union Road, Cambridge CB2 1EZ, UK (fax: (+44)1223-336-033; e-mail: deposit@ccdc.cam.ac.uk). Crystallographic data are presented in Table S2.

Table S2. Crystallographic Data for **1** and **2**.

	1	2
Formula	C ₂₀ H ₄₀ ClIrNP ₂	C ₂₀ H ₄₀ ClIrNP ₂ , C ₄ H ₈ O, PF ₆
Fw	584.14	801.21
Color / habit	blue / prism	red-brown / fragment
Crystal dimensions (mm ³)	0.13 × 0.15 × 0.64	0.18 × 0.25 × 0.38
Crystal system	monoclinic	monoclinic
Space Group	<i>P2/c</i> (no. 13)	<i>P2₁/n</i> (no. 14)
<i>a</i> (Å)	11.4939(5)	14.5723(4)
<i>b</i> (Å)	8.5651(4)	14.7565(5)
<i>c</i> (Å)	13.5064(6)	15.6793(5)
β (°)	113.325(1)	109.7116(15)
<i>V</i> (Å ³)	1220.99(10)	3174.05(17)
<i>Z</i>	2	4
<i>T</i> (K)	173	123
<i>D</i> _{calcd} (g cm ⁻³)	1.589	1.677
μ (mm ⁻¹)	5.712	4.496
F(000)	582	1600
θ Range (°)	2.38 – 25.33	1.65 – 25.38
Index ranges (<i>h</i> , <i>k</i> , <i>l</i>)	-12 – 11; ± 10 ; ± 16	± 17 ; ± 17 ; ± 18
No. of rflns. collected	48957	80345
No. of indep. rflns. / <i>R</i> _{int}	2155 / 0.042	5807 / 0.037
No. of obsd. rflns. [<i>I</i> _o > 2σ(<i>I</i> _o)]	2079	5382
No. of data/restraints/params	2155 / 0 / 121	5807 / 0 / 346
<i>R</i> ₁ / <i>wR</i> ₂ [<i>I</i> _o > 2σ(<i>I</i> _o)] ^a	0.0116 / 0.0278	0.0147 / 0.0324
<i>R</i> ₁ / <i>wR</i> ₂ (all data) ^a	0.0127 / 0.0297	0.0172 / 0.0333
GOF (on <i>F</i> ²) ^a	1.127	1.047
Largest diff. peak and hole (e Å ⁻³)	0.58 / -0.62	0.57 / -0.45

$${}^aR_1 = \Sigma(|F_o| - |F_c|) / \Sigma|F_o|; wR_2 = \{\Sigma[w(F_o^2 - F_c^2)^2] / \Sigma[w(F_o^2)^2]\}^{1/2}; GOF = \{\Sigma[w(F_o^2 - F_c^2)^2] / (n - p)\}^{1/2}$$

B.1.4.2 Neutron diffraction study of 1

General method: The neutron diffraction experiment was carried out with the Laue thermal-neutron diffractometer VIVALDI, located on the H22 thermal guide of the High Flux Reactor of the Institut Laue-Langevin (Grenoble, France). With its quasi-white wavelength bandwidth (0.8 to 5 Å), this instrument gives the opportunity to collect good quality neutron diffraction data even when the sample size is small, here 0.5 mm³. The sample was mounted in an orange cryostat and cooled to 174 K. To obtain good statistics and an adequate redundancy of reflections, it was necessary to collect 12 images, separated by 15° rotations around the φ vertical axis (perpendicular to the incident neutron beam), allowing a coverage of reciprocal space up to $d_{\min} = 0.66$ Å with a wavelength bandwidth of 0.8 – 5 Å. The data reduction was done with an adapted version CCP4 Laue suite^[261] providing a complete intensity file with 7375 unique reflections. After orientation refinement, reflections were indexed with the LAUEGEN program^[261a,262] and then integrated with ARGONNE_BOXES software.^[263] To take into account the incident beam wavelength distribution, normalization to a common wavelength was made, with the program LNORM.^[264] An empirical absorption correction was applied via the wavelength normalization process.

Table S3. Neutron diffraction data of **1**.

1	
Formula	C ₂₀ H ₄₀ ClIrNP ₂
Fw	584.14
Color / habit	Blue / prism
Crystal dimensions (mm ³)	0.50 × 1.00 × 1.04
Crystal system	monoclinic
Space Group	P2/c (no. 13)
<i>a</i> (Å)	11.4939(5) ^a
<i>b</i> (Å)	8.5651(4) ^a
<i>c</i> (Å)	13.5064(6) ^a
β (°)	113.325(1) ^a
<i>V</i> (Å ³)	1220.99(10) ^a

[261] a) J. W. Campbell, *J. Appl. Crystallogr.* **1995**, 28, 228; b) J. R. Helliwell, J. Habash, D. W. J. Cruickshank, M. M. Harding, T. J. Greenhough, J. W. Campbell, I. J. Clifton, M. Elder, P. A. Machin, M. Z. Papiz, S. Zurek, *J. Appl. Crystallogr.* **1989**, 22, 483.

[262] J. W. Campbell, Q. Hao, M. M. Harding, N. D. Nguti, C. Wilkinson, *J. Appl. Crystallogr.* **1998**, 31, 496.

[263] C. Wilkinson, H. W. Khamis, R. F. D. Stansfield, G. J. J. McIntyre, *Appl. Crystallogr.* **1988**, 21, 471.

[264] J. W. Campbell, J. Habash, J. R. Helliwell, K. Moffat, *Inf. Q. Protein Crystallogr.* **1986**, 18, 23.

Z	2
T (K)	173
D_{calcd} (g cm^{-3})	1.589
$F(000)$	582
Normalization wavelength range	0.8 – 2.3 Å
Index ranges (h, k, l)	-10 – 11; -10 – 9; ± 16
No. of rflns. collected	7375
No. of indep. rflns. / R_{int}	1498 / 0.147
No. of obsd. rflns. [$I_o > 2\sigma(I_o)$]	1298
No. of data/restraints/params	1498 / 0 / 295
R_1/wR_2 [$I_o > 2\sigma(I_o)$] ^b	0.0742 / 0.1804
R_1/wR_2 (all data) ^b	0.0877 / 0.1895
GOF (on F^2) ^b	1.160
Largest diff. peak and hole (fm)	0.87 / -0.53

^aThe unit cell dimensions were taken from the X-ray experiment.

^b $R_1 = \Sigma(|F_o| - |F_c|) / \Sigma|F_o|$; $wR_2 = \{\Sigma[w(F_o^2 - F_c^2)^2] / \Sigma[w(F_o^2)^2]\}^{1/2}$; $GOF = \{\Sigma[w(F_o^2 - F_c^2)^2] / (n - p)\}^{1/2}$

Details: Crystal of **1** were mounted on the vertical axis of the ILL VIVALDI Laue diffractometer with cylindrical neutron-sensitive image-plate detector, 4000 horizontal pixels, 2000 vertical pixels, subtending $\pm 144^\circ$ horizontal, $\pm 56^\circ$ vertical. Pixel size 200 x 200 μm^2 . Successive images were collected, each separated by 12-15° rotation around the vertical axis perpendicular to the neutron incident beam. Crystallographic data are presented in Table S3. The unit cell dimensions were taken from the X-ray experiment. The data has been deposited with the Cambridge Crystallographic Data Centre as supplementary publication no. CCDC-822069.

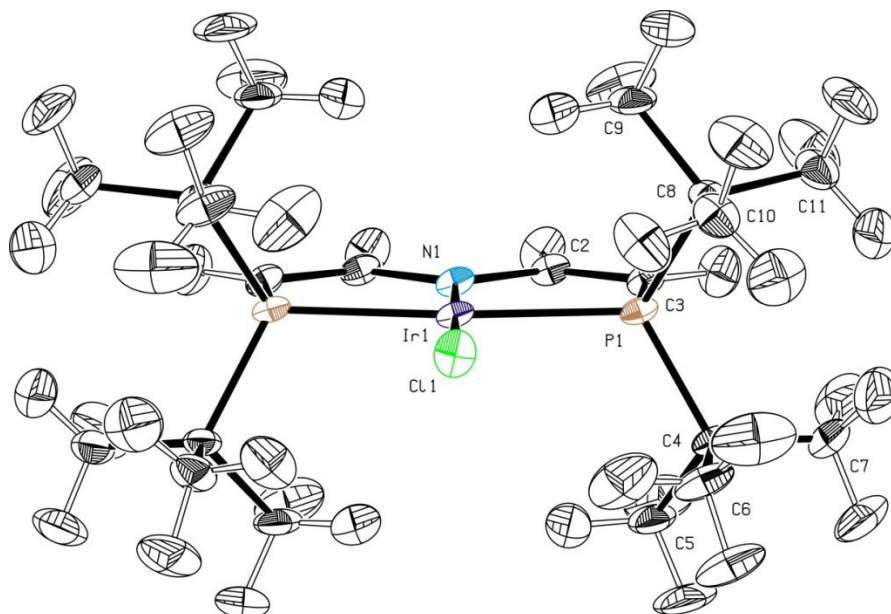


Figure S4. Molecular structure of **1** from single crystal neutron diffraction. Thermal ellipsoids are drawn at the 30 % probability level.

Table S4. Comparison of the molecular structures of **1** derived by single-crystal X-ray diffraction and neutron diffraction.

	1	
	<i>X-ray diffraction</i>	<i>Neutron diffraction</i>
Ir1–N1 [Å]	1.985(2)	1.975(2)
Ir1–C11 [Å]	2.3390(7)	2.340(2)
Ir1–P1 [Å]	2.3190(6)	2.320(3)
N1–C2 [Å]	1.387(2)	1.389(2)
C2=C3 [Å]	1.342(3)	1.348(4)

B.1.5 Computational examinations

B.1.5.1 Methods

The program package ORCA 2.7 revision 0 was used for all calculations.^[265] The geometries for the truncated models, where *t*-Bu-groups were replaced by Me-groups, were fully optimized by the spin-unrestricted DFT method with the BP86 functional including relativistic effects in zero order regular approximation (ZORA).^[266,267,268] All optimized geometries were verified as being true minima by the absence of negative eigenvalues in the vibrational frequency analysis. The single point calculations were performed with the B3LYP

[265] F. Neese, *ORCA – an Ab Initio, Density Functional and Semiempirical SCF-MO Package, version 2.7 revision 0*; Institut für Physikalische und Theoretische Chemie, Universität Bonn, Germany, **2009**.

[266] A. D. Becke, *Phys. Rev. A* **1988**, *38*, 3098.

[267] J. P. Perdew, *Phys. Rev. B* **1986**, *34*, 7406.

[268] C. van Wüllen, *The Journal of Chemical Physics* **1998**, *109*, 392.

functional^[269,270] including relativistic effects in zero order regular approximation (ZORA).^[268] The triple- ζ basis sets with one-set of polarization functions (TZVP)^[271] were used for Ir, N, Cl, and P atoms and the double- ζ basis sets with one-set of polarization functions (SVP)^[271] were used for C and H atoms. Conductor like screening model (COSMO) was routinely used for all calculations.^[272] Molecular orbitals and the spin density plot were visualized via the program Molekel.^[273]

B.1.5.2 Computational Results

Table S5. Comparison of the optimized geometries for **1^{Me}** and **2^{Me}** (spin unrestricted ZORA-BP86-DFT) with **1** and **2**.

	1^{Me}		2^{Me}		
	<i>X-ray</i> (1)	<i>DFT</i> ($S = 1/2$)	<i>DFT</i> ($S = 0$)	<i>DFT</i> ($S = 1$)	<i>X-ray</i> (2)
Ir-N [Å]	1.985(2)	1.972	1.911	1.998	1.922(2)
Ir-Cl [Å]	2.3390(7)	2.369	2.303	2.341	2.2966(6)
Ir-P [Å]	2.3190(6)	2.323	2.342	2.352	2.3416(6) / 2.3443(6)
N-C [Å]	1.387(2)	1.402	1.423	1.393	1.414(3) / 1.415(3)
C=C [Å]	1.342(3)	1.364	1.357	1.369	1.335(3) / 1.334(3)

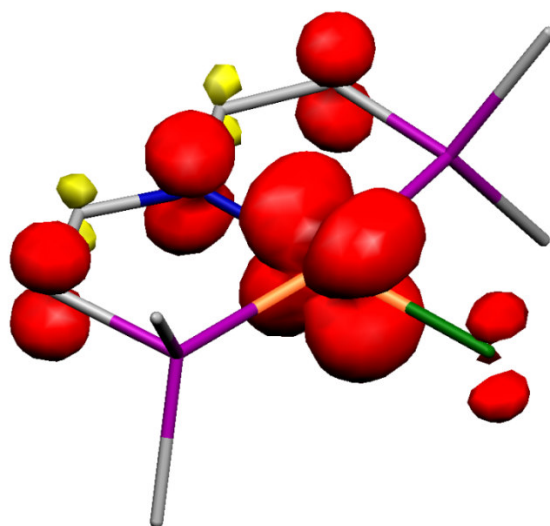


Figure S5. Spin density map for **1^{Me}** obtained from spin-unrestricted ZORA-B3LYP-DFT calculations.

[269] A. D. Becke, *J. Chem. Phys.* **1993**, 98, 5648.

[270] C. T. Lee, W. T. Yang, R. G. Parr, *Phys. Rev. B* **1988**, 37, 785.

[271] D. A. Pantazis, X. Y. Chen, C. R. Landis, F. Neese, *J. Chem. Theory Comput.* **2008**, 4, 908.

[272] A. Klamt, G. Schürmann, *J. Chem. Soc., Perkin Trans. 2* **1993**, 799.

[273] S. Portmann, *Molekel, version 4.3.win32*; CSCS/UNI Geneva, Switzerland, **2002**.

Table S6. Coordinates of **1^{Me}** ($S = 1/2$).

Ir	0.00000	0.00000	0.00000
Cl	2.36858	0.00000	0.00000
P	-0.25664	2.30848	0.00000
P	-0.25786	-2.30815	-0.02299
N	-1.97127	0.00040	0.02154
C	-2.69965	1.19887	0.03927
C	-2.07583	2.41186	0.03544
C	-2.69960	-1.19830	0.02200
C	-2.07684	-2.41168	0.00530
C	0.28447	3.30093	-1.46846
C	0.34666	3.32798	1.42427
C	0.28912	-3.28615	-1.49936
C	0.34323	-3.34130	1.39340
H	-3.79574	1.09845	0.05692
H	-2.64246	3.35146	0.05133
H	-3.79623	-1.09785	0.03512
H	-2.64417	-3.35128	0.00193
H	1.38963	3.30512	-1.51287
H	-0.08174	4.34247	-1.39700
H	-0.10732	2.83373	-2.38952
H	1.45281	3.32702	1.42360
H	-0.00921	2.88267	2.37050
H	-0.01732	4.36972	1.34573
H	1.39411	-3.28374	-1.54322
H	-0.10610	-2.81330	-2.41550
H	-0.07124	-4.33088	-1.43540
H	-0.01514	-2.90404	2.34236
H	1.44898	-3.34042	1.39292
H	-0.02152	-4.38214	1.30204

Table S7. Coordinates of **2^{Me}** ($S = 0$).

Ir	0.00000	0.00000	0.00000
----	---------	---------	---------

Cl	2.30289	0.00000	0.00000
P	-0.22941	2.33008	0.00000
P	-0.23455	-2.33040	-0.01921
N	-1.91081	0.00139	0.04532
C	-2.67817	1.19949	0.07765
C	-2.06032	2.40722	0.06652
C	-2.68035	-1.19595	0.06556
C	-2.06554	-2.40486	0.04335
C	0.24585	3.30078	-1.49383
C	0.36334	3.33462	1.42684
C	0.24145	-3.29140	-1.51952
C	0.35539	-3.34798	1.40120
H	-3.76875	1.07884	0.11252
H	-2.63601	3.34129	0.09502
H	-3.77131	-1.07346	0.09874
H	-2.64329	-3.33828	0.05738
H	1.34917	3.31275	-1.56454
H	-0.12918	4.33774	-1.41638
H	-0.16778	2.81661	-2.39555
H	1.46900	3.33665	1.41491
H	0.01433	2.87927	2.37005
H	-0.00746	4.37299	1.34909
H	1.34454	-3.29879	-1.59199
H	-0.17633	-2.80363	-2.41684
H	-0.12982	-4.33063	-1.44594
H	0.01072	-2.89639	2.34776
H	1.46054	-3.35692	1.38494
H	-0.02287	-4.38339	1.31514

Table S8. Coordinates of 2^{Me} ($S = 1$).

Ir	1.653075	3.430620	10.345330
Cl	1.031450	5.639047	10.810495
P	0.225553	2.435009	11.927073
P	3.093556	3.949953	8.560192

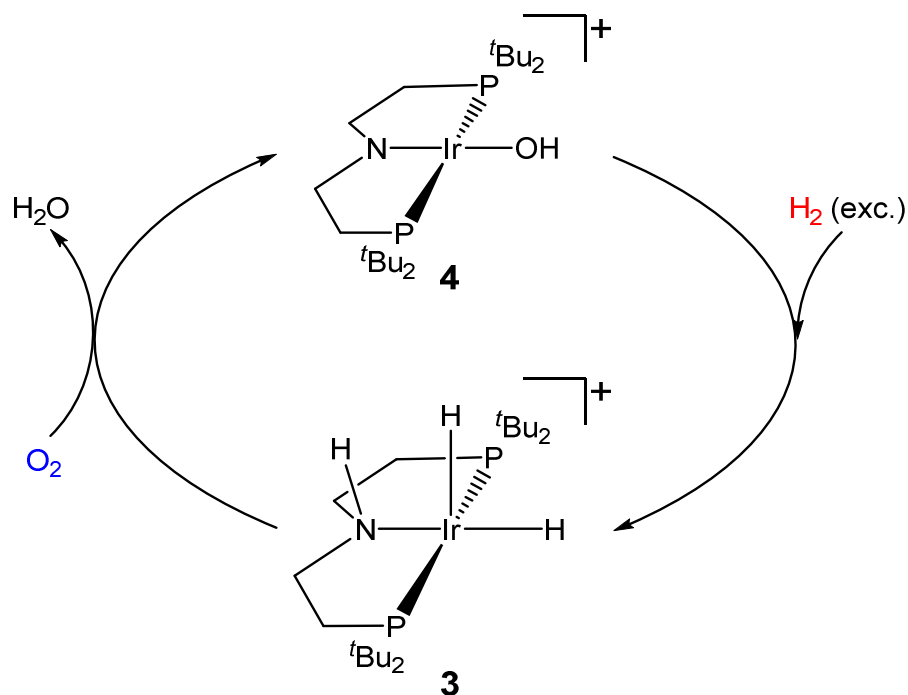
N	1.848293	1.559973	9.671532
C	1.203167	0.497079	10.300343
C	0.403894	0.699019	11.392695
C	2.669465	1.271092	8.583435
C	3.354264	2.258044	7.927729
C	-1.574878	2.818055	11.831649
C	0.634051	2.486104	13.721113
C	2.432322	4.936541	7.151298
C	4.760482	4.656304	8.900796
H	1.375384	-0.501110	9.873501
H	-0.096914	-0.141491	11.889598
H	2.731341	0.214671	8.284756
H	3.999046	2.024803	7.070690
H	-1.733384	3.857240	12.173639
H	-2.147261	2.125292	12.475339
H	-1.917337	2.725598	10.785998
H	0.491560	3.519686	14.087138
H	1.688187	2.192195	13.868701
H	-0.026802	1.802111	14.284968
H	2.275098	5.975819	7.493082
H	1.466702	4.512339	6.826026
H	3.148844	4.928575	6.308946
H	5.255382	4.067690	9.693225
H	4.636394	5.698975	9.246153
H	5.377120	4.643134	7.982806

B.2 Oxygenation of a dihydrido iridium complex toward a SP-coordinated Ir(III)hydroxo complex

unpublished results

J. Meiners, S. Schneider*

Georg August Universität Göttingen, Tammannstr 4, 37073 Göttingen/Germany



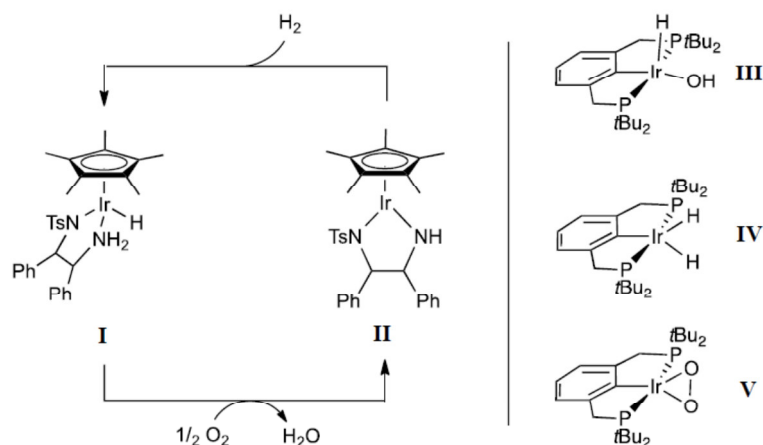
Reaction of an IrPNP Dihydrido complex with molecular oxygen O₂

B.2.1 Abstract

Reaction of the cationic iridium(III) dihydrido complex $[\text{Ir}(\text{H})_2\{\text{HPNP}^{\text{tBu}}\}]\text{PF}_6$ ($\text{HPNP}^{\text{tBu}} = \text{HN}(\text{CH}_2\text{CH}_2)\text{P}^{\text{tBu}}_2$) (**3**) with an excess of dioxygen leads to the SP-coordinated Ir(III) hydroxo complex $[\text{Ir}(\text{OH})\{\text{PNP}^{\text{tBu}}\}]\text{PF}_6$ (**4**), (and to one equivalent of water in case of CD_2Cl_2 as the solvent) and to formation of γ -butyrolactone in case of THF as the solvent. **3** can be hydrogenated to give back dihydrido complex (**3**) by treatment with H₂.

B.2.2 Introduction

The direct utilization of dioxygen for selective functionalization of organic compounds in oxidation or oxygenation reactions is a key goal of sustainable catalysis. Apart from synthetic transformations, oxygen reduction (ORR: $\text{O}_2 + 4\text{H}^+ + 4\text{e}^- \rightarrow 2 \text{H}_2\text{O}$) also defines a pivotal reaction for biological and technical processes of energy conversion, such as respiration and fuel cell applications.



Scheme B.2-1: *Left:* ORR catalysed by a bifunctional iridium hydride catalyst reported by *Heiden* and *Rauchfuss*. *Right:* Iridium pincer complexes examined in the context of O₂ reduction by *Goldberg, Mayer et al.*^[281]

However, the reduction of O₂ imposes several challenges:

1) O₂ splitting requires four electrons, which have to be provided by multiple redox centers. Metalloenzymes utilize multinuclear cofactors (e.g. tyrosinase),^[274] redox non-innocent ligands (e.g. cytochrome P450),^[275]

or both (e.g. cytochrome-c-oxidase)^[276] to accomplish four-electron redox chemistry, and bioinspired models have adopted these principles.^[277] However, both biological examples and synthetic systems can suffer from two-electron side reactions, such as H₂O₂ formation, which, at best, reduce catalytic efficiency or even result in undesired oxidation products or degradative processes.

2) Water formation requires the delivery of four protons. This has recently been taken into account for ORR catalyst design by tethering of acidic functional groups in the proximity of the oxygen binding site.^[278]

In this context, the *Rauchfuss* group reported the reduction of O₂ by H₂ within a synthetic cycle, catalyzed by a bifunctional catalyst (**Scheme B.2-1**).^[278a] This remarkable system combines both aspects, i.e. the use of a cooperating amine ligand and formal electron delivery

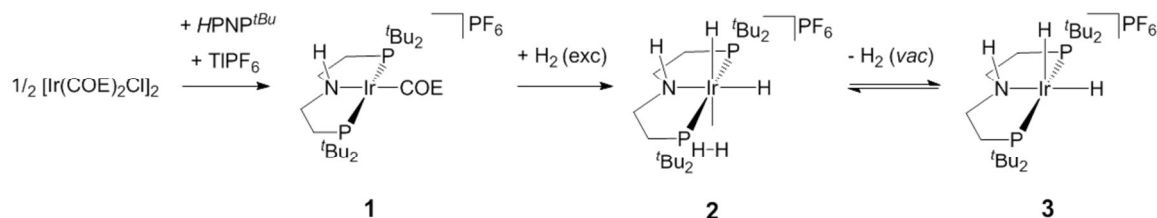
[274] a) P. M. Siegbahn, *J Biol Inorg Chem* **2003**, 8, 567-576; b) E. I. Solomon, P. Chen, M. Metz, S.-K. Lee, A. E. Palmer, *Angew. Chem. Int. Ed.* **2001**, 40, 4570-4590.

[275] I. G. Denisov, T. M. Makris, S. G. Sligar, I. Schlichting, *Chem. Rev.* **2005**, 105, 2253.

[276] J. P. Collman, N. K. Devaraj, R. A. Decréau, Y. Yang, Y.-L. Yan, W. Ebina, T. A. Eberspacher, C. E. D. Chidsey *Science* **2007**, 315, 1565.

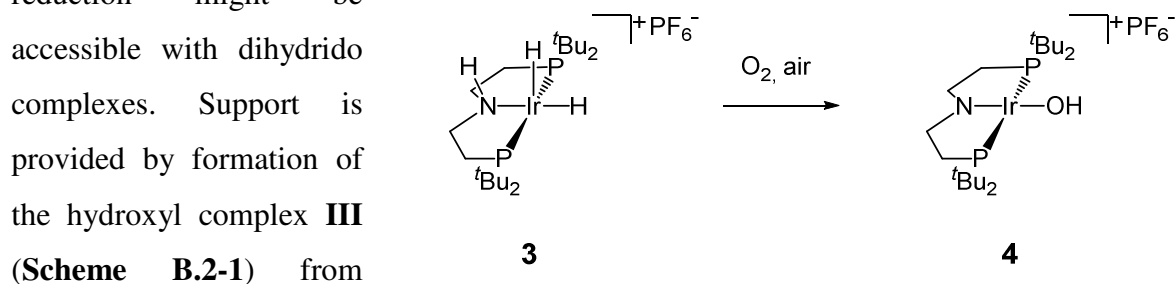
[277] L. Jr. Que, W. B. Tolman, *Nature* **2008**, 455, 333.

[278] Representative examples: (a) Z. M. Heiden, T. B. Rauchfuss, *J. Am. Chem. Soc.* **2007**, 129, 14303. (b) D. K. Dogutan, S. A. Stoian, R. Jr. McGuire, M. Schwalbe, T. S. Teets, D. G. Nocera, *J. Am. Chem. Soc.* **2011**, 133, 131. (c) C. T. Carver, B. D. Matson, J. M. Mayer, *J. Am. Chem. Soc.* **2012**, 134, 5444.



Scheme B.2-2: Synthesis of $[\text{Ir}(\text{H}_2)(\text{H})_2\{\text{HPNP}^{\text{tBu}}\}]\text{PF}_6$ (**2**) and $[\text{Ir}(\text{H})_2\{\text{HPNP}^{\text{tBu}}\}]\text{PF}_6$ (**3**).

by the hydride rather than the Ir^{III} -center.^[279] However, the monohydride complex **I** provides only two redox equivalents and ORR completion was proposed to proceed via reaction of a hydroperoxide-intermediate^[280] with a second equivalent of **I**. Hence, direct four-electron O_2 reduction might be



accessible with dihydrido complexes. Support is provided by formation of the hydroxyl complex **III** (Scheme B.2-1) from reaction of dihydride **IV**

Scheme B.2-3: Synthesis of hydroxo complex **4**

with O_2 , albeit only in minor amounts within a product mixture of mostly peroxo complexes, such as **V**.^[281]

The present study describes an approach to combine these two concepts within a mononuclear complex. The reactivity of dihydride $[\text{Ir}(\text{H})_2\{\text{HPNP}^{\text{tBu}}\}]\text{PF}_6$ (**3**) which splits O_2 and forms water beside the unusual, square-planar hydroxo complex $[\text{Ir}(\text{OH})\{\text{HPNP}^{\text{tBu}}\}]\text{PF}_6$ (**4**) is reported. In reverse, **4** affords H_2 heterolysis to complete a full ORR cycle without formal metal redox change within the overall four-electron reaction.

B.2.3 Results and Discussion

B.2.3.1 Synthesis of $[\text{Ir}(\text{H})_2\{\text{HPNP}^{\text{tBu}}\}]\text{PF}_6$ (**3**)

$[\text{Ir}(\text{H})_2\{\text{HPNP}^{\text{tBu}}\}]\text{PF}_6$ (**3**) can be obtained in good yield by treatment of the *in situ* generated cationic iridium(I) olefin complex $[\text{Ir}(\text{COE})\{\text{HPNP}^{\text{tBu}}\}]^+\text{PF}_6^-$ (**1**) with an excess of H_2 , formation of the iridium(III) dihydrogen dihydrido complex $[\text{Ir}(\text{H}_2)(\text{H})_2\{\text{HPNP}^{\text{tBu}}\}]^+\text{PF}_6^-$ (**2**) and dehydrogenation of the latter *in vacuo* toward **3** (Scheme B.2-2). **3** is stable in THF but slowly chlorinated in dichloromethane at r.t. over several hours.^[283] The signals of the room temperature ^1H and ^{13}C NMR spectra (s. 104) of **3** point toward a pyramidal, C_S -symmetric amino dihydrido iridium complex. A broad, mixed signal for the two hydrido ligands appears

[279] Owing to the high covalency of the M–H bonds of late transition metals the formal oxidation state may not be confused with real charge.

[280] Representative examples: (a) M. M. Konnick, S. S. Stahl, *Angew. Chem. Int. Ed.* **2006**, *45*, 2904. (b) M. C. Denney, N. A. Smythe, K. L. Cetto, R. A. Kemp, K. I. Goldberg, *J. Am. Chem. Soc.* **2006**, *128*, 2508.

[281] D. B. Williams, W. Kaminsky, J. M. Mayer, K. I. Goldberg, *Chem. Commun. (Cambridge, U. K.)* **2008**, 4195–4197.

[282] J. Meiners, A. Friedrich, E. Herdtweck, S. Schneider, *Organometallics* **2009**, *28* (21), 6331–6338.

[283] J. Meiners, S. Schneider, *unpublished results*

at -31.11 ppm and splits up into two signals at -47.06 ppm and -15.99 ppm, below the (estimated) coalescence temperature of $T_{c(\text{calc}, 400\text{MHz})} = -37^\circ\text{C}$. The latter peaks can be assigned to one *trans*-non-coordinated and one *trans*-N-coordinated hydrido ligand, respectively, which indicate **3** to be a *cis*-dihydrido complex with a square-pyramidal configuration, one hydride occupying the apical position. The activation parameters for the exchange of the two hydrido ligands of the dynamic compound **3** are calculated to $\Delta H^\ddagger = 40 \pm 0.5$ kJ/mol and $\Delta S^\ddagger = 10 \pm 2$ J/molK based on line shape analysis of the ^1H NMR spectra (s. 107).

$[\text{Ir}(\text{H}_2)(\text{H})_2\{\text{HPNP}^{\text{tBu}}\}]\text{PF}_6$ (**2**) can be generated in quantitative NMR spectroscopic yield by treatment of **3** with an excess of H_2 . The NMR spectra (s. 108) of **2** are in agreement with a C_S -symmetric amino complex, which is coordinated by four H atoms ($\delta = -9.91$ ppm, br, IrH_4).

The ^1H NMR VT spectra (s. 110) of dynamic compound **2** point toward coordination of the four hydrido ligands to iridium in a classical respective a nonclassical manner. There was no T_1 measurement performed to prove this assignment ultimately. However, according to established metal polyhydrides^[284] the chemical shifts of the two broadened peaks at $\delta = -14.83$ ppm (2H, $w_{1/2} = 80$ Hz, $\text{Ir}(\text{H})_2$) and -5.33 ppm (2H, $w_{1/2} = 130$ Hz, $\text{Ir}(\text{H}_2)$) at 190 K match the expected values accurately. The activation parameters for the putative exchange of the dihydrogen ligand with the two hydrido ligands are calculated to $\Delta H^\ddagger = 33.5 \pm 1$ kJ/mol, -23 ± 3 J/molK. The calculated coalescence temperature is $T_{c(\text{calc} 400\text{MHz})} = -42^\circ\text{C}$.

B.2.3.2 Reaction of **3** with an excess of dioxygen toward a SP coordinated Ir(III) hydroxo complex **4**

Treatment of $[\text{Ir}(\text{H})_2\{\text{HPNP}^{\text{tBu}}\}]\text{PF}_6$ (**3**) with air or an excess of O_2 in THF or dichloromethane at r.t. leads to formation of the complex $[\text{Ir}(\text{OH})\{\text{PNP}^{\text{tBu}}\}]\text{PF}_6$ (**4**) in almost quantitative spectroscopic yield (^{31}P and ^1H NMR) within ca. 30 minutes (**Scheme B.2-3**). Isolation of **4** is possible in moderate to good yields (62%). **4** decomposes noticeably in THF at r.t. (~25% per one day), but is more stable in dichloromethane at r.t.. Spectroscopic data (NMR: ^{31}P , ^1H , ^{13}C , ^1H , ^1H cosy, ^1H noesy, ^1H , ^{13}C hsqc (s. 112), high-resolution MS, IR) and elemental analysis of **4** point toward a diamagnetic, C_{2v} -symmetric, square planar Ir(III) amido hydroxo complex at room temperature. The O–H stretching vibration was assigned to a peak at 3604 cm^{-1} in the IR spectrum and the proton to a broad ^1H NMR peak at 11.6 ppm, which exhibits triplet multiplicity at low concentrations owing to $^3J_{\text{HP}}$ (7.4 Hz) coupling.

[284] examples: a) $[\text{W}(\text{CO})_5(\text{P}^i\text{Pr}_3)(\text{H}_2)]$: $\delta_{\text{W}(\text{H}_2)} = -4.21$ ppm; G. J. Kubas, R. R. Ryan, B. I. Swanson, P. J. Vergamini, H. J. Wasserman, *J. Am. Chem. Soc.* **1984**, *106*, 451-452; b) $[\text{Ir}(\text{H})_2(\text{H}_2)_2(\text{PCy}_3)_2]^+$: $\delta_{\text{Ir}(\text{H})_2} = -15.2$ ppm, $\delta_{\text{Ir}(\text{H}_2)} = -5.05$ ppm; R. H. Crabtree, M. Lavin, *J. Chem. Soc., Chem. Commun.* **1985**, 794-795 *ibid.* 1661-1662; c) $[\text{Ir}(\text{H})_2\text{bq}(\text{PPh}_3)_2]^+$ (bq = benzoquinoline): $\delta_{\text{Ir}(\text{H})_2} = -15.2$ ppm, $\delta_{\text{Ir}(\text{H}_2)} = -3.0$ ppm; *ibid.*

Addition of D₂O results in rapid disappearance of this signal, presumably due to H/D

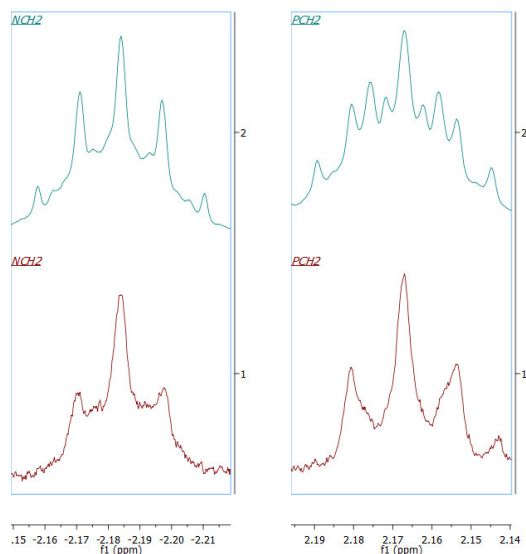


Figure B.2-1: $^1\text{H}\{^{31}\text{P}\}^{[288]}$ (left) and ^1H (right) NMR signals of NCH₂ and PCH₂ groups of **4**.

exchange.

The ^1H NMR signal of the NCH₂ groups occurs at -2.23 ppm and is therefore extraordinarily shifted from expected values, whereas the ^{13}C signal of NCH₂ and the ^1H NMR signal of the PCH₂ groups show up at usual shifts ($\delta = 88.80$ ppm, 2.16 ppm). The ^1H signal of NCH₂ does not exhibit any considerable temperature-dependent drift in VT NMR. Therefore no significant spin density can be assumed to be present at the NCH₂ group. In comparison, an unusual chemical shift for these protons was also found for square-planar d^6 complex $[\text{RuCl}\{\text{N}(\text{CH}_2\text{CH}_2\text{P}t\text{Bu}_2)_2\}]$.^[285,286] In that

case, the strong temperature dependence of the chemical shift and computational results point toward a low-lying intermediate-spin excited state that is thermally populated. However, this interpretation does not hold true for **4** (see below).

As early as in 1977 *Shaw et al.* presented an isoelectronic PCP complex $\text{Ir}(\text{Cl})\text{C}((\text{CH}_2\text{CH}_2)\text{P}t\text{Bu}_2)_2$ ^[287] wherein the formal carbene C atom is located 0.3 Å above the $\text{Ir}=\text{C}-\text{C}_\alpha\text{C}_\alpha$ plane in the crystal. They reported a noticeable shift (of only two) of the CCH₂ protons in ^1H NMR to $\delta = -2.77$ ppm (pseudo pentet, $J = 7.1$ Hz, triplet in $^1\text{H}\{^{31}\text{P}\}$ NMR) as well, and supposed this was caused by shielding due to a remarkable contribution of an ylid-like resonance structure of the seemingly Ir=C carbene complex.

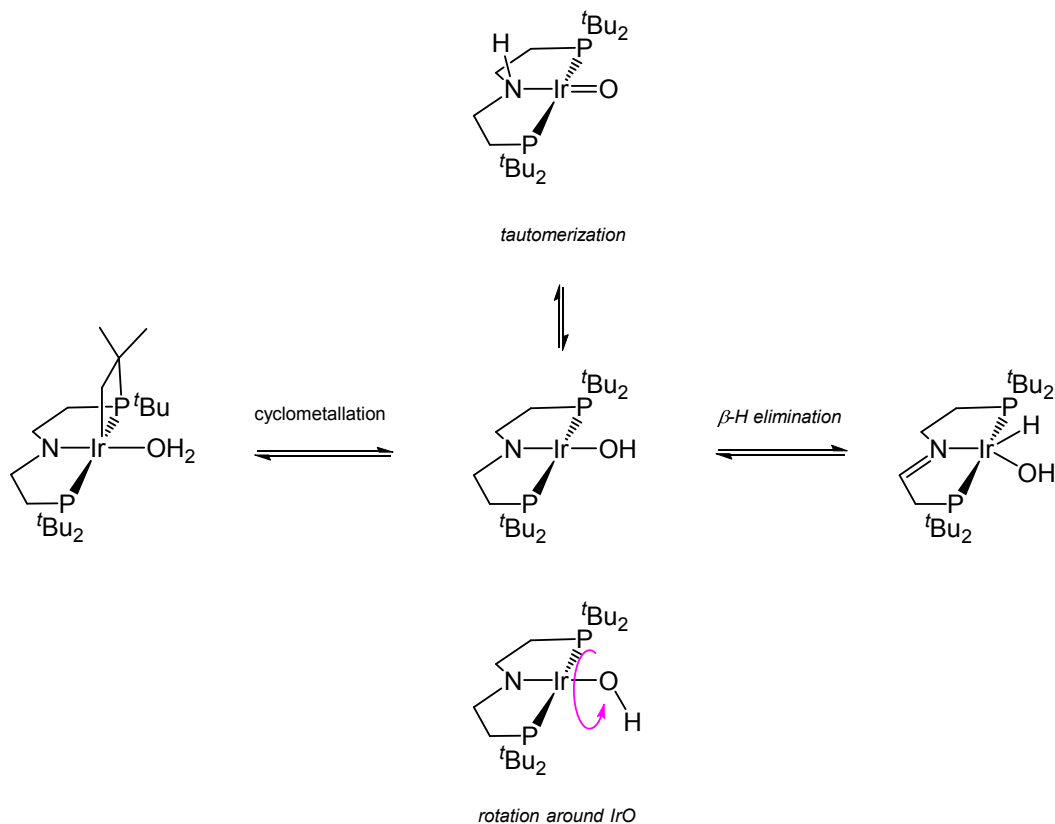
A likely shielding could be induced in **4** by a relevant charge density situated in the N p_π orbital, which should be located in a torsion angle ca 35° and 145° regarding the NCH₂ protons in the two rigid chelate rings, which would explain the absent affect toward the NCH₂ carbons.

[285] B. Askevold, M. M. Khusniyarov, E. Herdtweck, K. Meyer, S. Schneider, *Angew. Chem. Int. Ed.* **2010**, *49*, 7566.

[286] a) B. Askevold, M. M. Khusniyarov, E. Herdtweck, K. Meyer, S. Schneider, *Angew. Chem. Int. Ed.* **2010**, *49*, 7566; b) B. Askevold, J. Meiners, M. M. Khusniyarov, W. Kroener, K. Gieb, P. Müller, E. Herdtweck, F. Heinemann, M. Diefenbach, M. C. Holthausen, V. Vieru, L. F. Chibotaru, S. Schneider *submitted*.

[287] a) H. D. Empsall, E. M. Hyde, R. Markham, W. S. McDonald, M. C. Norton, B. L. Shaw, B. Weeks, *J. Chem. Soc., Chem. Commun.* **1977**, 589–90; b) C. Crocker, H. D. Empsall, R. J. Errington, E. M. Hyde, W. S. McDonald, R. Markham, M. C. Norton, B. L. Shaw, B. Weeks, *J. Chem. Soc., Dalton Trans.* **1982**, 1217–24.

The PCH₂ and NCH₂ methylene signals (**Figure B.2-1**) of the PNP ligand of **4** appear as pseudo triplets ($^3J_{\text{HH}} = 6.8$ Hz) in $^1\text{H}\{^{31}\text{P}\}$ spectroscopy^[288], leading to the assumption, that in solution the CH₂ protons stand staggered (by about 20°-50°)^[289] and thus the two five-rings are twisted. In ^1H spectroscopy they occur as a pseudo pentet and as a multiplet, respectively.



Scheme B.2-4: Potential dynamic processes within $[\text{Ir}(\text{OH})\{\text{PNP}^{\text{tBu}}\}]\text{PF}_6$ (**4**)

4^{PF₆} is a dynamic compound. In CD₂Cl₂, the singlet signal in ^{31}P spectroscopy (which shows a temperature dependent drift; $\delta = 62.87$ ppm at +35°C, $\delta = 62.05$ ppm at -35°C), splits up into two new signals (-90°C: 2 d, 60.67 ppm and 62.09 ppm, $\text{trans } ^2J_{\text{PP}} = 336$ Hz) below the coalescence temperature $T_{\text{c}(\text{calc } 500\text{MHz})} = -38^\circ\text{C}$. The activation parameters for this process are $\Delta H^\ddagger = 41 \pm 1$ kJ/mol and $\Delta S^\ddagger = -5 \pm 2$ J/molK. In VT ^1H NMR(500 MHz) one can also identify the splitting of the signals of the ^tBu groups (-60°C: 1.44 ppm, vt → -70°C: 1.41 ppm + 1.44 ppm, 2 m, br.) and the PCH₂ groups (-60°C: 2.08 ppm, m → -80°C: 2.02 ppm + 2.09 ppm, 2 t, br.), but no decoalescence of the NCH₂ groups down to -90°C. Interestingly, there is no splitting or broadening in THF as the solvent in ^{31}P or ^1H NMR until -100°C.

[288] Christoph Schiewek, Master thesis, Georg-August-Universität Göttingen 2013

[289] M. Hesse, H. Meier, B. Zeeh, *Spektroskopische Methoden in der organischen Chemie*, Georg Thieme Verlag, Stuttgart, 2005.

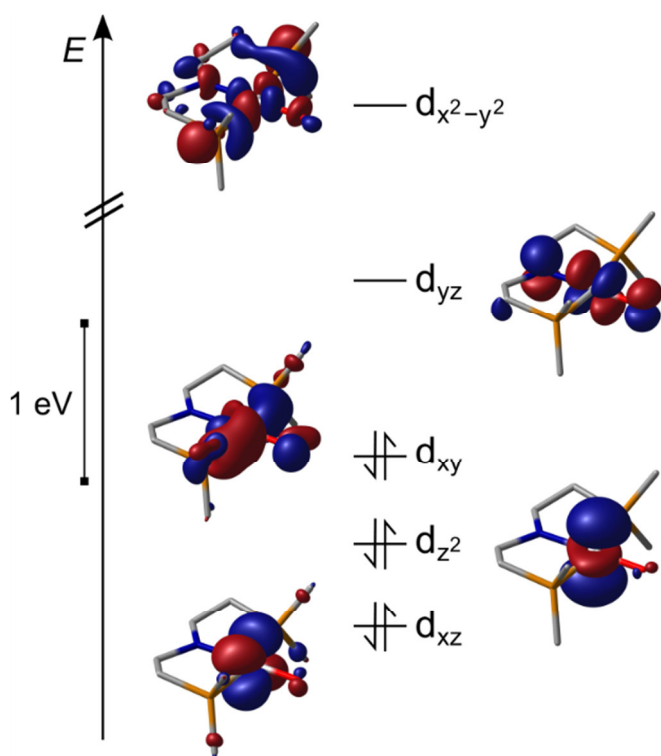


Figure B.2-2: Metal-centered Kohn–Sham frontier orbitals of **4** in the singlet state from spin-unrestricted B3LYP/SVP DFT calculations^[292] (the z axis is perpendicular to the {Ir(L4)} plane).

In a formally conceivable dynamic equilibrium between the amido hydroxo complex and e. g. an amino oxo complex (*tautomerization*) or an aquo or hydrido hydroxo imino complex (*β -H elimination*), the difference of the chemical shifts of the NCH₂ group in ¹H NMR should be much larger than one can estimate after the not decoalescence peaks until -90°C (with $k_c = \pi\Delta\nu_0/2^{1/2}$ and the Arrhenius equation for **4**: $\ln k = -5195,3 \cdot 1/T + 29,644$). Furthermore, in the first case, a singlet instead of two doublets would remain in ³¹P spectroscopy.

In the second case the differences of the chemical shifts of the two doublets in ³¹P NMR should be larger.^[290] In case of an addition of one ^tBu C-H bond along the Ir-O axis (*cyclometallation*), the ³¹P nmr signal of the affected phosphorous atom should be shifted significantly upfield^[291], due to ring torsion effects in the formed 5,4-fold bicyclus.

Regarding a representative *rotation around the Ir-OH bond axis* of **4**, it was consistently observed, that in case of THF as the solvent, no broadening or splitting of the singlet signal down to -100°C was found in ³¹P nmr spectroscopy. The rotation could be accelerated to such an extent, that it cannot be slowed down below the NMR time scale, e.g. due to the formation of H-bridge bonds in THF. Tunnel effects might also cause a fast interchange of proton positions. Therefore, the two ³¹P NMR signals observed at low temperatures are consistent with a hampered rotation of a bent hydroxide ligand. The energetic barrier for the probable OH rotation points toward a considerable O→Ir π -bonding interaction (see below).

Unfortunately no success in several deuteration attempts to clearly *isolate* [Ir(OD){PNP^tBu}]PF₆ (*D1-4*) or to prove the deuteration of OH by ²H NMR spectroscopy, to slow down the supposed rotation frequency and prevent tunneling effects, was achieved.

[290] A. Friedrich, M. Drees, M. Kaess, E. Herdtweck, S. Schneider, *Inorg. Chem.* 2010, 49, 5482–5494.

[291] a) O. Kühn, Phosphorus-³¹ NMR spectroscopy. A concise introduction for the synthetic organic and organometallic chemist, Springer, Berlin, 2008; b) L. D. Quin, J. G. Verkade, Phosphorus-31 NMR spectral properties in compound characterization and structural analysis, VCH, New York, 1994; c) H. A. Y. Mohammad, J. C. Grimm, K. Eichele, H.-G. Mack, B. Speiser, F. Novak, M. G. Quintanilla, W. C. Kaska, H. A. Mayer, *Organometallics* 2002, 21, 5775–5784.

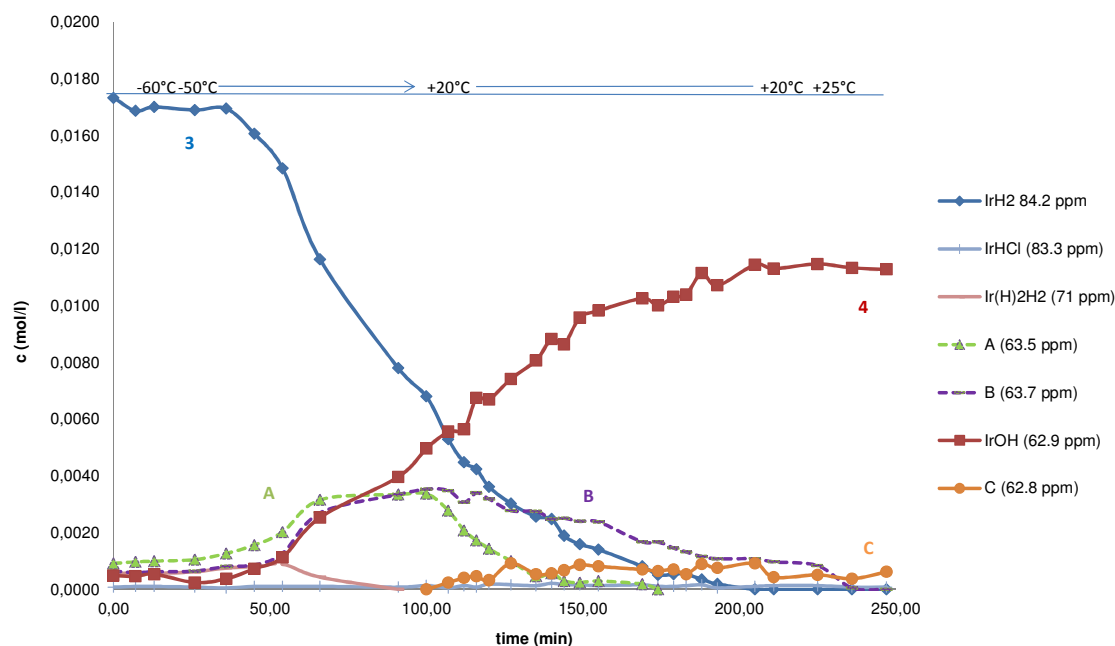


Figure B.2-3: Concentration of involved diamagnetic species due to evaluation of ^{31}P NMR spectra in the reaction of the dihydride **3** with 7 eq. O_2 in CD_2Cl_2 . The reaction is NOT monitored in inversed gated mode, which means that, due to NOE buildup, the integrals do not necessarily represent absolute concentrations. The integrals are normalized by referring them to the signal of PF_6^- , divided by the total amount of integrals at the reaction start referring them to the concentration of **3** before the reaction was started. Some ^1H NMR signals of **A** and **B** are discussed in the text.

Electronic structure calculations (DFT) by Förster *et al.*^[292] in further investigations confirm strong $\text{N} \rightarrow \text{Ir} \pi$ -bonding. Computed geometry (B3LYP/SVP, **Figure B.2-2**) in the singlet state is in good agreement with an Ir center, which is coordinated square planar by the $\text{N}(\text{CH}_2\text{CH}_2\text{P}^t\text{Bu}_2)_2$ ligand and is very similar to that of Ir(III) dieneamido complex $[\text{IrCl}(\text{N}(\text{CH}_2\text{CH}_2\text{P}^t\text{Bu}_2)_2)]\text{PF}_6$ (**B.1**). Particularly the Ir–N ($S=0$: 1.882 Å; $S=1$: 1.986 Å) bond is highly sensitive to spin multiplicity. This can be rationalized by evaluation of the molecular orbitals (**Figure B.2-2**): The LUMO in the singlet state, which is singly occupied for $S=1$, exhibits considerable Ir–N and some Ir–O π^* antibonding character. As was emphasized for d^6 ions (Ru^{II} , Ir^{III}) in a square-planar ligand field with these PNP pincer ligands, stabilization of the low-spin *vs.* intermediate-spin state is subject to the extent of $\text{N} \rightarrow \text{M} \pi$ -donation, which destabilizes this orbital.^[101,286,293] For **4**, the singlet state, which was calculated to be more stable by $\Delta E = 84 \text{ kJmol}^{-1}$, exhibits coplanar arrangement of the planes described by Ir–O–H and P–Ir–N, yet perpendicular arrangement for the triplet to avoid Ir–O π^* -destabilization of that SOMO. Computation of OH rotation ($S=0$) predicts a barrier around 50 kJmol^{-1} , in good

[292] M. Förster, M. Holthausen, *unpublished results*

[293] S. Schneider, J. Meiners, B. Askevold, *Eur. J. Inorg. Chem.* 2012 (3), 412–429.

agreement with the experimental value, which also suggests that this process occurs on the singlet surface.

During the oxidation reaction (**Scheme B.2-3**) one equivalent H_2O per introduced **3** is generated, which was shown by trap-to-trap transfer of the volatiles after complete conversion (**Figure B.2-37 exp data**). No indication for the formation of H_2O_2 was found. Hence, the

reaction is consistent with the overall stoichiometry $\mathbf{3} + \text{O}_2 \rightarrow \mathbf{4} + \text{H}_2\text{O}$. Furthermore, **3** does not react with water at room temperature, also ruling out hydrolysis as a pathway for the formation of **4**.

During VT NMR spectroscopy of the oxygenation of dihydride **3** with seven equivalents of O_2 in CD_2Cl_2 (**Figure**

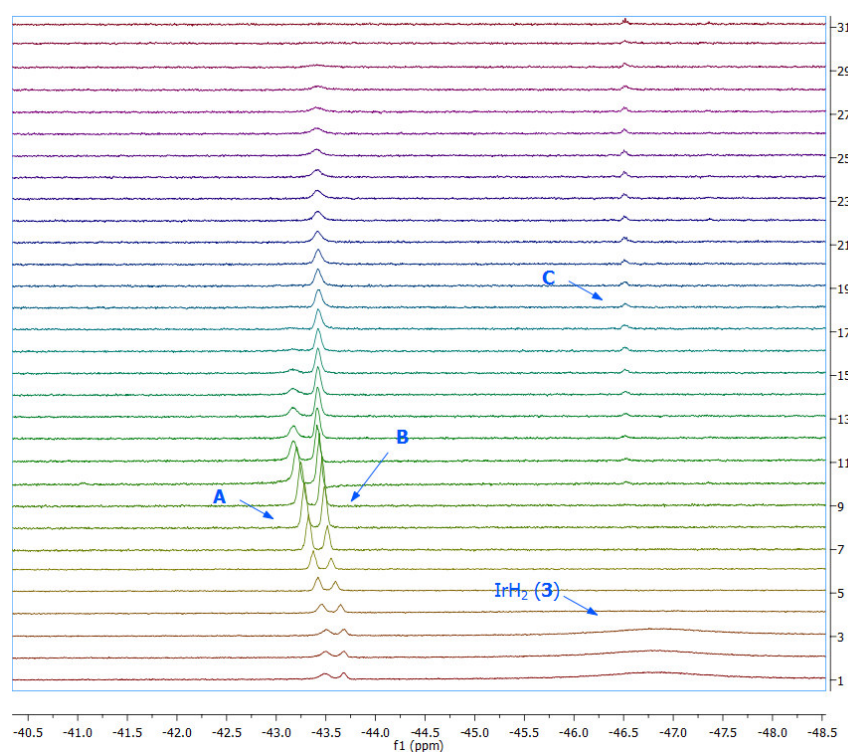


Figure B.2-4: Hydride region in ^1H NMR spectroscopy of the reaction: $\mathbf{3} + \text{O}_2 \rightarrow \mathbf{4}$, 1 = start, 31 = finish.

B.2-4) in ^{31}P NMR spectroscopy, one can observe the transient formation of three diamagnetic species: **A**, **B** and dihydrido dihydrogen complex **2**. Furthermore, small, constant amounts of chlorinated **3** ($[\text{IrH}(\text{Cl})\{\text{HPNP}^{\text{tBu}}\}]\text{PF}_6$, $\mathbf{3}^{\text{Cl}}$) can be identified, a species **C** is formed in small amounts and the formation of the hydroxide **4** occurs in ca. 75-80% d.Th.

A, **B** and **C** are C_5 -symmetric compounds (^{31}P NMR: δ [ppm] = **A**: 63.5 (s), **B**: 63.7 (s), **C**: 62.8 (s)). Referring to ^1H NMR spectroscopy, they contain one hydride ligand (δ 283 K [ppm]) = **A**: -43.21 (br, 1H), **B**: -43.43 (t, $^3J_{\text{HP}} = 8$ Hz, 1H), **C**: -46.53 (br, 1H,) each, which perceives no trans-ligand. Furthermore, there is one signal belonging to **A** (δ 293 K [ppm]) = 5.00 (br, 1H), which is presumed to represent an amino proton, while no such signal was found for **B** (**Figure B.2-5**). There is another signal in the region for NH protons (δ 293 K [ppm]) = 4.65 (br), which could belong to **C**. Although, the concentration of **C** is so small that this seems quite speculative, **C** and **B** should indeed be amino complexes as well. Coordination of an amido ligand as a strong π -donor would promote Y-shaped

geometry and thus introduce a downfield shift of the corresponding hydride signals. There could not be located any signal for a hydroperoxyde ligand. But maybe this would be difficult in any case due to the potential broadening of the corresponding peaks and the overlapping with other signals in the ^1H NMR spectrum during the reaction process.

While the mechanism of O_2 cleavage and formation of hydroxide **4** requires further examination, these preliminary results would be consistent with an insertion of O_2 into one of the Ir hydride bonds of **3** and formation of an amino hydrido hydroperoxo complex. **A** and **B** could represent each isomers of amino hydrido hydroperoxo complexes in which the NH moiety points up and down, respectively. Extrusion of oxen from the hydroperoxo ligand of **A** and **B** could lead to the formation of e.g. a transient amido aquo hydroxo complex in equilibrium with hydroxide **4**. These complexes could form **4** by dissociation of one molecule of H_2O . Whether hydride **C** plays a role in this scenario, e.g. by being in equilibrium with **4**, or if it is the product of a separate pathway is questionable.

These mechanistic assumptions, if they are true, would propose a rate law, which is first order in **3**. *Rauchfuss and co-workers* reported a rate law that is second order in **I** suggesting an intermolecular O_2 cleavage.

Regarding the ^1H NMR measurements of the last experiment, one can see that the omitted ~25% of dihydride **3** are not converted to hydroxide **4** but to paramagnetic compounds which have not been identified yet (**Figure B.2-41 exp. data**). During another oxygenation reaction of the dihydride **3** with an excess of O_2 in CH_2Cl_2 the reaction was observed at $\sim 0^\circ\text{C}$ via cryo mass spectroscopy^[294]. Educt **3**, product **4** and a species **P**, with $M/Z = 585.25$, which matches the formula $\text{C}_{20}\text{H}_{44}\text{IrNO}_2\text{P}_2^+$ were detected (**Figure B.2-42 exp. data**). According to the chemical formula, **P** should be a paramagnetic compound, at least at the time of detection by the mass spectrometer. It could be an amido dioxygen complex with Ir(II) emerged from dissociation of H_2 from dihydride **3** in combination with radical H atom abstraction at the

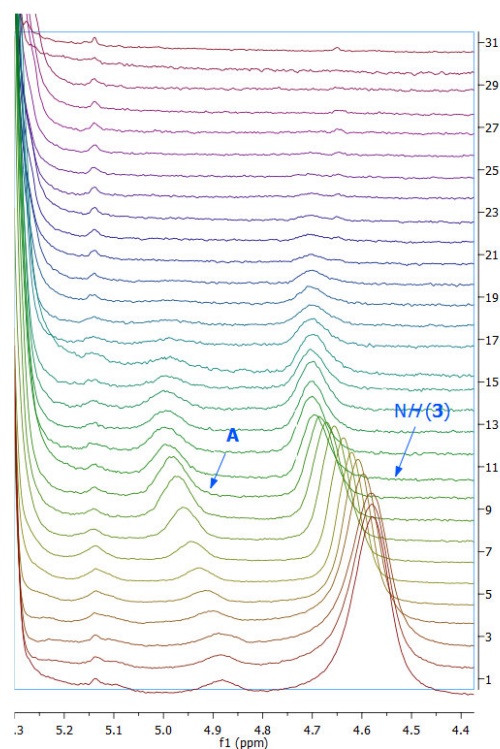


Figure B.2-5: Amine region in ^1H NMR spectroscopy of the reaction: **3** + $\text{O}_2 \rightarrow$ **4**, bottom = start, top = finish.

[294] J. Meiners, M. v. Gernerl, T. Drewello, I. Ivanović-Burmazović, FAU Erlangen, unpublished results.

ligand e.g. by O₂. Dissociation of H₂ would explain the formation of small amounts of dihydrido dihydrogen complex **2**, which is repeatedly observed during reaction of **3** with O₂. One could postulate that a total of two paths exist for the reaction of the dihydride **3** with O₂: The first is via the formation of diamagnetic intermediates leading (i.a.) to the formation of hydroxide **4**. The second path leads, probably under involvement of radical chain and/or free radical steps, to formation of paramagnetic, yet unidentified species. If any of these reaction sequences is thermodynamically or kinetically preferred or whether one can specifically facilitate one path, is not known yet.

B.2.3.3 Regeneration of 3 via treatment of 4 with an excess of hydrogen and O₂-splitting/hydrogenation cycle

[Ir(OH){PNP^{tBu}}]PF₆ (**4**) can be converted back to educt [Ir(H)₂{HPNP^{tBu}}]PF₆ (**3**) by treatment with an excess of H₂ at r.t. overnight (**Scheme B.2-5**). It has not been tested yet, if there is any generation of H₂O during the hydrogenation reaction. However, no other compound, which had incorporated the O-atom of the foregoing hydroxo ligand, was detected. Therefore, in the absence of any substrate other than H₂, the reaction should be consistent with the overall stoichiometry $\mathbf{4} + 2 \text{H}_2 \rightarrow \mathbf{3} + \text{H}_2\text{O}$.

Renewed oxidation of **3** with ca. three equivalents of O₂ toward **4** and once again the regeneration of **3** by treatment with H₂ can be shown in an oxygenation-hydrogenation cycle three times in CD₂Cl₂ with the same sample by keeping the same solvent mixture during all pump-freeze-thaw gassing/degassing cycles (**Figure B.2-39**).

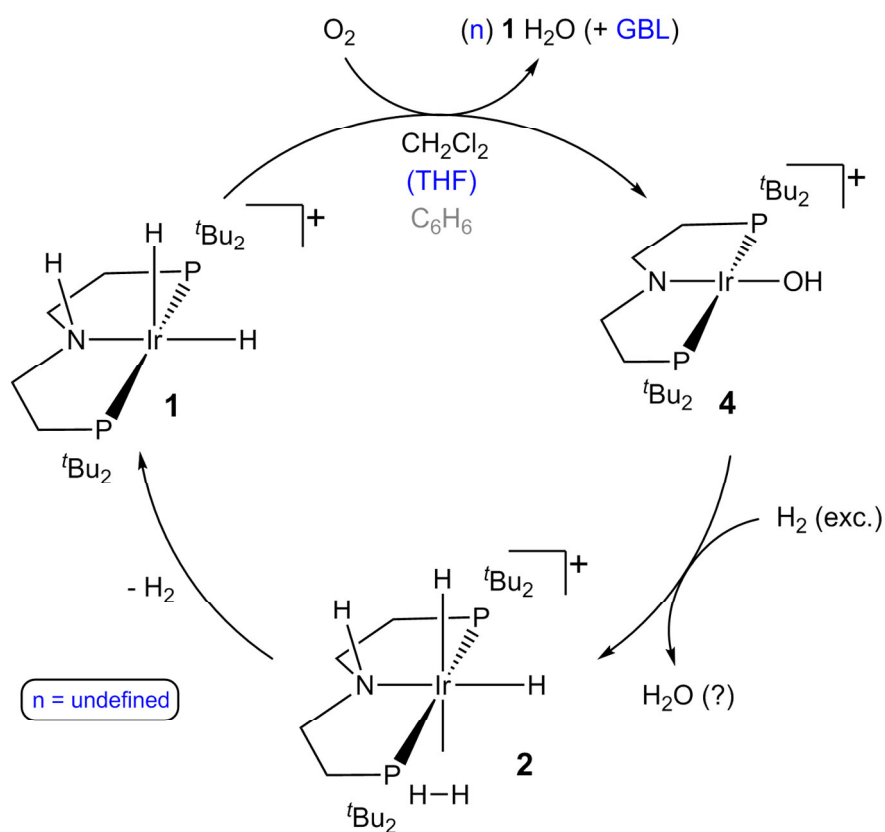
A more frequent iteration of the reaction cycle than three times is precluded by full conversion of **3** toward [Ir(HCl){HPNP^{tBu}}]PF₆ in dichloromethane over a few days. Furthermore, the hydrogenation step takes successively longer to be completed, presumably due to formation of H₂O, which could block the vacant coordination sites in [Ir(OH){PNP^{tBu}}]PF₆ (**4**). Perhaps, the cycle could be repeated more often in dichloromethane by removing the solvent mixture after every step and redissolving the solid residues again in dry dichloromethane.

Although, as mentioned above, **4** decomposes gradually in THF at r.t., the oxygenation-hydrogenation cycle can be completed three times in THF, until there are no diamagnetic species be observed anymore (no signal in ³¹P NMR, except of PF₆⁻). γ -Butyrolactone (GBL) is selectively generated during the oxidation of **3** towards **4** in THF. However, there was no success in quantitative experiments concerning the stoichiometry of the GBL formation.

The oxidation of **3** with O₂ toward **4** could be shown in C₆D₆ as well. The poor solubility of **4** in benzene in contrast to that of **3** could open up an easier synthesis route for **4** in benzene in the future.

B.2.4 Conclusion

In conclusion, an iridium complex that catalyzes ORR within several synthetic cycles was presented. Four-electron dioxygen splitting is accompanied by hydride oxidation of **3** and formation of a probable square-planar Ir^{III} complex **4**, thus, without a formal oxidation state change of the metal. At this point, preliminary mechanistic information and suggestions point toward insertion of O₂ in an Ir-H bond of the dihydride **3** as the first step, thereby formation of a hydroperoxo species and subsequently conversion to hydroxo complex **4** and H₂O. In this case, all four reduction equivalents would be stored within the Ir-H bonds of one molecule of



Scheme B.2-5: Oxygen splitting / hydrogenation cycle.

3. The vicinity of the amine moiety as Brønsted acid in **3** might facilitate oxygen activation but the possible role of coupled electron and proton transfer for the reaction kinetics needs to be examined further. However, amine deprotonation is highly instrumental in the ground-state stabilization of **4**, as the unusual electronic structure (*d*⁶, square-planar, low-spin) is subject to the strong π -donating character of the PNP dialkylamido ligand. Therefore, this process seems

to be truly 'bifunctional' to the effect that the ligand functions as a proton relay as amine and stabilizes coordinatively and electronically highly unsaturated intermediates like **4** in its deprotonated form.

Supporting Information:

B.2.5 Experimental Section

B.2.5.1 Materials and synthetic methods

All experiments were carried out under an atmosphere of argon using Schlenk and glove box techniques. Solvents were dried over Na/benzophenone/tetraglyme (benzene) and Na/benzophenone (THF, toluene), distilled under argon and deoxygenated prior to use or by passing through columns packed with activated alumina.

Pentanes and CH₂Cl₂ were dried by passing through columns packed with activated alumina. Deuterated solvents were obtained from Euriso-Top GmbH, dried over Na/K (C₆D₆) or CaH₂ (CD₂Cl₂), distilled by trap-to-trap transfer *in vacuo*, and degassed by three freeze-pump-thaw cycles. [IrCl(COE)₂]₂^[295] and HPNP^{*t*Bu}^[282] were prepared according to published procedures.

B.2.5.2 Analytical methods

Elemental analyses were obtained from the Microanalytical Laboratories of Friedrich-Alexander Universität Erlangen and Georg-August University of Göttingen. NMR spectra were recorded on the following spectrometers: Jeol Eclipse+ 400, Bruker Avance III 300, Bruker Avance 300, Bruker DRX 500 and were calibrated to the residual proton resonance of the solvent (CHDCl₂: δ = 5.32 ppm; C₆HD₅: δ = 7.16 ppm). ³¹P NMR chemical shifts are in case of present PF₆⁻ reported relative to PF₆⁻ (δ = -143.90 ppm) or in case of no PF₆⁻ reported relative to external phosphoric acid (δ = 0.0 ppm). ¹³C resonances are reported relative to CD₂Cl₂ (δ = 53.84 ppm). Signal multiplicities are abbreviated as: s (singlet), d (doublet), t (triplet), q (quartet), sept (septet), m (multiplet), br (broad). The mass spectrometry was performed with a maXis 3.2.12.6 spectrometer, acquired with the program micrOTOFcontrol 3.0.66.0 and processed with DataAnalysis 4.0.281.0.

B.2.5.3 Calculation of Eyring plots

VT NMR spectra were measured at a Bruker Avance III 400 spectrometer (**3** and **2**) and at a Bruker DRX 500 NMR spectrometer (**4**). NMR spectra for line shape analysis were processed with Nuts®. The simulation of the patterns was achieved with WinDNMR®^[296] using several mathematical approximations by the program. The rate constants *k* of the regions: *slow*, *intermediate* and *fast exchange*, were calculated by the following equations^[296]

[295] A. L. Onderlinden, A. van der Ent, *Inorg. Chim. Acta* **1972**, 6, 420.

[296] H. J. Reich, *J. Chem. Ed. Software* **1996**, 3D2, 17.

(region/approximations): *slow exchange*; $k = \pi(w_e - w_o)$, *intermediate exchange*; $k = \pi(\Delta\nu_o^2 - \Delta\nu_e^2)^{1/2}/2^{1/2}$, *fast exchange*; $k = \pi\Delta\nu_o^2/2(w_e - w_o)$ (with: ν_e = changing of the chemical shifts, w_e = line widths, w_e/w_o = full width at half maximum (fwhm) with or without exchange and ν_e/ν_o = chemical shifts of the decoalesced peaks with or without exchange^[297]). The natural line broadening w_o was assumed as the line broadening caused by window function of the spectra plus $3 \cdot 10^{-2}$ times of the fwhm of the overall CHDCl₂ signal (in case of **3** and **2**) or 1.5 times of the fwhm of the PF₆ signal (in case of **4**), because of broadening of the signals due to temperature dependent viscosity of CD₂Cl₂. The calculated rate constants were plotted in Excel®. The coalescence temperatures T_c were not directly observed but calculated from rate constant at the coalescence temperature k_c using the formulas: $k_c = \pi\Delta\nu_o/2^{1/2}$ in case of **3** and **2** and $k_c = \pi(\Delta\nu_o^2 + 6J^2)^{1/2}/2^{1/2}$ in case of **4** (with: $J = \textit{trans}^2 J_{PP}$) and the Arrhenius plots $\ln k$ vs $1/T$.

B.2.5.4 Syntheses:

B.2.5.4.1 [Ir(H)₂{HPNP^{tBu}}]PF₆ (**3**):

An orange solution of HPNP^{tBu} (442 mg, 1.22 mmol) and [Ir(COE)₂Cl]₂ (494 mg, 551 μ mol) in THF (25 mL) is stirred for 20 seconds at r.t. in the glove box. TlPF₆ (429 mg, 1.23 mmol) is added and the red mixture is stirred again for the same amount of time. The mixture is frozen (liquid N₂) at the Schlenk line with stirring and the atmosphere is changed from Ar to H₂ using a pressure-equalized Schlenk cross. The reaction is thawed by removing the cool bath and is stirred overnight at r.t. The resulting pale solution is filtered off and the grey residue is extracted with THF (5 x 5 ml). The combined filtrates are reduced *i. vac.* (~20 ml) until cloudiness appears in the now orange solution. It is then stored in the fridge (-17°C) overnight. The lye is filtered off and the orange, air-sensitive crystals are washed with pentanes (5 ml) and dried *i. vac.* (first yield: 279 mg, 389, μ mol, 35 %). The lye is recrystallized for two more times to obtain an overall yield of 645 mg, 899 μ mol, 82 % of orange **3** with 0.25 equivalents of THF (which could not be separated from the product after prolonged drying *i. vac.*). A distinct amount of **3** is chlorinated in dichloromethane at r.t. over several hours. Anal. calcd. for C₂₀H₄₇F₆IrNP₃ · (C₄H₈O)_{0.25} (717.74): C, 35.12; H, 6.74; N, 1.95. Found: C, 34.99; H, 6.74; N, 1.51. NMR (r.t., CD₂Cl₂, [ppm]): ¹H NMR (399.8 MHz): δ = -31.11 (br, 2H, IrH₂), 1.18 (A₉XX'A'₉, N = |³J_{HP} + ⁵J_{HP}| = 7 Hz, 18H, P^tBu^tBu), 1.23 (A₉XX'A'₉, N = |³J_{HP} + ⁵J_{HP}| = 7 Hz, 18H, P^tBu^tBu), 2.30 (m, 4H, PCH₂ + NCH₂), 2.51 (m, 2H, PCH₂), 3.71 (m,

[297] If one wants to calculate k by hand, because of a strong roof effect of the decoalesced ³¹P NMR signals in case of [Ir(OH){PNP^{tBu}}]PF₆ (**4**), the determination of the changing of the chemical shifts ν_e and the line widths w_e has to be done by referring the separate signals of the two doublets to their arithmetic average. See: H. Friebolin, *Ein- und zweidimensionale NMR-Spektroskopie. Eine Einführung*, Wiley-VCH, Weinheim, 2013.

2H, NCH₂), 4.67 (br, 1H, NH), ¹³C{¹H} NMR (75.5 MHz): δ = 27.63 (AXX'A', N = |¹J_{CP} + ³J_{CP}| = 10.8 Hz, PCH₂), 28.64 (A₃XX'A₃', N = |²J_{CP} + ⁴J_{CP}| = 2.5 Hz, PC(CH₃)₃), 28.75 (A₃XX'A₃', N = |²J_{CP} + ⁴J_{CP}| = 3.0 Hz, PC(CH₃)₃), 33.71 (AXX'A', N = |¹J_{CP} + ³J_{CP}| = 12.6 Hz, PC(CH₃)₃), 37.29 (AXX'A', N = |¹J_{CP} + ³J_{CP}| = 11.8 Hz, PC(CH₃)₃), 56.67 (AXX'A', N = |²J_{CP} + ³J_{CP}| = 2.4 Hz, NCH₂), ³¹P NMR (161.8 MHz): δ = 83.97 (s, P^tBu₂), -143.90 (sept, ¹J_{PF} = 712 Hz, PF₆), MS(ESI): m/z = 556.2819 ([M] - PF₆⁻, 100 %).

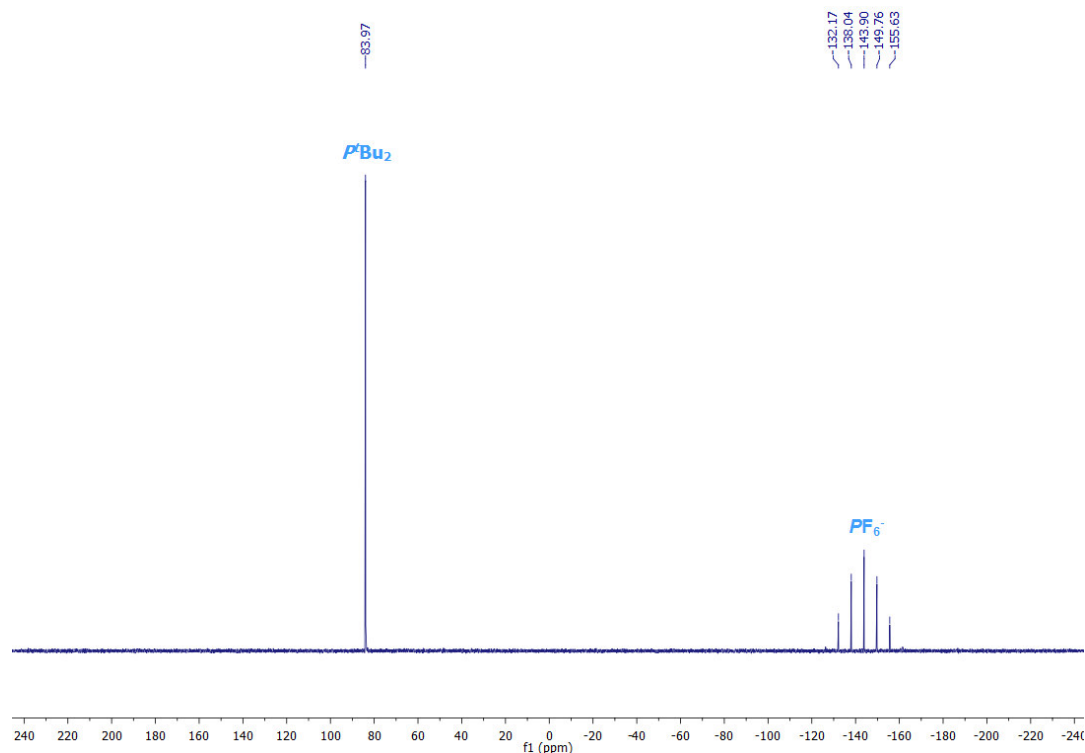


Figure B.2-6: ³¹P NMR spectrum (r.t., CD₂Cl₂) of [Ir(H)₂{HPNP^tBu}]PF₆ (3).

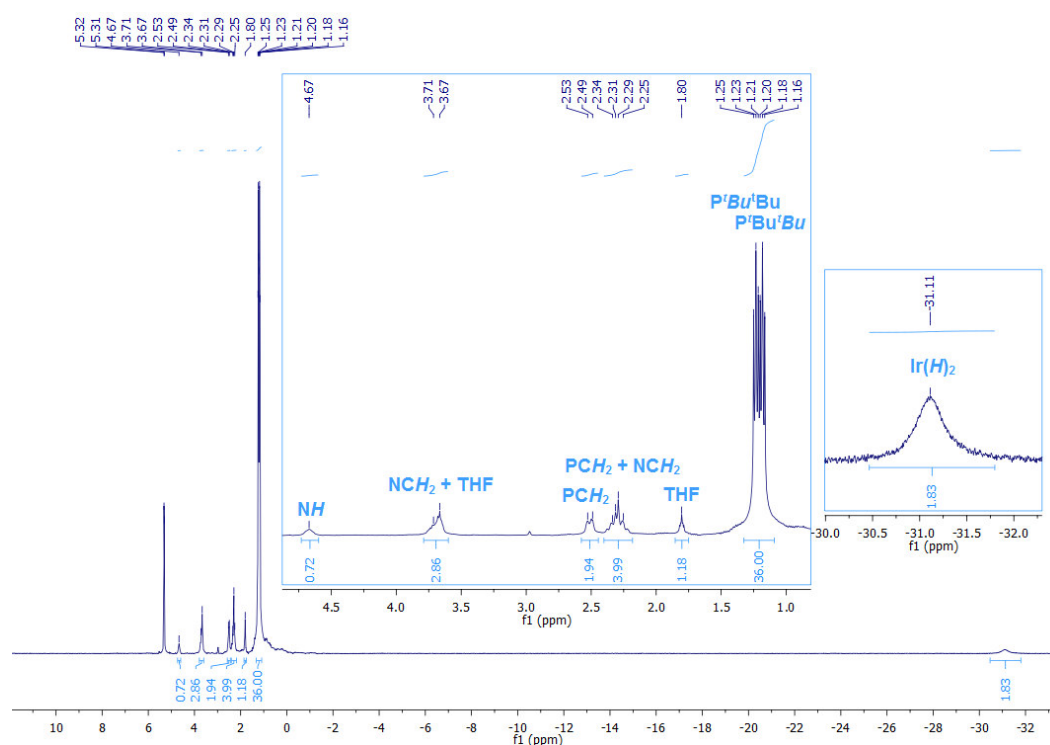


Figure B.2-7: ¹H NMR spectrum (r.t., CD₂Cl₂) of [Ir(H)₂{HPNP^tBu}]PF₆ (3).

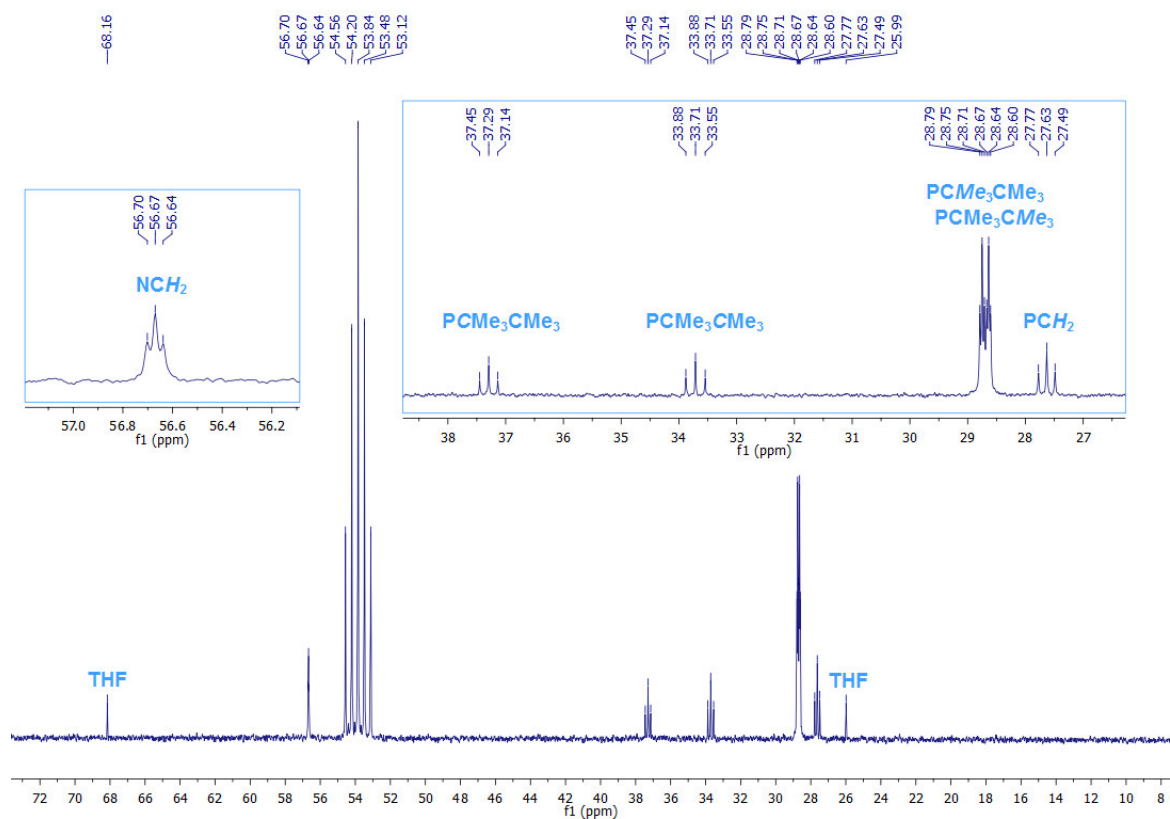


Figure B.2-8: ^{13}C NMR spectrum (r.t., CD_2Cl_2) of $[\text{Ir}(\text{H})_2\{\text{HPNP}^t\text{Bu}\}]\text{PF}_6$ (**3**).

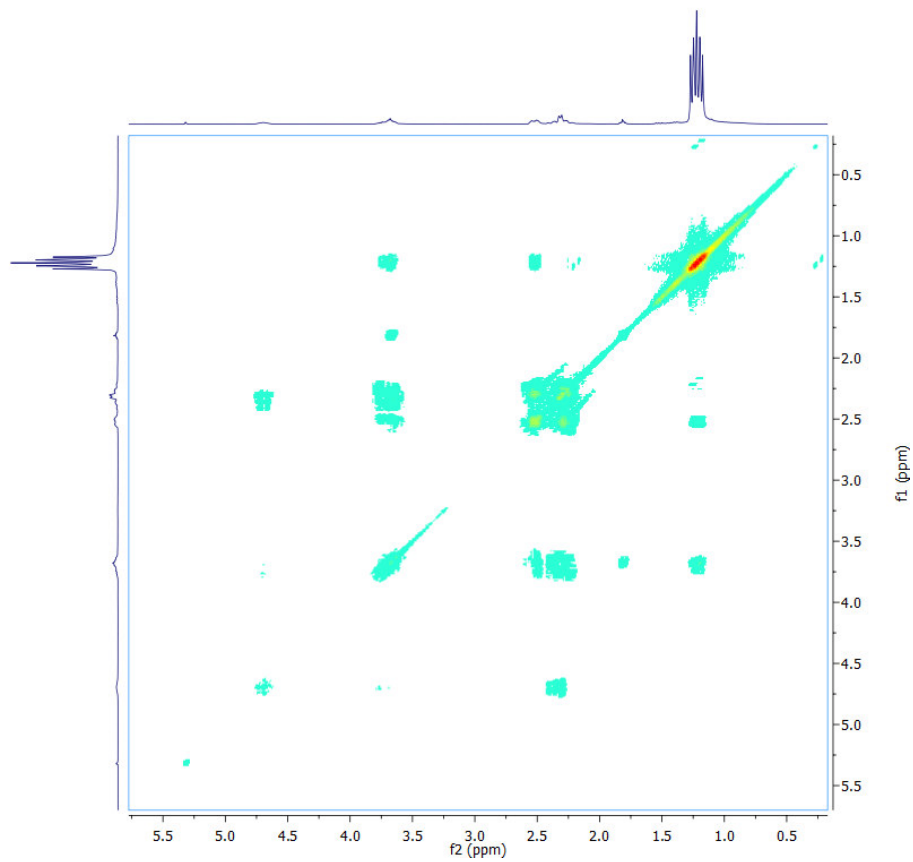


Figure B.2-9: ^1H cosy NMR spectrum (r.t., CD_2Cl_2) of $[\text{Ir}(\text{H})_2\{\text{HPNP}^t\text{Bu}\}]\text{PF}_6$ (**3**).

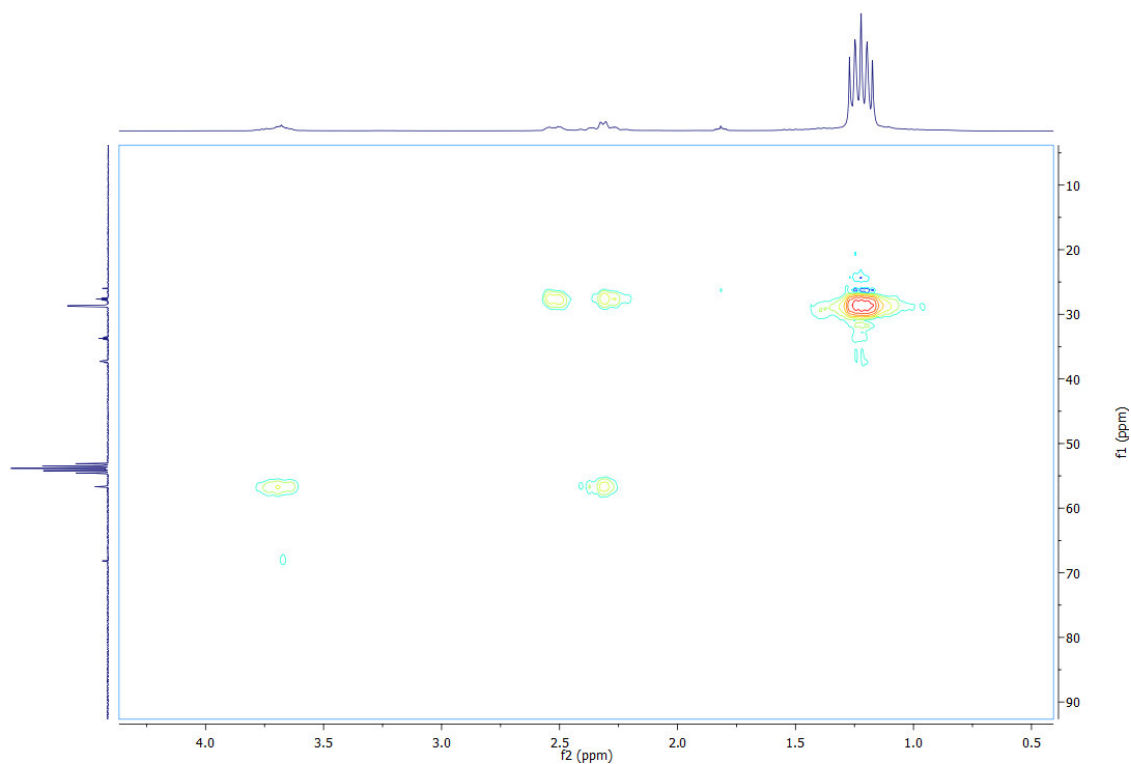


Figure B.2-10: ^1H , ^{13}C HSQC NMR spectrum (r.t., CD_2Cl_2) of $[\text{Ir}(\text{H})_2\{\text{HPNP}^{t\text{Bu}}\}]\text{PF}_6$ (**3**).

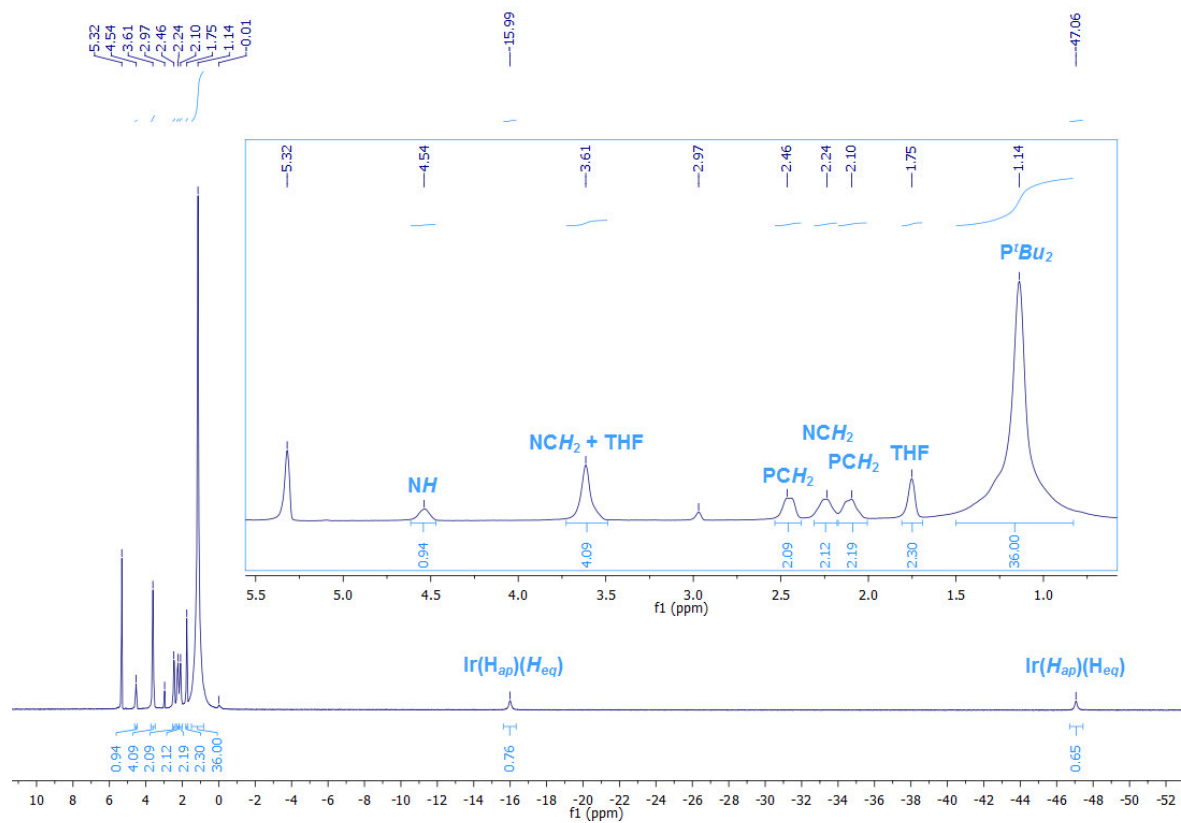


Figure B.2-11: ^1H NMR spectrum (190 K, CD_2Cl_2) of $[\text{Ir}(\text{H})_2\{\text{HPNP}^{t\text{Bu}}\}]\text{PF}_6$ (**3**).

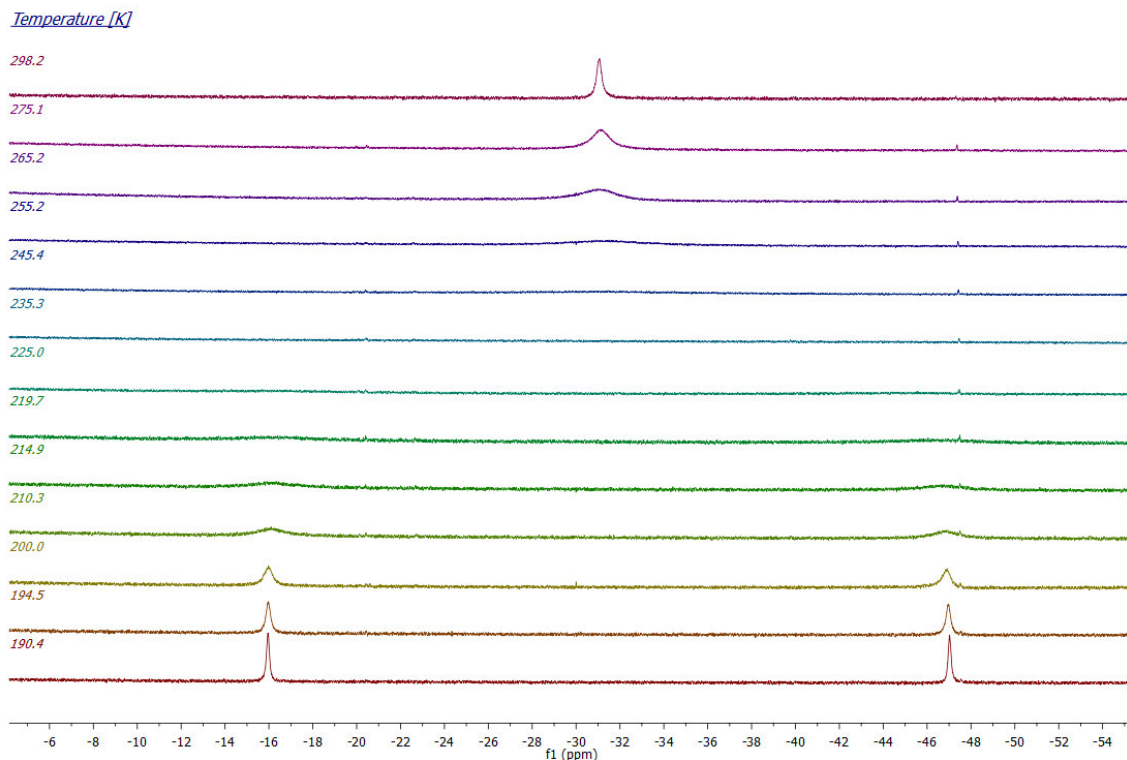


Figure B.2-12: ^1H NMR spectrum (VT, CD_2Cl_2 , high field region) of $[\text{Ir}(\text{H})_2\{\text{HPNP}^{\text{tBu}}\}]\text{PF}_6$ (**3**); $\delta(190.4 \text{ K}, [\text{ppm}]) = -47.06$ (br, 2H, $\text{Ir}(\text{H}_{\text{ap}})(\text{H}_{\text{eq}})$), -15.99 (br, 2H, $\text{Ir}(\text{H}_{\text{ap}})(\text{H}_{\text{eq}})$).

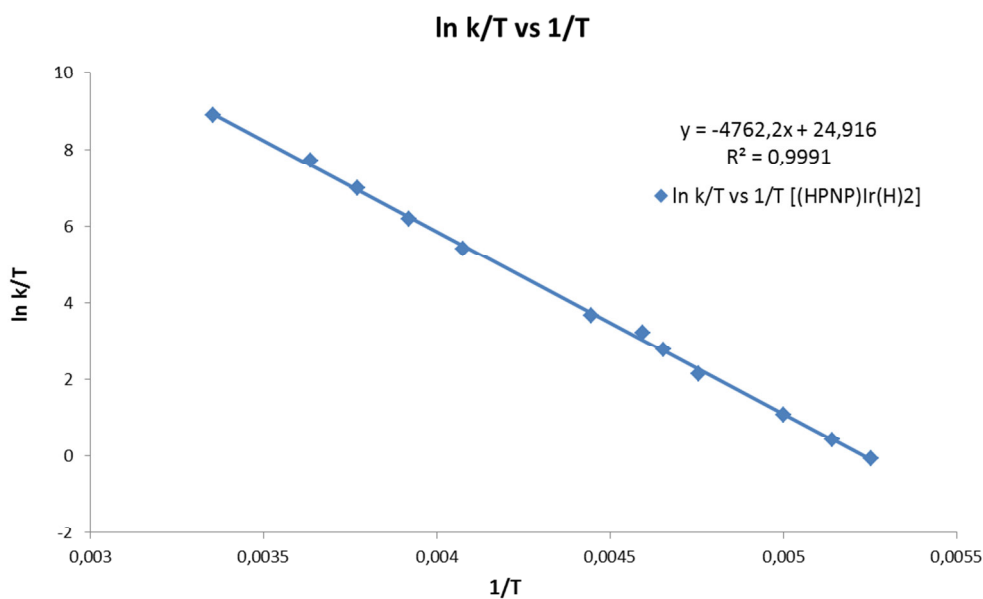


Figure B.2-13: Eyring plot of the symmetric exchange process between the apical and the equatorial hydrido ligand of $[\text{Ir}(\text{H})_2\{\text{HPNP}^{\text{tBu}}\}]\text{PF}_6$ (**3**); $\Delta H^\ddagger = 40 \pm 0.5 \text{ kJ/mol}$, $\Delta S^\ddagger = 10 \pm 2 \text{ J/molK}$, $T_{\text{c}}(\text{calc } 400\text{MHz}) = -37^\circ\text{C}$.

Compound Spectra

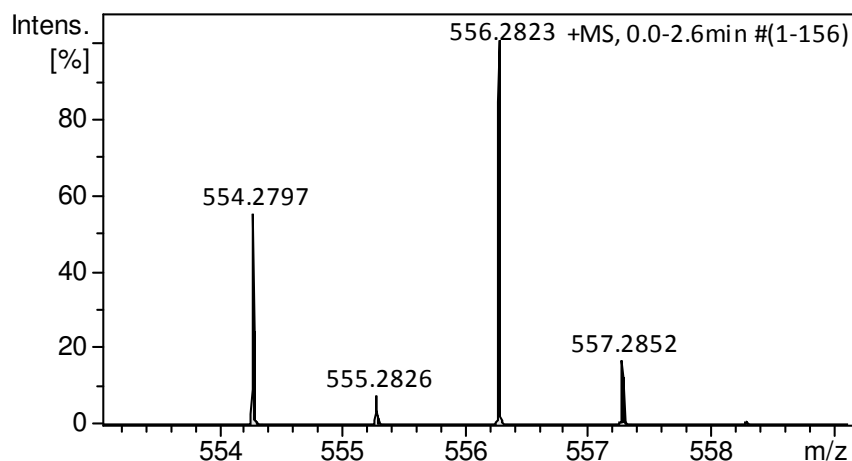


Figure B.2-14: High resolution MS spectrum of $[\text{Ir}(\text{H})_2\{\text{HPNP}^t\text{Bu}\}]\text{PF}_6$ (**3**)

B.2.5.4.2 $[\text{Ir}(\text{H}_2)(\text{H})_2\{\text{HPNP}^t\text{Bu}\}]\text{PF}_6$ (**2**):

An orange solution of $[\text{Ir}(\text{H})_2\{\text{HPNP}^t\text{Bu}\}]\text{PF}_6$ (**3**) (5 mg, 7 μmol in 0.5 ml CD_2Cl_2) is treated with an excess of H_2 . The resulting pale solution is studied by NMR spectroscopy. NMR (r.t., CD_2Cl_2 , [ppm]) ^1H NMR (400.12 MHz): $\delta = -9.91$ (br, 4H, $\text{Ir}(\text{H})_2\text{H}_2$), 1.29 ($\text{A}_9\text{XX}'\text{A}'_9$, $N = |^3J_{\text{HP}} + ^5J_{\text{HP}}| = 6.6$ Hz, 18H, $\text{P}^t\text{Bu}^t\text{Bu}$), 1.35 ($\text{A}_9\text{XX}'\text{A}'_9$, $N = |^3J_{\text{HP}} + ^5J_{\text{HP}}| = 6.1$ Hz, 18H, $\text{P}^t\text{Bu}^t\text{Bu}$), 1.97 (m, 2 H, CH_2), 2.30 (m, 4H, CH_2), 3.56 (m, 2H, CH_2), 5.16 (br, 1H, NH), ^{31}P NMR (162.0 MHz, 27°C): $\delta = 71.86$ (s, P^tBu_2), -143.90 (sept, $^1J_{\text{PF}} = 712$ Hz, PF_6).

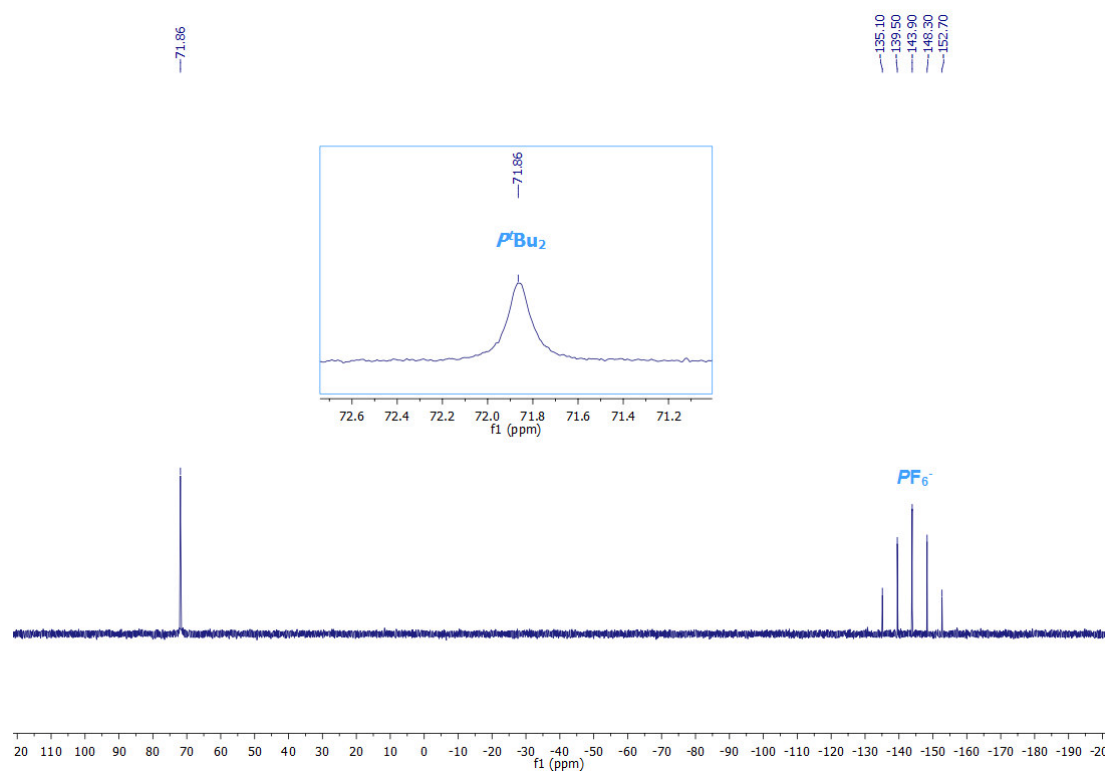


Figure B.2-15: ^{31}P NMR spectrum (r.t., CD_2Cl_2) of $[\text{Ir}(\text{H}_2)(\text{H})_2\{\text{HPNP}^t\text{Bu}\}]\text{PF}_6$ (**2**).

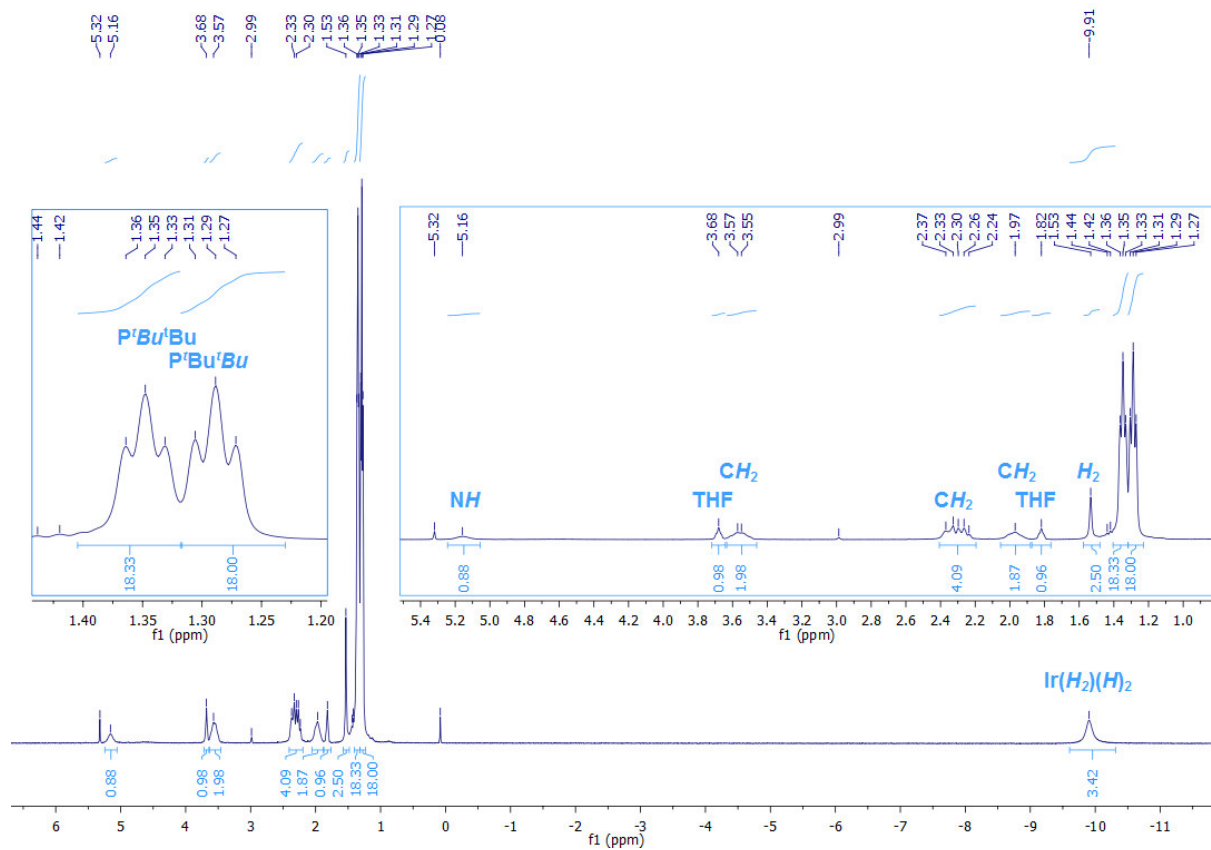


Figure B.2-16: ^1H NMR spectrum (r.t., CD_2Cl_2) of $[\text{Ir}(\text{H}_2)(\text{H})_2\{\text{HPNP}^{\text{tBu}}\}]\text{PF}_6$ (**2**).

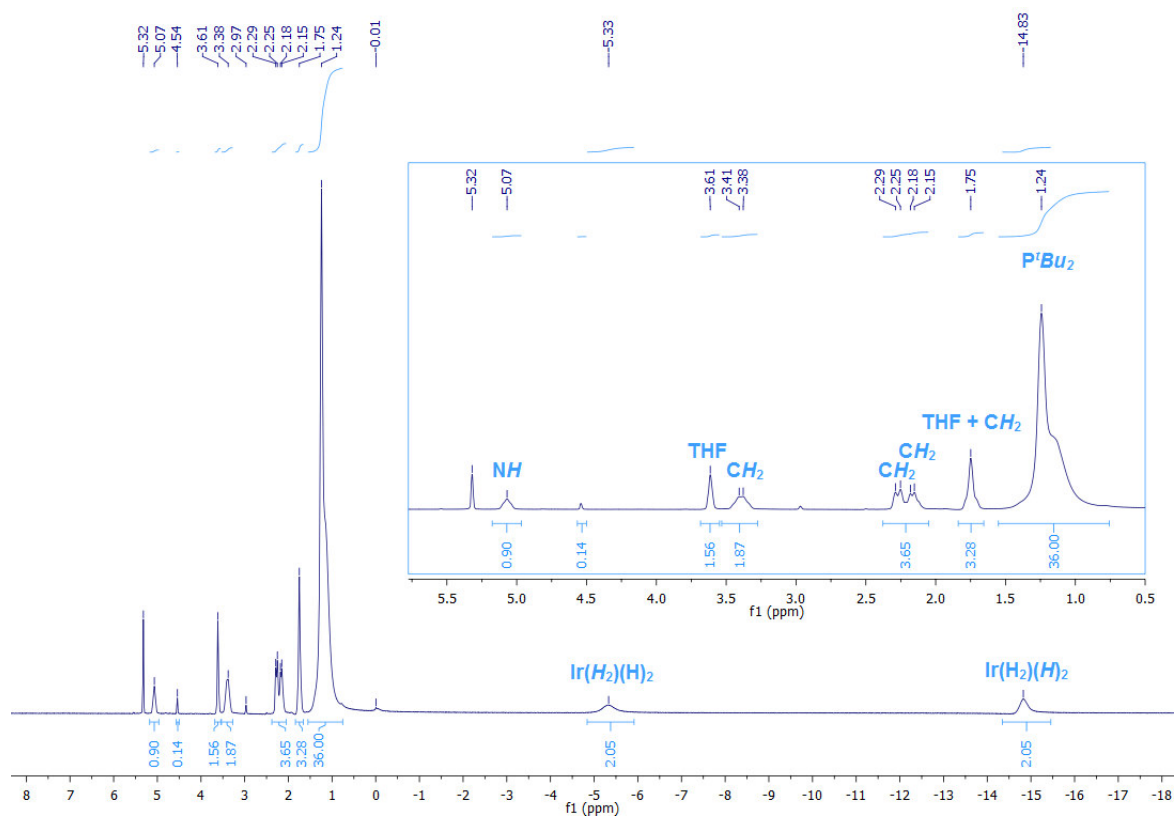


Figure B.2-17: ^1H NMR spectrum (190 K, CD_2Cl_2) of $[\text{Ir}(\text{H}_2)(\text{H})_2\{\text{HPNP}^{\text{tBu}}\}]\text{PF}_6$ (**2**).

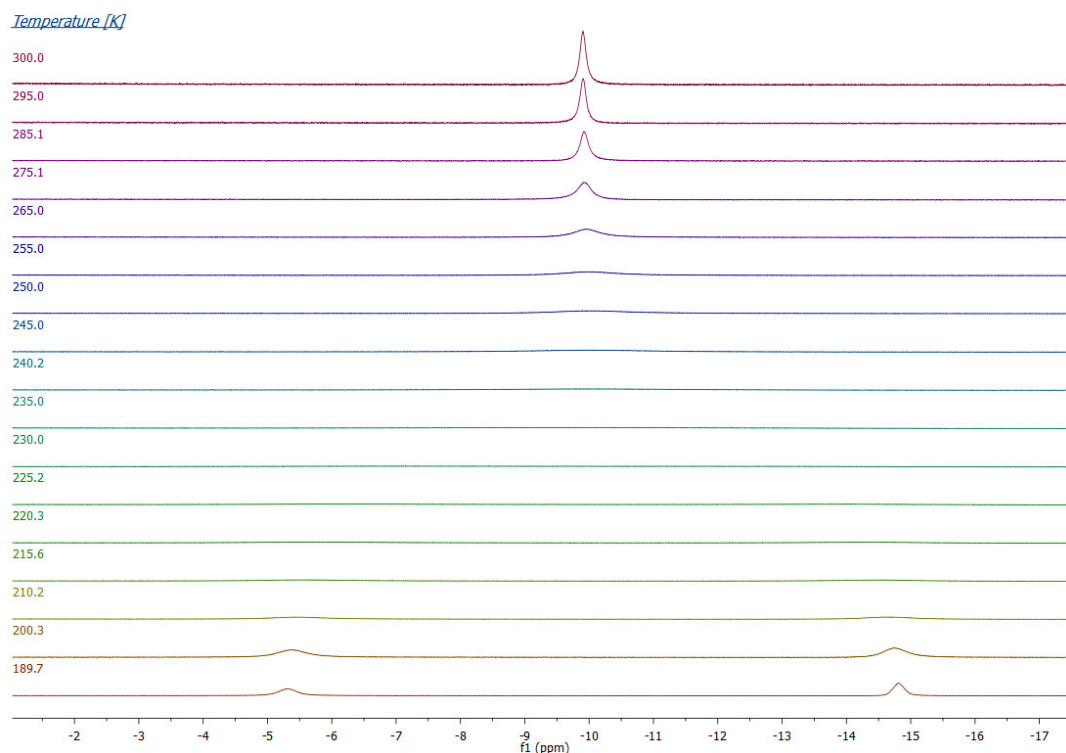


Figure B.2-18: ^1H NMR spectrum (VT, CD_2Cl_2 , high field region) of $[\text{Ir}(\text{H}_2)(\text{H})_2\{\text{HPNP}^{\text{tBu}}\}]\text{PF}_6$ (**2**); δ (189.7 K, [ppm]) = -14.83 (br, 2H, $\text{Ir}(\text{H}_2)(\text{H})_2$), -5.33 (br, 2H, $\text{Ir}(\text{H})_2(\text{H})_2$).

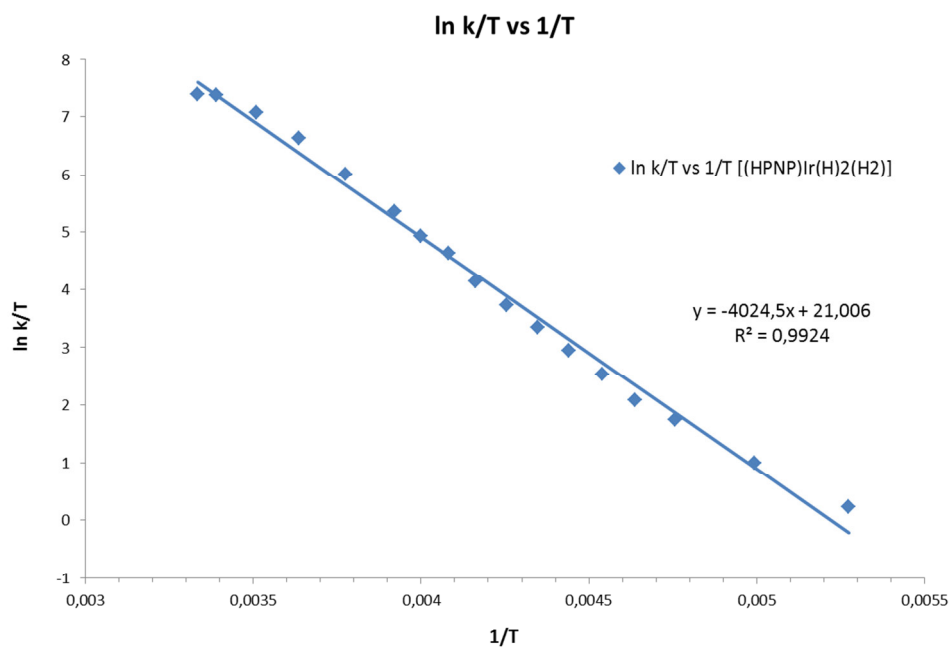


Figure B.2-19: Eyring plot of the symmetric exchange process between the two hydrido (not decoalescenced) ligands and the dihydrogen ligand of $[\text{Ir}(\text{H})_2(\text{H}_2)\{\text{HPNP}^{\text{tBu}}\}]\text{PF}_6$ (**2**); $\Delta\text{H}^\ddagger = 33.5 \pm 1$ kJ/mol, $\Delta\text{S}^\ddagger = -23 \pm 3$ J/molK, $\text{T}_{\text{C}(\text{calc } 400\text{MHz})} = -42^\circ\text{C}$.

B.2.5.4.3 [Ir(OH){PNP^{tBu}}]PF₆ (**4**):

[Ir(H)₂{HPNP^{tBu}}]PF₆ (**3**) (37 mg, 52 μmol) is dissolved in 15 ml of THF in a 50 ml *J*-Young flask, connected to a pressure equalized Schlenk cross, frozen, evacuated and purged with a dioxygen (overpressure = -0.25 bar) argon (overpressure of the Schlenk line = +0.2 bar) mixture. The flask is closed, disconnected and stirred from time to time for 30 minutes at r.t. The resulting pale brown solution is reduced *in vacuo* until crystallization appears (3 ml), cooled to -80°C and filtrated. The dark solid is washed with pentanes (2 x 3 ml) and dried *in vacuo* to yield 23 mg (32 μmol, 62 %) of grey **4**. **4** decomposes upon dissolution in THF at r.t. over several hours. Anal. calcd. for C₂₀H₄₅F₆IrNOP₃(714.70): C, 33.61; H, 6.35; N, 1.96. Found: C, 33.89; H, 6.15; N, 1.92. NMR (r.t., CD₂Cl₂, [ppm]): ¹H NMR (400.13 MHz): δ = -2.23 (m, 2H, NCH₂), 1.52 (A₁₈XX'A'₁₈, N = |³J_{HP} + ⁵J_{HP}| = 10.8 Hz, 36H, P^tBu₂), 2.16 (m, 2H, PCH₂) 11.62 (t, ³J_{HP} = 7.4 Hz, 1H, OH), ¹³C NMR (75.5 MHz): δ = 21.22 (AXX'A', N = |¹J_{CP} + ³J_{CP}| = 11.2 Hz, PCH₂), 30.07 (A₆XX'A₆', N = |²J_{CP} + ⁴J_{CP}| = 2.6 Hz, PC(CH₃)₃), 37.54 (A₄XX'A₄', N = |¹J_{CP} + ³J_{CP}| = 11.1 Hz, PC(CH₃)₃), 88.80 (AXX'A', N = |²J_{CP} + ³J_{CP}| = 3.1 Hz, NCH₂), ³¹P NMR (161.8 MHz): δ = 62.72 (s, P^tBu₂), -143.90 (sept, ¹J_{PF} = 711 Hz, PF₆), IR (Nujol [cm⁻¹]): ν = 3603.6 (w), 2721.3 (w), 1020.9 (w), 971.5 (w), 840.8 (s), 604.6 (w), 597.6 (w), 557.8 (m), 533.2 (w), 521.7 (w), 514.7 (w), 506.7 (w), Cryo Spray ESI-MS (0°C): m/z = 570.2614 ([M] - PF₆⁻, 100 %). In CD₂Cl₂ it is impossible to detect the number of equivalents of the water produced during the oxygenation reaction directly by ¹H NMR because of the overlapping signals of HDO (δ = 1.51 ppm) and of the ^{tert}Butyl groups (δ = 1.52). Therefore, the following experiment is carried out: **3** (17 mg, 24 μmol) is dissolved in 0.6 ml CD₂Cl₂ in a *J*-Young NMR tube and a defined amount of C₆H₆ is added. The tube is connected to a Schlenk cross, frozen, evacuated and purged with an excess of dioxygen (overpressure of the Schlenk line = +0.2 bar). The reaction is monitored at r.t. by ³¹P and ¹H NMR spectroscopy until no more educt **3** can be detected and the product **4** is formed for the most part (80 % by ³¹P NMR, 65% by ¹H NMR in around 16 hours). The mixture is frozen and all volatile parts are collected in another *J*-Young NMR tube by trap to trap condensation over a bridge and the mixture is studied by quantitative ¹H NMR spectroscopy.

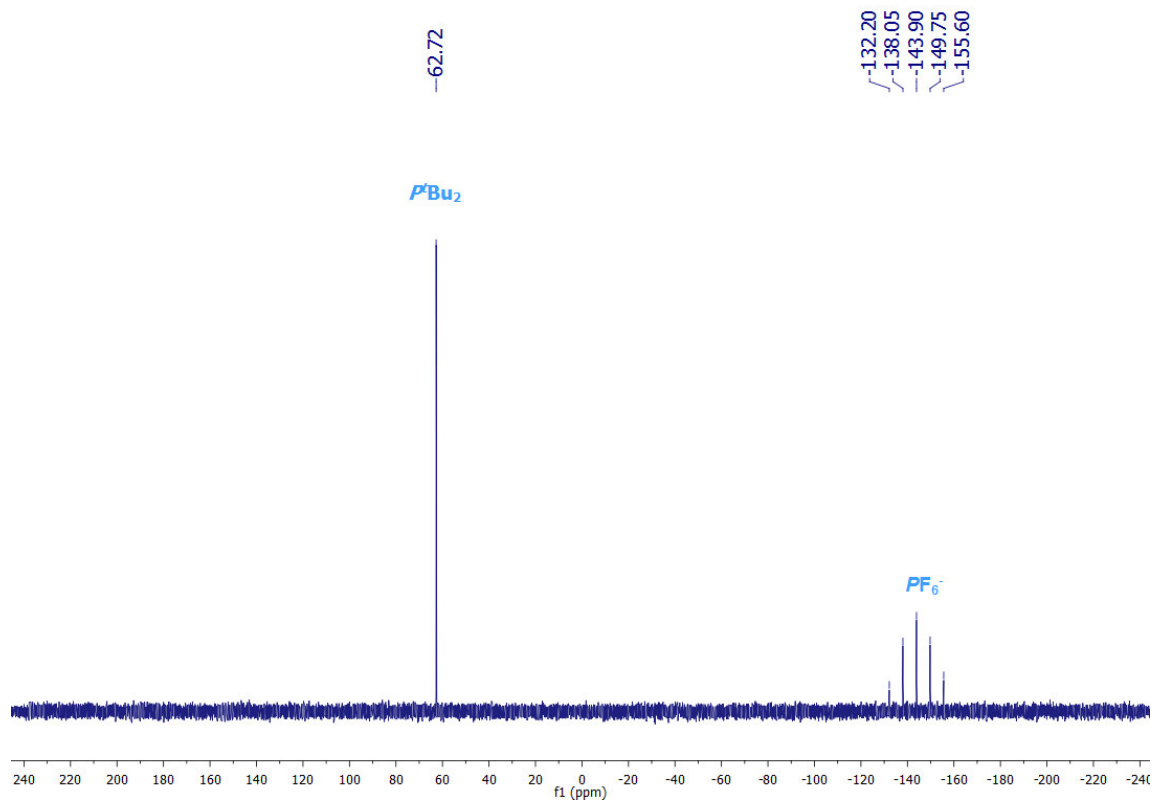


Figure B.2-20: ^{31}P NMR spectrum (r.t., CD_2Cl_2) of $[\text{Ir}(\text{OH})\{\text{PNP}^t\text{Bu}\}]\text{PF}_6$ (**4**).

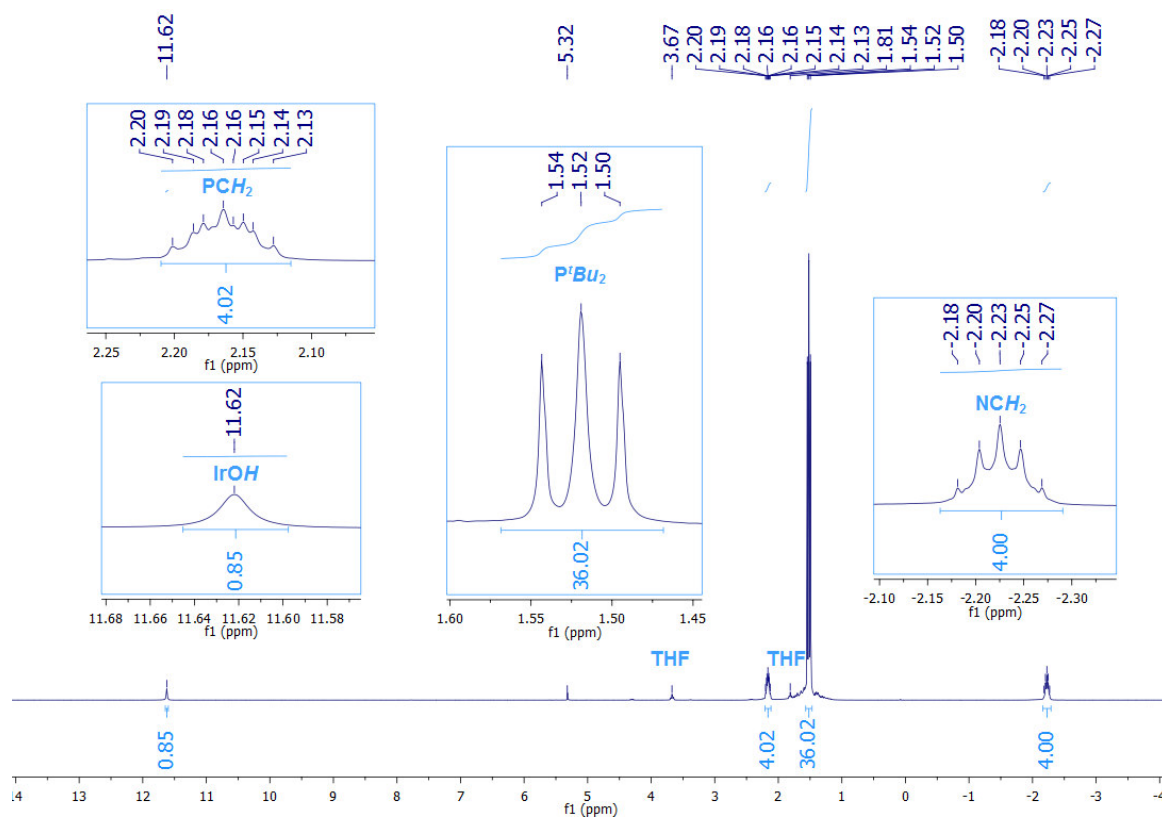


Figure B.2-21: ^1H NMR spectrum (r.t., CD_2Cl_2) of $[\text{Ir}(\text{OH})\{\text{PNP}^t\text{Bu}\}]\text{PF}_6$ (**4**).

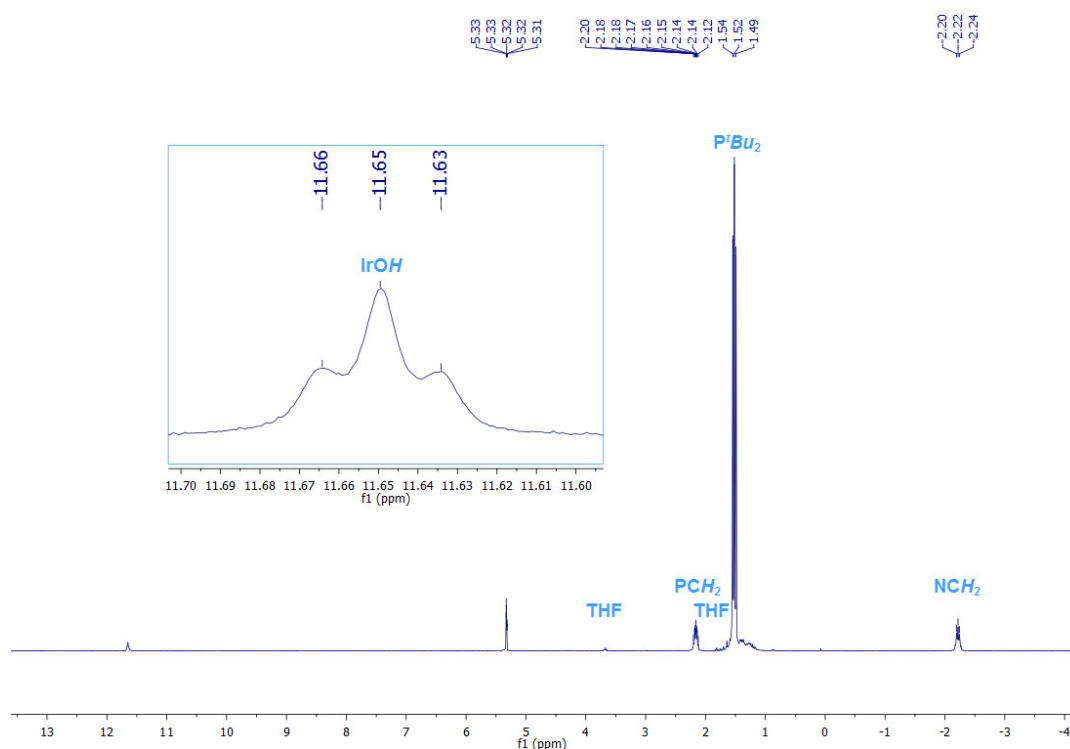


Figure B.2-22: ¹H NMR spectrum (r.t., CD₂Cl₂) of [Ir(OH){PNP^tBu}]PF₆ (**4**), lower concentration than in **Figure B.2-21**.

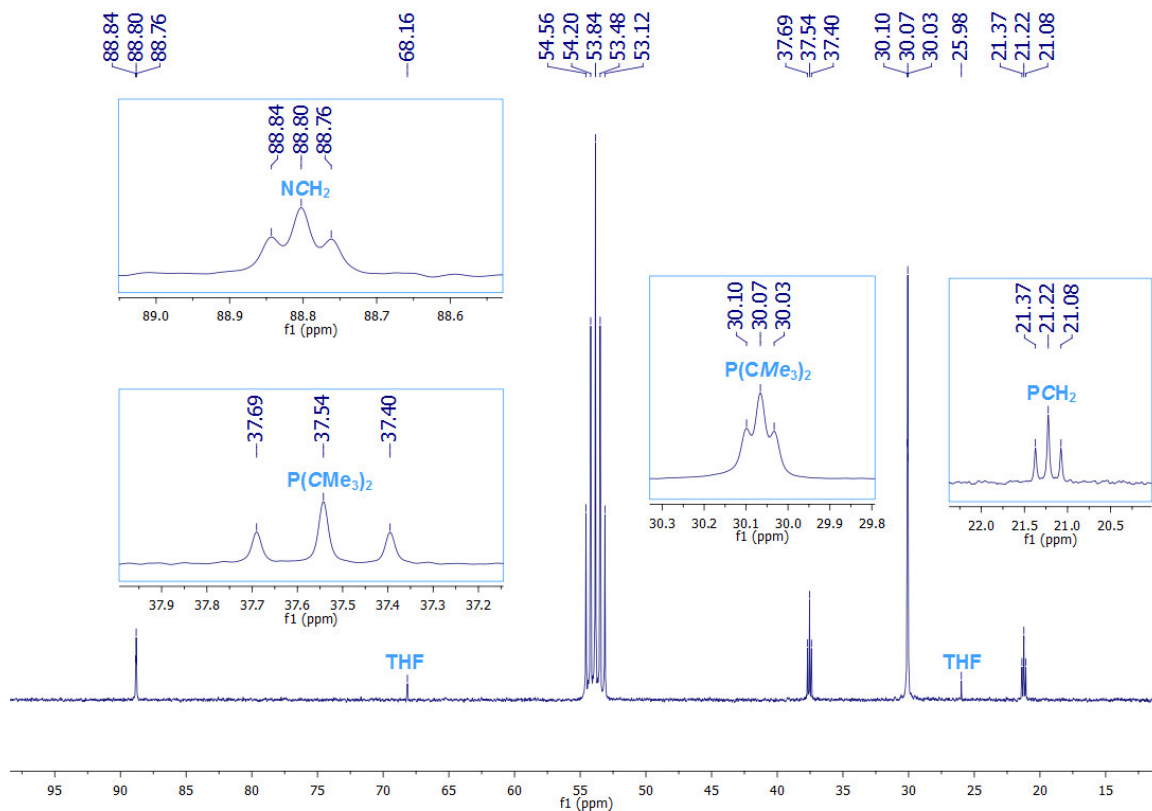


Figure B.2-23: ¹³C NMR spectrum (r.t., CD₂Cl₂) of [Ir(OH){PNP^tBu}]PF₆ (**4**).



Figure B.2-24: ^1H , ^1H COSY NMR spectrum (r.t., CD_2Cl_2) of $[\text{Ir}(\text{OH})\{\text{PNP}^{\text{tBu}}\}]\text{PF}_6$ (**4**).

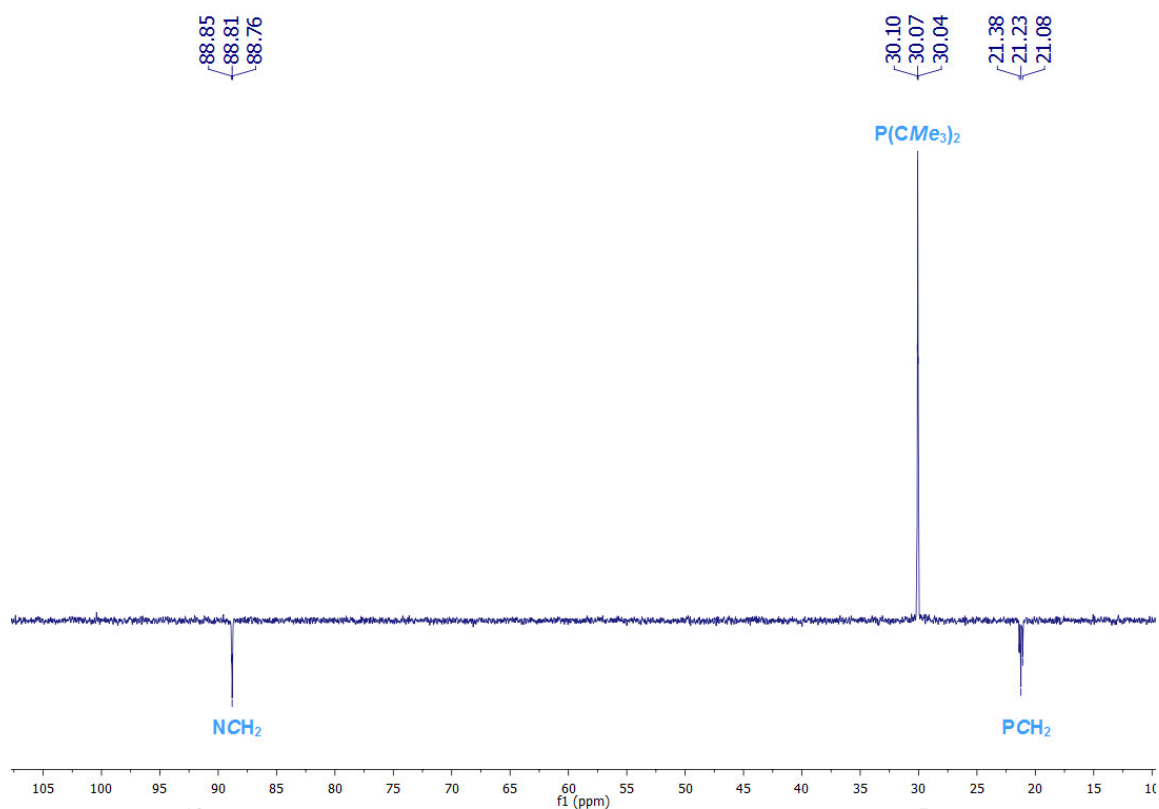


Figure B.2-25: ^{13}C DEPT NMR spectrum (r.t., CD_2Cl_2) of $[\text{Ir}(\text{OH})\{\text{PNP}^{\text{tBu}}\}]\text{PF}_6$ (**4**).

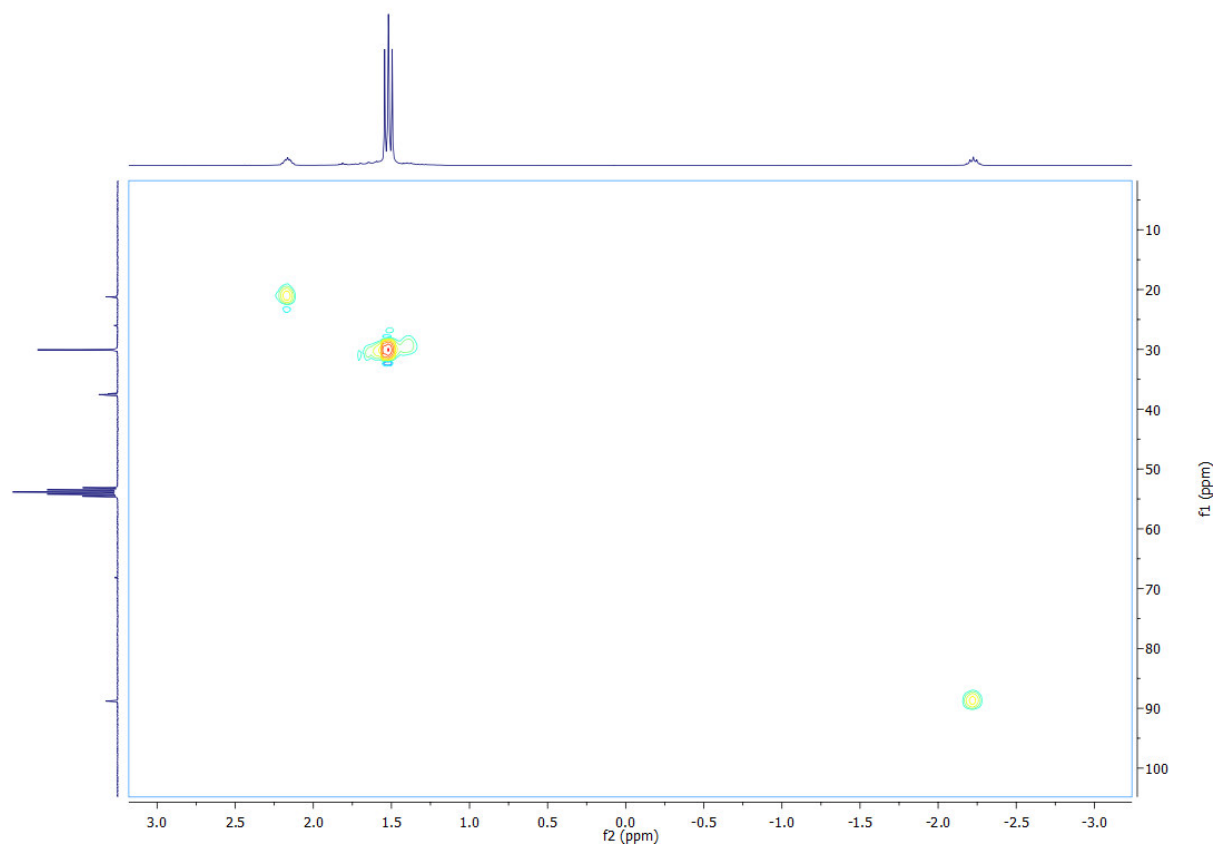


Figure B.2-26: ^1H , ^{13}C HSQC NMR spectrum (r.t., CD_2Cl_2) of $[\text{Ir}(\text{OH})\{\text{PNP}^t\text{Bu}\}]\text{PF}_6$ (**4**).

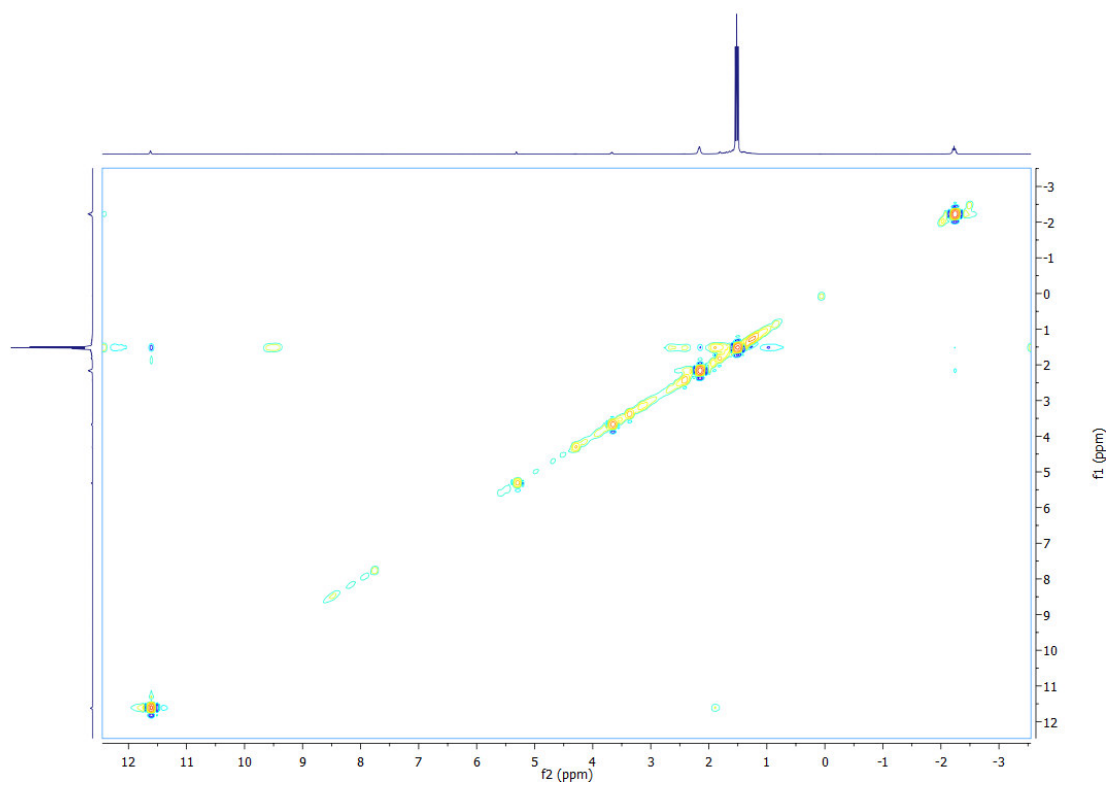


Figure B.2-27: ^1H , ^1H NOESY NMR spectrum (r.t., CD_2Cl_2) of $[\text{Ir}(\text{OH})\{\text{PNP}^t\text{Bu}\}]\text{PF}_6$ (**4**).

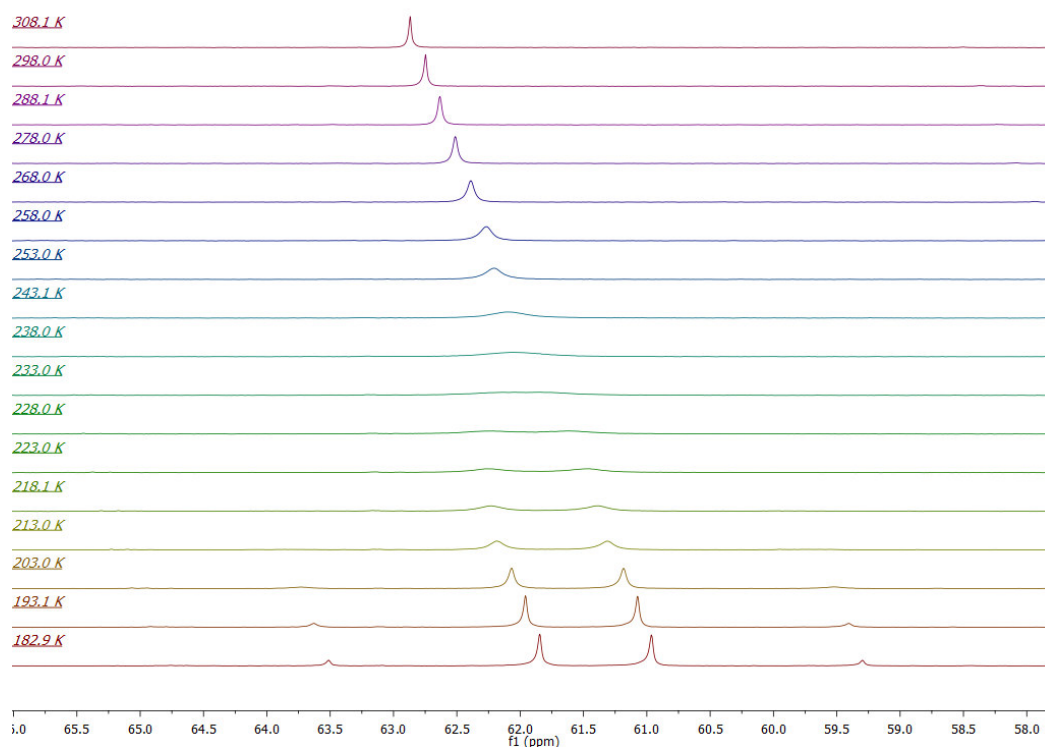


Figure B.2-28: ^{31}P NMR spectrum (VT, CD_2Cl_2) of $[\text{Ir}(\text{OH})\{\text{PNP}^{\text{tBu}}\}]\text{PF}_6$ (4); δ (182.9 K, [ppm]) = 60.67 (d, $\text{trans}^{-2}J_{\text{PP}} = 336$ Hz, $\text{Ir}(\text{P}_a^{\text{tert}}\text{Bu}_2)(\text{P}_b^{\text{tert}}\text{Bu}_2)$), 62.09 (d, $\text{trans}^{-2}J_{\text{PP}} = 336$ Hz, $\text{Ir}(\text{P}_a^{\text{tert}}\text{Bu}_2)(\text{P}_b^{\text{tert}}\text{Bu}_2)$).

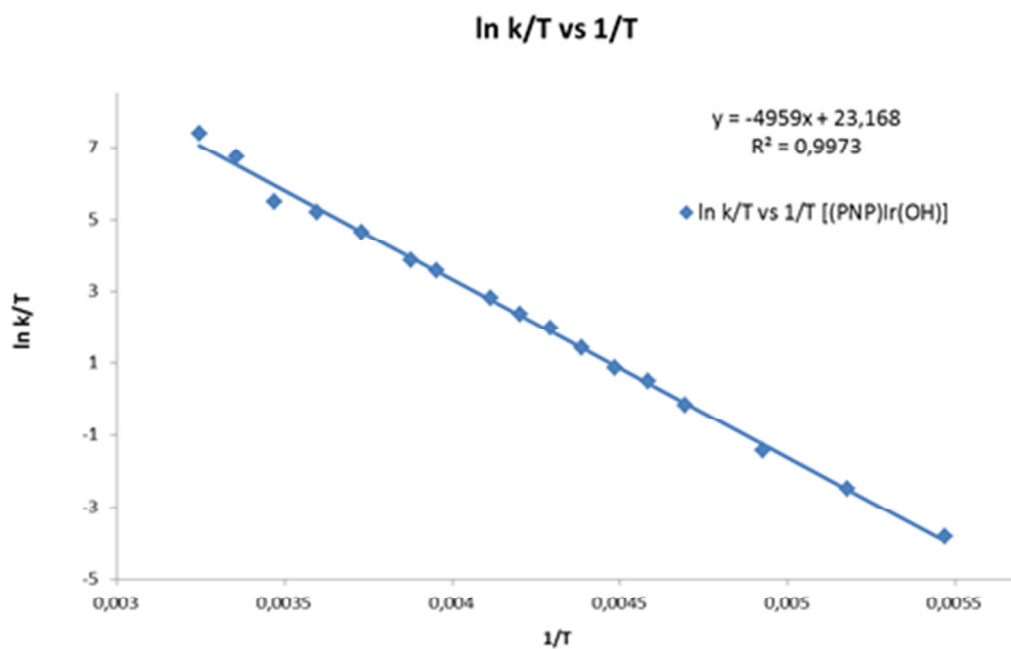


Figure B.2-29: Eyring plot for the dynamic process within $[\text{Ir}(\text{OH})\{\text{PNP}^{\text{tBu}}\}]\text{PF}_6$ (4) in CD_2Cl_2 ; $\Delta H^\ddagger = 41 \pm 1$ kJ/mol, $\Delta S^\ddagger = -5 \pm 2$ J/molK, $T_{\text{c}(\text{calc } 500\text{MHz})} = -38^\circ\text{C}$.

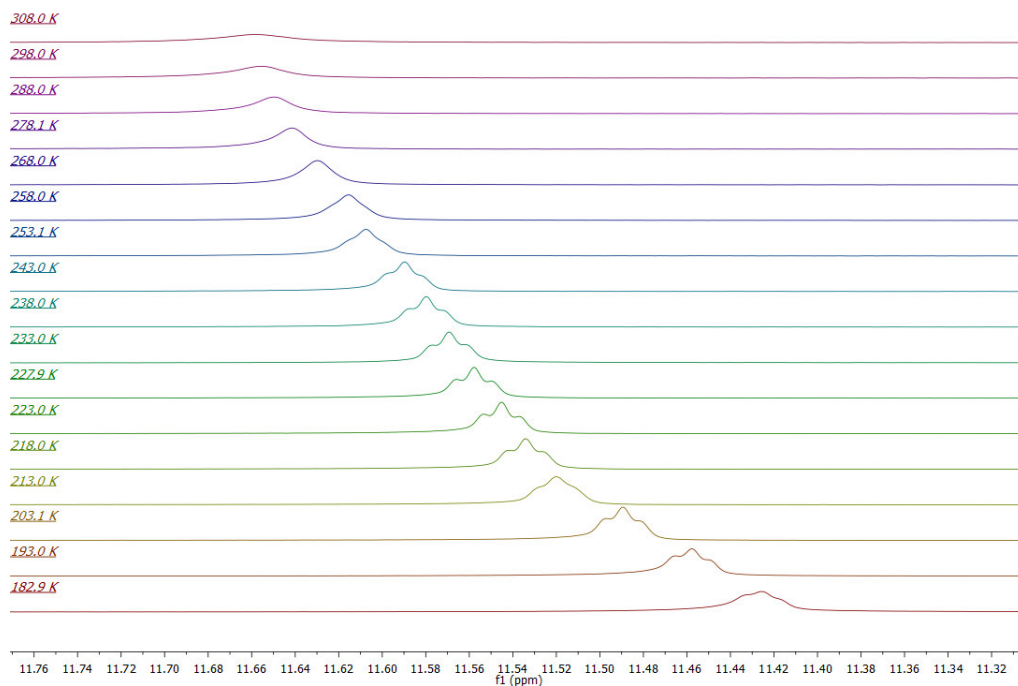


Figure B.2-30: ^1H NMR spectrum (VT, CD_2Cl_2) of $[\text{Ir}(\text{OH})\{\text{PNP}^t\text{Bu}\}]\text{PF}_6$ (4); IrOH signal

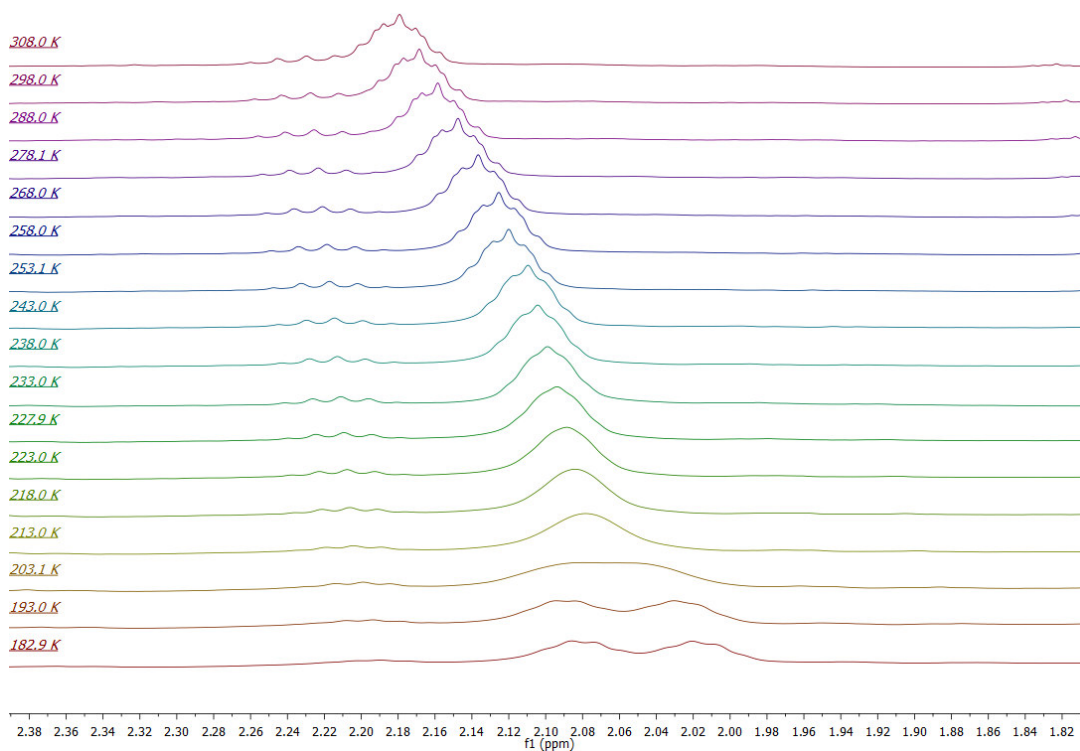


Figure B.2-31: ^1H NMR spectrum (VT, CD_2Cl_2) of $[\text{Ir}(\text{OH})\{\text{PNP}^t\text{Bu}\}]\text{PF}_6$ (4); PCH₂ signal

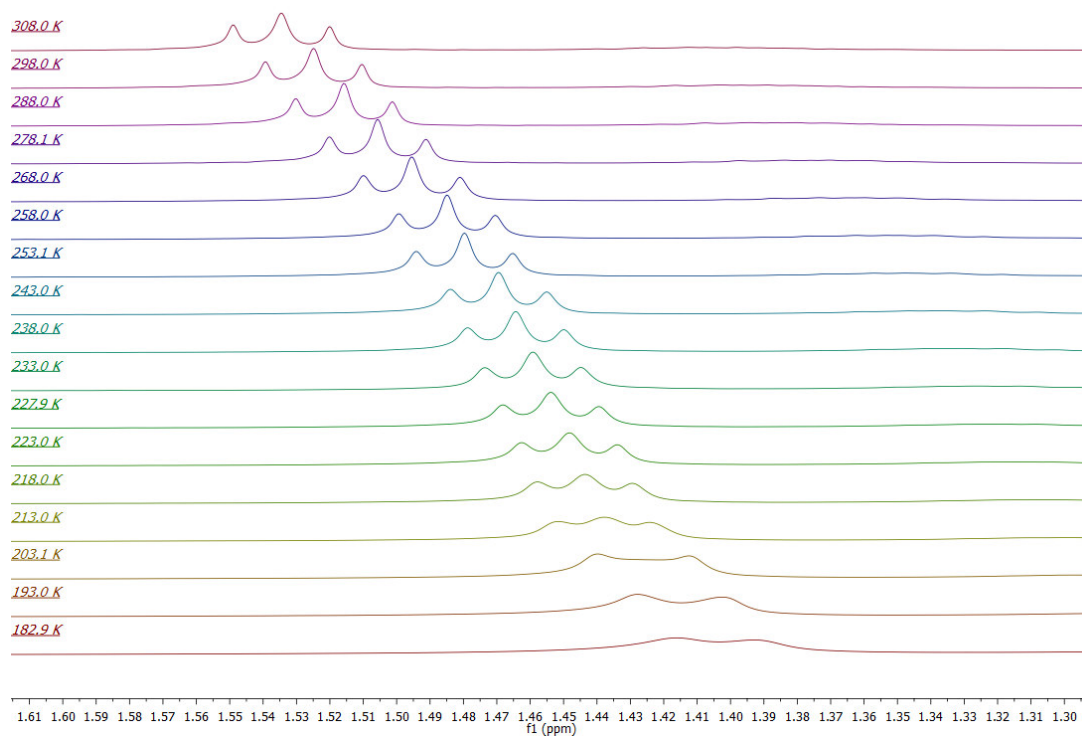


Figure B.2-32: ^1H NMR spectrum (VT, CD_2Cl_2) of $[\text{Ir}(\text{OH})\{\text{PNP}^{\text{tBu}}\}]\text{PF}_6$ (**4**); P^{tBu}_2 signal

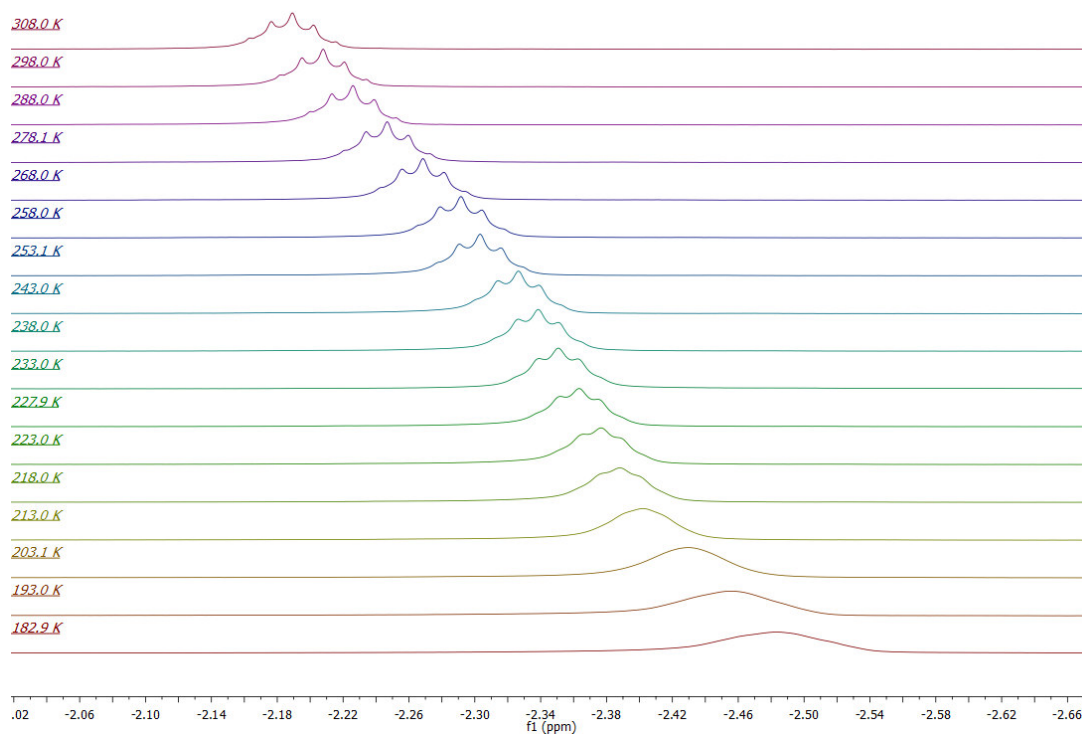


Figure B.2-33: ^1H NMR spectrum (VT, CD_2Cl_2) of $[\text{Ir}(\text{OH})\{\text{PNP}^{\text{tBu}}\}]\text{PF}_6$ (**4**); NCH_2 signal

Compound Spectra

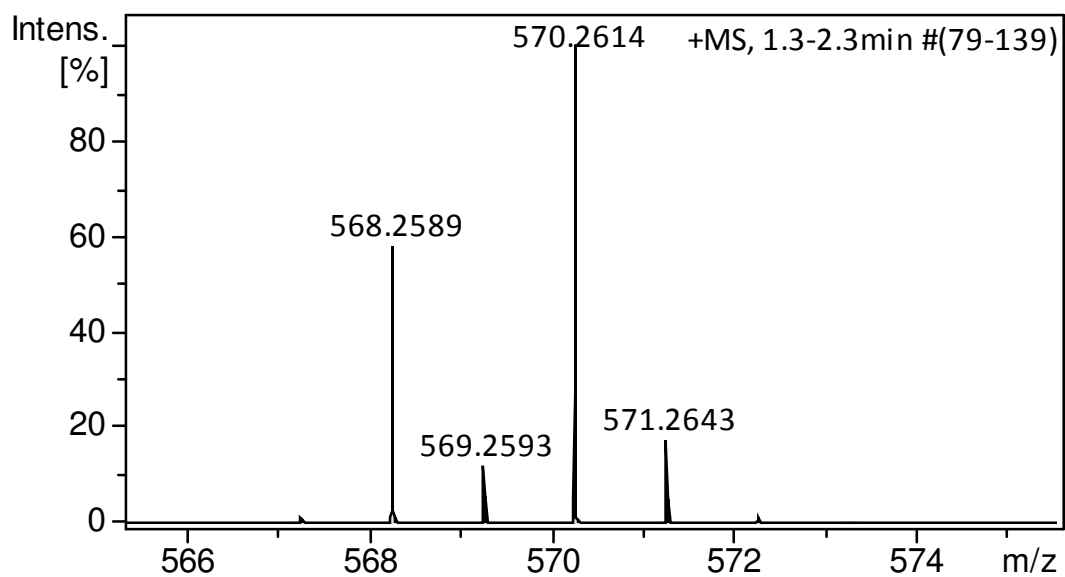
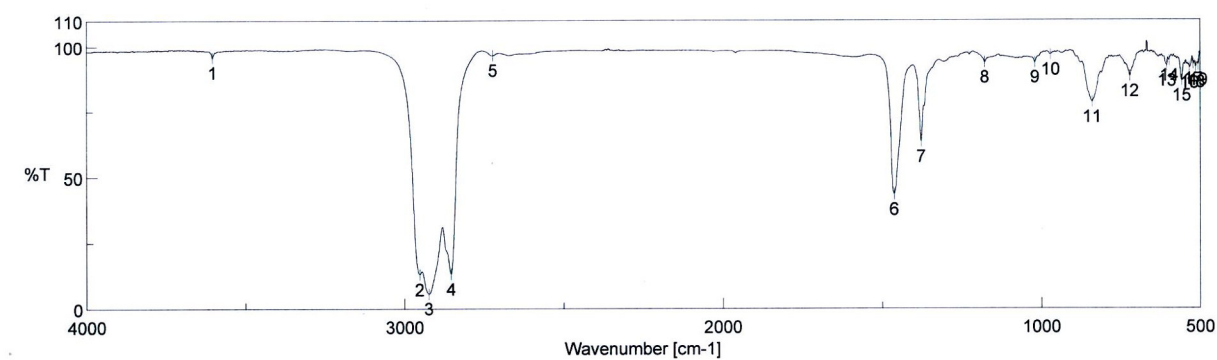


Figure B.2-34: High resolution MS spectrum of $[\text{Ir}(\text{OH})\{\text{PNP}^{t\text{Bu}}\}]\text{PF}_6$ (**4**)



[Result of Peak Picking]

No.	Position	Intensity	No.	Position	Intensity	No.	Position	Intensity
1	3603.58	95.617	2	2952.97	13.0605	3	2924.52	5.74979
4	2853.89	13.3004	5	2721.31	96.3895	6	1461.78	43.3784
7	1377.17	63.3312	8	1178.05	93.5993	9	1020.88	93.595
10	971.465	96.613	11	840.812	78.4331	12	721.97	88.2747
13	604.574	92.2499	14	597.584	94.2876	15	557.809	86.5921
16	533.221	91.4816	17	521.65	92.8776	18	514.66	91.7059
19	506.705	92.499						

Figure B.2-35: IR (nujol mull) spectrum of $[\text{Ir}(\text{OH})\{\text{PNP}^{t\text{Bu}}\}]\text{PF}_6$ (**4**)

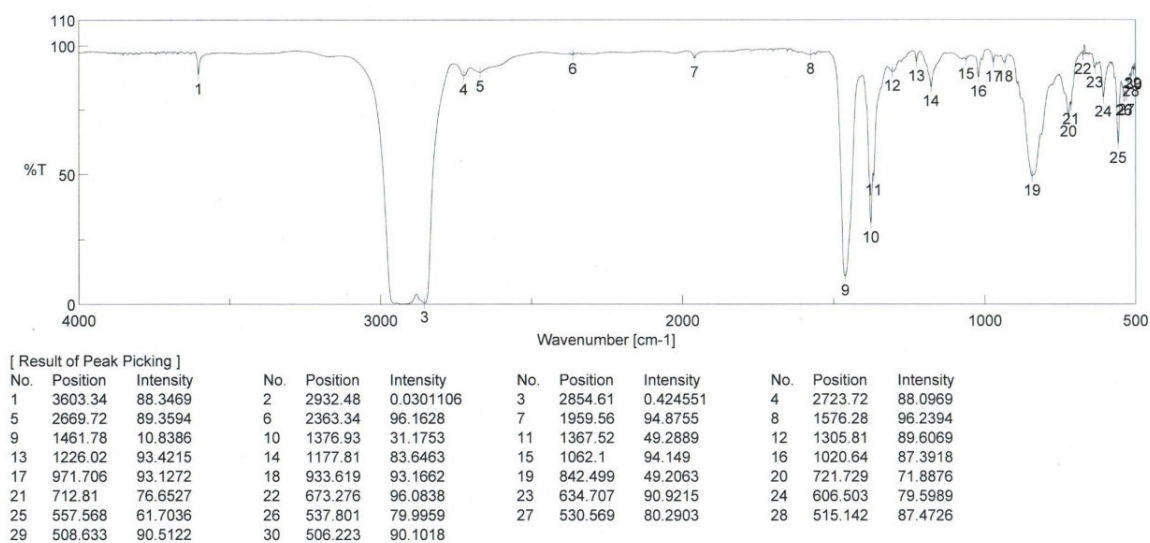


Figure B.2-36: IR (nujol mull) spectrum of $[\text{Ir}(\text{OH})\{\text{PNP}^{\text{tBu}}\}]\text{PF}_6$ (**4**) (higher concentration)

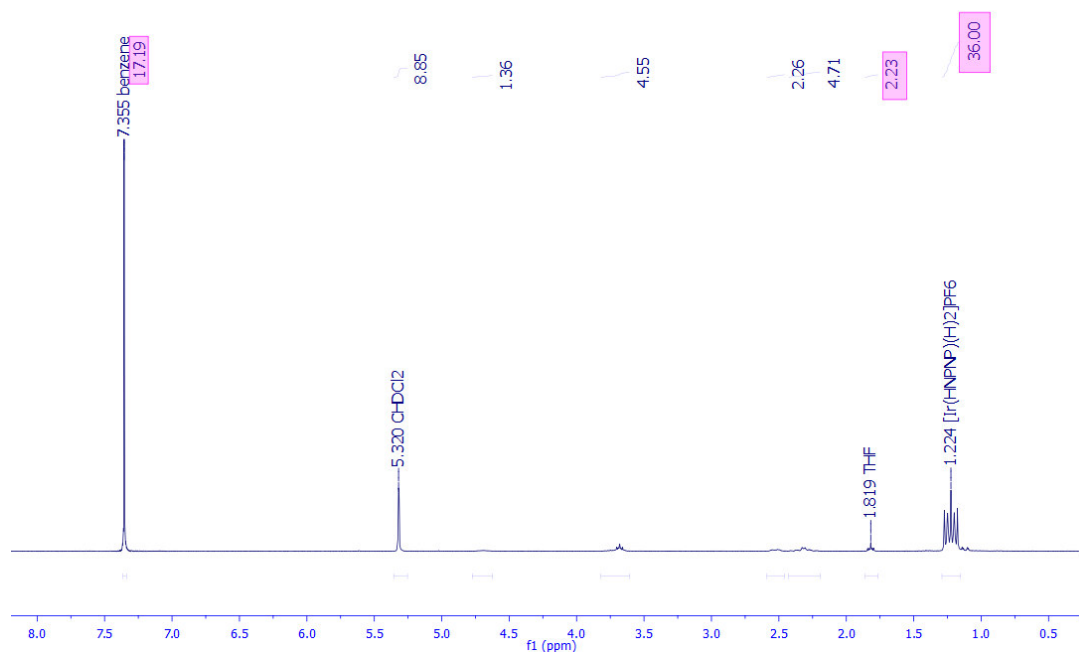


Figure B.2-37: Quantitative ^1H NMR monitoring (based on added C_6H_6 , $d1 = 20$ sec) of the reaction of $[\text{Ir}(\text{H})_2\{\text{HPNP}^{\text{tBu}}\}]\text{PF}_6$ (**3**) with O_2 toward $[\text{Ir}(\text{OH})\{\text{PNP}^{\text{tBu}}\}]\text{PF}_6$ (**4**) in CD_2Cl_2 at r.t.; before O_2 addition.

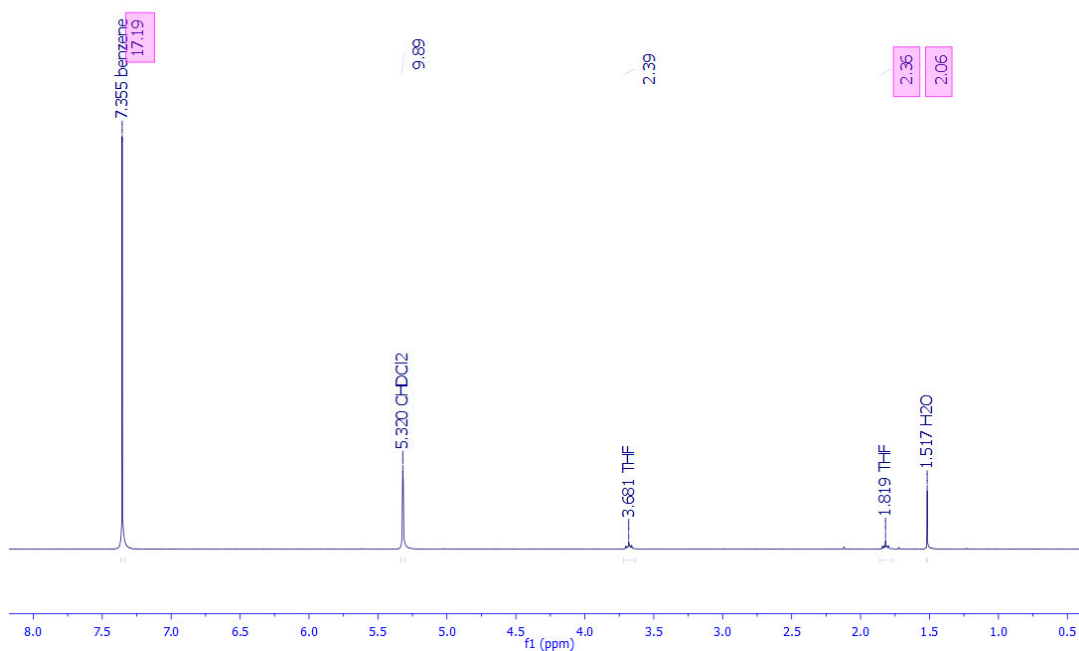


Figure B.2-38: Quantitative ^1H NMR monitoring (based on added C_6H_6 , $d1 = 20$ sec) of the reaction of $[\text{Ir}(\text{H})_2\{\text{HPNP}^{t\text{Bu}}\}]\text{PF}_6$ (**3**) with O_2 toward $[\text{Ir}(\text{OH})\{\text{PNP}^{t\text{Bu}}\}]\text{PF}_6$ (**4**) in CD_2Cl_2 at r.t.; condensate of the completed oxygenation reaction.

B.2.5.4.4 Cyclic oxygenation hydrogenation reactions:

Cyclic oxygenation/hydrogenation reaction in CD_2Cl_2 : $[\text{Ir}(\text{H})_2\{\text{HPNP}^{t\text{Bu}}\}]\text{PF}_6$ (**3**) (3.3 mg, 4.6 μmol) is dissolved in 0.45 ml of CD_2Cl_2 in a *J*-Young NMR tube, frozen, evacuated and treated with dioxygen as described for the synthesis of $[\text{Ir}(\text{OH})\{\text{PNP}^{t\text{Bu}}\}]\text{PF}_6$ (**4**) until no more **3** can be detected. Thereafter, the reaction mixture is pump-freeze degassed three times, treated with an excess of H_2 (in the same manner as before with O_2) and rotated over night with a rotary evaporator. When the reaction is finished, the sample is pump-freeze degassed three times again and treated with O_2 once more. In this fashion, three cycles of oxygenation/hydrogenation can be realized until no more **3**, **2** or **4** is detectable by ^{31}P NMR spectroscopy.

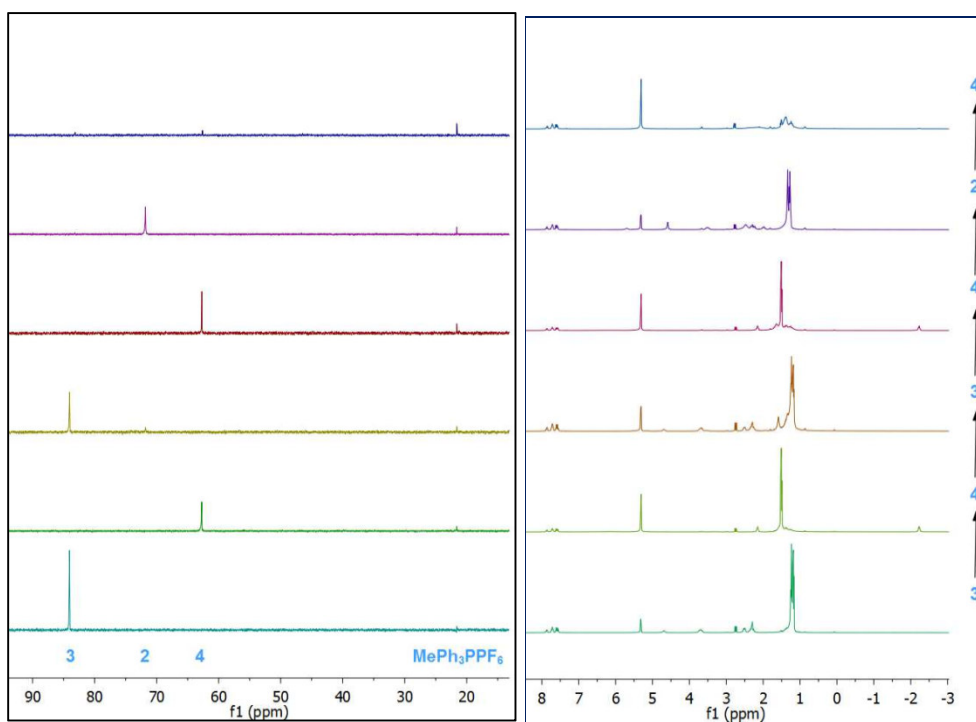


Figure B.2-39: ^{31}P (left) and ^1H NMR (right) spectra of successive O_2 -splitting/hydrogenation cycle in CD_2Cl_2 at r.t. with internal $^1\text{H}/^{31}\text{P}$ standard $[\text{PMePh}_3]\text{PF}_6$.

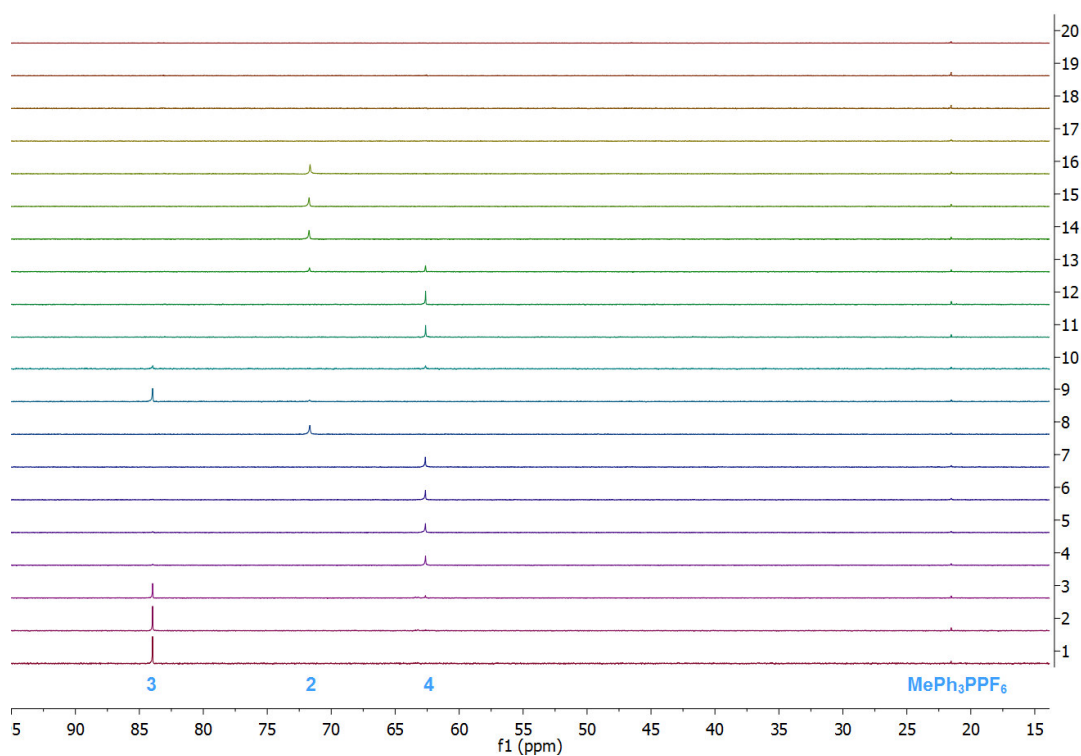


Figure B.2-40: Complete ^{31}P NMR spectra of above mentioned (**Figure B.2-39**) cyclic oxygenation-hydrogenation reaction in CD_2Cl_2 at r.t. with internal $^1\text{H}/^{31}\text{P}$ standard $\text{MePh}_3\text{PPF}_6$ (row 1: Initial \rightarrow row 20: Expiration).

B.2.5.4.5 Treatment of $[\text{Ir}(\text{H})_2\{\text{HPPNP}^{\text{B}^{\text{H}}}\}]\text{PF}_6$ (3**) with O_2 at low temperatures and observation of the reaction by NMR spectroscopy:**
 $[\text{Ir}(\text{H})_2\{\text{HPPNP}^{\text{B}^{\text{H}}}\}]\text{PF}_6$ (**3**) (7.0 mg, 10.0 μmol) is dissolved in 0.50 ml of CD_2Cl_2 in a *J-Young* NMR tube, frozen (N_2), evacuated and treated with an argon (overpressure of the Schlenk line = +0.2 bar) dioxygen (overpressure = -0.2 bar, volume of the tube: 2.6 ml, ~71 $\mu\text{mol O}_2$) mixture. The reaction is cooled down to -60°C and monitored by ^1H and ^31P VT NMR while successively warming the mixture.

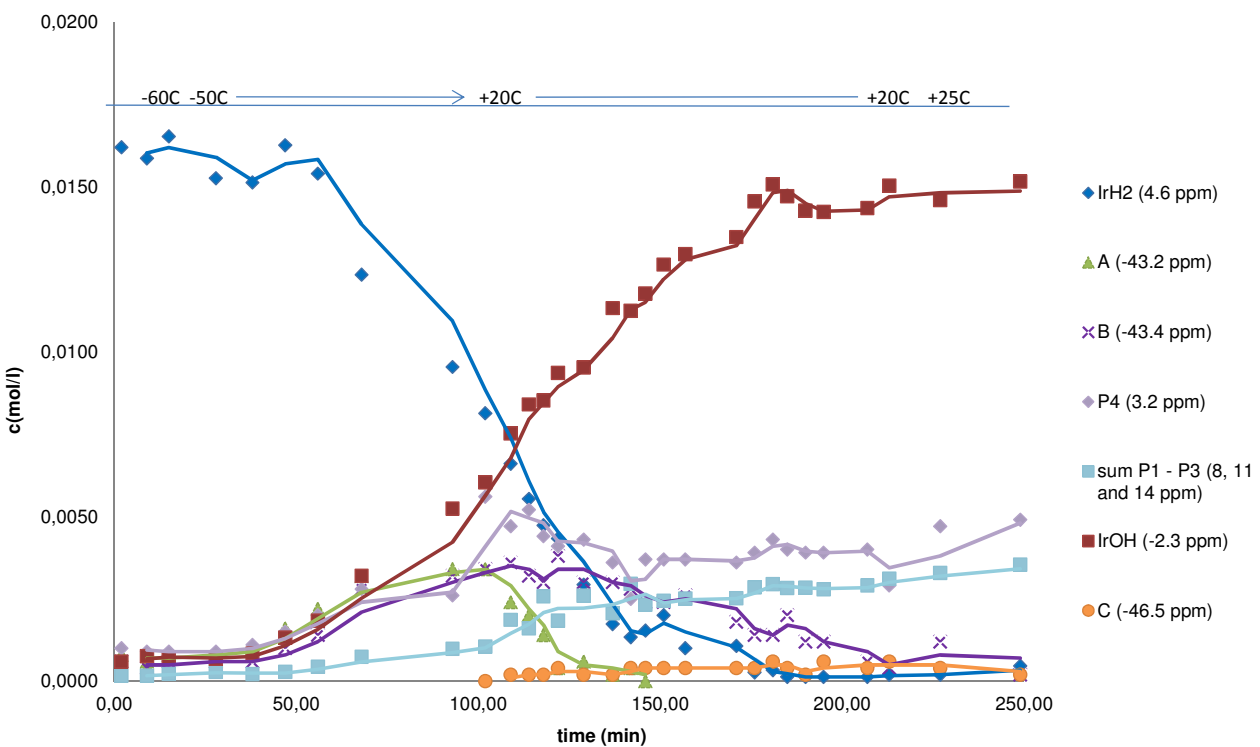


Figure B.2-41: Concentration of involved species due to evaluation of ^1H NMR spectra in the reaction of dihydride **3** with 7 eq. O_2 in CD_2Cl_2 . The reaction is NOT monitored in inverted gated mode, which means that, due to NOE buildup, these integrals do not necessarily represent absolute concentrations. The integrals are normalized by referring them to the integral of the CH_2Cl_2 signal, establishing an averaged factor for the proportion $f(^{31}\text{P NMR})/f(^1\text{H NMR})$ and referring them to the concentration of **3** before the reaction was started.

B.2.5.4.6 Treatment of $[\text{Ir}(\text{H})_2\{\text{HPNP}^t\text{Bu}\}]\text{PF}_6$ (3**) with O_2 at low temperatures and obseravtion of the reaction by cryo mass spectroscopy^[294]:**

$[\text{Ir}(\text{H})_2\{\text{HPNP}^t\text{Bu}\}]\text{PF}_6$ (**3**) (0.9 mg, 1.3 μmol) is dissolved in 1.0 ml of CH_2Cl_2 in a 50 ml flask, frozen (N_2), evacuated and treated with an argon (overpressure of the Schlenk line = +0.2 bar) dioxygen (overpressure = -0.2 bar) mixture. The reaction is cooled down to -78°C and several aliquots of the mixture are diluted with CH_2Cl_2 1/1000 and monitored by mass spectroscopy (0°C) while successively warming the reaction mixture to r.t. until the formation of $[\text{Ir}(\text{OH})\{\text{PNP}^t\text{Bu}\}]\text{PF}_6$ (**4**) is complete.

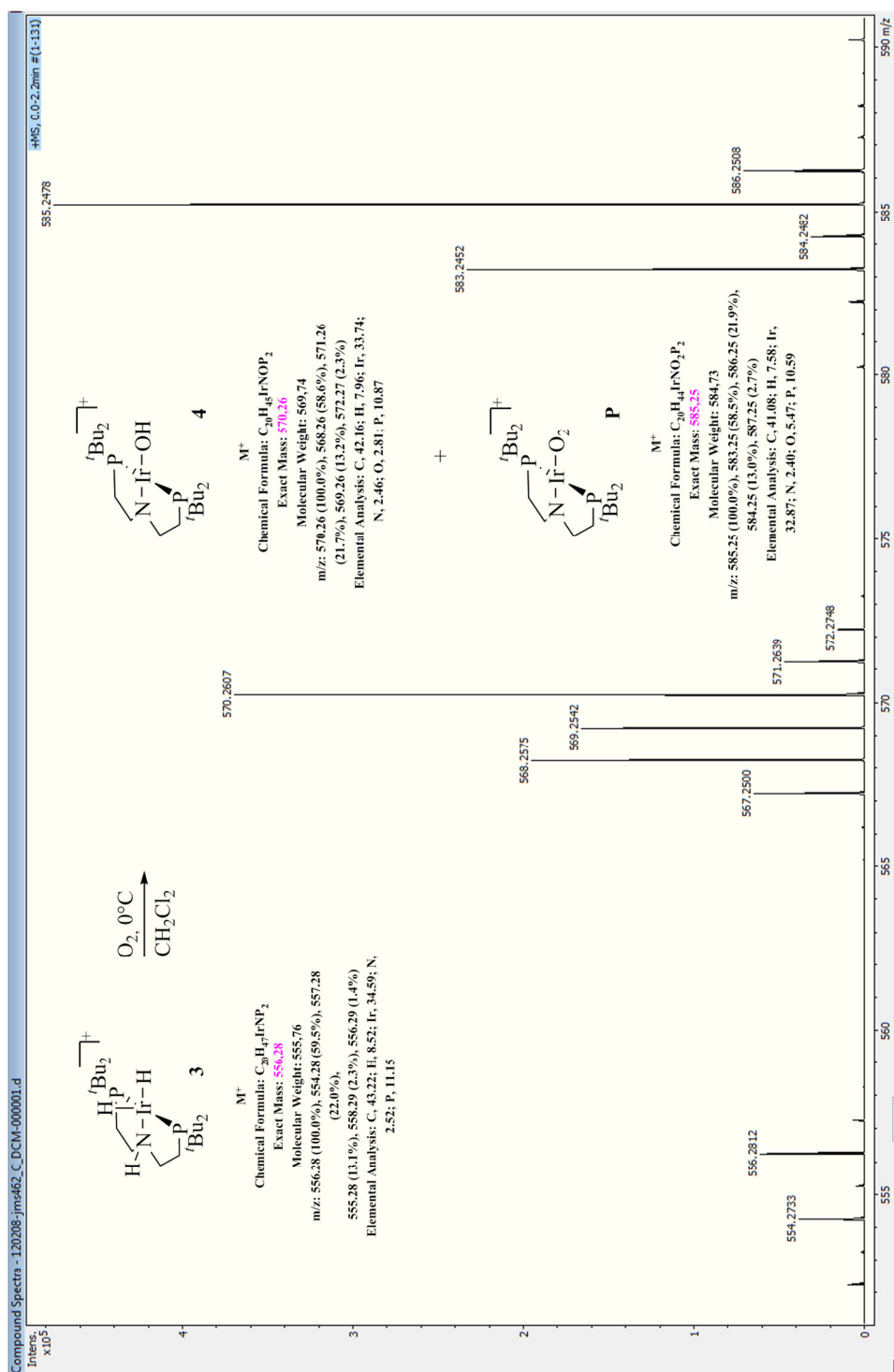


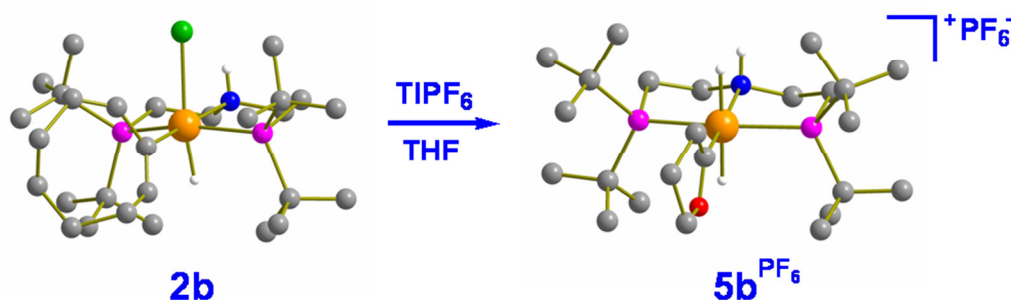
Figure B.2-42: Excerpt of a cryo mass spectrum^[294] measured during the observation of the reaction of dihydride **3** with O_2

B.3 CH activation of THF by a cationic HPNP iridium(I) complex

originated from the paper:

Facile double C-H Activation of Tetrahydrofuran by an Iridium PNP Pincer Complex

J. Meiners, A. Friedrich, E. Herdtweck, S. Schneider, *Organometallics* **2009**, 28, 6331-6338.



The reaction of [IrCl(COE)₂]₂ (COE = cyclooctene) with bulky PNP amino pincer ligand HN(CH₂CH₂P^{*t*}Bu₂)₂, (PNP^{*H*})^{*t*}Bu results in high yield formation of iridium(III) complex [IrH(C₈H₁₃)Cl(PNP^{*H*})^{*t*}Bu] after oxidative addition of a vinylic COE C-H bond. Upon dissolving the product in polar solvents or chloride abstraction with TIPF₆ the cationic iridium(I) complex [Ir(COE)(PNP^{*H*})^{*t*}Bu]⁺ is obtained, which is thermally unstable. This observation shows that the olefin isomer represents the thermodynamic minimum for the cationic complex, while the cyclooctenyl hydride isomer is trapped in unpolar solvents by anion coordination. Owing to the lability of the olefin ligand, [Ir(COE)(PNP^{*H*})^{*t*}Bu]⁺ undergoes facile intermolecular C-H activation. Fischer-carbene complex [Ir(H)₂(=CO(CH₂)₃)(PNP^{*H*})^{*t*}Bu]BPh₄ was isolated in good yield upon α,α -dehydrogenation of THF. Mechanistic examinations suggest olefin dissociation to be rate-determining.

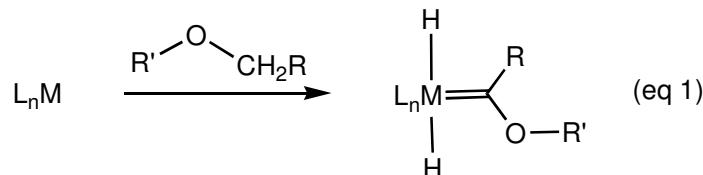
B.3.1 Introduction

After more than 25 years of extensive research, the activation of alkane C–H bonds remains a ‘holy grail’ of organometallic chemistry, and catalytic alkane C–H functionalization reactions, such as selective alkane oxidation or dehydrogenation, remain challenging goals.^[298] Particularly *d*⁸ metal complexes with cyclopentadienyl or related ligands have been successfully utilized for metal insertion into a C–H bond, which was attributed to an analogy

[298] (a) Arndtsen, B. A.; Bergman, R. G.; Mobley, T. A.; Peterson, T. H. *Acc. Chem. Res.* **1995**, 28, 154. (b) Shilov, A. E.; Shul'pin, G. B. *Chem. Rev.* **1997**, 97, 2879. (c) Labinger, J. A.; Bercaw, J. E. *Nature* **2002**, 417, 507. (d) Goldman, A. S.; Goldberg, K. I. in: K. I. Goldberg, A. S. Goldman (Eds.), *Activation and Functionalization of C-H Bonds*, ACS Symposium Series 885, American Chemical Society, Washington, DC, 2004, pp 1-43.

of the bent $[\text{CpM}^{\text{I}}\text{L}]$ fragment with isolobal carbene and favorable thermodynamics.^[299] Furthermore, 3-coordinate, T-shaped $[\text{L}_3\text{M}^{\text{I}}]$ fragments occupy a prominent role in C–H oxidative addition (OA) and reductive elimination (RE) reactions and several pincer chelate complexes have been successfully utilized in stoichiometric and catalytic C–H activation.^[300,301,302,303]

C–H activation is generally regarded a thermodynamic, rather than a kinetic problem, as demonstrated by methane oxidative addition to $\text{CpM}(\text{CO})$ ($\text{M} = \text{Rh}, \text{Ir}$) at temperatures as low as 12 K.^[304] Hence C–H bond addition of donor substituted hydrocarbons can be more favorable owing to directing pre-coordination and M–C bond stabilization to partially overcome entropic and enthalpic drawbacks. Accordingly, α -C–H bonds of ethers have been shown to undergo geminal double C–H oxidative addition to late metal centers, resulting in Fischer carbene complexes (eq. 1).^[305,306,307,308] Similarly, pyridines or vinyl ethers can undergo tautomerization in the coordination sphere of late transition metals toward heteroatom stabilized carbene complexes.^[309] Only recently, this reactivity has been used to functionalize the ether fragment by O- or NR-group transfer from heterocumulenes, such as CO_2 or azides.^[306e,310] However, mechanistic information about this relatively rare route of carbene formation remains scarce.^[308,311]



In our ongoing effort to explore the reactivity of late transition metal compounds with highly basic dialkylamido pincer ligands,^[312] we recently reported the synthesis of iridium(I) complex $[\text{Ir}(\text{COE})(\text{PNP}^{\text{H}})^{\text{iPr}}]\text{X}$ ($\mathbf{1a}^{\text{X}}$; COE = cyclooctene; $(\text{PNP}^{\text{H}})^{\text{iPr}} = \text{HN}(\text{CH}_2\text{CH}_2\text{P}^{\text{iPr}})_2$; $\text{X} = \text{PF}_6, \text{BPh}_4$).^[312a] A rapid equilibrium of the olefin complex with its

[299] (a) Saillard, J.; Hoffmann, R. *J. Am. Chem. Soc.* **1984**, *106*, 2066. (b) Stoutland, P. O.; Bergman, R. G.; Nolan, S. P.; Hoff, C. D. *Polyhedron* **1988**, *7*, 1429. [300] (a) Jensen, C. M. *Chem. Commun.* **1999**, 2443. (b) Goldman, A. S.; Renkema, K. B.; Czerw, M.; Krogh-Jespersen, K. In *Activation and Functionalization of C-H Bonds*; ACS Symposium Series 885; American Chemical Society: Washington, DC, 2004; pp 198-215.

[301] (a) Göttker-Schnetmann, I.; White, P.; Brookhart, M. *J. Am. Chem. Soc.* **2004**, *126*, 1804. (b) Göttker-Schnetmann, I.; Brookhart, M. *J. Am. Chem. Soc.* **2004**, *126*, 9330.

[302] Fan, L.; Parkin, S.; Ozerov, O. V. *J. Am. Chem. Soc.* **2005**, *127*, 16772.

[303] van der Boom, M.; Milstein, D. *Chem. Rev.* **2003**, *103*, 1759.

[304] Rest, A. J.; Whitwell, I.; Graham, W. A. G.; Hoyano, J. K.; McMaster, A. D. *J. Chem. Soc., Chem. Commun.* **1984**, 624.

[305] (a) Werner, H.; Weber, B.; Nürnberg, O.; Wolf, J. *Angew. Chem. Int. Ed.* **1992**, *104*, 1079. (b) Coalter III, J. N.; Ferrando, G.; Caulton, K. G. *New J. Chem.* **2000**, *24*, 835. (c) Ferrando-Miguel, G.; Coalter III, J. N.; Gérard, H.; Huffman, J. C.; Eisenstein, O.; Caulton, K. G. *New J. Chem.* **2002**, *26*, 687.

[306] (a) Boutry, O.; Gutiérrez, E.; Monge, A.; Nicasio, M. C.; Pérez, P. J.; Carmona, E. *J. Am. Chem. Soc.* **1992**, *114*, 7288. (b) Luecke, H. F.; Arndtsen, B. A.; Burger, P.; Bergman, R. G. *J. Am. Chem. Soc.* **1996**, *118*, 2517. (c) Guitérrez-Puebla, E.; Monge, Á.; Nicasio, M. C.; Pérez, P. J.; Poveda, M. L.; Carmona, E. *Chem. Eur. J.* **1998**, *4*, 2225. (d) Slugovc, C.; Mereiter, K.; Trofimenko, S.; Carmona, E. *Angew. Chem. Int. Ed.* **2000**, *39*, 2158. (e) Whited, M. T.; Grubbs, R. H. *J. Am. Chem. Soc.* **2008**, *130*, 5874. (f) Whited, M. T.; Zhu, Y.; Timpa, S. D.; Chen, C.-H.; Foxman, B. M.; Ozerov, O. V.; Grubbs, R. H. *Organometallics* **2009**, *28*, 4560. (g) Romero, P.; Whited, M. T.; Grubbs, R. H. *Organometallics* **2008**, *27*, 3422. (h) Verat, A. Y.; Pink, M.; Fan, H.; Tomaszewski, J.; Caulton, K. G. *Organometallics* **2008**, *27*, 166. (i) Carmona, E.; Paneque, M.; Santos, L. L.; Salazar, V. *Coord. Chem. Rev.* **2005**, *249*, 1729.

[307] Holtkamp, M. W.; Labinger, J. A.; Bercaw, J. E. *J. Am. Chem. Soc.* **1997**, *119*, 848.

[308] M. T. Whited, R. H. Grubbs, *Acc. Chem. Res.* **2009**, *42*, 1607–1616.

[309] Kunz, D. *Angew. Chem., Int. Ed.* **2007**, *46*, 3405.

[310] Whited, M. T.; Grubbs, R. H. *J. Am. Chem. Soc.* **2008**, *130*, 16476.

[311] Brookes, N. J.; Ariafard, A.; Stranger, R.; Yates, B. F. *J. Am. Chem. Soc.* **2009**, *131*, 5800.

[312] (a) Friedrich, A.; Ghosh, R.; Kolb, R.; Herdtweck, E.; Schneider, S. *Organometallics* **2009**, *28*, 708. (b) Käß, M.; Friedrich, A.; Drees, M.; Schneider, S. *Angew. Chem. Int. Ed.* **2009**, *48*, 905. (c) Marziale, A.; Herdtweck, E.; Eppinger, J.; Schneider, S. *Inorg. Chem.* **2009**, *48*, 3699. (d) A. Friedrich, M. Drees, S. Schneider, *Chem. - Eur. J.* **2009**, *15*, 10339-10342, S10339/1-S10339/22.

vinylcyclooctenyl hydrido isomer $[\text{IrH}(\text{C}_8\text{H}_{13})(\text{PNP}^{\text{H}i\text{Pr}})]^+$ was proposed to account for the highly fluxional behavior of $\mathbf{1a}^{\text{X}}$. This intramolecular C-H activation product could be trapped as $[\text{IrH}(\text{C}_8\text{H}_{13})\text{Cl}(\text{PNP}^{\text{H}i\text{Pr}})]$ ($\mathbf{2a}$) by addition of chloride. However, chloride ions also triggered N-H deprotonation and HCl oxidative addition to $\mathbf{1a}$, resulting in a mixture of $\mathbf{2a}$, $[\text{Ir}(\text{COE})(\text{PNP}^{\text{H}i\text{Pr}})]$ ($\mathbf{3a}$), and $[\text{IrHCl}_2(\text{PNP}^{\text{H}i\text{Pr}})]$ ($\mathbf{4a}$). Unfortunately, any effort to obtain intermolecular C-H activation starting from $\mathbf{1a}$, e.g., by thermolysis in several solvents, resulted in unselective decomposition. In this contribution the double C-H activation of THF by an Ir complex with a sterically modified PNP pincer ligand to give the corresponding dihydrido Fischer-carbene complex at very mild conditions is described. Kinetics suggest COE dissociation as the rate determining step.

B.3.2 Results and Discussion

B.3.2.1 Ligand synthesis

We reported that crystallization of $\mathbf{1a}^{\text{BPh}_4}$ resulted in a considerably disordered molecular structure.^[312a] In a further attempt to grow suitable crystals of $\mathbf{1a}^{\text{BPh}_4}$, colorless crystals were obtained from a saturated THF solution over several weeks at room temperature. Surprisingly, the molecular structure reveals the formation of Fischer-carbene $[\text{Ir}(\text{H})_2(=\text{CO}(\text{CH}_2)_3)(\text{PNP}^{\text{H}i\text{Pr}})]\text{BPh}_4$ ($\mathbf{5a}^{\text{BPh}_4}$, Figure 2). This result confirms the possibility of intermolecular C-H activation with the IrPNP fragment, albeit with *iso*-propyl substituted IrPNP compounds low selectivities were obtained. However, it is assumed that enhanced steric bulk could assist olefin dissociation from $\mathbf{1}$ facilitating intermolecular C-H activation at lower temperatures and with higher selectivities. Therefore, the bulkier ligand $(\text{PNP}^{\text{H}t\text{Bu}})$ ($\text{HN}(\text{CH}_2\text{CH}_2\text{P}^t\text{Bu}_2)_2$) was utilized. $(\text{PNP}^{\text{H}t\text{Bu}})$ can be synthesized by reaction of $\text{HN}(\text{CH}_2\text{CH}_2\text{Cl})_2$ with $^t\text{Bu}_2\text{PLi}$ from a protocol slightly modified from the one described earlier, and was isolated in good yields.^[313]

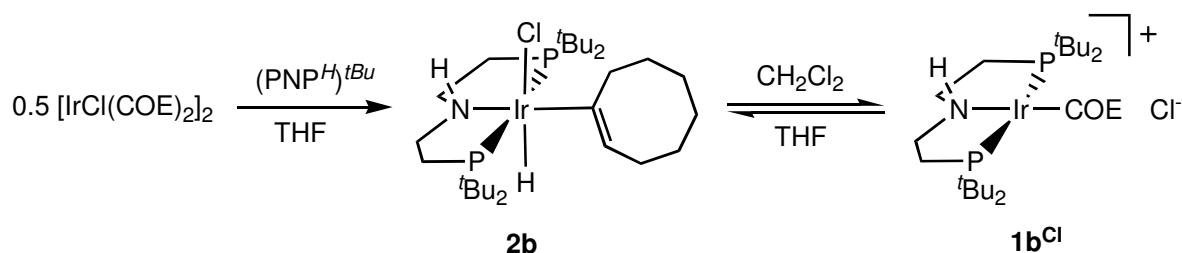
B.3.2.2 Intramolecular vinylc C-H activation of cyclooctene: Solvent dependent OA/RE

Reaction of $[\text{IrCl}(\text{COE})_2]_2$ with $(\text{PNP}^{\text{H}t\text{Bu}})$ gives colorless cyclooctenyl hydride complex $[\text{IrH}(\text{C}_8\text{H}_{13})\text{Cl}(\text{PNP}^{\text{H}t\text{Bu}})]$ ($\mathbf{2b}$) in good yields (Scheme 1). ^{31}P and ^1H NMR of $\mathbf{2b}$ in d^8 -THF are in agreement with a meridional arrangement of the PNP ligand in solution. The hydride chemical shift at -24.99 ppm suggests a *trans* position with respect to the chloride ligand ($\mathbf{2a}$: -24.40 ppm), and could be confirmed in the solid state by single crystal X-ray diffraction (Figure 1). The ^1H and ^{13}C chemical shifts and multiplicities of the vinylc functional group strongly resemble those of $\mathbf{2a}$ and the few other Ir^{III} cyclooctenyl complexes reported.^[312a,314]

[313] (a) Choualeb, A.; Lough, A. J.; Gusev, D. G. *Organometallics* **2007**, *26*, 3509. (b) Abdur-Rashid, K.; Graham, T.; Tsang, C.-W.; Chen, X.; Guo, R.; Jia, W.; Amoroso, D.; Sui-Seng, C. WO2008/141439.

[314] (a) Fernandez, M. J.; Rodriguez, M. J.; Oro, L. A.; Lahoz, F. J. *J. Chem. Soc., Dalton Trans.* **1989**, 2073. (b) Hermann, D.; Gandelman, M.; Rozenberg, H.; Shimon, L. J. W.; Milstein, D. *Organometallics* **2002**, *21*, 812. (c) Iimura, M.; Evans, D. R.; Flood, T. C. *Organometallics* **2003**, *22*, 5370.

The synthesis of **2b** was very recently described in a patent, as well, but the compound was not fully characterized.^[313b]



Scheme 1. Synthesis of hydrido vinyl complex **2b** and solvent dependence of the hydrido vinyl vs olefin complex isomer equilibrium (($\text{PNP}^H)^{t\text{Bu}} = \text{HN}(\text{CH}_2\text{CH}_2\text{P}^t\text{Bu}_2)_2$; COE = cyclooctene).

The molecular structure of **2b** in the solid state features six-coordinate iridium(III) with a meridional ($\text{PNP}^H)^{t\text{Bu}}$ pincer ligand and the cyclooctenyl ligand in *trans* position relative to N1 (Figure 1 and Table 1). The main deviation from ideal octahedral coordination is attributed to the pincer bite angle (P1–Ir1–P2 $159.49(3)^\circ$), which is approx. 5° smaller than found for other iridium ($\text{PNP}^H)^{i\text{Pr}}$ ^[312a,315] and ($\text{PNP}^H)^{t\text{Bu}}$ (vide infra) complexes indicating steric crowding. The Ir1–C1 bond length ($2.092(3) \text{ \AA}$) is very close to that in $[\text{IrH}(\text{C}_8\text{H}_{13})\text{Cl}(\text{PNP}^{\text{py}})]$ ($\text{PNP}^{\text{py}} = 2,6\text{-}(\text{CH}_2\text{P}^t\text{Bu}_2)_2\text{C}_5\text{H}_3\text{N}$) with a pyridine based pincer ligand ($2.094(8) \text{ \AA}$), and slightly longer than in $[\text{Ir}(\text{Tp})\text{H}(\text{C}_8\text{H}_{13})(\text{C}_8\text{H}_{14})]$ ($2.054(7) \text{ \AA}$; Tp = $\text{HB}(\text{N}_2\text{C}_3\text{H}_3)_3$), the only other structurally characterized vinylic cyclooctenyl iridium complexes.^[314a,b] The C1–C28 distance ($1.333(5) \text{ \AA}$) is in the typical range for olefinic bonds (free *trans*-COE: $1.363(8) \text{ \AA}$),³¹⁶ supporting the h^1 coordination mode of the hydrocarbon ligand.

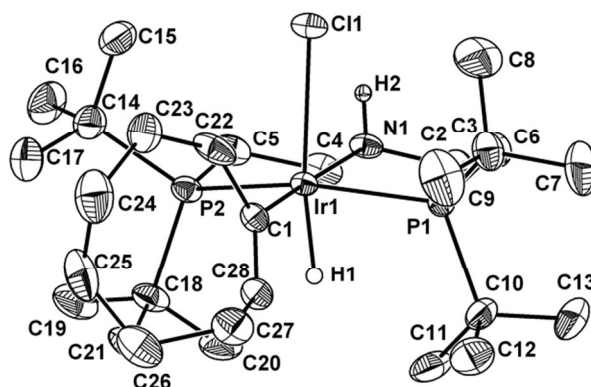


Figure 1. DIAMOND plot of **2b** in the crystal with thermal ellipsoids drawn at the 30% probability level. Hydrogen atoms other than H1 and H2 and split positions of C23 and C24 are omitted for clarity.

[315] Clarke, Z. E.; Maragh, P. T.; Dasgupta, T. P.; Gusev, D. G.; Lough, A. J.; Abdur-Rashid, K. *Organometallics* **2006**, *25*, 4113.

[316] Gavin, R. M.; Wang, Z. F. *J. Am. Chem. Soc.* **1973**, *5*, 1425.

Table 1. Selected bond lengths and angles of **2b** in the crystal.

Bond lengths (Å)	
Ir1–C1	2.092(3)
Ir1–Cl1	2.5639(9)
Ir1–N1	2.214(3)
Ir1–P1	2.345(1)
Ir1–P2	2.358(1)
C1–C28	1.333(5)
Bond angles (°)	
C1–Ir1–N1	175.4 (1)
P1–Ir1–P2	159.49(3)
Ir1–C1–C28	122.8(3)

Such vinyl hydride *vs.* olefin complex equilibria are of importance in C-H functionalization reactions. For example, [IrH(CHCH^tBu)(PCP)] (PCP = C₆H₃-2,6-(CH₂P^tBu)₂) represents the resting state in catalytic transfer dehydrogenation of cyclooctane with *tert*-butylethylene.^[300b] However, with olefins from dehydrogenation of *n*-alkanes thermally stable [Ir(olefin)(PCP)] complexes are formed eventually shutting down catalytic activity. Generally, the vinyl hydride can be preferred over the olefin isomer upon increased steric crowding or by intra- or intermolecular trapping.^[314b,317] Milstein and coworkers reported the synthesis of cyclooctenyl hydride complex [IrH(C₈H₁₃)Cl(PNP)^{py}] from the reaction of [IrCl(COE)₂]₂ with pincer ligand PNP^{py}.^[314b] On the other hand, starting from cationic [Ir(COE)₂(acetone)₂]⁺PF₆⁻ olefin complex [Ir(COE)(PNP)^{py}]⁺PF₆⁻ was obtained.^[318] Interestingly, dissolving colorless **2b** in methylene chloride results in a red solution, suggesting a considerable structural change. While such CH₂Cl₂ solutions rapidly decompose at room temperature, NMR examination at -50 °C, reveals the formation of a C₁-symmetric complex with two ³¹P NMR signals featuring a typical *trans* coupling constant (²J_{PP} = 323 Hz). Two ¹H NMR (3.46 and 4.08 ppm) and two ¹³C NMR signals (43.2 and 51.0 ppm) can be assigned to the olefin functional group of the p-bound COE ligand, respectively, and no free COE was detected. Furthermore, only small amounts of Ir-H species (~ 5 %) were found up to -100 ppm. Therefore, this compound is assigned to olefin complex [Ir(COE)(PNP^H)^tBu]Cl (**1b**^{Cl}). Accordingly, chloride abstraction from **2b**, e.g., with NaBPh₄ or TIPF₆, results in the same compound by ³¹P and ¹H NMR (vide infra). The broad ¹H NMR signal for the N-H proton of **1b**^{Cl} at 6.99 ppm suggests formation

[317] (a) Werner, H.; Dirnberger, T.; Schulz, M. *Angew. Chem.* **1988**, *100*, 993; *Angew. Chem. Int. Ed. Engl.* **1988**, *27*, 948. (b) Stoutland, P. O.; Bergman, R. G. *J. Am. Chem. Soc.* **1985**, *107*, 4581. (c) Ghosh, C. K.; Hoyano, J. K.; Krentz, R.; Graham, W. A. G. *J. Am. Chem. Soc.* **1989**, *111*, 5480. (d) Alvarado, Y.; Boutry, O.; Gutierrez, E.; Monge, A.; Nicasio, M. C.; Poveda, M. L.; Perez, P. J.; Ruiz, C.; Bianchini, C.; Carmona, E. *Chem. Eur. J.* **1997**, *3*, 860.

[318] Ben-Ari, E.; Gandelman, M.; Rozenberg, H.; Shimon, L. J. W.; Milstein, D. *J. Am. Chem. Soc.* **2003**, *125*, 4714.

of a weak Cl...H...N hydrogen bridge. These results confirm that even with the more sterically crowded P^tBu₂ substituted pincer ligand the olefin isomer represents the thermodynamic minimum of the cationic complex (Schemes 1+2). Apart from steric considerations, the positive charge can be expected to be a contributing factor in shifting the equilibrium from iridium(III) toward the iridium(I) olefin complex. The polar and weakly coordinating solvent CH₂Cl₂ facilitates ion pair formation with subsequent reductive elimination of COE. Generally, reductive elimination from *d*⁶ metal centers exhibits lower barriers for five-coordinate as compared with six-coordinate complexes.^[319] On the other hand, solvents which are less effective in ion pair stabilization (THF or benzene) favor trapping of the vinyl hydride isomer [Ir(H)(C₈H₁₃)(PNP^H)^{tBu}]⁺ by the chloride counter ion. Accordingly, evaporation of CH₂Cl₂ from a **1b**^{Cl} solution and redissolving in THF gives **2b** by ³¹P NMR.

Interestingly, in the patent mentioned earlier the authors obtained red solutions upon dissolving **2b** in THF/water or methanol, as well, and two signals were observed in the ³¹P NMR at 45.9 and 41.2 ppm (*J*_{PP} = 325 Hz), respectively, strongly resembling our spectra in CD₂Cl₂ (45.8 and 39.1 ppm, *J*_{PP} = 323 Hz).^[313b] However, this observation was attributed to HCl elimination from **2b** to give iridium(I) amido olefin complex [Ir(COE)(PNP)^{tBu}] (**3b**), although **3b** was reported to exhibit ³¹P NMR signals about Dd = +11 ppm at lower field.^[320] Therefore, it is evident that in fact Cl⁻ dissociation and not HCl elimination was observed in the polar solvents THF/water and methanol, confirming that the C–H activation equilibrium can be controlled by solvent dependent ion pair formation.

These results support our earlier proposal that the high fluxionality of complex **1a**^{PF₆} can be attributed to a rapid equilibrium between the olefin and the vinyl hydride complexes, which is strongly shifted toward the olefin complex.^[312a] **1b**^{Cl} exhibits two sharp doublets in the ³¹P NMR at -50 °C in CD₂Cl₂ (*w*_{1/2} ~ 11 Hz) and only slight broadening at room temperature in THF (*w*_{1/2} ~ 30 Hz). In contrast, the ³¹P NMR spectrum of **1a**^{PF₆} at -85 °C displays one broad signal (*w*_{1/2} ~ 550 Hz) and full decoalescence was not observed at temperatures down to -100 °C, indicating a higher barrier for the olefin / vinyl hydride equilibrium for the Ir(PNP^H)^{tBu} fragment as compared with Ir(PNP^H)^{iPr}.^[321] This observation suggests that COE dissociation is not rate-determining for this process, since higher rates would be expected for the bulkier pincer ligand. Furthermore, for **1a**^{PF₆} no olefin exchange was observed with free COE.^[312a] Therefore, the vinylic C–H activation is proposed to be an intramolecular process without initial olefin dissociation.^[322]

[319] Procelewska, J.; Zahl, A.; Liehr, G.; van Eldik, R.; Smythe, N. A.; Williams, B. S.; Goldberg, K. I. *Inorg. Chem.* **2005**, *44*, 7732.

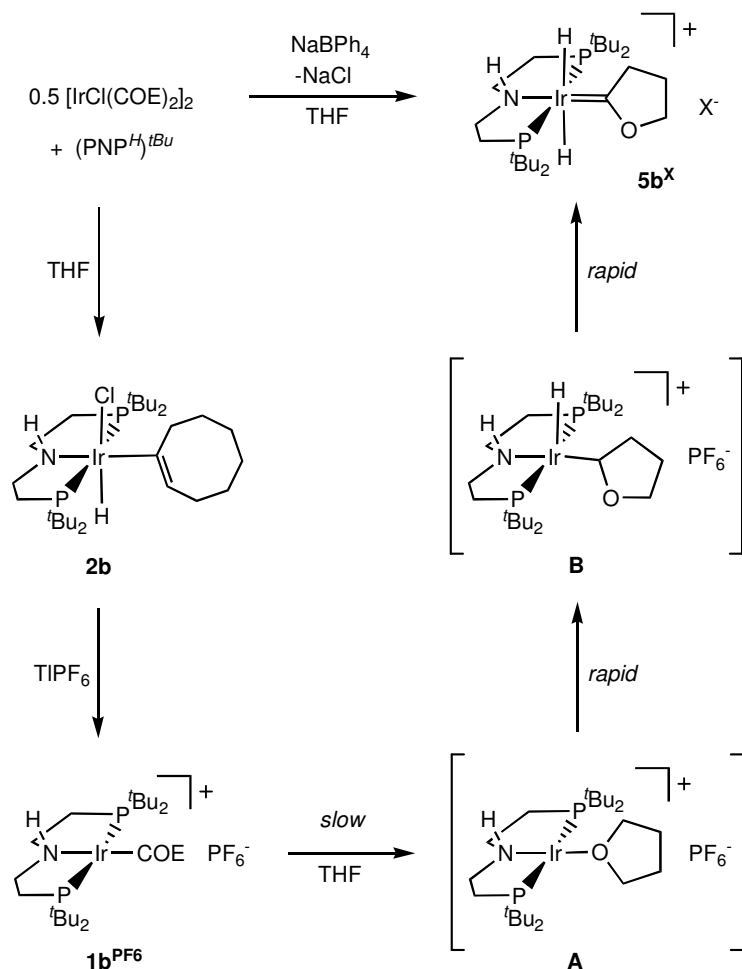
[320] We could confirm the spectroscopic data of **3b** by independent synthesis from [IrCl(COE)₂]₂, (PNP^H)^{tBu}, and KO^tBu (Yield: 72 %; ³¹P{¹H} NMR (161.8 MHz, C₆D₆, rt): δ = 52.4 (d, ²*J*_{PP} = 369 Hz), 56.4 (d, ²*J*_{PP} = 369 Hz)).

[321] The barrier of vinylic C–H activation in **1b**^{Cl} could not be obtained due to concomitant decomposition at higher temperatures in CD₂Cl₂.

[322] (a) Stoutland, P. O.; Bergman, R. G. *J. Am. Chem. Soc.* **1988**, *110*, 5732. (b) Smith, K. M.; Poli, R.; Harvey, J. N. *Chem. Eur. J.* **2001**, *7*, 1679.

B.3.2.3 Intermolecular double C-H activation of THF

For the preparation of **2b**, short reaction times are instrumental in obtaining high yields as slow decomposition is observed at room temperature both in the solid state and in organic solvents, such as benzene, THF, or CH₂Cl₂, to give mixtures of several products, respectively. However, the structural characterization of **5a**^{BPh₄} suggests that the IrPNP fragment should be well suitable for intermolecular C-H activation. As the presence of chloride could induce pathways for side reactions (*vide ultra*), [IrCl(COE)₂]₂ was reacted with (PNP^H)^{tBu} in THF in the presence of NaBPh₄. Facile conversion to iridium(III) complex



Scheme 2. Synthesis and proposed mechanism for the formation of Fischer-carbene complexes **5b**^X ((PNP^H)^{tBu} = HN(CH₂CH₂P^{tBu})₂; X = BPh₄, PF₆; COE = cyclooctene).

[Ir(H)₂(=CO(CH₂)₃)(PNP^H)^{tBu}]^{BPh₄} (**5b**^{BPh₄}), which features a Fischer-carbene ligand derived from THF, was observed in good yield at room temperature (Scheme 2). High selectivity for α,α -C-H activation and no signs for *b*-H elimination (vinyl ether formation) were observed. ¹H, ³¹P, and ¹³C NMR spectra are in agreement with a C_s-symmetric structure on the NMR time-scale. The downfield chemical shifts (-7.90 and -9.11 ppm) and ²J_{HH} (17 Hz) coupling

constant of the two hydride ligands indicate a mutual *trans* position, hence a meridional coordination mode of the (PNP^H)^{tBu} pincer ligand in solution. The carbene carbon atom was found in the ¹³C NMR spectrum at 261.9 ppm as a triplet coupling with the pincer ligand phosphine atoms (²J_{CP} = 5 Hz), comparing well with other Ir carbene complexes derived THF.^[306,323] In CD₂Cl₂, the chemical shifts of the pincer backbone protons show some counteranion dependence, with **5**^{BPh4} exhibiting ¹H signals for the N-H and the ethylene bridges shifted about 0.3-0.8 ppm to higher field, as compared with **5**^{PF6}. This observation points toward the formation of a contact ion pair in solution.

The molecular structures of octahedral carbene complexes **5a**^{BPh4} and **5b**^{BPh4} in the solid state was derived by single-crystal X-ray diffraction (Figure 2) confirming the meridional pincer coordination mode and *trans* dihydride configuration. While the pincer bite angle is almost identical in **5a**^{BPh4} and **5b**^{BPh4} the Ir-P and Ir-C1 lengths are slightly longer (~0.04 Å) in **5b**^{BPh4} as compared with **5a**^{BPh4}, presumably due to the increased steric bulk. The elongated Ir–C1 bond in **5b**^{BPh4} results in a slightly shorter C1–O1 distance (Δ*D* = 0.03 Å) compared with **5a**^{BPh4}, which could be explained with a stronger C1–O1 p-interaction. However, the Ir–C1 bond lengths (**5a**^{BPh4}: 1.905(4) Å; **5b**^{BPh4}: 1.942(3) Å) are in the range found for other alkoxy-carbene complexes of iridium in the literature.^[306,323,324]

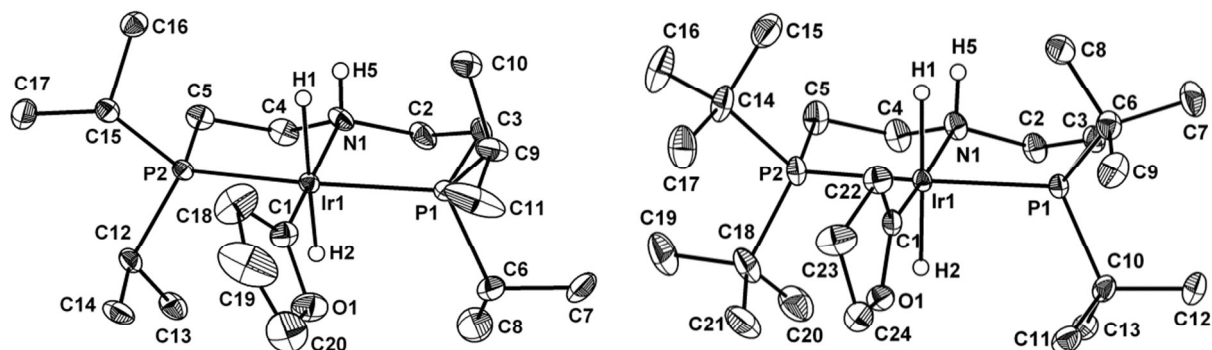


Figure 2. DIAMOND plot of the **5a**^{BPh4} (above) and **5b**^{BPh4} (below; one of two crystallographically independent molecules) cations in the crystal with thermal ellipsoids drawn at the 30% (**5a**^{BPh4}) and 50% (**5b**^{BPh4}) probability level. Hydrogen atoms other than H1, H2, and H5 are omitted for clarity.

[323] Ishii, Y.; Ogio, K.-I.; Nishio, M.; Retböll, M.; Kuwata, S.; Matsuzaka, H.; Hidai, M. *J. Organomet. Chem.* **2000**, 599, 221.

[324] (a) O'Connor, J. M.; Hiibner, K.; Closson, A.; Gantzel P. *Organometallics* **2001**, 20, 1482. (b) Ros, R.; Tassan, A.; Scopelliti, R.; Bondietti, G.; Roulet, R. *Inorg. Chim. Acta* **2005**, 358, 583. (c) O'Connor, J. M.; Pu, L.; Rheingold, A. L. *J. Am. Chem. Soc.* **1987**, 109, 7578. (d) O'Connor, J. M.; Pu, L.; Chadha, R. *Angew. Chem., Int. Ed.* **1990**, 29, 543. (e) O'Connor, J. M.; Pu, L.; Rheingold, A. L. *J. Am. Chem. Soc.* **1989**, 111, 4129. (f) O'Connor, J. M.; Merwin, R.; Rheingold, A. L.; Adams, M. L. *Organometallics* **1995**, 14, 2102.

Table 2. Selected bond lengths and angles of the **5a**^{BPh₄} and **5b**^{BPh₄} cations in the crystal (corresponding values for the second crystallographically independent molecule in italic).

	5a	5b
Bond Lengths (Å)		
Ir1–C1	1.905(4)	1.942(3) <i>1.934(3)</i>
Ir1–N1	2.201(4)	2.203(2) <i>2.200(3)</i>
Ir1–P1	2.306(1)	2.3453(8) <i>2.3347(8)</i>
Ir1–P2	2.307(1)	2.3333(8) <i>2.3326(8)</i>
C1–O1	1.340(6)	1.314(4) <i>1.330(5)</i>
Bond angles (°)		
N1–Ir1–C1	177.1(2)	176.4(1) <i>173.7(2)</i>
P1–Ir1–P2	164.32(4)	164.22(3) <i>163.51(3)</i>
O1–C1–C18/C22	108.9(4)	107.7(2) <i>109.9(3)</i>

B.3.2.4 Mechanistic considerations

The conversion of [IrCl(COE)₂]₂ to carbene complex **5b**^{BPh₄} in the presence of NaBPh₄ was monitored by ³¹P NMR. Only one intermediate species was detected featuring two doublets in the ³¹P NMR spectrum and was assigned to olefin complex **1b**^{BPh₄} by analogy to the spectrum of **1b**^{Cl} (vide ultra). This result suggests the initial formation of cyclooctenyl complex **2b** in THF and subsequent shift of the equilibrium toward **1b**^{BPh₄} by Cl[−] precipitation (Scheme 2). Therefore, we studied **5b**^{PF₆} formation starting from **2b** in THF using TlPF₆ (1.3 eq.) for chloride abstraction. Immediate formation of **1b**^{PF₆} and subsequent smooth conversion to **5b**^{PF₆} with no other intermediates are observed. The reaction is first order in **1b**^{PF₆} with a pseudo first order rate of $k = 0.0023 \text{ min}^{-1}$ at 298 K. Activation parameters of $\Delta H^\ddagger = 125(4) \text{ kJ/mol}$ and $\Delta S^\ddagger = 90(14) \text{ J/molK}$ were derived from an Eyring plot (Figure 3). Furthermore, no H/D kinetic isotope effect is found upon reaction in *d*⁸-THF, suggesting that C–H activation is not rate-determining. These results are consistent with slow formation of an *O*-bound ether complex intermediate (Scheme 2, A), which readily forms the Fischer-carbene upon rapid α,α -dehydrogenation or with direct C–H oxidative addition to a three-coordinate Ir(PNP^H) species. Such ether complexes have been proposed earlier as intermediates.^[311] A hydrido oxyalkyl intermediate like **B** has recently been trapped with CO.^[306i] The large positive ΔS^\ddagger suggests dissociative substitution of COE and the intermediacy of a highly reactive Ir(PNP^H) species, explaining as well the much more rapid reaction upon switching

from the ⁱPr to the ^tBu substituted pincer ligand and the unselective reactivity in solvent mixtures.^[325]

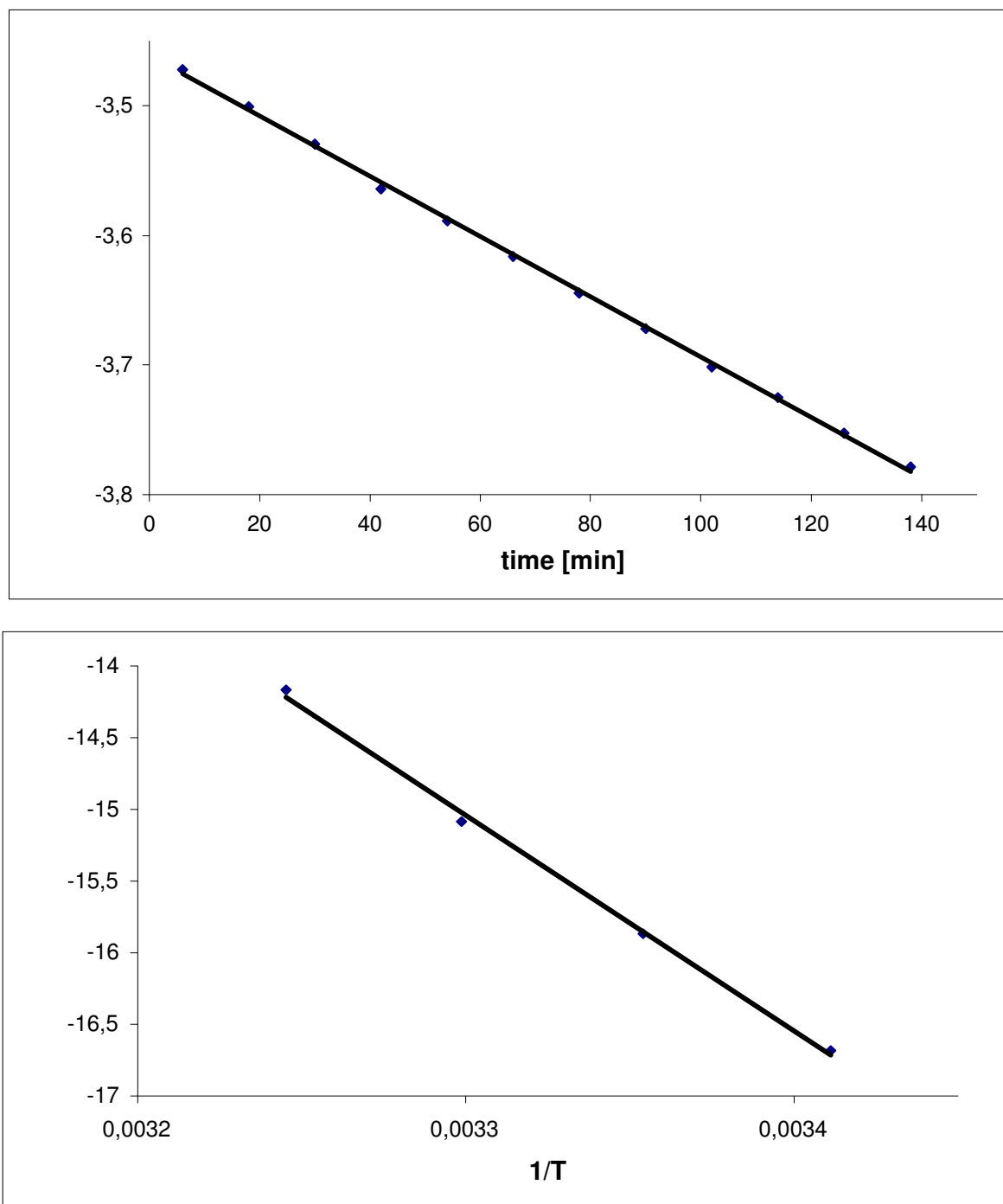


Figure 3. 1st order plot at 298 K (above) and Eyring plot (below) for the reaction of **2b** with TIPF_6 in THF giving **5b**^{PF₆}.

In contrast to this system, dehydrogenation of the amido pincer complex $[\text{Ir}(\text{H})_2(\text{PNP}^{\text{Ar}})]$ (**6**; $(\text{PNP}^{\text{Ar}}) = \text{N}(\text{C}_6\text{MeH}_3\text{P}^i\text{Pr}_2)_2$) with norbornene in methyl-*tert*-butylether was reported by Grubbs and co-workers to give iridium(I) carbene complex $[\text{Ir}(=\text{C}(\text{H})\text{O}^t\text{Bu})(\text{PNP}^{\text{Ar}})]$ (**7**), i.e., 2 eq. of H_2 per iridium are transferred to norbornene.^[306e] For dehydrogenation of THF

[325] Addition of up to 0.32 equiv. free COE with respect to THF resulted in no change of the reaction rate. However, higher concentrations of COE to probe for a dissociative pathway could not be used due to insolubility of the starting material.

with **6**/norbornene dihydride $[\text{Ir}(\text{H})_2(=\text{CO}(\text{CH}_2)_3)(\text{PNP}^{\text{Ar}})]$ (**8**) was identified spectroscopically as an intermediate and full dehydrogenation to $[\text{Ir}(=\text{CO}(\text{CH}_2)_3)(\text{PNP}^{\text{Ar}})]$ (**9**) required elevated temperatures. Finally, upon dehydrogenation of TMEDA ($\text{Me}_2\text{N}(\text{CH}_2)_2\text{NMe}_2$) only 1 eq. H_2 was transferred to norbornene, giving aminocarbene dihydride $[\text{Ir}(\text{H})_2(=\text{C}(\text{H})\text{NMe}(\text{CH}_2)_2\text{NMe}_2)(\text{PNP}^{\text{Ar}})]$ (**10**), in analogy to **5a/5b**.^[326] While π -donation of an amido ligand stabilizes an electrophilic Fischer-carbene in *trans*-position by a *push-pull* interaction,^[312a,c] octahedral coordination is unfavorable for d^6 amido complexes due to antibonding $d_{\pi}p_{\pi}$ interactions exemplified by the high basicity of $[\text{Ru}(\text{NH}_2)\text{H}(\text{Me}_2\text{PCH}_2\text{CH}_2\text{PMe}_2)_2]$.^[327] As an explanation for the distinctly different reactivity of **6**/norbornene with tertiary methylamines *vs.* methylethers the authors proposed, that the stronger $\text{E} \rightarrow \text{C}$ p -donation ($\text{E} = \text{N}, \text{O}$) in the aminocarbene *vs.* the alkoxy carbene results in higher basicity of the metal center in the $[\text{Ir}(=\text{C}(\text{H})\text{NMe}(\text{CH}_2)_2\text{NMe}_2)(\text{PNP}^{\text{Ar}})]$ fragment. Hence, dehydrogenation of the aminocarbene dihydrides could be thermodynamically unfavorable. However, the cationic fragment $[\text{Ir}(=\text{CO}(\text{CH}_2)_3)(\text{PNP}^{\text{H}})]^+$ should be even less basic at the metal center than $[\text{Ir}(=\text{C}(\text{H})\text{OR})(\text{PNP}^{\text{Ar}})]$, but our efforts to selectively dehydrogenate **5b**^{BPh₄} by reaction with potential hydrogen acceptors remained unsuccessful, so far.^[328] Furthermore, based on DFT calculations Yates and co-workers have recently proposed a mechanism for the formation of **7**.^[311] From the thermochemical calculations provided in this paper, the hypothetical dehydrogenation of $[\text{Ir}(\text{H})_2(\text{C}(\text{H})\text{O}^t\text{Bu})(\text{PNP}^{\text{Ar}})]$ with norbornene toward **7** can be estimated to be highly exothermic ($\Delta\text{H} = -93.9$ kJ/mol). In this context, it seems unlikely for dehydrogenation of **10** with norbornene to be endothermic. Therefore, the formation of iridium(I) *vs.* iridium(III) Fischer-carbenes might at least in part be attributed to kinetic arguments. Particularly steric factors which control the barrier of α -oxyalkyl rotation around the Ir–C bond in the proposed intermediate five-coordinate complex (**B**) should be important, since isomerization of the *trans*- to a *cis*-hydride would be necessary for H_2 loss.

B.3.3 Conclusions

In conclusion we have demonstrated the ability of the $\text{Ir}(\text{PNP}^{\text{H}})$ fragment to undergo facile activation of vinyl and alkyl C–H bonds, exemplified by reversible intramolecular vinylic oxidative addition of cyclooctene and intermolecular formation of Fischer-carbenes **5a/b** by geminal dehydrogenation of THF. Our results suggest that olefin complex **1b** readily loses COE to undergo intermolecular C–H activation. A frequently used method for *in situ* generation of such three-coordinate iridium(I) fragments is reductive elimination from five-

[326] Whited, M. T.; Grubbs, R. H. *Organometallics* **2008**, *27*, 5737.

[327] Fulton, J. R.; Bouwkamp, M. W.; Bergman, R. G. *J. Am. Chem. Soc.* **2000**, *122*, 8799.

[328] **5b**^{BPh₄} showed no reaction with norbornene in THF after 24 h at 70 °C by ³¹P NMR. In acetone, **5b**^{BPh₄} very slowly decomposed to a mixture of unidentified products upon prolonged heating at 60°C over several days.

coordinate iridium(III), e.g., by dehydrogenation of an iridium(III) dihydride with a strained olefin, such as norbornene.^[300b,302,306c] Here, we presented an alternative pathway making of the iridium(I) olefin *vs.* iridium(III) vinyl hydride complex equilibrium. While six coordinate cyclooctenyl hydride **2b** can be handled at room temperature for some time without considerable decomposition, the cationic complex rapidly converts to the olefin complex by reductive elimination. COE then readily dissociates assisted by the steric bulk of the (PNP^H)^{tBu} pincer ligand. Hence, intermolecular C–H activation can be controlled by ion pair formation, e.g., via chloride abstraction or polar solvent choice. To date, our efforts to dehydrogenate **5b** or functionalize the carbene ligand at the carbon atom with nucleophiles (e.g. amines, water) or electrophiles (e.g. CO₂) have been unsuccessful but will be further examined in the future.

B.3.4 Experimental Section

B.3.4.1 General Methods

All manipulations of air-sensitive materials were performed with the rigorous exclusion of oxygen and moisture in flame-dried Schlenk-type glassware either on a dual manifold Schlenk line, interfaced to a vacuum (<8 x 10⁻² Torr) line, or in an argon-filled M. Braun glovebox. THF and toluene were predried over Na wire and distilled under nitrogen from Na and benzophenone ketyl (stabilized with tetraglyme for toluene) prior to use. All other solvents were dried by passing over columns packed with activated alumina. Deuterated solvents were obtained from Euriso-Top GmbH, dried over Na/K (*d*⁸-THF, C₆D₆), CaH₂ (CD₂Cl₂), or molecular sieves and activated B₂O₃ (*d*⁶-acetone), distilled by trap-to-trap transfer *in vacuo*, and degassed by three *freeze-pump-thaw* cycles, respectively.

B.3.4.2 Analytical Methods

NMR spectra were recorded on JEOL 400 or BRUKER DPX 500 FT-NMR spectrometers. Chemical shifts are referenced to internal residual solvent resonances (¹H, ¹³C) or an external standard, and are reported relative to tetramethylsilane and 85% phosphoric acid (³¹P NMR), respectively. Signal multiplicities are abbreviated as: s (singlet), d (doublet), t (triplet), vt (virtual triplet), q (quadruplet), m (multiplet), br (broad). Reactions were monitored by ³¹P NMR without lock. [Ir(COE)₂Cl]₂ was synthesized according to literature procedures, respectively.^[329]

B.3.4.3 Syntheses

HN(CH₂CH₂P^{tBu})₂ ((PNP^H)^{tBu})^tBu₂PCl: A ^tBuMgCl Grignard solution (151 mmol), prepared from ^tBuCl and Mg in Et₂O, was added to PCl₃ (8.8 g; 65.0 mmol) in Et₂O (300 mL) at 0 °C and heated for 5 hours until full conversion is observed by ³¹P monitoring

[329] Onderlinden, A. L.; van der Ent, A. *Inorg. Chim. Acta* **1972**, *6*, 420.

(146.0 ppm). After filtration and distillation of the solvent, ${}^t\text{Bu}_2\text{PCl}$ is obtained as a colourless liquid (Yield: 7.20 g; 40.0 mmol; 62 %). ${}^t\text{Bu}_2\text{PH}$: LiAlH_4 (4.0 n in Et_2O ; 10.0 mL; 40.0 mmol) is added to ${}^t\text{Bu}_2\text{PCl}$ (7.2 g; 40.0 mmol) in Et_2O (200 mL) and heated for 4 h. The reaction is quenched by addition of MeOH at $-30\text{ }^\circ\text{C}$ and filtered. Removal of the solvents at ambient pressure and trap to trap condensation of the crude product affords a colourless liquid (${}^{31}\text{P}$ NMR: 20.0 ppm; Yield: 4.33 g; 29.6 mmol; 74 %). ${}^t\text{Bu}_2\text{PLi}$: ${}^t\text{Bu}_2\text{PH}$ (2.1 g; 14.4 mmol) is deprotonated with ${}^n\text{BuLi}$ (1.6 n in hexanes, 12 mL; 19.2 mmol) at $-50\text{ }^\circ\text{C}$ in pentanes (30 mL) and heated to reflux overnight. The product is filtered off, washed with pentanes (2 x 10 mL), and dried *i. vac.* (${}^{31}\text{P}$ NMR: $\delta = 35.8$ ppm (THF); Yield: 2.15 g; 14.1 mmol; 98%). $\text{HN}(\text{CH}_2\text{CH}_2{}^t\text{Bu})_2$: After addition of $\text{Me}_3\text{SiN}(\text{CH}_2\text{CH}_2\text{Cl})_2$ ^[315a] (460 mg; 2.15 mmol) to ${}^t\text{Bu}_2\text{PLi}$ (676 mg; 4.44 mmol) in THF (30 mL) at $-60\text{ }^\circ\text{C}$ the reaction is heated overnight (${}^{31}\text{P}$ NMR = 23.8 ppm). The amine is deprotected by addition of water (10 mL) and heating under reflux for 16 hours. The product is isolated by extraction with THF, drying of the organic layers with MgSO_4 , and evaporation of the solvent to give a viscous, light yellow liquid (Yield: 590 mg; 1.63 mmol; 76%). NMR (C_6D_6 , [ppm], $25\text{ }^\circ\text{C}$) ${}^1\text{H}$ NMR (399.78 MHz): $\delta = 1.05$ (s, 18H, $\text{C}(\text{CH}_3)_3$), 1.07 (s, 18H, $\text{C}(\text{CH}_3)_3$), 1.61 (m, 4H, PCH_2), 2.84 (m, 4H, NCH_2), 3.37 (br, 1H, NH). ${}^{13}\text{C}\{{}^1\text{H}\}$ NMR (100.6 MHz): $\delta = 22.4$ (d, ${}^1J_{\text{CP}} = 22$ Hz, PCH_2), 29.9 (d, ${}^2J_{\text{CP}} = 14$ Hz, $\text{C}(\text{CH}_3)_3$), 30.0 (d, ${}^2J_{\text{CP}} = 14$ Hz, $\text{C}(\text{CH}_3)_3$), 31.3 (d, ${}^1J_{\text{CP}} = 22$ Hz, $\text{C}(\text{CH}_3)_3$), 50.7 (d, ${}^2J_{\text{CP}} = 33$ Hz, NCH_2). ${}^{31}\text{P}\{{}^1\text{H}\}$ NMR (161.8 MHz): $\delta = 22.3$ (s).

[IrH(C₈H₁₃)Cl(PNP^H)^{tBu}] (2b) A solution of $(\text{PNP}^{\text{H}})^{t\text{Bu}}$ (164 mg; 454 μmol) and $[\text{Ir}(\text{COE})_2\text{Cl}]_2$ (204 mg; 227 μmol) in THF (10 mL) is stirred for 5 minutes at r.t. After concentration of the solvent to 1 mL *in vacuo*, the crude product is precipitated upon addition of 10 mL of pentanes, washed with pentanes (3 x 4 mL), dissolved in toluene (25 mL) and filtered. Crystallization from a saturated toluene solution at $-37\text{ }^\circ\text{C}$ over night gives microcrystalline, air-sensitive **2b** as a colourless solid (Yield: 190 mg; 271 μmol ; 60 %). Anal. calcd. for $\text{C}_{28}\text{H}_{59}\text{NCIrP}_2$ (699.39): C, 48.08; H, 8.50; N, 2.00. Found: 48.31; H, 8.49; N, 2.00. NMR (d^8 -THF, [ppm]) ${}^1\text{H}$ NMR (399.78 MHz, $-60\text{ }^\circ\text{C}$): $\delta = -24.99$ (t, ${}^2J_{\text{PH}} = 17.2$ Hz, 1H, Ir-H), 1.37 (m, 42H, $4 \times \text{C}(\text{CH}_3)_3 + 3 \times \text{CH}_2^{\text{COE}}$), 1.63 (m, 2H, CH_2^{COE}), 1.89 (m, 2H, CH_2^{COE}), 2.00 (m, 2H, CH_2^{PNP}), 2.25 (m, 4H, CH_2^{PNP}), 2.79 (m, 2H, CH_2^{COE}), 3.02 (m, 2H, CH_2^{PNP}), 5.27 (br, 1H, NH), 5.64 (t, ${}^2J_{\text{HH}} = 7$ Hz, 1 H, IrC=CH). ${}^{13}\text{C}\{{}^1\text{H}\}$ NMR (100.6 MHz, $-50\text{ }^\circ\text{C}$): $\delta = 27.9$ (s, CH_2^{COE}), 28.2 (s, CH_2^{COE}), 29.2 (vt, $J_{\text{CP}} = 9.5$ Hz, $\text{NCH}_2\text{CH}_2\text{P}$), 31.0 (s, CH_2^{COE}), 31.2 (s, CH_2^{COE}), 31.6 (br, $\text{PC}(\text{CH}_3)_3$), 32.2 (s, CH_2^{COE}), 39.0 (vt, $J_{\text{CP}} = 12.5$ Hz, PCMe_3), 39.5 (vt, $J_{\text{CP}} = 8.0$ Hz, PCMe_3), 42.1 (s, CH_2^{COE}), 53.4 (s, 2 NCH_2CH_2), 122.8 (t, ${}^2J_{\text{CP}} = 7.6$ Hz, Ir-C=CH(CH_2)₆), 137.3 (s, Ir-C=CH(CH_2)₆). ${}^{31}\text{P}\{{}^1\text{H}\}$ NMR (161.8 MHz, $-60\text{ }^\circ\text{C}$): δ

= 30.3 (s). Assignments were confirmed by ^1H COSY (-60 °C) and ^{13}C DEPT (-50°C) NMR spectroscopy.

Dissolving **2b** (30 mg; 42.9 μmol) in CD_2Cl_2 gives a red solution, which was assigned to olefin isomer **1b^{Cl}**. NMR (CD_2Cl_2 , [ppm], -50°C) ^1H NMR (399.78 MHz): δ = 1.20 (d, $^3J_{\text{PH}}$ = 12 Hz, 9H, C(CH_3)₃), 1.26 (m, 9H, C(CH_3)₃), 1.36 (d, $^3J_{\text{PH}}$ = 12 Hz, 15H, C(CH_3)₃ + 3 \times CH_2^{COE}), 1.43 (d, $^3J_{\text{PH}}$ = 12 Hz, 9H, C(CH_3)₃), 1.57 (m, 4H, 2 \times CH_2^{COE}), 1.88 (m, 1H, CH_2^{PNP}), 2.04 (m, 2H, CH_2^{PNP} + CH_2^{COE}), 2.24 (m, 4H, CH_2^{PNP}), 2.47 (m, 1H, CH_2^{COE}) 3.12 (m, 1H, CH_2^{PNP}), 3.21 (m, 1H, CH_2^{PNP}), 3.46 (m, 1H, CH^{COE}), 4.08 (m, 1H, CH^{COE}), 6.99 (br, 1 H, NH). $^{13}\text{C}\{^1\text{H}\}$ NMR (100.6 MHz, -50°C): δ = 24.4 (d, $^1J_{\text{PC}}$ = 23 Hz, PCH_2), 25.9 (s, CH_2^{COE}), 26.3 (s, CH_2^{COE}), 28.7 (d, $^1J_{\text{PC}}$ = 23 Hz, PCH_2), 29.1 (s, C(CH_3)₃), 30.5 (s, C(CH_3)₃), 31.1 (s, CH_2^{COE}), 32.1 (s, CH_2^{COE}), 33.9 (s, CH_2^{COE}), 34.6 (m, 2 \times C(CH_3)₃), 34.7 (s, CH_2^{COE}), 36.0 (dd, $^1J_{\text{PC}}$ = 14 Hz, $^3J_{\text{PC}}$ = 3 Hz, C(CH_3)₃), 36.7 (dd, $^1J_{\text{PC}}$ = 18 Hz, $^3J_{\text{PC}}$ = 3 Hz, C(CH_3)₃), 43.2 (s, $\text{CH}=\text{CH}^{\text{COE}}$), 51.0 (s, $\text{CH}=\text{CH}^{\text{COE}}$), 53.1 (s, NCH_2), 56.2 (s, NCH_2). $^{31}\text{P}\{^1\text{H}\}$ NMR (161.8 MHz): δ = 39.1 (d, $^2J_{\text{PP}}$ = 323 Hz), 45.8 (d, $^2J_{\text{PP}}$ = 323 Hz). Assignments were confirmed by ^1H COSY NMR (-60 °C) and ^{13}C DEPT and APT NMR (-50°C).

[Ir(=CO(CH₂)₃)(H)₂(PNP^H^{tBu})]X (5b^X; X = PF₆, BPh₄). Method A: THF (10 mL) is added to a solid mixture of **2b** (59 mg; 84 μmol) and TIPF₆ (31 mg; 89 μmol) and stirred for 16 h at r.t. After filtration the product is precipitated from a saturated THF solution by addition of pentanes (10 mL), washed with pentanes (3 \times 5 mL) and dried *in vacuo* to give light-brown, analytically pure **5b^{PF6}** (Yield: 49 mg; 63 μmol ; 75 %). Anal. calcd. for C₂₄H₅₃NF₆IrOP₃ (770.81): C, 37.40; H, 6.93; N, 1.82. Found: 37.31; H, 6.76; N, 1.77. NMR (25°C, CD_2Cl_2 , [ppm]): ^1H NMR (399.78 MHz): δ = -8.84 (dt, $^2J_{\text{HH}}$ = 17 Hz, $^2J_{\text{PH}}$ = 16 Hz, 1H, Ir-H), -7.85 (dt, $^2J_{\text{HH}}$ = 17 Hz, $^2J_{\text{PH}}$ = 13 Hz, 1H, Ir-H), 1.35 (vt, J_{HP} = 7 Hz, 18H, C(CH_3)₃), 1.39 (vt, J_{HP} = 7 Hz, 18H, C(CH_3)₃), 1.82 (m, 2H, 2 PCH_2), 1.89 (m, 2H, Ir=C($\text{CH}_2\text{CH}_2\text{CH}_2\text{O}$)), 2.21 (m, 4H, NCH_2 + PCH_2), 2.91 (t, $^3J_{\text{HH}}$ = 8 Hz, 2H, Ir=C($\text{CH}_2\text{CH}_2\text{CH}_2\text{O}$)), 3.37 (m, 2H, NCH_2), 4.29 (br, 1H, NH), 4.50 (t, $^3J_{\text{HH}}$ = 7 Hz, 2H, Ir=C($\text{CH}_2\text{CH}_2\text{CH}_2\text{O}$)). $^{31}\text{P}\{^1\text{H}\}$ NMR (161.8 MHz): δ = 68.0 (s, P^{PNP}), -144 (sept, $^1J_{\text{PF}}$ = 711 Hz, PF_6).

Method B: (PNP^H^{tBu}) (27 mg; 75 μmol) and NaBPh₄ (26 mg; 76 μmol) are added to a solution of $[\text{Ir}(\text{COE})_2\text{Cl}]_2$ (34 mg; 38 μmol) in THF (10 mL) and stirred for 16 h at r.t. The solution is filtered and the residue extracted with THF (twice 3 mL). Upon evaporation of the solvent, the light-yellow crude product is dried *in vacuo* and washed with pentane (3 \times 3 mL). Recrystallization from THF gives colourless analytically pure **5b^{BPh4}** (Yield: 42 mg; 44 μmol ; 59 %). NMR (CD_2Cl_2 , 25°C, [ppm]) ^1H NMR (399.78 MHz): δ = -9.11 (dt, $^2J_{\text{HH}}$

= 17 Hz, $^2J_{\text{PH}} = 15$ Hz, 1H, Ir-H), -7.90 (dt, $^2J_{\text{HH}} = 17$ Hz, $^2J_{\text{PH}} = 13$ Hz, 1 H, Ir-H), 1.32 (vt, $J_{\text{HP}} = 7$ Hz, 18H, C(CH₃)₃), 1.34 (vt, $J_{\text{HP}} = 7$ Hz, 18H, C(CH₃)₃), 1.42 (m, 2 H, PCH₂), 1.84 (m, 2 H, Ir=C(CH₂CH₂CH₂O)), 1.87 (m, 2 H, NCH₂), 1.96 (m, 2 H, PCH₂), 2.69 (m, 2 H, NCH₂), 2.86 (t, $^3J_{\text{HH}} = 8$ Hz, 2 H, Ir=C(CH₂CH₂CH₂O)), 3.46 (br, 1H, NH), 4.45 (t, $^3J_{\text{HH}} = 7$ Hz, 2 H, Ir=C(CH₂CH₂CH₂O)), 6.87 (t, $^3J_{\text{HH}} = 7$ Hz, 4 H, 4 CH_{Ar} para), 7.02 (t, $^3J_{\text{HH}} = 7$ Hz, 8 H, 8 CH_{Ar} ortho), 7.28 – 7.36 (br, 8 H, 8 CH_{Ar} meta). ¹³C{¹H} NMR (100.6 MHz): $\delta = 24.0$ (s, Ir=C(CH₂CH₂CH₂O)), 28.0 (t, $^1J_{\text{CP}} = 12$ Hz, PCH₂), 29.3 (s, C(CH₃)₃), 30.4 (s, C(CH₃)₃), 34.3 (vt, $J_{\text{CP}} = 12$ Hz, C(CH₃)₃), 37.6 (vt, $J_{\text{CP}} = 13$ Hz, 2 C(CH₃)₃), 56.2 (s, NCH₂), 65.5 (s, Ir=C(CH₂CH₂CH₂O)), 82.9 (s, Ir=C(CH₂CH₂CH₂O)), 122.1 (s, 4 C_{Ar} para), 126.0 (br, C_{Ar} ortho), 136.3 (s, C_{Ar} meta), 164.4 (q, $^1J_{\text{CB}} = 49$ Hz, C_{Ar} ipso), 261.9 (t, $^2J_{\text{CP}} = 5$ Hz, Ir=C(CH₂CH₂CH₂O)). ³¹P{¹H} NMR (161.8 MHz): $\delta = 67.8$ (s). Assignments were confirmed by ¹H COSY, ¹H-¹³C HMQC, and ¹H-¹³C HMBC NMR spectra.

B.3.4.4 Kinetic Experiments

2b (10.4 mg; 14.9 μmol) and TIPF₆ (6.8 mg; 19.5 μmol) are mixed in a septum cap nmr tube equipped with a sealed capillary of phosphoric acid as internal standard. THF or *d*⁸-THF (0.47 mL), respectively, is added through a syringe. The reaction is followed by ³¹P{¹H} NMR spectroscopy at a preset temperature in the inverse-gated mode to avoid NOE buildup. The relaxation delay (6 sec) is chosen as $> 5T_1$, as derived by ³¹P NMR inversion recovery experiments. Activation parameters are derived from an Eyring plot upon rate measurements at +20, +25, +30, and +35 °C, respectively.

B.3.4.5 X-ray Crystal-Structure Determinations

Crystal data and details of the structure determination are presented in **Table 3**. Suitable single crystals were grown by diffusion of pentanes into a THF solutions at -37 °C (**2b**) or at r.t. (**5a**^{BPh₄}, **5b**^{BPh₄}), respectively. Crystals were stored under perfluorinated ether, transferred in a Lindemann capillary, fixed, and sealed. Preliminary examinations and data collection were carried out with area detecting systems and graphite-monochromated Mo K α radiation ($\lambda = 0.71073$ Å). The unit cell parameters were obtained by full-matrix least-squares refinements during the scaling procedures. Data collection was performed at low temperatures (Oxford Cryosystems), and each crystal measured with a couple of data sets in rotation scan modus. Intensities were integrated and the raw data were corrected for Lorentz, polarization, and, arising from the scaling procedure, latent decay and absorption effects. The structures were solved by a combination of direct methods and difference Fourier syntheses. All non-hydrogen atoms were refined with anisotropic displacement parameters. The iridium hydride positions were taken tentatively from the difference peak lists and were fixed with reasonable Ir–H distances. Full-matrix least-squares refinements were carried out by minimizing

$\Sigma[w(F_o^2 - F_c^2)^2]$ with the SHELXL-97 weighting scheme and stopped at shift/err < 0.003. The final residual electron density maps showed no remarkable features. Neutral atom scattering factors for all atoms and anomalous dispersion corrections for the non-hydrogen atoms were taken from International Tables for Crystallography. All calculations were performed on an Intel Pentium 4 PC, with the WinGX system, including the programs PLATON, SIR92, and SHELXL-97.^[330] **2b**: Nine data sets were measured in rotation scan modus with $\Delta\phi/\Delta\Omega = 1.0^\circ$ (APEX II, κ -CCD) at the window of a rotating anode (Bruker AXS, FR591). A disorder of the cyclooctene ligand [0.63(1):0.37(1)] could be resolved clearly. In the final stage of the refinements the residual highest difference peaks suggest highly disordered solvent molecules. The problem was solved with the PLATON calc squeeze procedure. **5a**: Six data sets were measured in rotation scan modus with $\Delta\phi = 1.00^\circ$ (IPDS 2T) at the window of a rotating anode (Bruker AXS, FR591). Numerical absorption correction after crystal shape optimization with the programs XSHAPE and XRED. **5b**: Five data sets were measured in rotation scan modus with $\Delta\phi/\Delta\Omega = 0.50^\circ$ (APEX II, κ -CCD) at the window of a rotating anode (Bruker AXS, FR591). The asymmetric unit cell contains two crystallographic independent molecules **A**⁺, **A**⁻, **B**⁺ and **B**⁻. In the final stage of the refinements the residual highest difference peaks suggests highly disordered solvent molecules. The problem was solved with the PLATON calc squeeze procedure.

Table 3. Crystallographic data for $[\text{IrH}(\text{C}_8\text{H}_{13})\text{Cl}(\text{PNP}^{\text{H}})^{\text{tBu}}]$ (**2b**), $[\text{Ir}(\text{H})_2(=\text{CO}(\text{CH}_2)_3)(\text{PNP}^{\text{H}})^{\text{iPr}}][\text{BPh}_4]$ (**5a**^{BPh4}), and $[\text{Ir}(\text{H})_2(=\text{CO}(\text{CH}_2)_3)(\text{PNP}^{\text{H}})^{\text{tBu}}][\text{BPh}_4]$ (**5b**^{BPh4}).

	2b	5a ^{BPh4}	5b ^{BPh4}
formula	C ₂₈ H ₅₉ ClIrNP ₂	C ₄₄ H ₆₅ BIrNOP ₂	C ₄₈ H ₇₃ BIrNOP ₂
fw	699.37	888.94	945.04
color/habit	colorless/fragment	colorless/fragment	colorless/fragment
cryst dimensions (mm ³)	0.15 × 0.36 × 0.56	0.20 × 0.20 × 0.61	0.18 × 0.23 × 0.38
cryst syst	triclinic	triclinic	triclinic
space group	<i>P</i> $\bar{1}$ (no. 2)	<i>P</i> $\bar{1}$ (no. 2)	<i>P</i> $\bar{1}$ (no. 2)
<i>a</i> , Å	10.5995(4)	11.4149(3)	16.0820(12)
<i>b</i> , Å	12.0821(4)	13.8996(4)	16.5792(13)

[330] (a) APEX suite of crystallographic software. APEX 2 Version 2008.4. Bruker AXS Inc., Madison, Wisconsin, USA (2008). (b) SAINT, Version 7.56a and SADABS Version 2008/1. Bruker AXS Inc., Madison, Wisconsin, USA (2008). (c) Data Collection Software and Data Processing Software for Stoe IPDS 2T diffractometer, X-ARERA, Version 1.26; Stoe & Cie: Darmstadt, Germany, 2004. (d) Data Processing Software for Stoe IPDS 2T diffractometer, XRED, XSHAPE, Version 1.26; Stoe & Cie: Darmstadt, Germany, 2004. (e) Farrugia, L. J. WinGX (Version 1.70.01 January 2005). *J. Appl. Crystallogr.* **1999**, *32*, 837. (f) Altomare, A.; Cascarano, G.; Giacovazzo, C.; Guagliardi, A.; Burla, M. C.; Polidori, G.; Camalli, M. *SIR92*. *J. Appl. Crystallogr.* **1994**, *27*, 435. (g) *International Tables for Crystallography*; Wilson, A. J. C., Ed.; Kluwer Academic Publishers: Dordrecht, The Netherlands, 1992; Vol. C, Tables 6.1.1.4, 4.2.6.8, and 4.2.4.2. (h) Spek, A. L. *PLATON, A Multipurpose Crystallographic Tool*; Utrecht University: Utrecht, The Netherlands, **2001**. (i) Sheldrick, G. M. *SHELXL-97*; Universität Göttingen: Göttingen, Germany, **1998**.

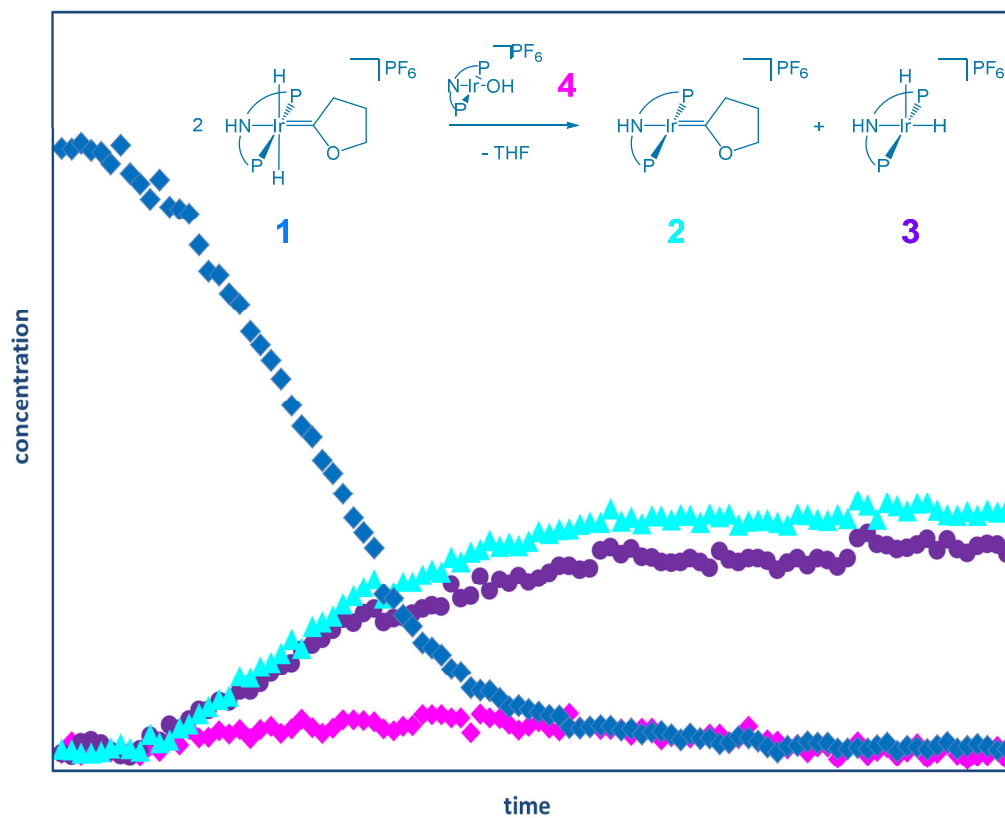
c , Å	15.4891(5)	14.3394(4)	19.2566(14)
α , deg	67.976(1)	75.453(2)	75.202(3)
β , deg	84.985(2)	69.695(2)	88.153(3)
γ , deg	71.147(1)	86.219(2)	84.312(3)
V , Å ³	1738.91(11)	2064.78(10)	4939.5(6)
Z	2	2	4
T , K	173	123	173
D_{calcd} , g cm ⁻³	1.336	1.430	1.271
μ , mm ⁻¹	4.023	3.344	2.800
$F(000)$	716	912	1952
θ range, deg	1.42 – 25.40	4.69 – 25.35	3.40 – 25.34
index ranges (h, k, l)	$\pm 12, -12-13, \pm 18$	$\pm 13, \pm 16, \pm 17$	$-18-19, \pm 19, \pm 23$
no. of rflns collected	86394	91296	79377
no. of indep rflns/ R_{int}	6145/0.035	7499/0.057	17481/0.030
no. of obsd rflns ($I > 2\sigma(I)$)	5820	7117	16158
no. of data/restraints/params	6145/0/329	7499/0/471	17481/0/997
$R1/wR2$ ($I > 2\sigma(I)$) ^a	0.0221/0.0510	0.0270/0.0624	0.0251/0.0653
$R1/wR2$ (all data) ^a	0.0244/0.0529	0.0301/0.0634	0.0274/0.0667
GOF (on F^2) ^a	1.212	1.093	1.042
largest diff peak and hole (e Å ⁻³)	1.66/-1.17	1.20/-1.39	3.27/-1.62

B.4 Hydrogen elimination from a PNP Iridium(III) Dihydrido Carbene Complex

unpublished results

J. Meiners, S. Schneider*

Georg August Universität Göttingen, Tammannstr 4, 37073 Göttingen/Germany



Desymmetrization of a PNP iridium dihydrido carbene complex **1** toward carbene and dihydrido complex **2** and **3** is accelerated by presence of both O₂ or oxygenation product Ir(III) hydroxo complex **4**.

B.4.1 Abstract

The cationic iridium(III) Fischer carbene complex $[\text{HPNP}^{\text{tBu}}\text{Ir}=\text{CO}(\text{CH}_2)_3(\text{H})_2]\text{PF}_6$ ($\text{HPNP}^{\text{tBu}} = \text{HN}(\text{CH}_2\text{CH}_2)\text{P}^{\text{tBu}}_2$) (**1**)^[331] undergoes a desymmetrization reaction toward the corresponding dehydrogenated iridium(I) carbene complex $[\text{HPNP}^{\text{tBu}}\text{Ir}=\text{CO}(\text{CH}_2)_3]\text{PF}_6$ (**2**) and the iridium(III) dihydrido complex $[\text{HPNP}^{\text{tBu}}\text{Ir}(\text{H})_2]\text{PF}_6$ (**3**)^[332]. The reaction shows complex kinetic curves and is accelerated by the addition of dioxygen in terms of air (but not by addition of AIBN). Reaction of each of the three reactants with an excess of dioxygen leads to the formation of the earlier described SP coordinated Ir(III) hydroxo complex $[\text{PNP}^{\text{tBu}}\text{Ir}(\text{OH})]\text{PF}_6$ (**4**) (**B.2**)^[332]. **4** itself accelerates the above mentioned desymmetrization reaction as well.

B.4.2 Introduction

Oxidative functionalization of Alkyl ethers through reaction of hetero cumulenes with an iridium PNP pincer carbene complex

Grubbs and co-workers described a catalytic process for geminal CH_2 functionalization of dialkyl ethers with 1-Azidoadamantane (AdN_3) as an oxidizing agent utilizing the complex $[(\text{PNP}^{\text{Ar}})\text{Ir}(\text{N}_2)]$ ^[333] ($\text{PNP}^{\text{Ar}} = [\text{N}(2\text{-P}^i\text{Pr}_2\text{-4-Me-C}_6\text{H}_3)_2]$)^[334] as the catalyst (**Scheme B.4-1**).^[308] This catalytic double C-H activation-group transfer reaction was performed with 10 mol-% of [Ir] catalyst and yielded up to > 90 %. The authors proposed a mechanism that can be split up into three sub-reactions of two interconnected catalytic cycles, which were also subject of a theoretical study^[335].

1) CH activation

Dehydrogenation of the dihydrido complex $(\text{PNP}^{\text{Ar}})\text{IrH}_2$ ^[336] (**I**) with 1 equivalent of norbornene (NBE) in the presence of a dialkyl ether (butylmethylethers, e.g. MTBE, SBME, NBME, or cyclic ethers, e.g. THF) leads to formation of the corresponding Ir(I) Fischer carbene complex $(\text{PNP}^{\text{Ar}})\text{Ir}=\text{C}(\text{R}^1)\text{OR}^2$ ($\text{R}^1 = \text{H}$; $\text{R}^2 = \textit{t}/\textit{sec}/\textit{n}\text{Bu}$ (**IV^{tBu/secBu/nBu}**), $\text{R}^1 = \text{R}^2 = \text{CH}_2\text{CH}_2$ (**IV^{THF}**)).^[337] In analogy to previous work on ether double CH activation^[305,306a-d,306h-i,307] and CH activation with Ir(I) pincer systems^[338,339], the authors proposed for this reaction a mechanism via CH activation by the 14 VE, T-shaped

[331] J. Meiners, A. Friedrich, E. Herdtweck, S. Schneider, *Organometallics* **2009**, 28 (21), 6331–6338.

[332] C. Schiwiek, J. Meiners, C. Würtele, M. Finger, H. Wolf, D. Stalke, S. Schneider, *in preparation*

[333] M. T. Whited, R. H. Grubbs, *J. Am. Chem. Soc.* 2008, 130, 16476–16477.

[334] L. Fan, B. M. Foxman, O. V. Ozerov, *Organometallics* 2004, 23, 326–328.

[335] N. J. Brookes, A. Ariafard, R. Stranger, B. F. Yates, *J. Am. Chem. Soc.* **2009**, 131, 5800–5808.

[336] L. Fan, S. Parkin, O. V. Ozerov, *J. Am. Chem. Soc.* **2005**, 127, 16772–16773.

[337] N. J. Brookes, M. T. Whited, A. Ariafard, R. Stranger, R. H. Grubbs, B. F. Yates, *Organometallics* **2010**, 29, 4239–4250.

[338] A. S. Goldman, K. I. Goldberg, *Organometallic C–H Bond Activation: An Introduction*, Bd. 885, S. 1–43.

[339] (a) K. I. Goldberg, A. S. Goldman, S. R. Klei, K. L. Tan, J. T. Golden, C. M. Yung, R. K. Thalji, Activation and Functionalization of C-H Bonds, ACS Symposium Series Volume 885, (b) K. A. Ahrendt, J. A. Ellman, T. D. Tilley, R. G. Bergman, *chapter 2: Carbon–Hydrogen Bond Activation by Iridium and Rhodium Complexes: Catalytic Hydrogen/Deuterium Exchange and Carbon–Carbon Bond-Forming Reactions*, S. 46–55.

Ir(I)-intermediate **II**. **II** is supposed to be formed in a preceding dehydrogenation step through reaction of **I** with NBE ($\mathbf{I} + \text{NBE} \rightarrow \mathbf{II} + \text{NBA}$). Electronically and coordinatively unsaturated **II** undergoes C-H oxidative addition twice: The first one leads to formation of the five-fold coordinated hydrido alkyl species **III**. **III** is via a second α CH activation in equilibrium with the dihydrido carbene **IV-H₂** ($\mathbf{II} \rightarrow \mathbf{III} \rightarrow \mathbf{IV-H_2}$), which finally eliminates H₂ to generate **IV**^[340,341]. The reaction of **II** toward **IV^{tBu}** was probed by DFT computations with a simplified model ($\text{PNP}^{\text{Ar}}\text{Ir} = \text{N}((\text{CH}_2\text{CH}_2)\text{PMe}_2)_2\text{Ir}$), which corroborates this view.^[335] The authors also calculated the equilibrium between *cis*-**IV^{tBu}-H₂**, **III^{tBu}**, and *trans*-**IV^{tBu}-H₂**. While *trans*-**IV^{tBu}-H₂** is slightly lower in energy, the formation of *cis*-**IV-H₂** is a prerequisite for H₂ reductive elimination. However, the highest barrier for the overall reaction $\mathbf{I} \rightarrow \mathbf{IV}$ was calculated at +76.2 kJ mol⁻¹ (H₂ reductive elimination from *cis*-**IV-H₂**), thus thermally accessible. The free reaction enthalpy for this part of the mechanism was computed to be almost thermoneutral. They suggest that the consumption of H₂ represent the overall thermodynamic driving force (see below).

2) Oxidative functionalization

According to electronic structure calculations of **IV^{tBu}**, the HOMO-1 exhibits large Ir dz^2 character, explaining the nucleophilic reactivity at Ir, while the LUMO has predominant C p-orbital character (Ir=C π^*).^[342] Consequently this *Roper-type nucleophilic-at-metal carbene*^[343] effects multiple-bond metatheses leading to atom and group transfer from electrophilic heterocumulenes (e.g., CO₂, CS₂, PhNCS, N₂O, AdN₃, Me₃SiN₃, 2,6-diisopropylphenylazide), releasing the corresponding formate, thioformate or formimidate and iridium(I) N₂, CO, CS, or PhNC complexes, respectively.^[333]

3) H₂ transfer

The calculations in the proposal^[335] of Yates and co-workers suggest that the amounts of H₂, which were formed in the *CH activation* step by elimination of H₂ from *cis*-**IV^{tBu}-H₂** toward **IV^{tBu}** are added to **III^{tBu}**, followed by the reductive elimination of the alkyl ligand due to the trans-influence of the now trans-bound hydrido species to furnish **I** and unbound MTBE highly exothermic (-79.3 kJ mol⁻¹). This exothermic H₂ transfer reaction provides efficiently energy to repeat the cycle until **IV^{tBu}** is obtained quantitatively by an all-over consumption of two equivalents of NBE. Thus the H₂ transfer step is representing the thermodynamic driving force of the whole reaction from **I** toward **IV^{tBu}**.

[340] P. E. Romero, M. T. Whited, R. H. Grubbs, *Organometallics* **2008**, *27*, 3422–3429.

[341] M. T. Whited, R. H. Grubbs, *J. Am. Chem. Soc.* **2008**, *130*, 5874–5875.

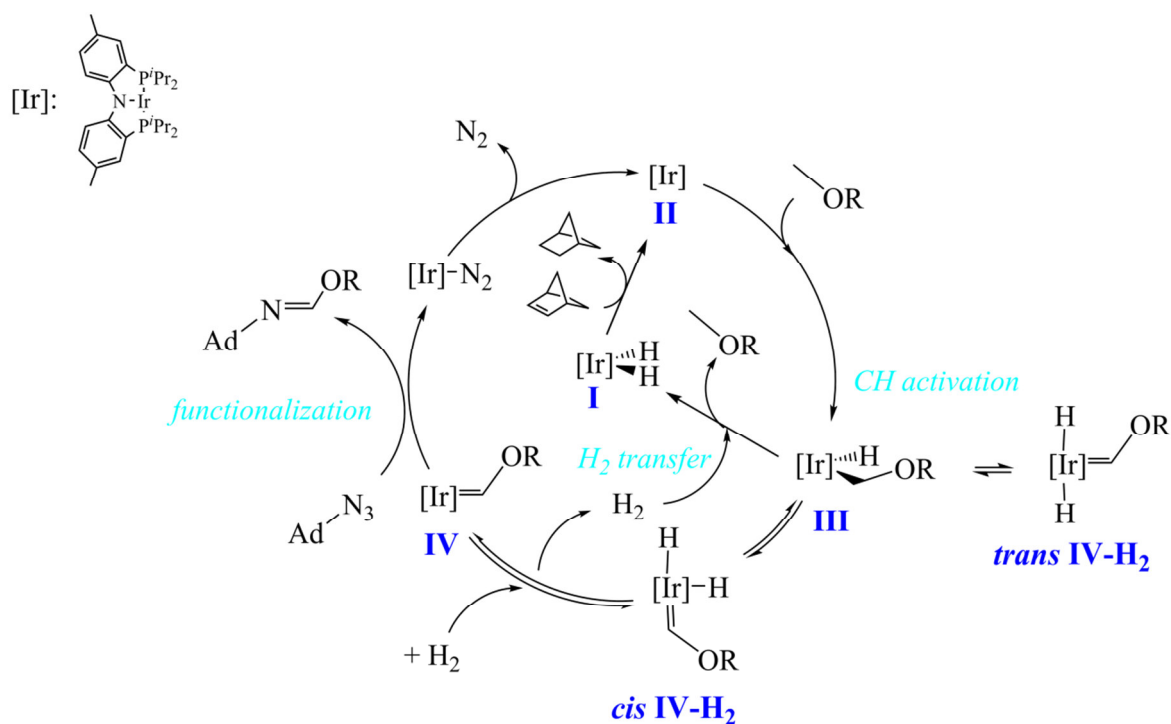
[342] M. T. Whited, R. H. Grubbs, *Organometallics* **2009**, *28*, 161–166.

[343] M. A. Gallop, W. R. Roper in *Advances in Organometallic Chemistry*, Elsevier, **1986**, *25*, 121–198.

Grubbs and co-workers demonstrated within stoichiometric reactions, that the dehydrogenative C-H activation (**I** → **IV**) and the carbene functionalization (**IV** → [Ir-N₂] + organic product) are viable reactions. However, the proposed hydrogen transfer pathway:



which was only suggested theoretically before,^[344] has not been shown experimentally. The formation of the cationic dihydrido iridium(III) carbene complex [HPNP^{tBu}Ir={CO(CH₂)₃}(H)₂]PF₆ (**1**)^[331] with the neutral, aliphatic HPNP^{tBu} ligand system, which is similar to the above-mentioned *trans*-**IV-H₂** gained by an equal *CH activation* substep, have previously been presented. Hence, these findings offer the opportunity to study the H₂ transfer mechanism, which will be described below.



Ad: Adamantyl, [Ir]: 10%,

yield: > 90% (R = ^tBu), less efficient (R = ^{sec}Bu, ⁿBu)

Scheme B.4-1: Grubbs ether functionalization cycle

[344] M. T. Whited, Y. Zhu, S. D. Timpa, C.-H. Chen, B. M. Foxman, O. V. Ozerov, R. H. Grubbs, *Organometallics* **2009**, 28, 4560–4570.

B.4.3 Results and Discussion

B.4.3.1 Study of the subsequent dehydrogenation of a dihydrido iridium carbene complex

The iridium(III) carbene dihydrido complex $[HPNP^{tBu}Ir=\{CO(CH_2)_3\}(H)_2]PF_6$ (**1**)^[331], which was previously obtained by chloride abstraction of the Ir(III) cyclooctenyl complex $[HPNP^{tBu}IrH(C_8H_{13})Cl]$ (**6**)^[331] with $TiPF_6$ and following a double α CH activation of the solvent THF, could not be dehydrogenated by H_2 trapping sources like NBE or acetone or by irradiation with UV light.^[345] Addition of PMe_3 or CH_3CN during the synthesis of **1**^[282] led to buildup of a new C_s -symmetric product by ^{31}P NMR, presumably due to formation of an alkyl

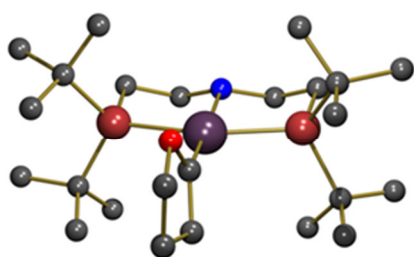


Figure B.4-1: POV-ray depiction^[346] of **2** in the crystal (Hydrogen atoms are omitted for clarity).

Bond lengths (Å)	Bond Angles (deg)
Ir1-C21 1.900(3)	N1-Ir1-C21 173.56(14)
Ir1-N1 2.194(3)	P1-Ir1-P2 162.73(3)
Ir1-P1 2.3179(8)	O1-C21-C22 107.0(3)
Ir1-P2 2.3168(9)	
C21-O1 1.339(4)	

Table B.4-1: Selected bond length and bond angles of **2** in the crystal.^[346]

hydrido complex.^[345] But treatment with the heterocumulene CO_2 or the nucleophile *para*-Toluidin did not lead to any reaction such as carbene functionalization.

However, continual warming over several days of a solution of **1** in THF led to the generation of one new product, namely the iridium(I) carbene complex $[HPNP^{tBu}Ir=CO(CH_2)_3]PF_6$ (**2**) and the familiar iridium(III) dihydrido complex $[HPNP^{tBu}Ir(H)_2]PF_6$ (**3**)^[332] (**Scheme B.4-2**, **Scheme B.4-5**, **B.2**). **3** can be obtained by an additional pathway by treatment of **1** with an excess of H_2 , the formation of the also known iridium(III) dihydrido dihydrogen complex $[HPNP^{tBu}Ir(H)_2(H_2)]PF_6$ (**5**)^[332] (**Scheme B.4-5**, **B.2**) and dehydrogenation of the latter *in vacuo* toward **3**.

$[HPNP^{tBu}Ir=CO(CH_2)_3]PF_6$ (**2**) could be synthesized with a yield of 15% in one attempt by complete desymmetrization of dihydrido carbene **1** toward carbene **2** and dihydride **3** and subsequent recrystallization in THF to separate **3** from **2**.

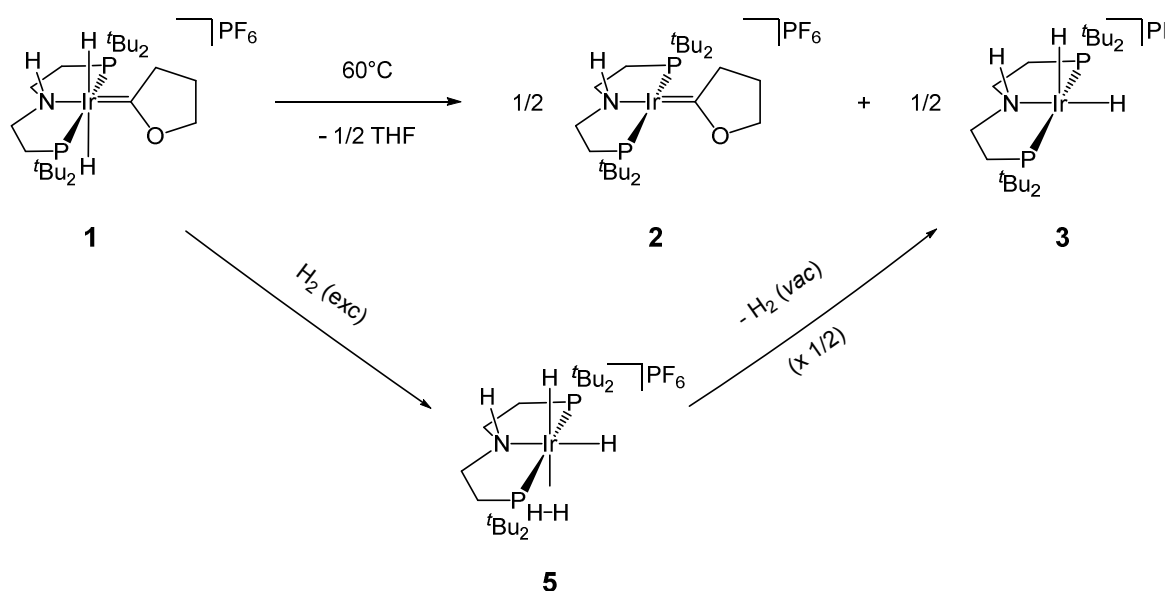
Although no dehydrogenation of **1** with NBE was achieved before, the trapping of H_2 during the desymmetrization reaction turned out to be reasonable. In a NMR scale experiment, six

[345] J. Meiners, S. Schneider, *unpublished results*

eq. NBE were added to the reaction, which resulted in a product mixture **2:3** of 0.7/0.3 by ^{31}P NMR.^[345] Therefore, it could be useful for syntheses of **2** in the future to proceed the reaction under addition of NBE.

The signals of the room temperature ^{31}P and ^1H NMR spectra (s. 158) of **2** are in agreement with a C_S -symmetric carbene amino complex.

An x-ray structure which was obtained from single-crystal x-ray diffraction measured by *Bechlars*^[346] of orange crystals of **2** derived from THF/pentanes solution shows a square planar coordinated iridium center with the carbene ligand perpendicular to the Ir-P1-P2-N plane (**Figure B.4-1**). The pincer bite angle, the N1-Ir1-C21 bond angle and the O1-C21-C22 bond angle in **2** are slightly smaller ($\sim 1\text{-}2^\circ$, **Table B.4-1**) than in $[\text{HPNP}^{\text{tBu}}\text{Ir}=\{\text{CO}(\text{CH}_2)_3\}(\text{H})_2\text{PF}_6$ **1**^[331]. While the Ir bond distances in the iridium(I) compound **2** toward N1, P1, P2 and C21 are a little shorter ($\sim 0.01\text{-}0.04 \text{ \AA}$) than in the iridium(III) compound **1**, the C21-O1 bond shows a small elongation ($\sim 0.02 \text{ \AA}$) in **2**, probably revealing a weaker C21-O1 π -interaction due to an increased push-pull-interplay between N1, Ir1 and C21. The Ir1-C21 bond length ($1.900(3) \text{ \AA}$) is within the range found for other alkoxy-carbene complexes of iridium in the literature.^[331,306,323,324] There could not be located a reason to explain, why the direct bond distances Ir- ηE (E = P, N, C) in the compound **2** with lower oxidation state are shorter than in the Ir(III) compound **1**.



Scheme B.4-2: Desymmetrization reaction and synthesis of the dihydride **3** by hydrogenation of dihydrido carbene **1**.

[346] TU München, unpublished results

B.4.3.2 Kinetic investigations of the desymmetrization reaction

In order to study the reaction mechanism of the reaction of **1** toward **2** and **3**, ^{31}P NMR kinetic measurements at 60°C have been examined (e.g.

Figure B.4-2). However, it turned out that the kinetic behavior is complex.

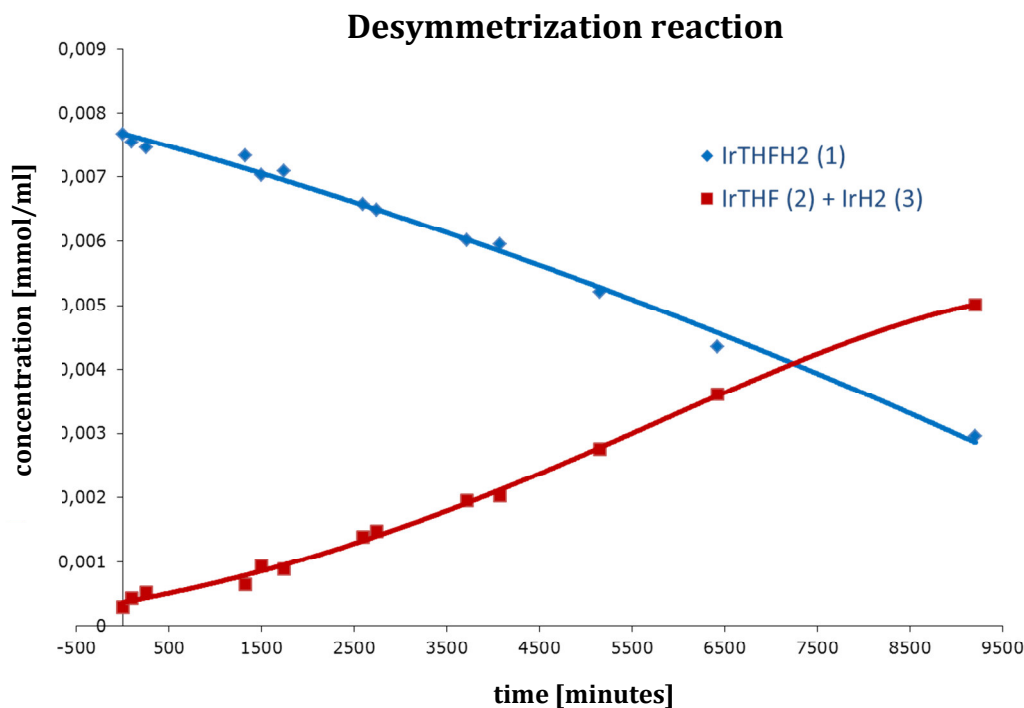


Figure B.4-2: Example of the desymmetrization reaction of $[\text{HPNP}^{\text{tBu}}\text{Ir}=\text{CO}(\text{CH}_2)_3(\text{H})_2]\text{PF}_6$ (**1**); decay of **1** (blue) and buildup of the products **2** plus **3** (red)

The reaction could not be prepared with reproducible rates under initial conditions and therefore it was not possible to determine the order of the reaction in $[\text{Ir}(\text{HPNP})=\text{CO}(\text{CH}_2)_3(\text{H})_2]^+$ (**1**), because of a lack of a decisive trend even in the starting velocities v_0 within the measured curves. Highly irreproducible rates are indicative for the involvement of radical intermediates, as it was found e.g. for insertion reactions of O_2 in M-H bonds.^[347] In this case, the presence of AIBN can be used to overcome the initiation periods and thus leads to reproducible rates.^[347] However, when the reaction of **1** toward **2** and **3** was carried out by addition of 3.0 equivalents of AIBN, no reaction at all occurred at 60°C in 1000 minutes.

Within the measurements, there was no apparent influence or trend of added N_2 .

[347] L. Boisvert, M. C. Denney, H. S. Kloek, K. I. Goldberg, *J. Am. Chem. Soc.* **2009**, *131*, 15802–15814.

A trend of a reaction order = 0.3 regarding the starting velocities versus adding 0, 1, 40, 60 and 500 equivalents of degassed water, was ascribed to be caused by polarity effects.

B.4.3.3 Acceleration of the reaction by the addition of oxygen

After checking solvent batches, solvent drying and degassing protocols, a potential influence of the counter-anions PF_6^- , BPh_4^- and CF_3SO_3^- , batches of **1**, glassware and potential rests of

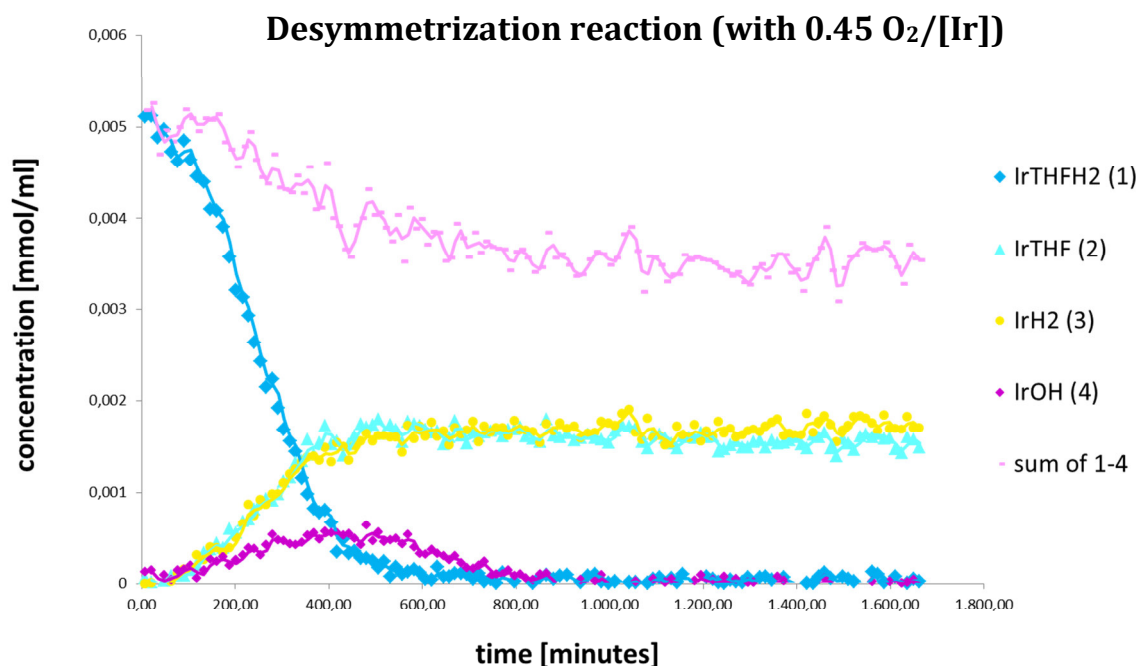


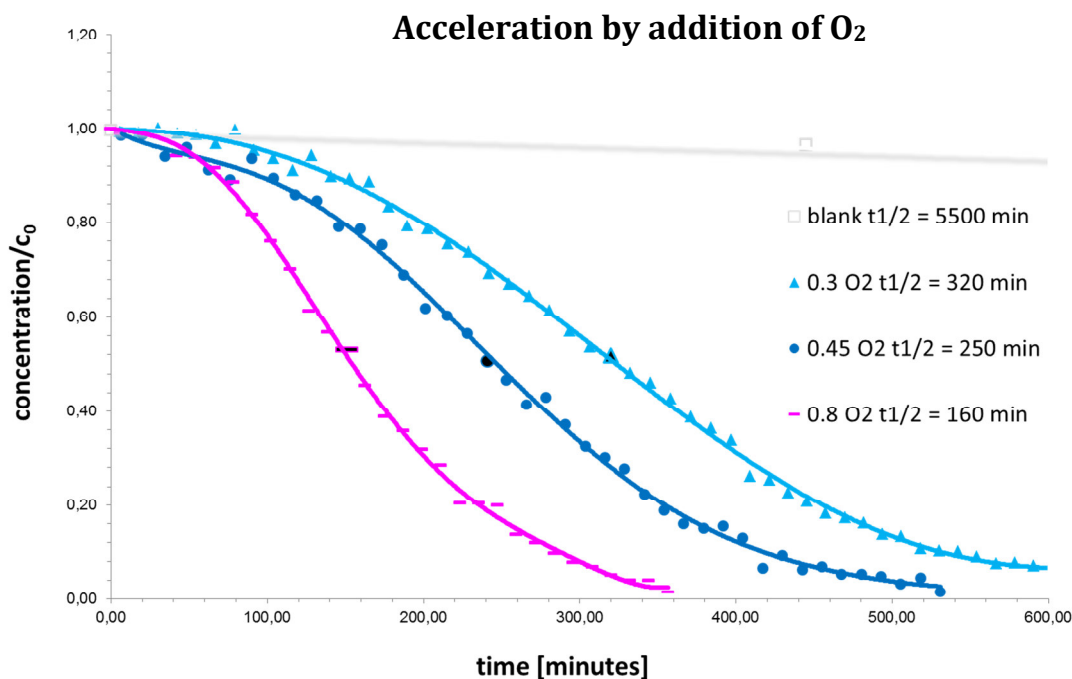
Figure B.4-3: Plot of the reaction under addition of 0.45 equivalents of O₂ per $[\text{HPNP}^{\text{tBu}}\text{Ir}=\text{CO}(\text{CH}_2)_3(\text{H})_2]\text{PF}_6$ (**1**)

acid on the surface, it turned out that the addition of O₂ accelerates the reaction. Thus the reaction was presumably not reproducible before due to potential changeable traces of oxygen in the solvent, glove box, argon line and maybe due to not fully tight *J*-Young NMR tubes during the whole reaction time and all temperature differences.

To investigate the influence of O₂ on the reaction, a series of preliminary experiments with different equivalents of O₂ (in terms of added argon/air mixtures to a degassed, dry solution of **1** in THF) between 0 and 1 equivalents in total in the gas phase per **1** in solution was analyzed (Figure B.4-3, Scheme B.4-3, exp. data).

At the beginning, an initiation period can be identified, which is typically either due to autocatalytic reactions or a delay caused by diffusion phenomena in e.g. heterogeneous reactions. After passing through this induction, the reaction rate increases, which results in a sigmoidal curve shape. By precisely monitoring the experiment, a reduction of the sum of the reactants during the reaction and furthermore, the intermediate formation of the familiar oxygenation product the SP coordinated Ir(III) hydroxo complex [PNP^{tBu}Ir(OH)]PF₆ (**4**)^[332] can be observed.

The reaction of molecular oxygen with five-fold coordinated *d*⁶ iridium metal hydrides



Scheme B.4-3: Series of the desymmetrization reaction of [HPNP^{tBu}Ir=CO(CH₂)₃(H)₂]PF₆ (**1**) with defined quantities of added O₂.

IrPCP^{tBu}HX (**A**) (PCP^{tBu} = [1,3-(CH₂P^{tBu})₂C₆H₃]⁻, X = H, Ph, C≡CPh) that were examined by the group of Goldberg^[348,349] leads to the corresponding peroxo complex IrPCP(O₂) (**B**) and the bis-dioxygen complex IrPCP(O₂)₂ (**C**). No direct oxygenation products or reaction

[348] W. D. Bridget, W. Kaminsky, J. M. Mayer, K. I. Goldberg, *Chem. Commun.* **2008**, 4195–7.

[349] L. Boisvert, K. I. Goldberg, *Acc. Chem. Res.* **2012**, *45*, 899–910.

products due to any insertion of O₂ into Ir-H or Ir-C bond are observed (except for traces of IrPCP^{tBu}(OH)H (**D**) in case of X = H). Because of the fact that IrPCP^{tBu}(H)₂ and IrPCP(H)C≡CPh do not perform any reductive elimination of HX in absence of O₂, an initial association of O₂ to **A** and a by O₂ assisted subsequent reductive elimination of HX is assumed by the authors. A mechanism similar to this could be present in the case of the reaction of [HPNP^{tBu}Ir=CO(CH₂)₃(H)₂]PF₆ (**1**) with O₂ as well at least in part when **1**, in

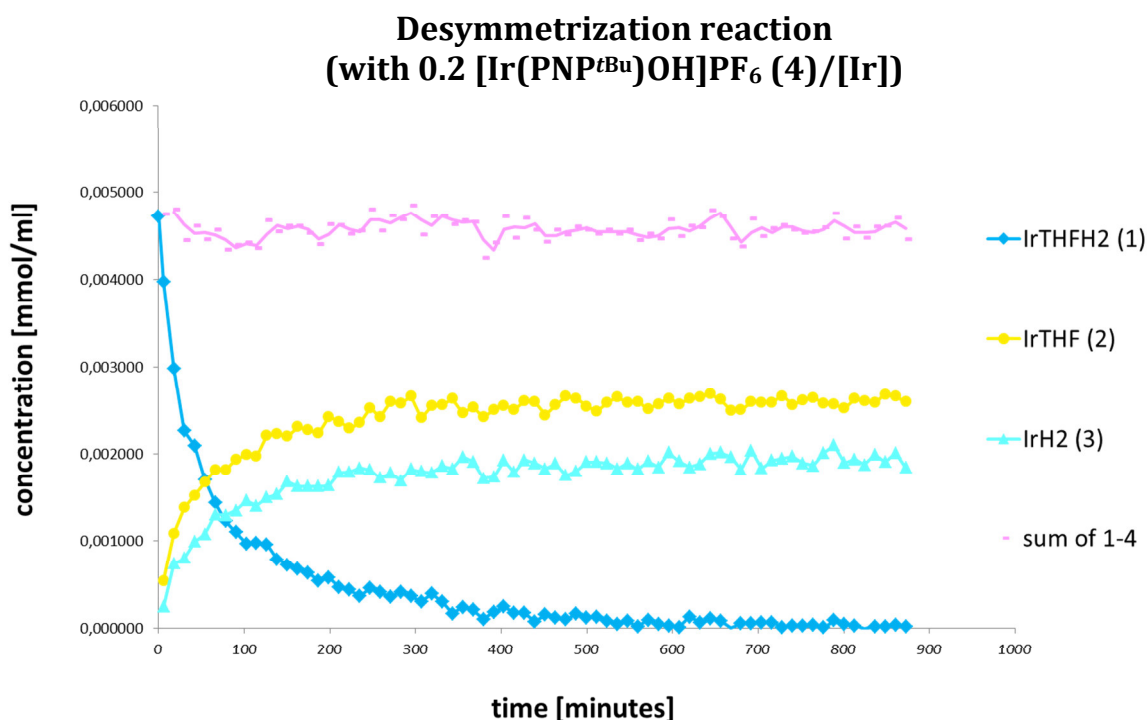


Figure B.4-4: Plot of the reaction under addition of 0.45 equivalents of **4** per [HPNP^{tBu}Ir=CO(CH₂)₃(H)₂]PF₆ (**1**).

terms of the five-fold coordinated species [HPNP^{tBu}Ir(H)-CH(O)(CH₂)₃]PF₆, which is assumed to be in dynamic equilibrium with **1**, or the dihydride **3**, which reacts with oxygen toward [PNP^{tBu}Ir(OH)]PF₆ (**4**).

The Pt(IV) complex Tp^{Me2}PtMe₂H^[350] (**E**) (Tp^{Me2} = hydridotris(3,5-dimethylpyrazolyl)borate), which formally inserts dioxygen into the Pt-H bond, produces the hydroperoxo Pt(IV) species Tp^{Me2}PtMe₂(OOH) (**F**).^[349,351] **F** is stable at ambient temperature but results upon extended thermolysis in solution at 79 °C or by treatment with oxygen-atom-acceptors predominantly

[350] O'Reilly, S. A.; White, P. S.; Templeton, J. L. *J. Am. Chem. Soc.* **1996**, *118*, 5684.

[351] D. D. Wick, K. I. Goldberg, *J. Am. Chem. Soc.* **1999**, *121*, 11900–11901.

in formation of the hydroxo species $\text{Tp}^{\text{Me}_2}\text{PtMe}_2(\text{OH})$ (**G**). The first step (**E** \rightarrow **F**) is supposed to proceed via a radical chain mechanism.

The autoxidation of $(\text{bipy})\text{PdMe}_2$ (**H**), which results in the formation of the Pd(II) methylperoxide complex $(\text{bipy})\text{Pd-Me}(\text{OOMe})$, was determined to be one-half-order in both [**H**] and [AIBN], and zero-order in $[\text{O}_2]$. The involvement of a radical chain mechanism is suggested and stepwise homolytic substitution reactions at the metal center of **H** are proposed as key steps.^[349,347]

The hydride complex $\text{PCP}^{\text{tBu}}\text{PdH}$ (**I**)^[352] in benzene-*d*₆ reacts cleanly to form $(\text{PCP}^{\text{tBu}})\text{Pd}(\text{OOH})$ (**J**) and subsequently $(\text{PCP}^{\text{tBu}})\text{Pd}(\text{OH})$ (**K**).^[349,353] The first process (**I** \rightarrow **J**) is not affected by radical starters, light or radical inhibitors and is assumed to be first order in **I** as well as in O_2 . The reaction product **K** is in contrast presumably formed by a radical reaction.

However, as mentioned above, the reaction of **1** toward **2** and **3**, is not accelerated by an addition of AIBN. Therefore a crucial reactivity of O_2 due to its diradical character should be neglectable.

B.4.3.4 Acceleration of the reaction by addition of $[\text{Ir}(\text{PNP})\text{OH}]\text{PF}_6$

By treatment of **1** with an excess of dioxygen, the hydroxo complex $[\text{Ir}(\text{PNP})\text{OH}]\text{PF}_6$ (**4**) is formed (**chapter B.2**). In preliminary attempts, addition of **4** to **1** also accelerates the desymmetrization reaction (**Figure B.4-4, Scheme B.4-4, exp. data**). Albeit, there is no induction period and therefore no sigmoidal curve shape as in the case of O_2 addition.

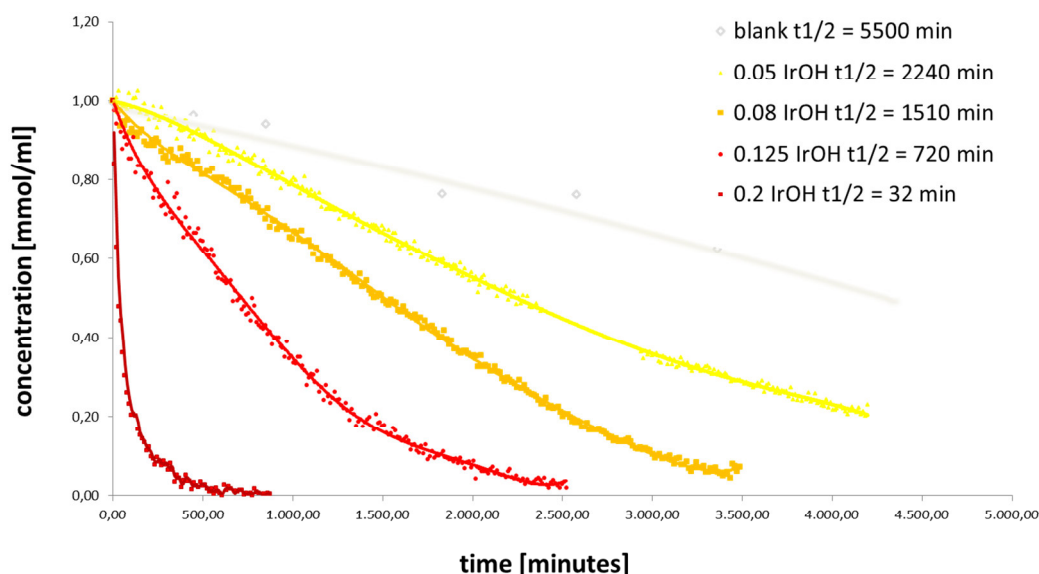
Milstein et al. found in a series of oxidative addition of several aliphatic alcohols to $(\text{COE})\text{IrCl}(\text{PMe}_3)_3$ (**L**), which yields the cis-hydridoalkoxo products *mer-cis*- $\text{HIr}(\text{OR})\text{Cl}(\text{PMe}_3)_3$ (with R = Me, Et, *n*-pentyl, *i*-propyl), a first-order dependence in **L** and “a best fit for a fourth-order dependence in methanol was obtained” although a third- or fifth-order was not ruled out. They assumed that due to retardation of the reaction in polar solvents, the high order in methanol is owed to its protic nature, and not to its polarity. Protic solvent aggregation in the transition state in an apolar medium is suggested. They proposed that hydrogen bonding of free methanol to the addendum might weaken the O-H bond prior to cleavage and stabilize the basic oxygen on the forming product.^[354] However, in case of the reaction of **1** toward **2** and **3** in the polar solvent THF, relationships like the one mentioned last are doubtful.

[352] C. J. Moulton, B. L. Shaw, *J. Chem. Soc., Dalton Trans.* **1976**, 1020-1024.

[353] M. C. Denney, N. A. Smythe, K. L. Cetto, R. A. Kemp, K. I. Goldberg, *J. Am. Chem. Soc.* **2006**, *128*, 2508–2509.

[354] O. Blum, D. Milstein, *J. Am. Chem. Soc.* **2002**, *124*, 11456–11467.

Acceleration by addition of $[\text{Ir}(\text{PNP}^{t\text{Bu}})\text{OH}]\text{PF}_6$ (**4**)



Scheme B.4-4: Series of the desymmetrization of **1** with defined quantities of added $[\text{Ir}(\text{PNP}^{t\text{Bu}})\text{OH}]\text{PF}_6$ (**4**).

B.4.4 Mechanistic considerations

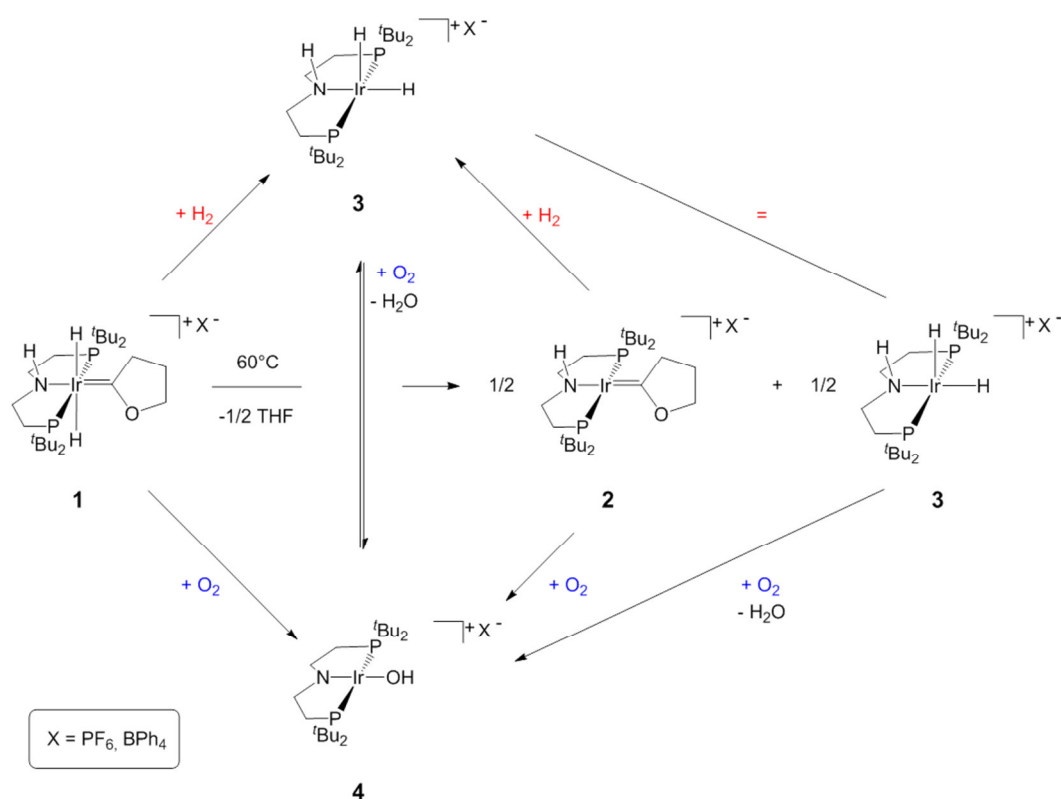
Interestingly, a similar combination of double α -CH activation at THF and desymmetrization reaction, which is at least in the overall stoichiometry identical to that of **1**, was found by *Caulton et al.*^[355]:

Dimeric $[\text{RuHCl}(\text{P}^i\text{Pr}_3)_2]_2$ (**M**), as a source of the 14 VE $\text{RuHCl}(\text{P}^i\text{Pr}_3)_2$ fragment, reacts in THF at elevated temperatures to one equivalent of the carbene complex $[\text{Ru}=\{\text{CO}(\text{CH}_2)_3\}\text{HCl}(\text{P}^i\text{Pr}_3)_2]$ (**N**) and one equivalent of the dihydrogen complex $[\text{RuH}(\text{H}_2)\text{Cl}(\text{P}^i\text{Pr}_3)_2]$ (**O**). The formation of an intermediate dihydrogen alkyl complex $[\text{Ru}\{\text{CHO}(\text{CH}_2)_3\}(\text{H}_2)\text{Cl}(\text{P}^i\text{Pr}_3)_2]$ (**P**), generated by single α -H elimination, is not observed, but seems presumeable. At higher temperatures TBE induces the decomposition of **M**. But in similar reactions^[355] in dioxolane or the cyclic amine pyrrolidine, which can be carried out at r.t., by the addition of TBE, the formation of **O** can be suppressed completely and thus the corresponding carbene complex is generated exclusively. The desymmetrization step is assumed to take place via dehydrogenation of **N** by the trapping of one equivalent H_2 by **M** or $\text{RuHCl}(\text{P}^i\text{Pr}_3)_2$.

The reaction of **1** in the presence of O_2 shows sigmoidal curve shapes and is accelerated by the addition of dioxygen without the production of any noticeable new product, except of

[355] a) I. J. N. Coalter, G. Ferrando, K. G. Caulton, *New J. Chem.* **2000**, *24*, 835–836; b) G. Ferrando-Miguel, J. N. Coalter III, H. Gerard, J. C. Huffman, O. Eisenstein, K. G. Caulton, *New J. Chem.* **2002**, *26*, 687–700.

[PNP^{tBu}Ir^{III}(OH)]PF₆ (**4**). But the reaction is not accelerated by the addition of AIBN. This contradicts a radical mechanism in case of the desymmetrization reaction of **1** by itself



Scheme B.4-5: Correlation between the above discussed compounds involved in the desymmetrization reaction of [HPNP^{tBu}Ir=CO(CH₂)₃(H)₂]PF₆ (**1**) toward [HPNP^{tBu}Ir=CO(CH₂)₃]PF₆ (**2**) and [HPNP^{tBu}Ir(H)₂]PF₆ (**3**).

without further additives. In THF **4** is known to react to other products that have not been identified yet, (**chapter B.2**), which are probably paramagnetic and thus not detectable in ³¹P NMR. Therefore it is consistent, that the total amount of detectable reactants in the measurements under O₂ addition decreases with time. The reaction of each of the three reactants **1**, **2** and **3**^{[332][345]} with an excess of dioxygen leads to the formation of **4** (**Scheme B.4-5**).

Furthermore, the direct addition of **4** to **1** also accelerates the reaction without any induction period and without decreasing the sum more than the initial amount of the substance of **4**. There are no experimental hints how the presence of **4** could accelerate the reaction, but an action as a Brønsted base at the amido or the hydroxo function which activates **1** via the formation of hydrogen bridge bonds at the NH function of **1** would be conceivable, due to the stabilization of a fivefold coordinated ML₅ d⁶ species in gradual modification of the

π -bonding strength of the pincer ligand^[356]. In any case, treatment of **1** with one equivalent of strong base KO^tBu results in the formation of a new, not yet identified species^[357], but not in a buildup of any of the desymmetrization products (and no **4**, too). On the other hand, if the hydroxo ligand of **4** acts as a hydrogen bridge bond source, a potential enhancement in bifunctional hydrogen exchange processes, as it was enclosed previously in the case of [Ru(H)₂PMe₃(HN(CH₂CH₂PⁱPr₂)₂)]^[358] (**6**), was plausible. By addition of two equivalents of H₂O to **6**, a dramatic increase of the proton exchange rates of H₂O was observed. According

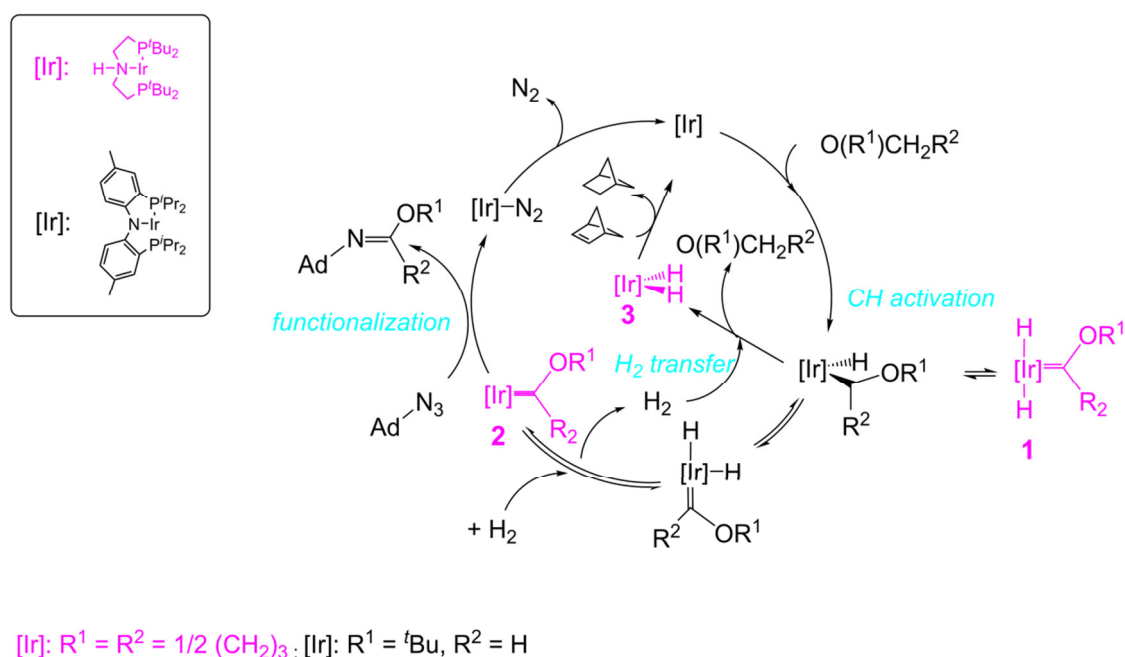


Figure B.4-5: Three fold CH functionalization scheme postulated by *Grubbs et al.* (formulas in pink: compounds that are experimental corroborated with the ethylene bridged *HPNP*^{*t*Bu} ligand).

to calculations, this reaction is assumed to take place via a lower-lying six-membered-ring transition state, which is stabilized by a polar interaction with H₂O by a contribution of the NH moiety and selectively the hydrido ligand adjacent to NH.^[358] However, treatment of **4** with one and two equivalents of KO^tBu does not lead to the deprotonation at the OH-moiety.^[359]

An accurate fitting of the measured kinetic curves into a simulation program (e.g. COPASI) seemed to be affected by to large incalculabilities due to a lack of known concentrations v_t of O₂ in the solution and v_t of the reaction products of **4**. Furthermore, the side reaction of THF to GBL is not well-established.

[356] Y. Jean, O. Eisenstein, *Polyhedron* 1988, 7, 405–7; b) J. F. Riehl, Y. Jean, O. Eisenstein, M. Pelissier, *Organometallics* 1992, 11, 729–37.

[357] J. Meiners, S. Schneider, *unpublished results*; ³¹P and ¹H NMR data point out toward an opening of the THF ring.

[358] A. Friedrich, M. Drees, a. d. G. J. Schmedt, S. Schneider, *J. Am. Chem. Soc.* 2009, 131, 17552–17553.

[359] J. Meiners, S. Schneider, *unpublished results*; according to ¹H and ³¹P NMR data, imine formation is presumed.

The qualitative relationships between the debated reactants are outlined in Scheme B.4-5.

B.4.5 Conclusion

The first two steps of the previously postulated pathway for ether C-H functionalization, consisting of α,α CH activation followed by H₂ transfer and C-E coupling (E = N, O, S), were also shown with the ethylene-bridged, aliphatic Ir(HPNP^{tBu}) platform (**Figure B.4-5**). The H₂ transfer step was shown experimentally for the first time. Selective desymmetrization of the first intermediate **1** to the dihydride complex **3** and Ir(I) carbene **2** was directly observed and kinetically examined. While the exact mechanism of H₂ transfer remains to be elucidated fully, some insights into that reaction could be accumulated:

(a) The desymmetrization is accelerated by the addition of oxygen in terms of air

(b) The dependency of O₂ addition was just uncovered by a process of eliminating all other conceivable influences but was not noticeable e.g. in the detection of oxidated side products. It is thus conceivable, that similar O₂-accelerated processes probably frequently play a role although without being noticed.

(b) Excess of air leads to the formation of Ir(III) hydroxo complex **4**. This compound also accelerates the desymmetrization of **1**. Hence it is possible that **4** is an active catalyst for this reaction, which could explain qualitatively the observation of an induction period as well.

However, further experiments will be necessary to understand the complete mechanism. E.g. an equimolar reaction of **1** with **4** and the measurement of ¹H NMR kinetic curves, in order to observe potential paramagnetic intermediates, could be meaningful. This kind of work would be particularly interesting in the context of oxidative CH functionalization, as demonstrated by the formation of γ -butyrolactone originated from THF.

Supporting Information

B.4.6 Experimental Section

B.4.6.1 Materials and synthetic methods

All experiments were carried out under an atmosphere of argon using Schlenk and glove box techniques. Solvents were dried over Na/benzophenone/tetraglyme (benzene) and Na/benzophenone (THF, toluene), distilled under argon and deoxygenated prior to use or by passing through columns packed with activated alumina.

Pentanes and CH₂Cl₂ were dried by passing through columns packed with activated alumina. Deuterated solvents were obtained from Euriso-Top GmbH, dried over Na/K (C₆D₆) or CaH₂ (CD₂Cl₂), distilled by trap-to-trap transfer *in vacuo*, and degassed by three freeze-pump-thaw

cycles. $[\text{IrCl}(\text{COE})_2]_2$ ^[360], $[\text{IrHPNP}^t\text{Bu}=\text{C}(\text{OCH}_2\text{CH}_2\text{CH}_2)(\text{H})_2]\text{PF}_6$ ^[331,282] and HPNP^tBu ^[331] were prepared according to published procedures.

B.4.6.2 Analytical methods

NMR spectra were recorded on the following spectrometers: Jeol Eclipse+ 400, Bruker Avance III 300, Bruker Avance 300, Bruker DRX 500 and were calibrated to the residual proton resonance of the solvent (CH_2Cl_2 : $\delta = 5.32$ ppm; C_6HD_5 : $\delta = 7.16$ ppm). ^{31}P NMR chemical shifts are in case of present PF_6^- reported relative to PF_6^- ($\delta = -143.90$ ppm) or in case of no PF_6^- reported relative to external phosphoric acid ($\delta = 0.0$ ppm). ^{13}C resonances are reported relative to CD_2Cl_2 ($\delta = 53.84$ ppm). Signal multiplicities are abbreviated as: s (singlet), d (doublet), t (triplet), q (quartet), sept (septet), m (multiplet), br (broad).

B.4.6.3 Syntheses: $[\text{IrHPNP}^t\text{Bu}=\text{COCH}_2\text{CH}_2\text{CH}_2]\text{PF}_6$ (**2**)

A solution of $[\text{Ir}(\text{COE})_2\text{Cl}]_2$ (160 mg, 178 μmol) and HPNP^tBu (140 mg, 387 μmol) in THF (15 mL) is treated with TIPF_6 (134 mg, 384 μmol). The resulting orange mixture is stirred overnight at r.t. The solution is filtered off, reduced *in vacuo* and treated with pentanes until precipitation occurs. The light brown solid is filtered off and washed with pentanes (3 x 5 ml) and dried *in vacuo* to yield a mixture of **1**, **2** and **3**. The mixture is dissolved in THF (15 mL), frozen, evacuated, thawed *in vacuo* and heated ($\sim 60^\circ\text{C}$) in a *J*-Young flask with stirring for 3.5 days to complete the desymmetrization reaction. The resulting brown solution is filtered into a Schlenk flask, reduced *in vacuo* (5 ml) and stored in the fridge (-37°C) over night. The lye is filtered off and the resulting yellowish crystals are recrystallized once more to separate **3** from the better crystallizing **2**. NMR measurements of **2** have been done in C_6D_6 under addition of three drops of CD_2Cl_2 due to poor solubility in benzene. **2** is not stable in pure CD_2Cl_2 at r.t. Yield: 44.2 mg (57.5, μmol , 15 %) of yellow, air sensitive microcrystalline powder. NMR (r.t., $\text{C}_6\text{D}_6/\text{CD}_2\text{Cl}_2$, [ppm]): ^1H NMR (400.12 MHz): $\delta = 0.99$ ($\text{A}_9\text{XX}'\text{A}'_9$, $\text{N} = |^3J_{\text{HP}} + ^5J_{\text{HP}}| = 6.5$ Hz, 18 H, $\text{P}^t\text{Bu}^t\text{Bu}$), 1.09 ($\text{A}_9\text{XX}'\text{A}'_9$, $\text{N} = |^3J_{\text{HP}} + ^5J_{\text{HP}}| = 6.8$ Hz, 18 H, $\text{P}^t\text{Bu}^t\text{Bu}$), 1.17 ($\text{A}_2\text{M}_2\text{X}_2$, $^1J_{\text{HH}} = 7.6$ Hz, 7.1 Hz, 2 H, $\text{Ir}=\text{C}(\text{O})\text{CH}_2\text{CH}_2\text{CH}_2$), 1.66 (m, 2 H, $\text{N}(\text{CH}_2)_2\text{P}$), 1.89 (m, 2 H, $\text{N}(\text{CH}_2)_2\text{P}$), 2.01 (m, 2 H, $\text{N}(\text{CH}_2)_2\text{P}$), 2.05 (A_2M_2 , $^1J_{\text{HH}} = 7.6$ Hz, 2 H, $\text{Ir}=\text{C}(\text{O})\text{CH}_2\text{CH}_2\text{CH}_2$), 3.50 (m, 2 H, $\text{N}(\text{CH}_2)_2\text{P}$), 3.58 (A_2M_2 , $^1J_{\text{HH}} = 7.1$ Hz, 2 H, $\text{Ir}=\text{C}(\text{O})\text{CH}_2\text{CH}_2\text{CH}_2$), 4.85 (AXX' , $^3J_{\text{HH}} = 11.1$ Hz, 1 H, NH), $^{31}\text{P}\{^1\text{H}\}$ NMR (162.0 MHz): $\delta = 71.64$ (s, P^tBu_2), -143.90 (sept, $^1J_{\text{PF}} = 713$ Hz, PF_6).

[360] (a) Onderlinden, A. L.; van der Ent, A. *Inorg. Chim. Acta* **1972**, *6*, 420; (b) J. L. Herde; J. C. Lambert, C. V. Senoff, *Inorg. Synth.* **1974**, *15*, 18.

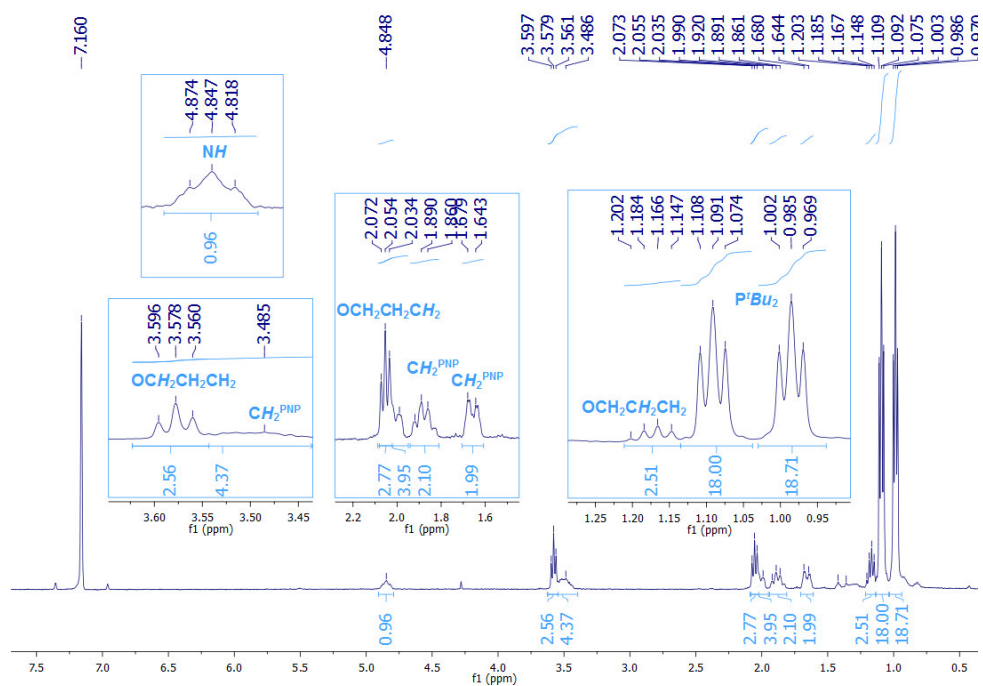


Figure B.4-6: ^{31}P NMR spectrum (r.t., C_6D_6) of $[\text{Ir}=\text{CO}(\text{CH}_2)_3\{\text{HPNP}^t\text{Bu}\}]\text{PF}_6$ (**2**).

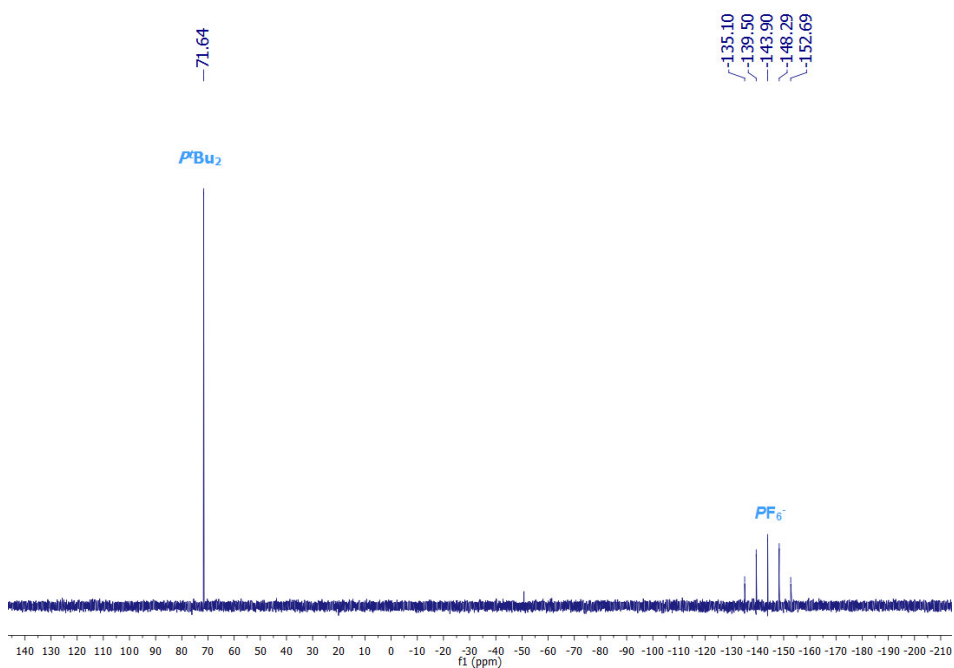


Figure B.4-7: ^1H NMR spectrum (r.t., C_6D_6) of $[\text{Ir}=\text{CO}(\text{CH}_2)_3\{\text{HPNP}^t\text{Bu}\}]\text{PF}_6$ (**2**).

B.4.6.4 Kinetic experiments: General procedure and air and [Ir] catalyzed, respectively

General: In a typical desymmetrization experiment $[\text{Ir}\{\text{HN}(\text{CH}_2\text{CH}_2\text{P}^t\text{Bu}_2)_2\}=\text{C}(\text{OCH}_2\text{CH}_2\text{CH}_2)(\text{H})_2]\text{PF}_6$ (**1**), (2.0 mg, 2.6 μmol) is dissolved in 0.5 ml of THF- H_8 in a *J-Young* NMR tube. The reaction at 60°C is monitored by $^{31}\text{P}\{^1\text{H}\}$ NMR spectroscopy in the inverse-gated mode to avoid NOE buildup. The relaxation delay (6 sec) is chosen as $> 5T_{1(1)}$, as derived by ^{31}P NMR inversion recovery experiments.

In case the reaction lasts longer than 16 hours, the following protocol is used: To compare the absolute intensities of the reaction participants, a saturated solution of $[\text{PCH}_3\text{Ph}_3]\text{PF}_6$ (gained from salt metathesis of $\text{PCH}_3\text{Ph}_3\text{I}$ with TIPF_6 in acetone) in THF- H_8 (24 $\mu\text{mol}/\text{ml}$) is used as an internal ^{31}P standard and as the solvent instead of neat THF. The samples are heated in a tempered silicon oil bath and cooled to r.t. for the time of NMR measurements (~15 min). The time that the measurement takes is excluded in the calculation of the reaction time.

In case of shorter reaction times, either the $[\text{PCH}_3\text{Ph}_3]\text{PF}_6$ solution is used or a sealed capillary of 1% H_3PO_4 is included into the sample. To observe the external standard, spinning of the sample is switched off because of the inhomogeneity of the sealed capillary. Either a programmed 2D kinetic measurement file is used (JEOL) or a multi zg measurement is started (BRUKER).

In case of air-catalyzed reactions the sample is first prepared as usual. Outside of the glove box, the NMR tube is connected to a septum equipped Schlenk apparatus (the volume of both was measured beforehand). The sample is frozen and the whole apparatus is evacuated. The frozen NMR tube is closed under vacuum. A calculated volume of air is added with a syringe through the septum into the stationary evacuated apparatus. The remaining volume is as quickly as possible filled with Ar (overpressure of the line = +0.2 bar). After waiting for 10 min. for the gas to shuffle, the NMR tube is opened and purged with the mixture. The missing pressure of the apparatus is filled with Ar and the NMR tube is closed immediately. The total of the equivalents of O_2 that can participate in the reaction are approached using the *ideal gas law* (the **initial concentration** c_0 in the solution is represented by an equilibrium between gas phase and solution in front of, which can be estimated by *Henry's law*, that is distinctly **smaller** than the over-all equivalents of O_2 divided by the total volume and multiplied with the volume of the solvent).

In case of $[\text{Ir}\{\text{N}(\text{CH}_2\text{CH}_2\text{P}^t\text{Bu}_2)_2\}(\text{OH})]\text{PF}_6$ (**4**) catalyzed reactions an amount of a titer solution (5.4 $\mu\text{mol}/\text{ml}$) of **4** in THF is added via a Hamilton glass syringe to the prepared sample.

The accumulated kinetic spectra were analysed with the Delta® kinetics tool (Jeol spectra) or with the advanced data analysis in Mestre® in the stacked spectra modus (BRUKER and Jeol spectra) and were plotted in Excel®.

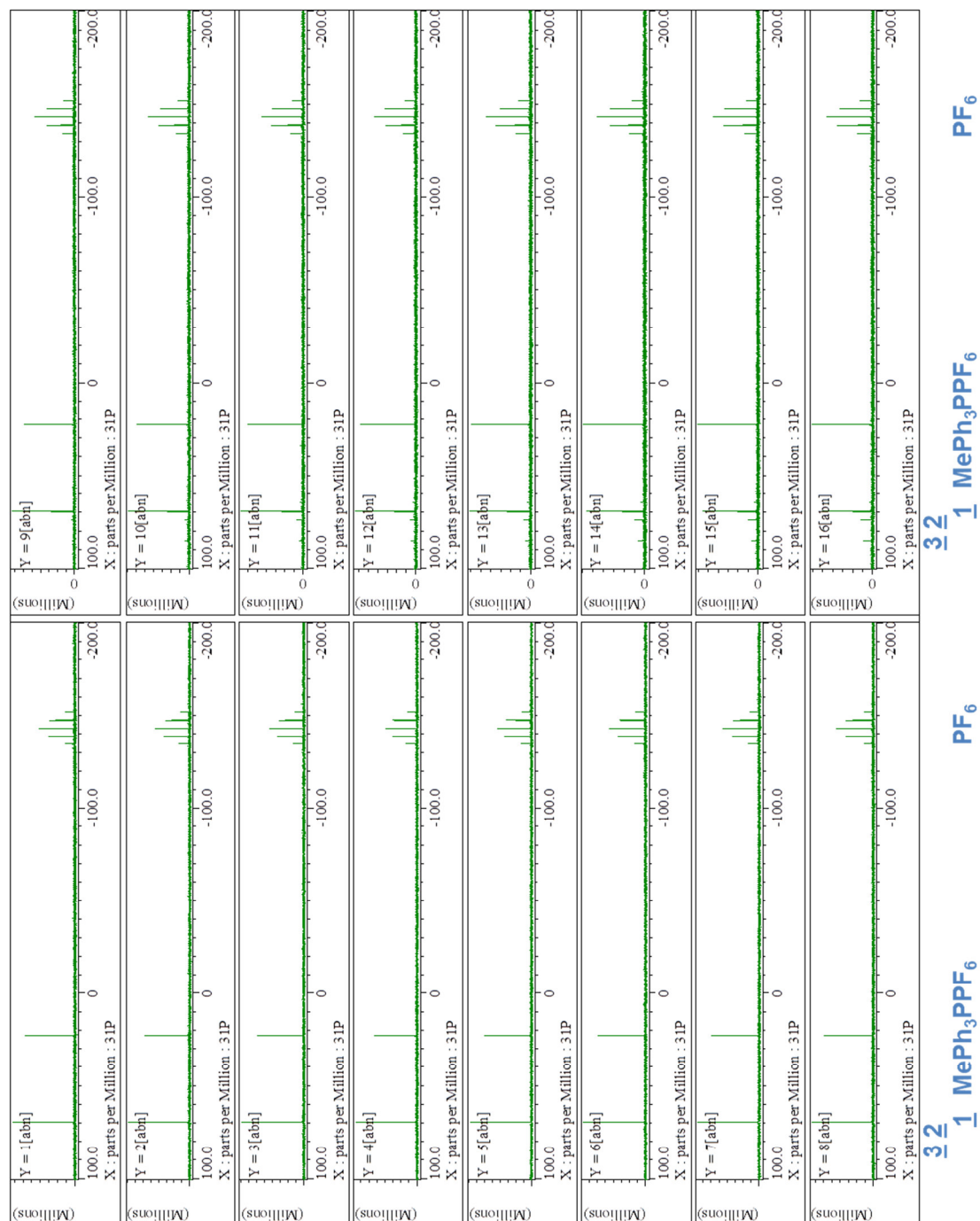


Figure B.4-8: Excerpt of a ^{31}P NMR kinetic measurement; multiple spectra arrayed in a Delta 2D plot (1: Start, $t = 6$ min, 16: $t = 186$ min).

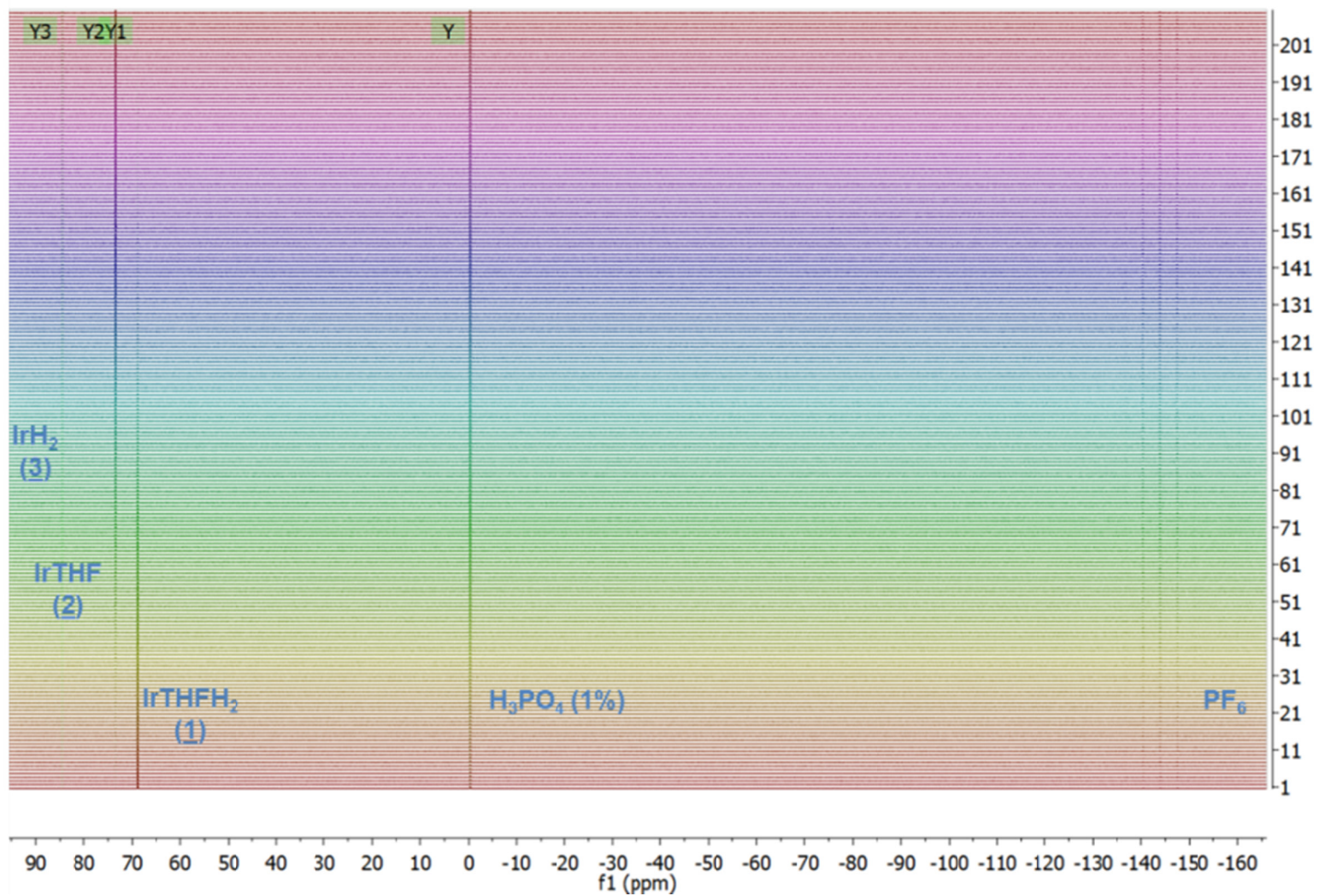


Figure B.4-9: Example of a ^{31}P NMR kinetic measurement; multiple spectra arrayed in a Mestrescope plot (1: Start, $t = 6$ min, 210: Finish, $t = 2514$ min).

Desymmetrization reaction (with 0.3

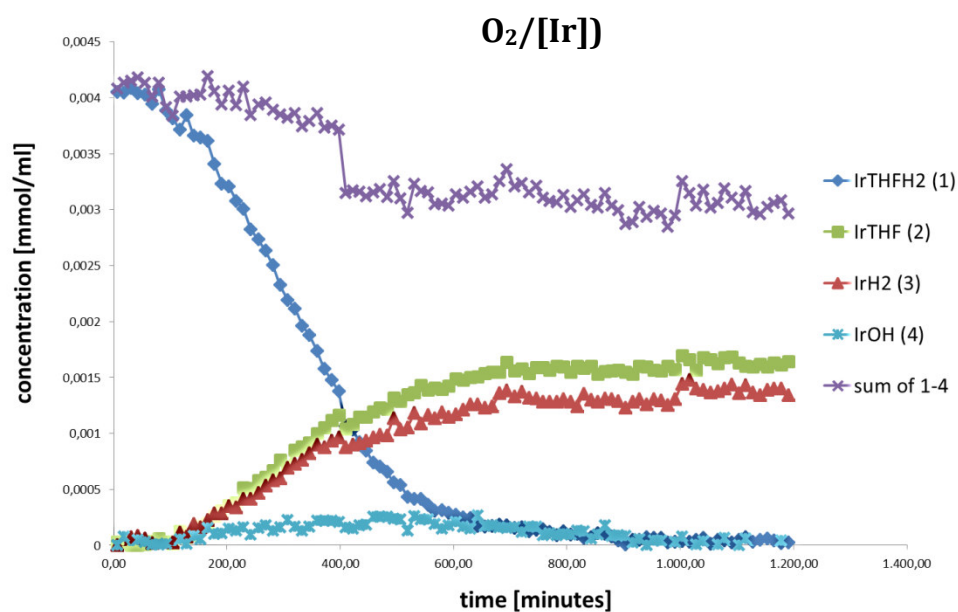


Figure B.4-10: Plot of the desymmetrization reaction by addition of 0.3 equivalents of O_2 per $[HPNP^{tBu}Ir=CO(CH_2)_3(H)_2]PF_6$ (**1**).

Desymmetrization reaction (with 0.45

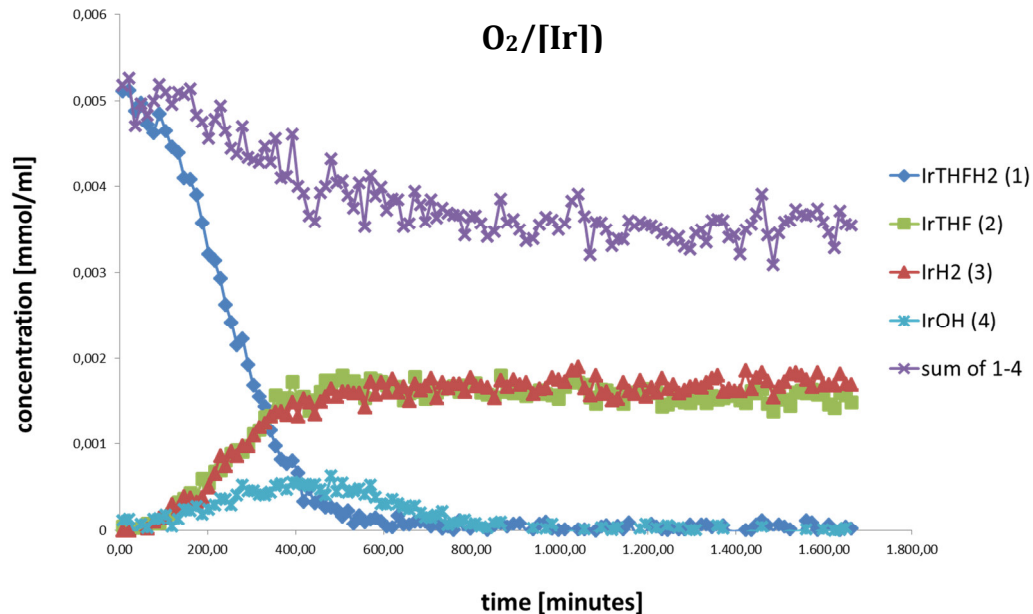


Figure B.4-11: Plot of the desymmetrization reaction by addition of 0.45 equivalents of O_2 per $[HPNP^{tBu}Ir=CO(CH_2)_3(H)_2]PF_6$ (**1**).

**Desymmetrization reaction
(with 0.05 [Ir(PNP^tBu)OH]PF₆ (4)/[Ir])**

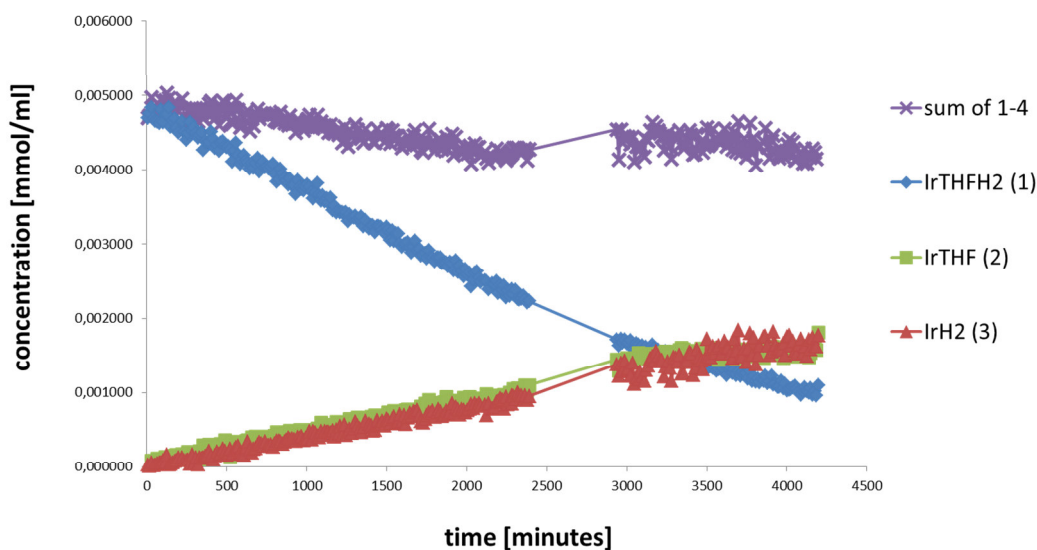


Figure B.4-12: Plot of the desymmetrization reaction by addition of 0.05 equivalents of [Ir(PNP^tBu)OH]PF₆ (4) per [HPNP^tBuIr=CO(CH₂)₃(H)₂]PF₆ (1) (discontinuity of the plots is due to interruption of the NMR scans, but not of the heater in the spectrometer and resuming of the measurement afterwards).

**Desymmetrization reaction
(with 0.08 [Ir(PNP^tBu)OH]PF₆
(4)/[Ir])**

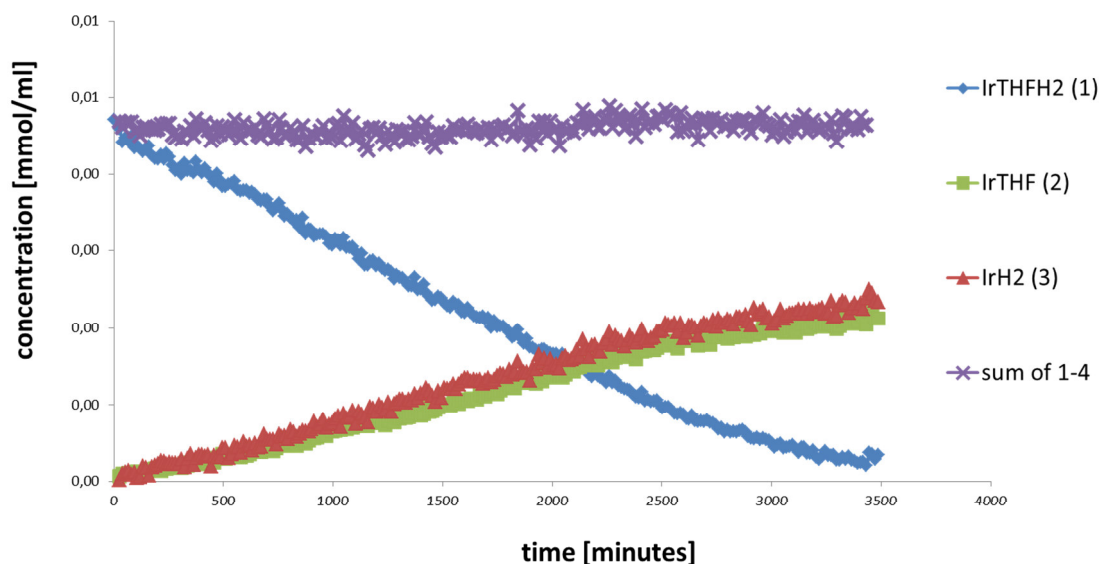


Figure B.4-13: Plot of the desymmetrization reaction by addition of 0.08 equivalents of [Ir(PNP^tBu)OH]PF₆ (4) per [HPNP^tBuIr=CO(CH₂)₃(H)₂]PF₆ (1).

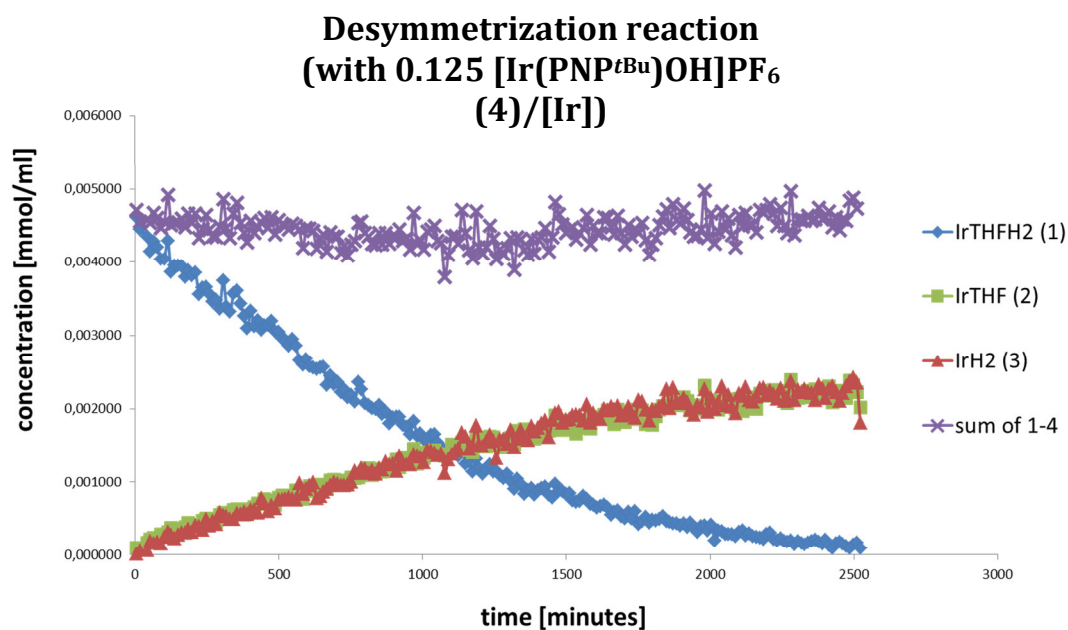


Figure B.4-14: Plot of the desymmetrization reaction by addition of 0.125 equivalents of [Ir(PNP^tBu)OH]PF₆ (4) per [HPNP^tBuIr=CO(CH₂)₃(H)₂]PF₆ (1).

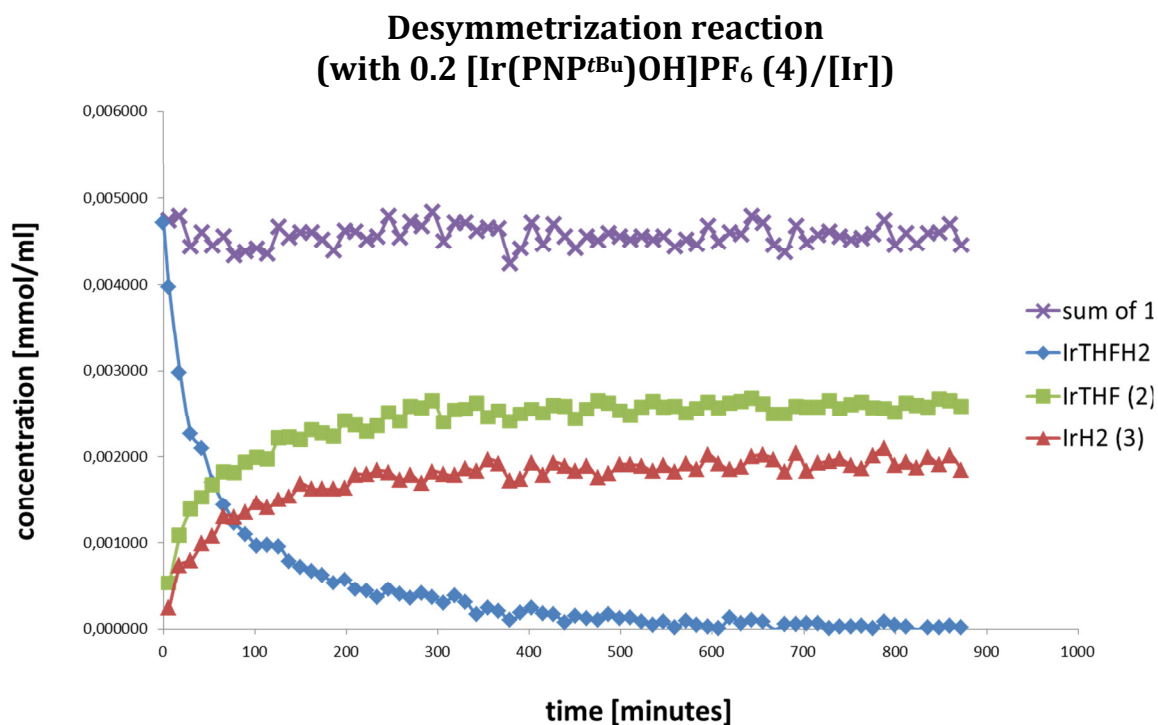


Figure B.4-15: Plot of the desymmetrization reaction by addition of 0.2 equivalents of [Ir(PNP^tBu)OH]PF₆ (4) per [HPNP^tBuIr=CO(CH₂)₃(H)₂]PF₆ (1).

Overview: Addition of O₂ vs addition of [Ir(PNP^tBu)OH]PF₆ (4)

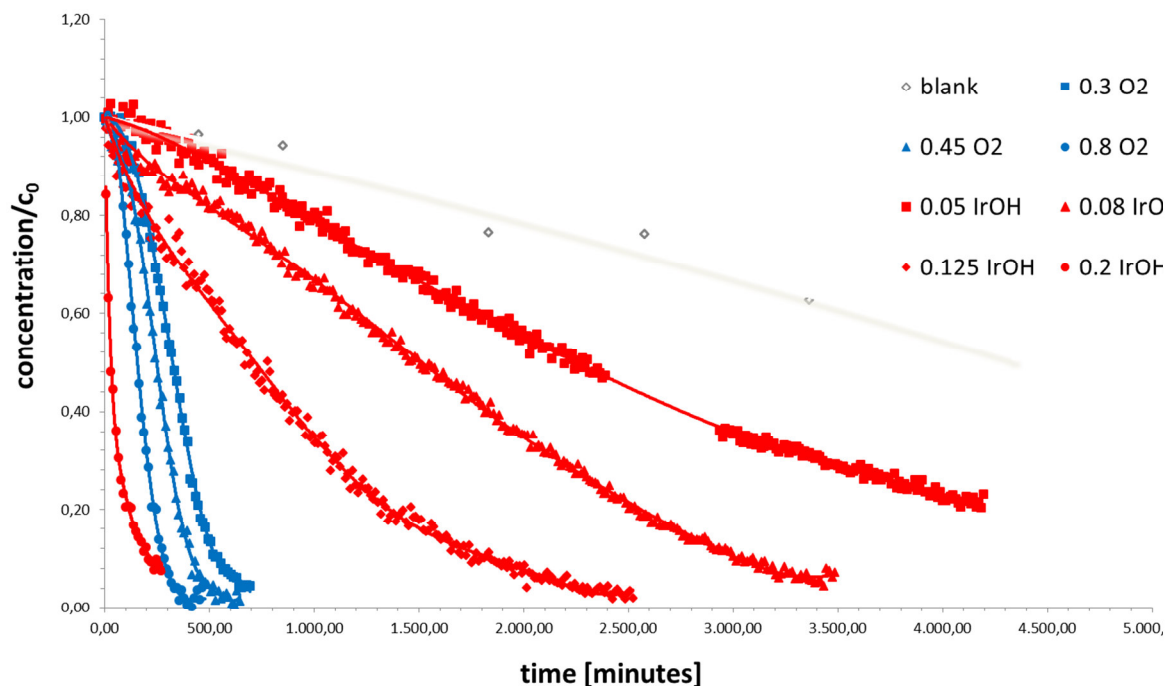


Figure B.4-16: Comparison of the decay of [HPNP^tBuIr=CO(CH₂)₃(H)₂]PF₆ (**1**) over time in a reaction without additive (grey), by addition of O₂ (blue) and addition of [Ir(PNP^tBu)OH]PF₆ (**4**) (red), respectively.

Desymmetrization reaction (with 3.0 AIBN/[Ir])

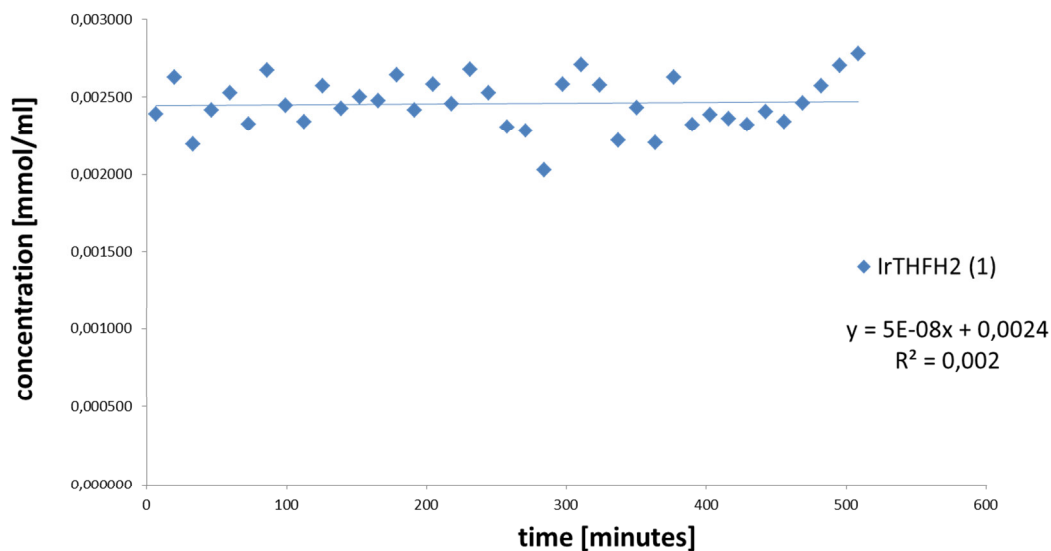


Figure B.4-17: Plot of the desymmetrization reaction by addition of 3.0 equivalents of AIBN 0.8 [HPNP^tBuIr=CO(CH₂)₃(H)₂]PF₆ (**1**).

C Summary and outlook

C.1 Overview

The coordination chemistry of *d6*, *d7* and *d8* iridium amino and amido PNP pincer complexes was investigated throughout this cumulative PhD thesis. Owing to *electronic*, *steric* and *bifunctional* features of the utilized PNP ligand system, the accessibility of unique oxidation states and coordination geometries as well as cooperative reactivity and facile activation of C-H bonds with the Ir(PNP) platform could be presented.

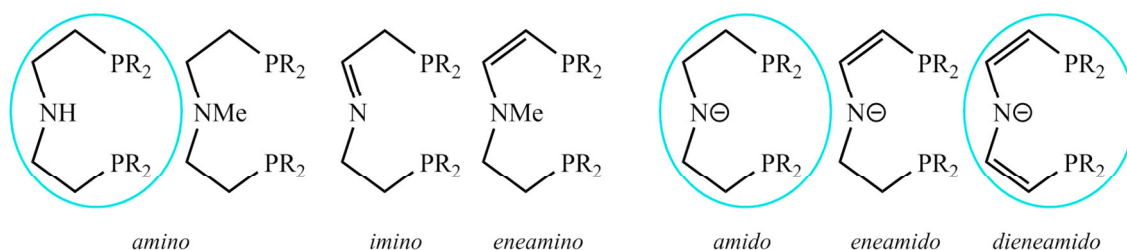


Figure C.1-1: Collection of several neutral and anionic PNP pincer systems generated by *NH* deprotonation, *NH* methylation or oxidative dehydrogenation of coordinated $\text{HN}(\text{CH}_2\text{CH}_2\text{PR}_3)_2$ ($\text{R} = \textit{i}\text{Pr}, \textit{t}\text{Bu}$)^[7,365]. In circles, $\text{R} = \textit{t}\text{Bu}$: Ligands examined during this work.

The chelating, ethylene bridged amine $\text{HN}(\text{CH}_2\text{CH}_2\text{P}^t\text{Bu}_3)_2$ shows a remarkable versatility acting as pincer ligand system. Amido, imino, enamido, and dienamido coordination modes are accessible by template or *in situ* synthesis starting from an amino metal complex via *NH* deprotonation or oxidative dehydrogenation of the aliphatic backbone (**Figure C.1-1**). This kind of modification leads to fine tuning of the electronic donor properties of the system, which strongly influences the stability of coordination geometries as well as oxidation and spin states. Furthermore, potential *non-innocent* and also cooperative reactivity of the complexes are influenced by tuning the system. As a result of the high electron density at the PNP amido center, unusual oxidation states and coordination modes of late transition metal centers as e.g. very rare square planar coordinated iridium(III), can be stabilized leading to electronic and coordinative unsaturated complexes with unexpected stability and reactivity.

C.2 Square-planar iridium d^7 and d^6 complexes

When the coordination chemistry of iridium with the aliphatic PNP pincer platform was investigated in the course of this thesis (**B.1**), it was disclosed how simple oxidative ligand functionalization of the aliphatic PNP ligand framework allows for the versatile isolation of unusual square-planar iridium d^7 and d^6 complexes. Synthesis via dehydrogenation of the PNP backbone with benzoquinone led to isolation of the stable, paramagnetic, square planar coordinated, dieneamido Ir(II) complex **1** in moderate to good yield. In addition, this complex could be oxidized to the first known square planar coordinated Ir(III) complex **2**^[361] (**Figure C.2-1**). Compared with the ethylene bridged PNP amido ligand, the generated unsaturated pincer is characterized by higher conformational rigidity but electronic flexibility: While the radical complexes from the oxidation of iridium(I) dialkylamides are transient species with N centered reactivity, the metallo-radical **1** and the oxidation product **2**^[361] are sufficiently stable to be easily isolated.^[239,73] Hence, the dieneamido ligand opens up the opportunity to

examine an unusual 1-electron reactivity of iridium. In the meantime, the corresponding Ir(I) equivalent was prepared by *Kinauer et al.*^[362]. Taken together, the compounds represent a suitable RedOx series Ir I/II/III with conclusive alteration of e.g. the N-Ir bond lengths due to successive electron filling of the LUMO/SOMO with mainly N-Ir π^* -character (**Figure C.2-2**). Differentiated reactivity is observed: While

Ir(III) can be attacked by nucleophiles, Ir(I) shows facile nucleophilic CH activation. The reactivity of the Ir(II) analogue is unclear. The main part of the Mulliken spin density is situated at the Ir central atom and thus consistently, no ligand-centered 1-electron-reactivity is detected. However, no distinct reactivity regarding the radical Ir(II) metal center could be located, either, perhaps due to sterical protection by the bulky *t*butyl groups.

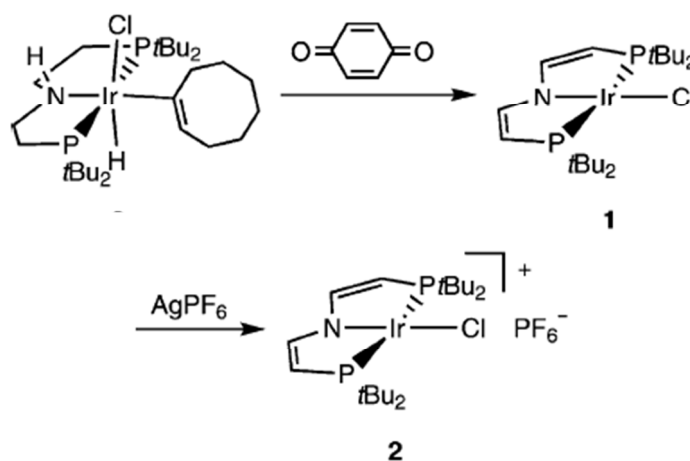


Figure C.2-1: Synthesis of stable, square planar coordinated iridium(II) and (III) complexes^[361].

[361] Complex **2** was synthesized by Markus Scheibel, Komplex **2** wurde von Markus Scheibel synthetisiert.

[362] M. Kinauer, M. G. Scheibel, J. Abbenseth, F. W. Heinemann, P. Stollberg, C. Würtele, S. Schneider, *Dalton Trans.* 2014, 43, 4506.

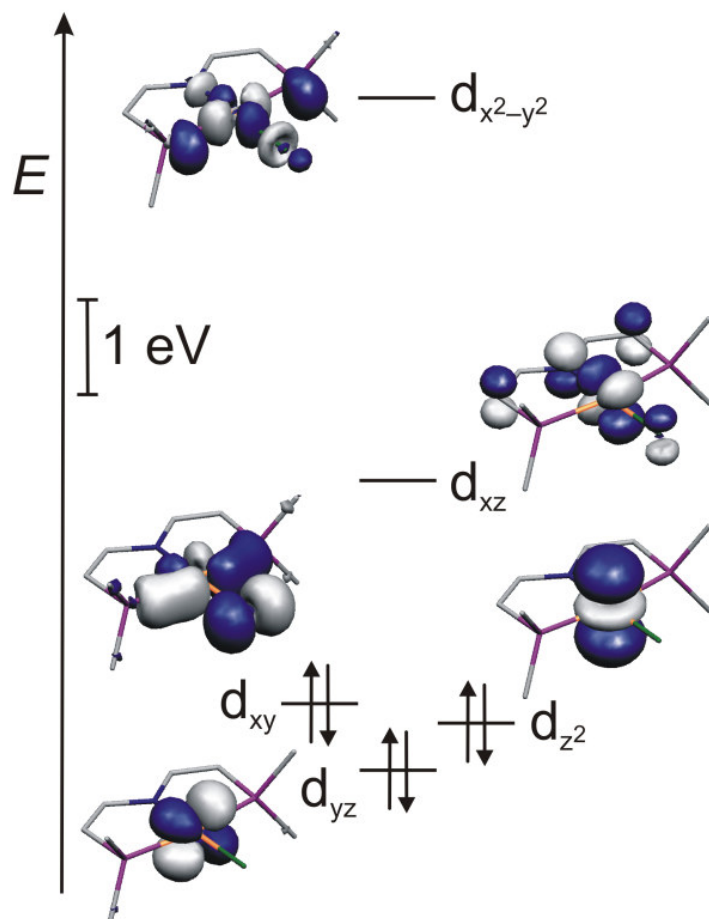


Figure C.2-2: Metal centred Kohn-Sham frontier orbitals of IrCl{N(CHCHPMe₂)₂} (**2**^{Me}) in the singlet state from spin-unrestricted ZORA-B3LYP-DFT calculations (the z-axis is perpendicular to the Ir{N(CHCHP)₂}-plane).

Diamagnetic (*d*6 low-spin) Ir(III) complex **2**^[361] is furthermore of great interest, because the set *d*6 ML4, which is very rare at any rate, is normally represented in the form of intermediate spin complexes (eg Fe coordinated with porphyrinato ligands) or is twisted toward butterfly-shaped complexes with one or two additional CH agostic interactions. The π -donating character of the dieneamido ligand leads to an uplifting of the weak antibonding orbitals in the square planar coordination mode and thus introduces spin pairing. In case of heavy 5*d* transition metal Ir, which exhibits a large splitting of the energy levels, the comparable weaker π -donor sufficiently influences the HOMO LUMO gap towards spin pairing (**Figure C.2-3**^[363,364]).

Interestingly, the *d*6 Ru(II) dieneamido analog complex, which is subject to a path-breaking work by Askevold^[365], exhibits intermediate spin configuration, suspected to be caused by smaller intrinsic orbital splitting in case of the 4*d* transition metal. If an even stronger π -donor i.e. the amido PNP ligand, is implemented, the low-spin *d*6 configuration can be accessed in case of Ru(II) as well. Thus, the tuning of π -donor strength of the used PNP pincer system can also be used to guide desired spin states.

[363] B. Askevold, M. M. Khusniyarov, E. Herdtweck, K. Meyer, S. Schneider, *Angew. Chem.* **2010**, *122*, 7728-7731; *Angew. Chem. Int. Ed.* **2010**, *49*, 7566-7569.

[364] S. Schneider, J. Meiners, B. Askevold, *Eur. J. Inorg. Chem.* **2012** (3), 412-429.

[365] *Late Transition Metal Amido Complexes: Electronic Structure and Reactivity*, Bjoern B. Askevold PhD Thesis TU München 2012.

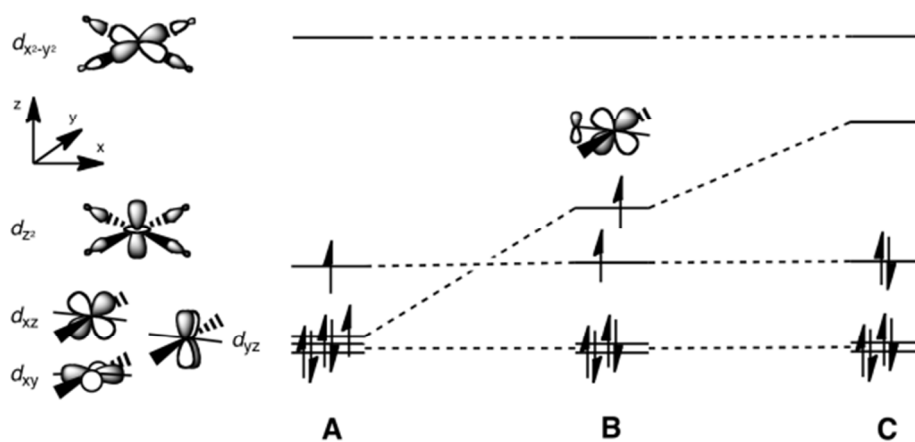


Figure C.2-3^[363,364]: Valence d -orbital splitting in square-planar coordination for a d^6 ion with pure σ -donor ligands (A) and one weak (B) or strong (C) single faced, perpendicular π -donor, respectively.

C.3 Oxygen reduction reaction (ORR)

In favor of gaining information about the potential of the estimated Ir(PNP) platform toward oxygenation, the Ir(III) dihydrido amino complex **3** was treated with dioxygen leading to the formation of the diamagnetic hydroxo amido Ir(III) complex **4**. The electronic structure (d^6 , square-planar, low-spin) of the latter is, again similar as in the case of the dieneamido complex **2**^[361], subject to the strong π -donating character of the PNP dialkylamido ligand and perhaps the sterical protection by the bulky *t*-butyl groups.

During the reaction of the dihydride **3** with oxygen, one equivalent of water arises as well. According to preliminary mechanistic information and suggestions, all four reduction equivalents are stored within the Ir–H bonds of one molecule of **3**. Dioxygen complexes of Iridium^[366] and the reductive scission of O_2 by iridium^[367] are known, but not the direct four-electron O_2 reduction by a monomolecular redox-center, taking all known facts into account. It was also discovered that starting from the dihydride, the oxidation reaction could be reversed by gassing with H_2 (Figure C.3-1). There were several such cycles, which can be

[366] a) D. B. Williams, W. Kaminsky, J. M. Mayer, K. I. Goldberg, *Chem. Commun. (Cambridge, U. K.)* **2008**, 4195–4197; b) S. Thewissen, D. A. Plattner, B. de Bruin, *International Journal of Mass Spectrometry* **2006**, 249–250, 446–450; c) M. A. Ciriano, J. A. Lopez, L. A. Oro, J. J. Perez-Torrente, M. Lanfranchi, A. Tiripicchio, M. T. Camellini, *Organometallics* **1995**, 14, 4764–4775; d) H. J. Lawson, J. D. Atwood, *J. Am. Chem. Soc.* **1989**, 111, 6223–6227; e) H. J. Lawson, J. D. Atwood, *J. Am. Chem. Soc.* **1988**, 110, 3680–3682.

[367] e.g. Z. M. Heiden, T. B. Rauchfuss, *J. Am. Chem. Soc.* **2007**, 129, 14303.

looped in the circuit in CH₂Cl₂ or THF. Taken together, although it is not yet clear whether H₂O is also formed in the reaction of the hydroxide with H₂, the cycle represents the gradually carried out catalytic, bifunctional oxygen reduction reaction, in this case the oxyhydrogen reaction. This could be a possible setting for a future experimental area towards creating a fuel cell.

O-O bond cleavage, which is a fundamental reaction, is not only of interest to ORR but also to potential selective oxidative CH functionalization

reactions. In the reactions of dihydride **3** with O₂ in the case of THF as the solvent, γ -butyrolactone (GBL) was formed. Therefore, a prospective combination of the O₂ splitting reaction of the PNP iridium fragment with CH activation

features (see below) should be very productive. For instance, it would be very interesting to ascertain whether it is possible to selectively oxygenate THF or other hydrocarbons catalytically in a mixed atmosphere 2 H₂/O₂.

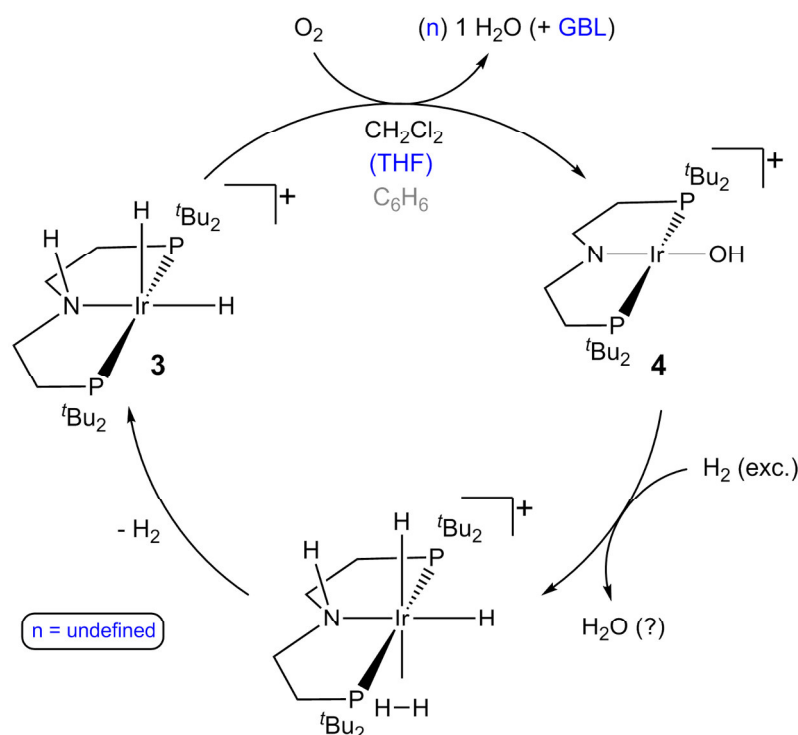


Figure C.3-1: O₂-splitting-hydrogenation cycle

C.4 Intermolecular CH activation

In favor of examining the ability of the Ir(PNP^{*t*Bu}) platform to activate organic substrates, potential CH activation features were examined. In preceding, motivating work by Friedrich^[71] it was disclosed that with the use of the Ir(HPNP^{*i*Pr}) system, vinylic oxidative addition of coordinated cyclooctene as well as intermolecular, double CH activation of the solvent THF towards an iridium dihydrido Fischer carbene complex is accessible, whereby the intramolecular pathway is predominant. When the modification of the phosphanyl groups was changed from ^{*i*Pr} to the bulkier ^{*t*Bu} in this work, quantitative intermolecular, geminal CH

activation of THF and formation of the corresponding dihydrido carbene complex **5** resulted (Figure C.4-1). Due to higher sterical pressure into the active site of the Ir(PNP) platform, the equilibrium of the formation of transient T-shaped d^8 $[(HPNP^{tBu})Ir]^+$ by dissociation of coe from $[(HPNP^{tBu})Ir(coe)]^+$

(**6**), which represents the rate determining step, is shifted toward the product.

Hence control of the reaction pathway arises from detailed design of the pincer ligand environment.

Furthermore, depending on the solvent medium, the reductive elimination equilibrium between six coordinate, moderately stable cyclooctenyl hydride **7**,

which exists predominantly in THF, and the cationic ion pair $[(HPNP^{tBu})Ir(coe)]^+Cl^-$ (**6**^{Cl})

in CH_2Cl_2 , is effectively directed. The opportunity to control the *in situ* generation of three-

coordinate iridium(I) fragments and thus C-H activation by solvent choice as well as by chloride abstraction, represents an alternative to the generation by five-coordinated iridium(III), e.g., by dehydrogenation of an iridium(III) dihydride with a strained olefin, which is frequently used.

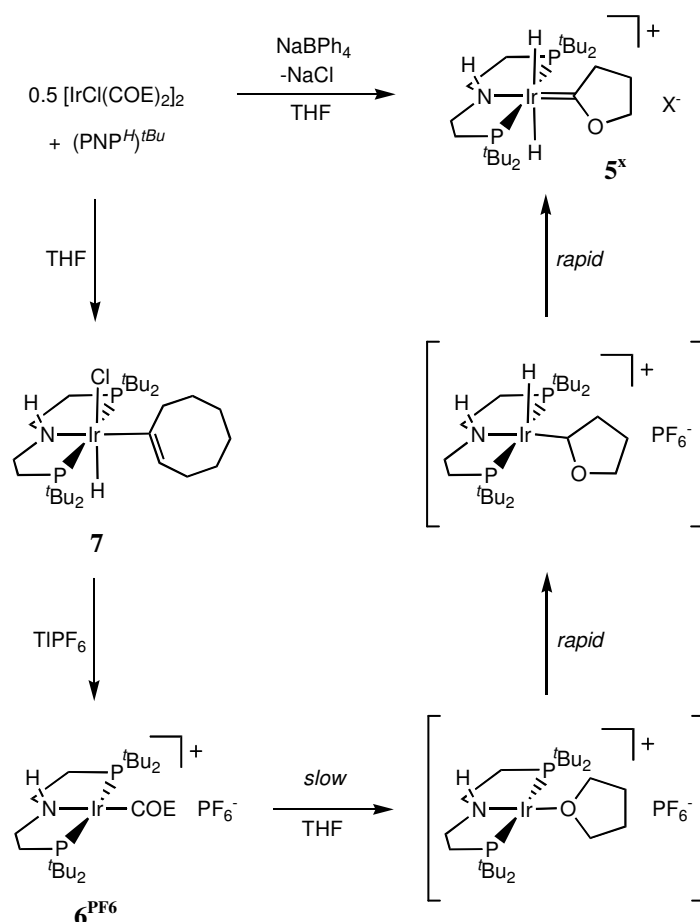


Figure C.4-1: Synthesis and proposed mechanism of the formation of Fischer-carbene complex **5** ($X = BPh_4, PF_6^-$).

C.5 Desymmetrization reaction accelerated by presence of O_2 or an Ir(III) hydroxo complex

Almost at the same time when the double CH activation of THF by Ir with the aliphatic PNP system was disclosed, *Grubbs et al.*^[203] discovered a very similar reaction using the monoanionic, diaryl *Ozerov* PNP pincer platform, which led to the formation of several

iridium carbene complexes by the double CH activation of different aliphatic ethers. However, in these reactions, the corresponding, dehydrogenated carbene would be produced. Thus, there are two free coordination sites available, and thereby the possibility to functionalize the carbene by the reaction with further substrates. In fact, the achievement by

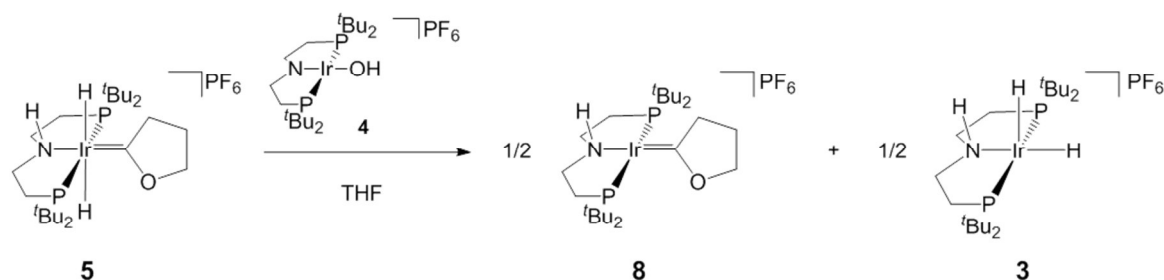


Figure C.5-1: Desymmetrization reaction of dihydrido Fischer carbene complex **5**, which is presumably catalyzed by addition of oxygenation product **4**.

Grubbs et al. is very impressive, since they obtained the corresponding formates, thioformates or formimidates by the use of several heterocumulenes as substrates in the *Grubbs* functionalization cycle^[203]. In contrast, functionalization or dehydrogenation of the dihydrido carbene with the neutral, aliphatic PNP system, did not succeed e.g. by addition of CO₂, norbornene or acetone. However, under defined conditions, a selective desymmetrization reaction of **5** towards the dihydride complex **3** and Ir(I) carbene **8** takes place (**Figure C.5-1**), which was directly observed and kinetically examined. But it was not demonstrated that any of the investigated aspects, e.g. choice of the counter anion, has an effect on the reaction rate, except for the addition of understoichiometric amounts of O₂ in terms of air or the hydroxo amido Ir(III) complex **4** (see above), respectively. Hence it is possible that **4** is an active catalyst for this reaction. Attempts with higher amounts of oxygen revealed that both desymmetrization products **5** and **8** can be converted to **4** and similarly to **3** by gassing with H₂. During the study of the desymmetrization reaction, a sub step of the *Grubbs* reaction cycle, the step of H₂ transfer was examined as well. Thereby, evidence was provided for the reaction of a transient five-fold coordinated complex with H₂ by experimental presentation of the H₂ transfer step for the first time.

In summary, during this thesis, the possibility of intermolecular CH activation, the bifunctional, catalytic reduction of O₂ and the stabilization of unusual oxidation states and geometries with iridium owing to the aliphatic PNP pincer platform were shown (**Figure C.5-2**). Significant experiments for future investigations should be: The potential CH activation and at best functionalization of unsubstituted hydrocarbons and further aliphatic

ethers and the improvement of the stability of the O₂-splitting cycle and thus the potential future implementation of a fuel cell.

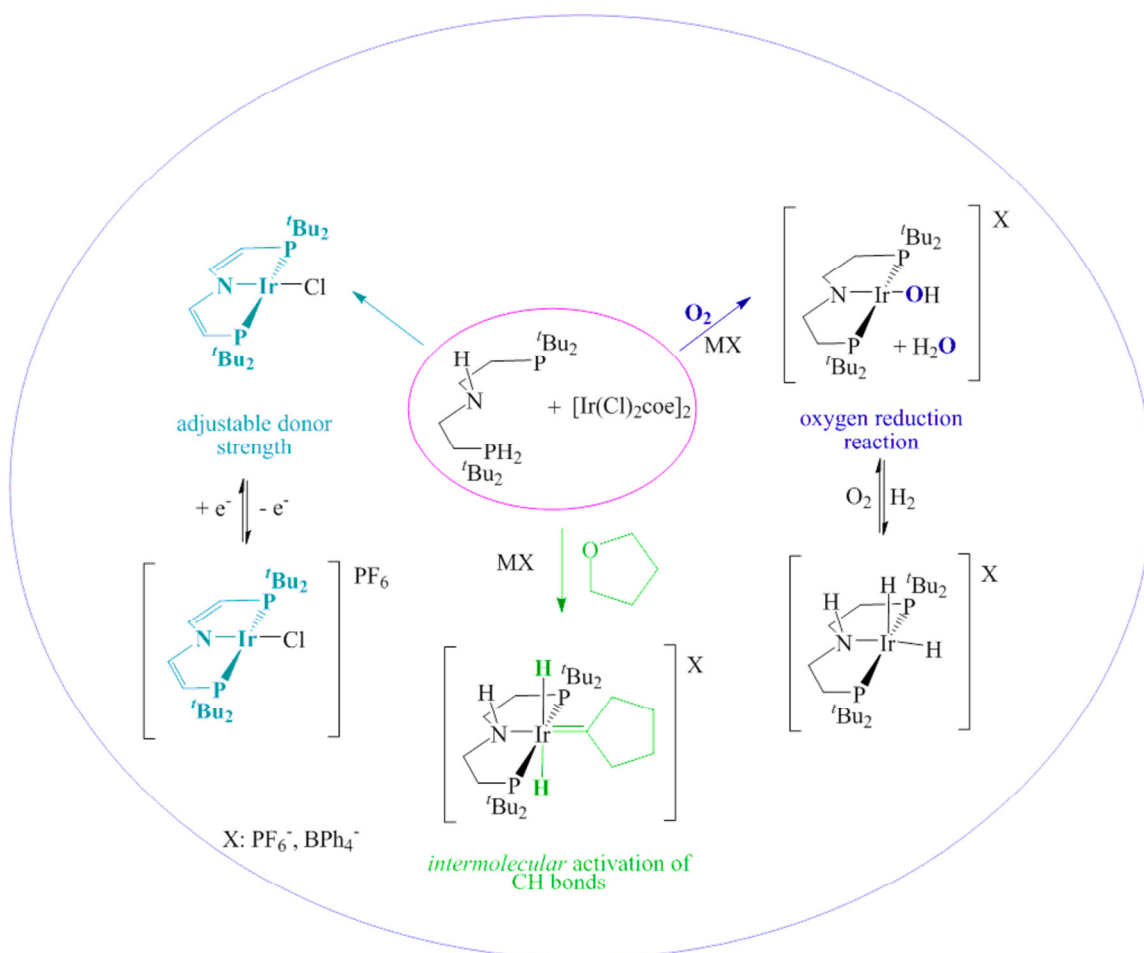


Figure C.5-2: Examined fields within this thesis.

D Zusammenfassung und Ausblick

D.1 Überblick

In dieser kumulativen Dissertation wurde die Koordinationschemie von *d6*, *d7* und *d8* Amino- und Amido-Iridium-PNP-Pinzettenkomplexen untersucht. Aufgrund *elektronischer*, *sterischer* und *bifunktioneller* Eigenschaften des verwendeten PNP-Ligandensystems, konnte die Zugänglichkeit von einzigartigen Oxidationsstufen und Koordinationsgeometrien, sowie kooperative Reaktivität und die ungehinderte Aktivierung von CH-Bindungen mit Hilfe der Ir(PNP)-Plattform vorgestellt werden.

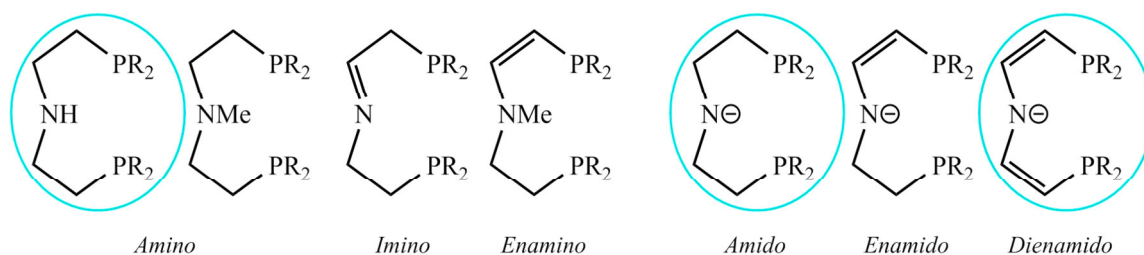


Abb. D.1-1: Kollektion verschiedener neutraler und anionischer PNP-Pinzetten-Liganden erhalten durch NH-Deprotonierung, -Methylierung oder Dehydrogenierung von koordiniertem $\text{HN}(\text{CH}_2\text{CH}_2\text{PR}_3)_2$ ($\text{R} = \text{}^i\text{Pr}$, $\text{}^t\text{Bu}$)^[7,365]. Umkreist, $\text{R} = \text{}^t\text{Bu}$: Liganden, die während dieser Arbeit untersucht wurden.

Das chelatisierende, ethylenverbrückte Amin $\text{HN}(\text{CH}_2\text{CH}_2\text{P}^t\text{Bu}_3)_2$ zeigt eine bemerkenswerte Vielseitigkeit als Pinzettenligand. Amido, Imino-, Enamido- und Dienamidokomplexe sind durch Templat- oder *in situ*-Synthese ausgehend vom Aminokomplex über NH-Deprotonierung oder oxidative Dehydrierung des aliphatischen Ligandrückgrats zugänglich (**Abb. D.1-1**).

Diese Art der Modifikation zur Feinabstimmung der elektronischen Donor-Eigenschaften des Systems beeinflusst die Stabilität der Koordinationsgeometrien sowie der Oxidations- und Spinzustände stark. Auch potenzielle *nicht-unschuldige* und kooperative Reaktivität der Komplexe werden durch diese Feineinstellung des Liganden beeinflusst. Aufgrund der hohen Elektronendichte am PNP-Amidozentrum, werden ungewöhnliche Oxidationsstufen und Koordinationsgeometrien der späten Übergangsmetallzentren, wie z.B. sehr seltenes quadratisch-planar koordiniertes Iridium(III), stabilisiert. Dies führt zu elektronisch und koordinativ ungesättigten Komplexen mit unerwarteter Stabilität sowie Reaktivität.

D.2 Quadratisch-planare Iridium *d7* und *d6* Komplexe

Während der Untersuchung der Koordinationschemie von Iridium mit dem aliphatischen PNP-Pinzettensystem im Rahmen dieser Arbeit (**B.1**) zeigte sich, wie unkompliziert oxidative Ligandenfunktionalisierung des aliphatischen PNP-Liganden die Isolierung von ungewöhnlichen, quadratisch-planaren Iridium *d7* und *d6*-Komplexen ermöglicht. Die

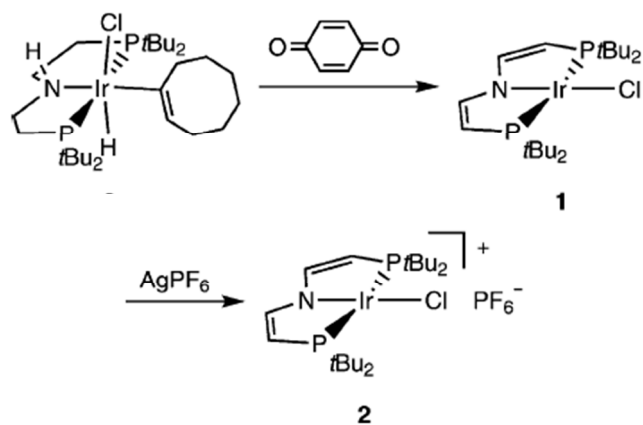


Abb. D.2-1: Synthese von stabilen, quadratisch planar koordinierten Ir(II)- und Ir(III)-Komplexen^[361].

Dehydrogenierung des PNP-Rückrats mit Benzochinon führte zur Isolierung des stabilen, paramagnetischen, quadratisch-planar-koordinierten, Dienamido-Ir(II)-Komplex **1** in mäßigen bis guten Ausbeuten. Darüber hinaus konnte **1** zum ersten bekannten quadratisch-planar koordinierten Ir(III)-Komplex **2**^[361] oxidiert werden (**Abb. D.2-1**).

Im Vergleich mit dem ethylenverbrückten PNP-Amidoligand zeichnet sich der erzeugte ungesättigte Ligand durch höhere Rigidität im Hinblick auf Konformationsänderungen aber durch größere elektronische Flexibilität aus: Während die Radikalkomplexe durch Oxidation von Iridium(I)-Dialkylamiden kurzlebige Spezies mit N-zentrierter Reaktivität sind, sind Metallo-Radikal **1** und das Oxidationsprodukt **2**^[361] stabil genug, um leicht isoliert werden.^[239,73] Daher eröffnet der Dienamidoligand die Möglichkeit einer ungewöhnlichen 1-Elektronen-Reaktivität von Iridium.

In der Zwischenzeit wurde das entsprechende Ir(I)-Äquivalent von *Kinauer et al.* präpariert^[362]. Die Verbindungen zusammen repräsentieren eine geeignete RedOx Serie Ir I/II/III mit schlüssiger Änderung z.B. der

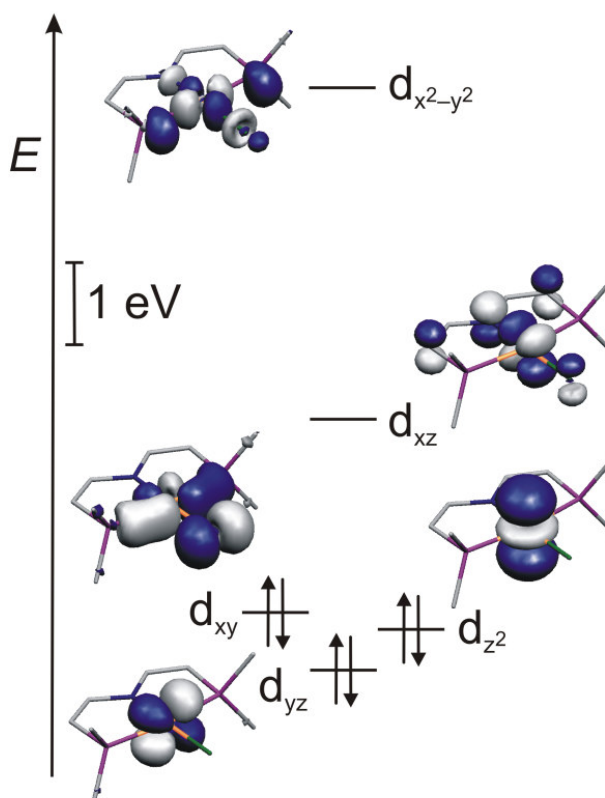


Abb. D.2-2: Metallzentrierte Kohn-Sham Grenz-Orbitale von IrCl{N(CH₂CHPMe₂)₂} (**2**^{Me}) im Singulettzustand aus Spin-unrestricted-ZORA-B3LYP-DFT Rechnungen (die z-Achse steht senkrecht zur Ir{N(CH₂CHP)₂}-Ebene).

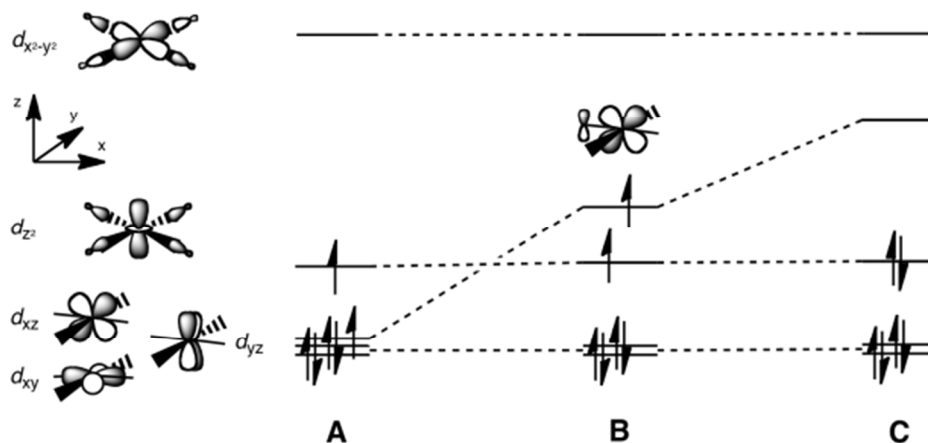


Abb. D.2-3^[363,364]: Valenz-*d*-Orbitalaufspaltung in quadratisch planarer Koordination für ein Ion mit reinen σ -Donor Liganden (A), beziehungsweise einem schwachen (B) oder starken (C) einseitigen, senkrechten π -Donor.

N-Ir-Bindungslängen durch sukzessive Befüllung des LUMO bzw. SOMO mit überwiegend N-Ir- π^* -Charakter mit Elektronen (**Abb. D.2-2**). Differenzierte Reaktivität tritt auf: Während Ir(III) durch Nukleophile angegriffen werden kann, aktiviert Ir(I) CH-Bindungen nukleophil. Die Reaktivität des Ir(II)-Analogons ist unklar. Der überwiegende Teil der Mulliken-Spindichte befindet sich auf dem Ir-Zentralatom und somit wird folgerichtig keine ligandenzentrierte 1-Elektronen-Reaktivität beobachtet. Es konnte aber auch keine ausgeprägte Reaktivität des radikalischen Ir(II)-Metallzentrums lokalisiert werden, vielleicht aufgrund einer sterischen Abschirmung durch die voluminösen ^tButylgruppen.

Der diamagnetische (*d6* Low-spin (LS)) Ir(III)-Komplex **2**^[361] ist darüber hinaus von großem Interesse, da das Set *d6* ML₄, welches ohnehin sehr selten ist, in der Regel in Form von intermediate-spin (IS) Komplexen repräsentiert wird (z.B. Fe koordiniert mit Porphyrinato) oder in Richtung C_{2v} Symmetrie (*butterfly*) verzerrt, mit einer oder zwei zusätzlichen CH-agostischen Wechselwirkungen vorliegt. Der π -Donor-Charakter des Dienamidoliganden führt zum Anheben der schwach antibindenden Orbitale in quadratisch-planarer Koordination und dadurch tendenziell zur Spinpaarung. Im Fall vom schweren 5*d* Übergangsmetall Ir, welches eine große Aufspaltung der Energieniveaus aufweist, beeinflusst der vergleichbar schwächere π -Donor ausreichend den HOMO-LUMO-Abstand in Richtung Spinpaarung (**Abb. D.2-3**^[363,364]). Interessanterweise besitzt das *d6* Ru(II)-Dienamido-Analogon, welches Gegenstand einer bahnbrechenden Arbeit von Askevold^[365] ist, IS-Konfiguration, vermutlich aufgrund einer kleineren intrinsischen Orbitalaufspaltung im Falle des 4*d* Übergangsmetalls.

Wenn ein stärkerer π -Donor wie z.B. der Amido-PNP-Ligand, eingesetzt wird, kann auch im Fall von Ru(II) LS $d6$ -Konfiguration erreicht werden. So kann die Abstimmung der π -Donorstärke des verwendeten PNP-Pinzettensystems auch genutzt werden, um zu gewünschten Spinzuständen zu gelangen.

D.3 Sauerstoff-Reduktions-Reaktion (ORR)

Um Informationen über das Potenzial der untersuchten Ir(PNP)-Plattform im Hinblick auf eine Oxygenierung zu gewinnen, wurde der Dihydridoamino-Ir(III)-Komplex **3** mit Sauerstoff umgesetzt, was zur Bildung des diamagnetischen Hydroxoamido-Ir(III)-Komplexes **4** führte. Für die elektronische Struktur ($d6$, quadratisch-planar, LS) des letzteren ist, wieder wie im Fall von Dienamido-Komplex **2**, der starke π -Donor-Charakter des Dialkylamido-PNP-Liganden und möglicherweise zusätzlich die sterische Abschirmung durch die sperrigen t Butylgruppen verantwortlich.

Bei der Reaktion des Dihydrids **3** mit Sauerstoff entsteht auch ein Äquivalent Wasser. Nach vorläufigen

mechanistischen

Informationen und Hinweisen werden alle vier

Reduktionsäquivalente innerhalb der Ir-H-Bindungen eines Moleküls **3** gespeichert.

Disauerstoff-Komplexe von Iridium^[366] und die reduktive Spaltung von O_2 durch Iridium^[368] sind bekannt, allerdings nach

bestem Wissen nicht die unmittelbare Vier-Elektronen- O_2 -Reduktion

durch ein monomolekulares RedOx-Zentrum. Weiterhin stellte sich heraus, dass ausgehend vom Dihydridokomplex **3** die Oxygenierungsreaktion durch Begasen mit H_2 rückgängig gemacht werden kann (**Abb. D.3-1**). Es konnten mehrere solcher Zyklen in CH_2Cl_2 oder THF

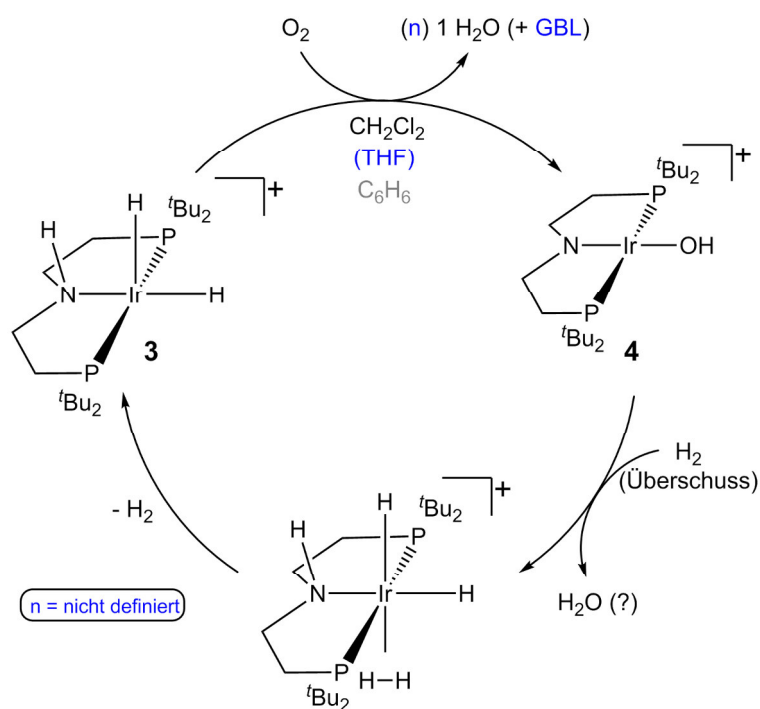


Abb. D.3-1: O_2 -Spaltungs-Hydrogenierungs-Zyklus

[368] z.B.: Z. M. Heiden, T. B. Rauchfuss, *J. Am. Chem. Soc.* **2007**, *129*, 14303.

gefahren werden. Zusammen genommen, wenn auch noch nicht klar ist, ob auch H₂O in der Reaktion des Hydroxids **4** mit H₂ gebildet wird, stellt der Zyklus die sukzessive, katalytische, bifunktionelle Variante der Sauerstoffreduktion, in diesem Fall die Knallgasreaktion, dar. Dies könnte ein mögliches Setting für ein zukünftiges Experimentalfeld in Richtung der Entwicklung einer Brennstoffzelle darstellen.

Die O-O-Bindungsspaltung, welche eine fundamentale Reaktion ist, ist nicht nur von Interesse für die ORR, sondern auch für mögliche selektive oxidative CH-Funktionalisierungen. In den Reaktionen des Dihydridokomplex **3** mit O₂ im Falle von THF als Lösungsmittel wurde γ -Butyrolacton (GBL) gebildet. Daher sollte eine zukünftige Kombination der O₂-Spaltreaktion mit den CH-Aktivierung-Fähigkeiten (siehe unten) des PNP-Iridiumfragments sehr produktiv sein z.B. wäre es interessant zu wissen, ob es möglich ist, in einer gemischten Atmosphäre 2 H₂/O₂ THF oder andere Kohlenwasserstoffe katalytisch selektiv mit Sauerstoff zu oxygenieren.

D.4 Intermolekulare CH-Aktivierung

Um das Potenzial der Ir(HPNP^{*t*Bu})-Plattform im Hinblick auf die Funktionalisierung organischer Substrate zu untersuchen, wurden potenzielle CH-Aktivierungsmöglichkeiten untersucht. In einer vorhergehenden, vielversprechenden Arbeit von Friedrich *et al.*^[71] wurde gezeigt, dass mit dem dort verwendeten Ir(HPNP^{*i*Pr})-System vinylische, oxidative Addition von koordiniertem Cycloocten sowie intermolekulare,

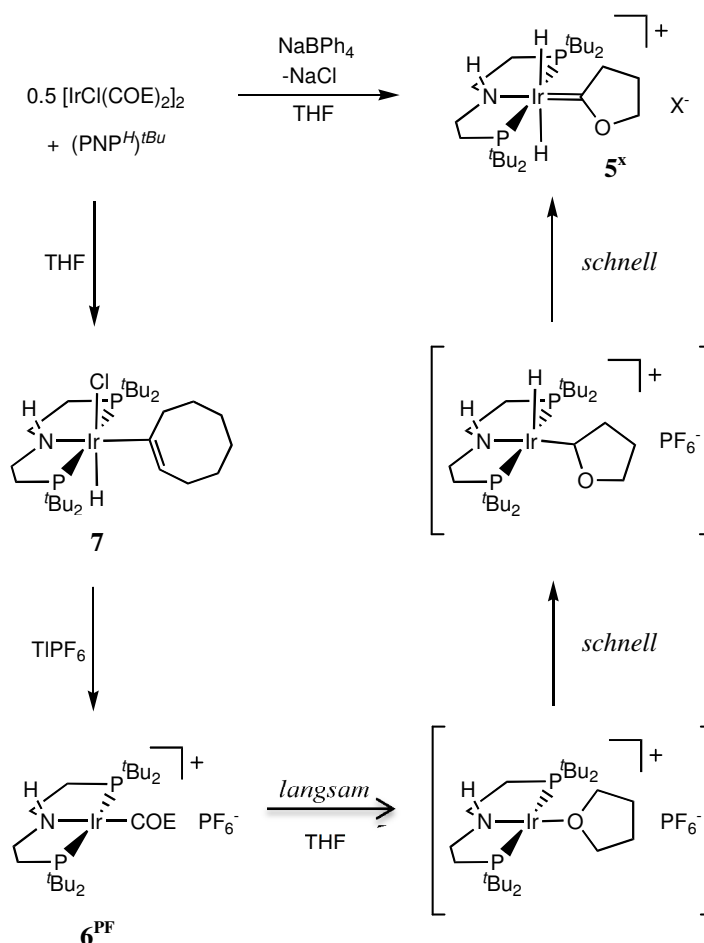


Abb. D.3-2: Synthese und angenommener Mechanismus der Bildung von Fischer-Carben Komplex **5** (X = BPh₄, PF₆⁻).

doppelte CH-Aktivierung des Lösungsmittels THF zu einem Iridium-Dihydrido-Fischer-Carbenkomplex möglich ist, wobei der intramolekulare Pfad überwiegt. Als die Modifikation der Phosphanylgruppen von ⁱPr- zu den voluminöseren ^tBu-Gruppen geändert wurde, führte dies zu quantitativer intermolekularer, geminaler CH-Aktivierung von THF und zur Bildung des entsprechenden Dihydrido-Carbenkomplex **5** (Abb. D.3-2). Aufgrund des höheren sterischen Drucks auf das aktive Zentrum der Ir(HPNP)-Plattform wird das Gleichgewicht der Bildung der kurzlebigen, T-förmigen *d8*-Spezies [(HPNP^{tBu})Ir]⁺ durch die Dissoziation von COE aus [(HPNP^{tBu})Ir(COE)]⁺ (**6**), die den geschwindigkeitsbestimmenden Schritt darstellt, auf die Produktseite verschoben. Das heißt, die Kontrolle des Reaktionsverlaufs ergibt sich aus dem detaillierten Design des Pinzettenumfeldes. Außerdem wird das Gleichgewicht der reduktiven Eliminierung zwischen sechsfachkoordiniertem, mäßig stabilen Cyclooctenylhydrid **7**, welches in THF überwiegend vorliegt und dem Ionenpaar [(HPNP^{tBu})Ir(COE)]⁺Cl⁻ (**6**^{Cl}) welches quantitativ in CH₂Cl₂ gebildet wird, in Abhängigkeit vom Lösungsmittel effektiv beeinflusst. Mit der *in situ*-Darstellung eines T-förmig koordinierten Iridium(I)-Fragments und somit der Möglichkeit zur CH-Aktivierung durch die Wahl des Lösungsmittels sowie durch Chloridabstraktion wird eine Alternative zur Erzeugung aus fünffach koordinierten Iridium(III)-Komplexen (beispielsweise durch Dehydrierung ein Iridium(III)-Dihydrids mit einem Opferolefin), die häufig genutzt wird, aufgezeigt.

D.5 Beschleunigte Desymmetrisierung in Anwesenheit von O₂ oder einem Ir(III)-Hydroxokomplex

Zu einem ähnlichen Zeitpunkt, als die doppelte CH-Aktivierung von THF durch Ir mit dem aliphatischen PNP-Ligand gelang, präsentierten *Grubbs et al.*^[203] eine sehr ähnliche Reaktion unter Verwendung des monoanionischen, Diaryl-Ozerov-PNP-Pinzettensystems, die zur Bildung von verschiedenen Iridiumcarbenkomplexen durch doppelte CH-Aktivierung von diversen aliphatischen Ethern führte. Bei diesen Reaktionen wurde das entsprechende dehydrierte Carben gebildet. Somit waren zwei freie Koordinationsstellen verfügbar und dadurch die Möglichkeit, das Carben durch Reaktion mit weiteren Substraten zu funktionalisieren. In der Tat konnte durch Umsetzen mit mehreren Heterokumulenen die Bildung der entsprechenden Formate, Thioformate oder Formimidate im *Grubbs*-Funktionalisierungs-Zyklus^[203] in beeindruckender Weise ermöglicht werden. Im Gegensatz dazu gelang die Funktionalisierung oder Dehydrierung des Dihydridocarbens **5** mit dem neutralen, aliphatischen PNP-Liganden, z.B. durch Zugabe von CO₂, Norbornen oder

Aceton, nicht. Hingegen fand unter definierten Bedingungen eine selektive Desymmetrisierungsreaktion von **5** zum Dihydridokomplex **3** sowie zum Ir(I)carben **8** statt (**Abb. D.5-1**), die beobachtet und kinetisch untersucht wurde. Aber es konnte nicht gezeigt werden, dass einer der untersuchten Aspekte, z.B. die Wahl des Gegenions, einen Effekt auf die Reaktionsgeschwindigkeit hätte, mit Ausnahme der Zugabe von unterstöchiometrischen Mengen an O₂ in Form von Luft oder dem Hydroxoamido-Ir(III)-Komplex **4** (siehe oben).

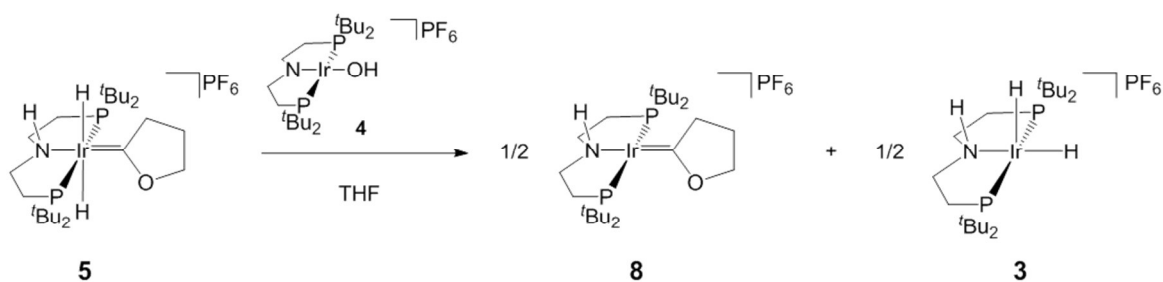


Abb. D.5-1: Desymmetrisierung des Dihydrido-Fischer-Carben-Komplex **5**, die wahrscheinlich durch das Oxygenierungs-Produkt **4** katalysiert wird.

Daher erscheint es möglich, dass **4** ein aktiver Katalysator für diese Reaktion ist. Versuche mit höheren Mengen an Sauerstoff zeigten, dass beide Desymmetrisierungsprodukte **5** und **8** zu **4** und gleichfalls durch Begasen mit H₂ zu **3** umgesetzt werden können. Während der Studie der Desymmetrisierungsreaktion wurde dadurch auch ein Teilschritt des *Grubbs*-Reaktionszyklus, der Schritt der H₂-Übertragung, näher beleuchtet. Dabei wurde der Nachweis für die postulierte Reaktion einer fünffach koordinierten Übergangsstufe mit H₂ durch experimentelle Darstellung des H₂-Übertragungsschrittes zum ersten Mal erbracht.

Zusammenfassend wurde während dieser Arbeit die Möglichkeit der intermolekularen CH-Aktivierung, die katalytische, bifunktionelle Reduktion von O₂ und die Stabilisierung von ungewöhnlichen Oxidationsstufen und Geometrien durch Iridium mit dem aliphatischen PNP-Pinzettenliganden gezeigt (**Abb. D.5-2**). Wichtige Experimente für zukünftige Untersuchungen sollten sein: Die potenzielle CH-Aktivierung und am besten Funktionalisierung von unsubstituierten Kohlenwasserstoffen und weiteren aliphatischen Ethern und die Verbesserung der Stabilität des O₂-Spaltzyklus und damit die mögliche zukünftige Implementierung einer Brennstoffzelle.

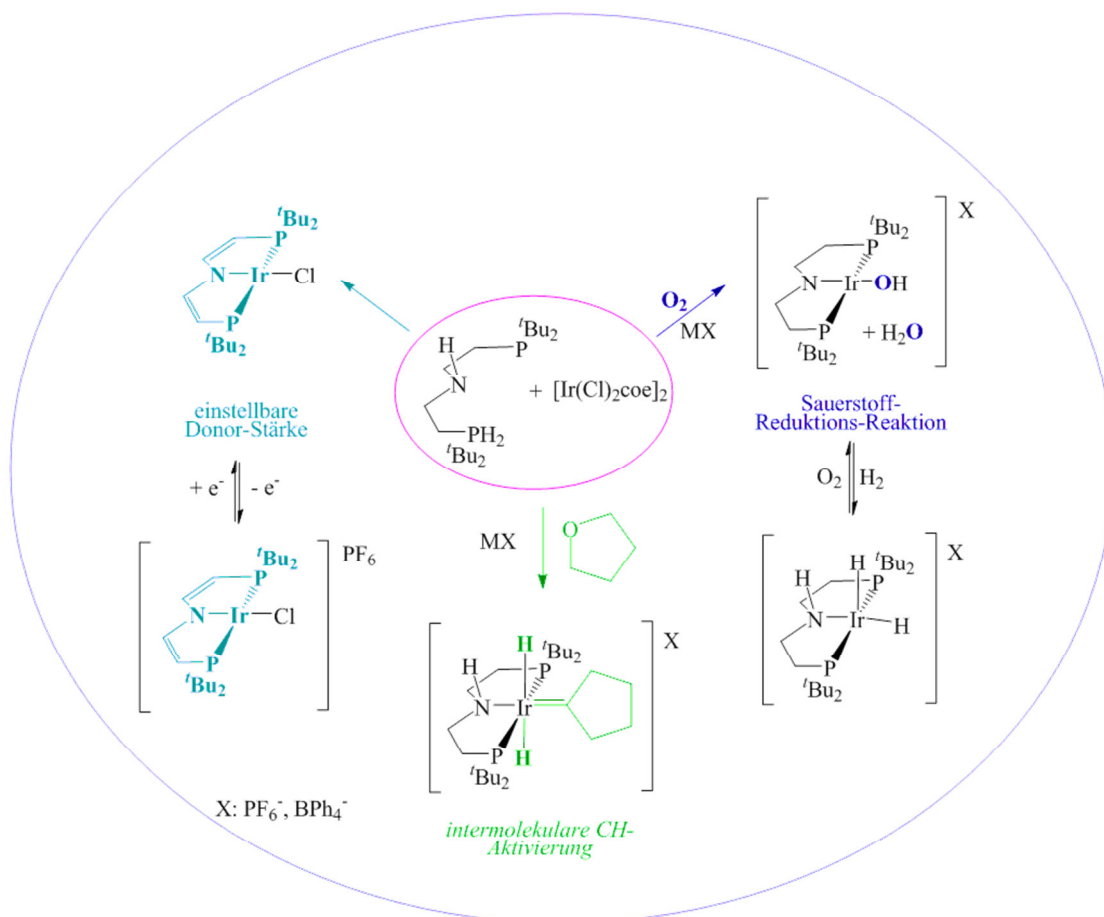


Abb. D.5-2: Untersuchte Arbeitsfelder dieser Dissertation.

E List of Publications

List of publications originating from this thesis released until now:

Review: "Cooperative Aliphatic PNP Amido Pincer Ligands – Versatile Building Blocks for Coordination Chemistry and Catalysis." S. Schneider, J. Meiners, B. Askevold, *Eur. J. Inorg. Chem.* **2012**, 3, 412-429

"Square-Planar Iridium(II) and Iridium(III) Amido Complexes." J. Meiners, M. Scheibel, M.-H. Lemée-Cailleau, S. A. Mason, M. B. Boeddinghaus, T. F. Fässler, E. Herdtweck, M. M. Khusniyarov, S. Schneider, *Angew. Chem. Int. Ed.* **2011**, 50(35), 8184-8187

Oral Presentation at the ACS 240th ACS National Meeting, Boston, MA, United States, August 22-26, **2010**: "Four-coordinate Ru(II) amido PNP-pincer complexes" by B. Askevold (presenting author), J. Meiners, M. Khusniyarov, E. Herdtweck, S. Schneider

Oral Presentation at the ACS 239th ACS National Meeting, San Francisco, CA, United States, March 21-25, **2010**: "Facile double C-H activation of tetrahydrofuran by an iridium PNP pincer complex." by J. Meiners (presenting author), A. Friedrich, E. Herdtweck, S. Schneider

"Facile C-H Activation of Tetrahydrofuran by an Iridium PNP Pincer Complex." J. Meiners, A. Friedrich, E. Herdtweck, S. Schneider, *Organometallics* **2009**, 28(21), 6331-6338

F Curriculum Vitae

Name	Jenni Meiners
Date and place of birth	03.10.1978 Berlin
Employment	
Oct. 2014 – today	Employment at ADAM OPEL AG Rüsselsheim in the chemical division of Prof. Dr. Hartmut Baumgart of the ITDC
Feb. 2014 – July 2014	Employment at <i>FFO Automotive Rüsselsheim</i> and work in the quality analysis at ADAM OPEL AG Rüsselsheim
University	
Dec. 2014	Defense of the PhD thesis at Technical University of Munich (<i>magna cum laude</i>)
Sept. 2013 – Jan. 2014	Writing of the cumulative dissertation and preparation of defense
June 2012 - August 2013	PhD candidate in organometallic chemistry at the Georg August University Göttingen, supervised by Prof. Dr. Sven Schneider
Jan. 2012 - May 2012	PhD candidate in organometallic chemistry at the Friedrich Alexander University Erlangen, supervised by Prof. Dr. Sven Schneider
March 2008 – Dec. 2011	PhD candidate in organometallic chemistry at the Technical University of Munich, supervised by Dr. Sven Schneider at the chair for inorganic chemistry Prof. W. A. Herrmann
Study	
Oct. 2007 - Feb. 2008	Study Physics for the teaching at University Potsdam
June 2006 – March 2007	Diploma thesis supervised by Prof. Dr. Peter W. Roesky at the Freie University Berlin with the topic: „ <i>Aminotroponiminato- und Aminotroponatogoldkomplexe; trigonal koordinierte Gold(I)verbindungen</i> “ publication: ‘ <i>Three Coordinated Aminotroponiminate and Aminotroponate Complexes of Gold(I)</i> ’ J. Meiners, J. S. Herrmann, P. W. Roesky, <i>Inorg. Chem.</i> 2007 , 46(11), 4599 – 4604, poster presentation: “ <i>Aminotroponiminato-Gold(I)-Komplexe</i> “ J. Meiners (presenting author), P. W. Roesky, J. S. Herrmann, <i>Wöhler</i> conference 2006 Aachen/D grade Diploma thesis: 1,3, overall grade: 1,7
Oct. 2005 - March 2007	Resumption of studies
Jan. 2004 - Dec. 2005	Provisional guidance of the artist and restoration store <i>PROPOLIS Farben Meiners</i> of my mother, working as a student assistant in the preparation and implementation of experimental lectures,

	October 2004 - Sept. 2005: Two semester leave of absence
Oct. 2003 - Sept. 2004	Interruption of studies for competitive sports
Oct. 1999 - Sept. 2003	Change to graduate study in chemistry at the Humboldt University Berlin
Oct. 1998 - Sept. 1999	Two semesters studying computer science at the Humboldt University Berlin
June 1998	Abitur at Sophie-Scholl-School Berlin Schöneberg

Qualifications

Synthesis and experiment planning, evaluation and interpretation, synthesis, purification, analysis, redox reactions, hydrogenation and oxygenation of sensitive to temperature, water, light, air and pyrolysis organometallic compounds using Schlenk and glovebox inert gas techniques and cryogenic techniques, purification methods under inert gas such as crystallization, distillation, condensation, sublimation, column chromatography and analytical techniques such as inert gas NMR, VT-NMR, two-dimensional NMR, kinetic NMR measurements and IR, single crystal breeding, drying, purification and degassing of solvents and starting compounds, study of reaction rates and mechanisms, design and construction of Schlenk and *J*-Young glassware apparatuses, work with the following pure gases: nitrogen, argon, hydrogen and oxygen, building, furnishing and relocating of inert gas labs, supervision of students and academic staff, planning and implementation of chemical internships and seminars for major and minor students, literature research, writing scientific publications and review articles

IT

Excel, Word, Citavi	Good knowledge
MestreNova, DeltaJeol,	Good to very good knowledge
Topspin, Nuts, WinDNMR	Basic knowledge

Language

English	Fluent
French and Latin	School knowledge